Dipl.-Ing. Alexander Klippel

# Investigations into the influence of dustiness on the course of vented dust explosions

BAM-Dissertationsreihe • Band 123
Berlin 2015

Die vorliegende Arbeit entstand an der BAM Bundesanstalt für Materialforschung und -prüfung.

Impressum

**Investigations into the influence**
**of dustiness on the course**
**of vented dust explosions**

2015

Herausgeber:
BAM Bundesanstalt für Materialforschung und -prüfung
Unter den Eichen 87
12205 Berlin
Telefon: +49 30 8104-0
Telefax: +49 30 8112029
E-Mail: info@bam.de
Internet: www.bam.de

Layout: BAM-Referat Z.8

ISSN 1613-4249
ISBN 978-3-9816668-2-3

# Investigations into the influence of dustiness on the course of vented dust explosions

**Dissertation**

zur Erlangung des akademischen Grades

**Doktoringenieur**

**(Dr.-Ing.)**

von Dipl.-Ing. Alexander Klippel

geb. am 11.08.1983 in Berlin

genehmigt durch die Fakultät für Verfahrens- und Systemtechnik der Otto-von-Guericke-Universität Magdeburg

| | |
|---|---|
| Promotionskommission: | Prof. Dr.-Ing. Eckehard Specht (Vorsitz) |
| | Prof. Dr-Ing. habil. Ulrich Krause (Gutachter) |
| | Prof. (Emeritus) Rolf K. Eckhoff (Gutachter) |
| | Dr.-Ing. Martin Schmidt (Mitglied) |
| eingereicht am: | 02.07.2014 |
| Promotionskolloquium am: | 17.11.2014 |

Berlin 2015

***”We have first raised a dust and then complain we cannot see.“***

George Berkeley ( † 1753)

# Zusammenfassung

Eine neue sicherheitstechnische Kennzahl, das Staubungsverhalten gemäß VDI Richtlinie VDI 2263 – Blatt 9, wird hinsichtlich ihres Nutzens für den Staubexplosionsschutz untersucht. Unter Staubungsverhalten versteht man die Tendenz eines Staubes, Wolken aufgrund eines festgelegten mechanischen Stimulus zu bilden. Stäube können sich bei vergleichbareren physikalischen Eigenschaften wie Dichte oder Partikelgrößenverteilung, teilweise sehr unterschiedlich in einem Staub/Luft-Gemisch oder im Falle einer Staubexplosion verhalten. Um den Einfluss des Staubungsverhaltens auf die Staubwolkenbildung und den Ablauf von Explosionen zu untersuchen, wurden Experimente und Simulationen in einer vertikalen 75 L Rohrapparatur durchgeführt. Mit den Erkenntnissen aus diesen Laborversuchen wurden weitere Versuche im Realmaßstab in einem 50 m³ Silo durchgeführt.

Versuche im Labormaßstab in einem druckentlasteten 75 L Behälter haben gezeigt, dass das Staubungsverhalten einen Einfluss auf die reduzierten Explosionsdrücke, die zeitlichen Druckanstiege und die Flammengeschwindigkeiten hat. Um die Versuchsergebnisse für den industriellen Maßstab zu belegen, wurden Versuche in einem 50 m³ Silo durchgeführt. Dabei wurde zunächst die Reproduzierbarkeit von Befüllungsvorgängen mit Staubkonzentrationsmessungen durch mehrere Wiederholungsversuche überprüft. Dabei ergaben sich Abweichungen von 30 % und mehr im Vergleich zum Mittelwert der Versuche. Erste Explosionsversuche eines Worst-Case-Szenarios mit hoher Turbulenz und möglichst homogenen Staubwolken ergaben deutlich niedrigere reduzierte Explosionsdrücke als die mit den empirischen Gleichungen berechneten. Der Explosionsverlauf war in Übereinstimmung mit den Kenngrößen $p_{max}$ und $K_{St}$.

Bei der Simulation von Staub/Luft-Gemischen wurden mit dem Euler/Lagrange- und dem Euler/Euler-Ansatz verwendet. Dabei wurde vor allem untersucht inwiefern das Sedimentations- und Staubungsverhalten modelliert werden können. Es zeigte sich, dass der Euler/Lagrange-Ansatz besser geeignet ist lokale Staubkonzentrationsverteilungen, Partikelgrößenverteilungen und -kräfte zu simulieren. Der Euler/Euler-Ansatz ermöglicht generelle Aussagen in kürzerer Rechenzeit für eine definierte Partikelgröße. Der numerische Strömungslöser ANSYS CFX V14 wurde für alle Simulationen benutzt.

**Schlagwörter:** Staubungsverhalten, druckentlastete Staubexplosionen, Staubexplosionsschutz, CFD, Euler/Lagrange-Ansatz

# Abstract

A new safety characteristic named “dustiness” according to the German guideline VDI 2263 – part 9 is investigated. Dustiness describes the tendency of a powder to form airborne dust by a prescribed mechanical stimulus. Dusts often behave differently in a dust/air mixture or in the case of a dust explosion, even if they have comparable physical properties such as particle size and density. In order to look into the effects of dustiness on dust cloud formation and explosion properties experiments and simulations in a 75 L vertical dust dispersion glass tube apparatus were carried out. In a second step industrial-scale experiments were carried out in a 50 m³ silo.

Experiments showed that particle size and density are not the only factors which influence dustiness, since the chosen dusts with comparable densities and particle size distributions showed very different behavior in the flow. Other dust properties such as particle shape, specific surface area, humidity and agglomeration processes have an influence which can outweigh size and density. Preliminary explosion experiments showed that dustiness has an influence on the reduced explosion pressure and pressure rise in a vented 75 L test apparatus. In order to verify the results for applications in the process industries further tests with different settings were carried out in industrial-scale experiments. First dust concentration measurements were done in order to evaluate the reproducibility of filling processes. Experiments showed that single tests differed by 30 % and more from the average depending on dust sample and filling method. First explosion experiments with a worst-case scenario in terms of high turbulence and homogenous dust distribution showed that the maximum reduced explosion pressures were well below the calculated values. Reduced explosion pressures and rates of pressure rise of the three tested dust were as their explosion characteristics $p_{max}$ and $K_{St}$ let suggest.

The Euler/Lagrange and the Euler/Euler approaches were compared simulating dust/air mixtures. Especially sedimentation and the ability of the approaches to simulate the tendency of dust to stay airborne were investigated. The Euler/Lagrange approach is better suited for simulating local dust concentrations, particle size distributions and particle forces. With the Euler/Euler method it is possible to achieve fast solutions for one specified diameter. The computational fluid dynamics code ANSYS CFX R14 was used for all simulations.

**Keywords:** dustiness, vented dust explosion, dust explosion protection, CFD, Euler/Lagrange approach

# Table of contents

# List of figures

# List of tables

# Abbreviations

| | |
|---|---|
| acc. to | according to |
| approx. | approximately |
| BAM | Federal Institute for Materials Research and Testing |
| CAD | computer aided design |
| CFD | computational fluid dynamics |
| CTA | constant temperature anemometry |
| DIN | German Institute for Standardization |
| eq. | equation |
| EN | European standard |
| FSA | Research Establishment for Applied System Safety and Health |
| GSBL | Joint Substance Data Pool of the German Federal Government and the German Federal States |
| gsf | global scale factor |
| LDA | Laser-Doppler anemometer |
| LEL | lower explosion limit |
| NFPA | National Fire Protection Association |
| SC | safety characteristics |
| SKG 5 | dust concentration meter |
| SST | Shear Stress Transport |
| VDI | Association of German Engineers |

# Nomenclature

| | | |
|---|---|---|
| $1 - norm$ | average deviation compared to finest grid | $[m/s]$ |
| $2 - norm$ | standard deviation compared to finest grid | $[m/s]$ |
| $A$ | constant of van-der-Wals force | $[-]$ |
| $A_{\alpha\beta}$ | contact surface | $[m^2]$ |
| $\tilde{A}_{\alpha\beta}$ | modified contact surface | $[m^2]$ |
| $a$ | minimum distance between two particles | $[m]$ |
| $c(t)$ | dust concentration as function of time | $[-]$ |
| $C_C$ | Cunningham correction | $[-]$ |
| $C_{CD}$ | coefficient of momentum transfer | $[-]$ |
| $C_D$ | drag coefficient | $[-]$ |
| $C_l$ | Saffman coefficient | $[-]$ |
| $C_{TD}$ | turbulent dispersion coefficient | $[-]$ |
| $C_v$ | concentration by volume | $[-]$ |
| $C_{VM}$ | virtual mass coefficient | $[-]$ |
| $D_{max}$ | maximum dispersibility | $[kg/J]$ |
| $D_{real}$ | real dispersibility | $[kg/J]$ |
| $d$ | diameter | $[m]$ |
| $d(0.1)$ | 10 % of sample particles have smaller diameters | $[m]$ |
| $d(0.5)$ | median diameter | $[m]$ |
| $d(0.9)$ | 90 % of sample particles have smaller diameter | $[m]$ |
| $d_0$ | diameter of equal surface sphere | $[m]$ |
| $d_1$ | diameter of larger particle | $[m]$ |
| $d_2$ | diameter of smaller particle | $[m]$ |
| $d_c$ | diameter of dust cloud | $[m]$ |
| $d_e$ | equivalent diameter | $[m]$ |

| | | |
|---|---|---|
| $d_S$ | Stokes diameter | $[m]$ |
| $d_V$ | diameter of equal volume sphere | $[m]$ |
| $d_\beta$ | particle diameter | $[m]$ |
| $(dp/dt)$ | rate of pressure rise | $[bar/s]$ |
| $(dp/dt)max$ | maximum rate of pressure rise | $[bar/s]$ |
| E | extinction | $[-]$ |
| $F_B$ | buoyancy force | $[N/m^3]$ |
| $F_D$ | drag force | $[N/m^3]$ |
| $F_E$ | electrical force | $[N]$ |
| $F_P$ | pressure gradient force | $[N]$ |
| $F_S$ | Saffman force | $[N/m^3]$ |
| $F_v$ | van-der-Wals force | $[N]$ |
| $F_{TD}$ | turbulent dispersion force | $[N/m^3]$ |
| $F_{VM}$ | virtual mass force | $[N/m^3]$ |
| $f_D$ | Doppler frequency | $[1/s]$ |
| $f_{Hey}$ | Heywood factor | $[-]$ |
| $f_k$ | error of simulated velocity | $[m/s]$ |
| $g$ | gravitational acceleration | $[m/s^2]$ |
| $I$ | received light intensity | $[-]$ |
| $I_0$ | emitted light intensity | $[-]$ |
| $K_{St}$ | dust explosion constant | $[bar \cdot m/s]$ |
| $k$ | factor of efficiency | $[-]$ |
| $l$ | measurement distance | $[m]$ |
| $m_\alpha$ | mass of displaced fluid | $[kg]$ |
| $max - norm$ | maximum deviation | $[m/s]$ |
| $\dot{m}$ | mass flow | $[kg/h]$ |
| $N$ | number of nodes | $[-]$ |
| $P$ | potential between two particles | $[V]$ |

| | | |
|---|---|---|
| $p$ | pressure | $[bar]$ |
| $p_{ex}$ | explosion pressure | $[bar]$ |
| $p_{max}$ | maximum explosion pressure | $[bar]$ |
| $p_{red}$ | reduced explosion pressure | $[bar]$ |
| $p_{red,max}$ | maximum reduced explosion pressure | $[bar]$ |
| $p_{stat}$ | static activation pressure | $[bar]$ |
| $p_{static}$ | static pressure | $[bar]$ |
| $p_{tot}$ | total pressure | $[bar]$ |
| $q_1$ | charge of larger particle | $[C]$ |
| $q_2$ | charge of smaller particle | $[C]$ |
| $r_\alpha$ | volume fraction of fluid | $[-]$ |
| $r_\beta$ | volume fraction of solid | $[-]$ |
| $\tilde{r}_\beta$ | modified volume fraction of solid | $[-]$ |
| $Re$ | Reynolds number | $[-]$ |
| $Re_p$ | particle Reynolds number | $[-]$ |
| $S$ | dustiness number | $[-]$ |
| $S_i$ | dustiness number of test I | $[-]$ |
| $T$ | temperature | $[K]$ |
| $t_F$ | conveying time | $[s]$ |
| $t_S$ | settling time | $[s]$ |
| $U$ | average velocity | $[m/s]$ |
| $U_\infty$ | average velocity of surrounding flow | $[m/s]$ |
| $U_{DC}$ | measured dust cloud settling velocity | $[m/s]$ |
| $U_c$ | cloud settling velocity | $[m/s]$ |
| $U_{RMS}$ | RMS velocity | $[m/s]$ |
| $U_S$ | terminal velocity of particle | $[m/s]$ |
| $U_{Sch}$ | cloud settling velocity of dust cloud in enclosure | $[m/s]$ |
| $U_\alpha$ | velocity of fluid | $[m/s]$ |

| | | |
|---|---|---|
| $U_\beta$ | velocity of solid | $[m/s]$ |
| $LEL$ | lower explosion limit | $[kg/m^3]$ |
| $u_x$ | partial velocity in x | $[m/s]$ |
| $u_y$ | partial velocity in y | $[m/s]$ |
| $u_z$ | partial velocity in z | $[m/s]$ |
| $t_{diff}$ | time difference between first detection of dust | $[m/s]$ |
| $V$ | volume | $[m^3]$ |
| $V_A$ | total volume of agglomerate | $[m^3]$ |
| $V_{AH}$ | volume particles in an agglomerate | $[m^3]$ |
| $V_c$ | volume of cloud | $[m^3]$ |
| $V_H$ | volume of hollow space | $[m^3]$ |
| $V_{Hg}$ | volume of closed pores | $[m^3]$ |
| $V_{Ho}$ | volume of open pores | $[m^3]$ |
| $V_{HP}$ | volume of all pores | $[m^3]$ |
| $V_P$ | total volume of particle | $[m^3]$ |
| $V_S$ | volume of solid | $[m^3]$ |
| $\dot{V}$ | volume flow | $[m^3/h]$ |
| $W_{min}$ | specific dispersibility | $[J/kg]$ |
| $y^+$ | dimensionless distance from wall | $[-]$ |
| $\alpha$ | fluid | $[-]$ |
| $\beta$ | solid | $[-]$ |
| $\epsilon$ | porosity | $[-]$ |
| $\epsilon_0$ | permittivity vacuum | $[F/m]$ |
| $\epsilon_A$ | agglomerate porosity | $[-]$ |
| $\epsilon_p$ | particle porosity | $[-]$ |
| $\epsilon_\alpha$ | permittivity of gas | $[F/m]$ |
| $\kappa$ | extinction coefficient | $[m^2/kg]$ |
| $\lambda$ | wavelength of light | $[m]$ |

| | | |
|---|---|---|
| $\eta$ | dynamic viscosity of air | $[kg/(m \cdot s)]$ |
| $\eta_c$ | dynamic viscosity of a cloud | $[kg/(m \cdot s)]$ |
| $\rho_0$ | density | $[kg/m^3]$ |
| $\rho_a$ | density of raw material | $[kg/m^3]$ |
| $\rho_{air}$ | density of air | $[kg/m^3]$ |
| $\rho_c$ | density of dust cloud | $[kg/m^3]$ |
| $\rho_{eq}$ | equivalent density | $[kg/m^3]$ |
| $\rho_\alpha$ | density of fluid | $[kg/m^3]$ |
| $\rho_\beta$ | density of solid | $[kg/m^3]$ |
| $\sigma_{t\alpha}$ | turbulent Schmidt number | $[-]$ |
| $\Theta$ | angle between laser beams | $[rad]$ |
| $\chi$ | shape factor of particle | $[-]$ |
| $\psi_{Wa}$ | sphericity according to Wadell | $[-]$ |

# Vorwort

Die vorliegende Arbeit zum Thema „Investigations into the influence of dustiness on the course of vented dust explosions“ entstand aus einer Zusammenarbeit der Fakultät für Verfahrens- und Systemtechnik der Otto-von-Guericke-Universität Magdeburg, speziell dem Institut für Apparate- und Umwelttechnik, unter der Leitung von Herrn Prof. Dr.-Ing. habil. Ulrich Krause und der BAM Bundesanstalt für Materialforschung und -prüfung, Fachbereich 2.2 „Reaktionsfähige Stoffe und Stoffsysteme“ auf dem Gebiet „brennbaren Schüttgüter und Stäube, feste Brennstoffe“ bei Herrn Dr.-Ing. Martin Schmidt. Herrn Prof. Dr.-Ing. habil. Ulrich Krause danke ich für die Übernahme der Betreuung und für seine Hilfe bei Fachfragen. Durch seine lange Erfahrung auf unterschiedlichen Gebieten der Sicherheitstechnik und seine tiefe Verbundenheit zur wissenschaftlichen Herangehensweise, waren die Gespräche eine große Unterstützung. Professor Rolf K. Eckhoff danke ich für seine Bereitschaft das Zweitgutachten zu übernehmen und am Kolloquium teilzunehmen.

Ganz besonders möchte ich mich bei Herrn Dr.-Ing. Martin Schmidt bedanken, der mir durch seine engagierte Betreuung bei allen auftretenden Problemen sehr geholfen hat und auch nach Dienstschluss das Wohl seiner Mitarbeiter nie aus den Augen verliert. Bei der BAM möchte ich ebenfalls Herrn Dr.-Ing. Marc Scheid danken, der mir gerade in der Anfangszeit mit vielen Denkanstößen und seiner Diskussionsbereitschaft geholfen hat. Ohne die gute Zusammenarbeit mit Herrn Olaf Mücke wäre der Aufbau bzw. die Steuerung der Versuchsapparaturen sehr viel aufwändiger gewesen. Bei Katharina Wegener bedanke ich mich für die schnelle Prüfung der verwendeten Substanzen. Herr Dipl.-Ing. Stefan Zirker unterstützte mich bei allen Fragestellungen zur Mess- und Elektrotechnik. Bei der praktischen Arbeit haben mich insbesondere Herr Dipl.-Ing. Mike Wappler, Herr January Kopersski und Herr Alexander Przybilski sehr unterstützt. Für die Hilfe zu allen chemischen Fragestellungen und seine Anmerkungen zur schriftlichen Arbeit danke ich Herrn Dr. rer. nat. Marcus Malow. Dr. rer. nat. Kai Holtappels, Dr.-Ing. Martin Kluge und M.Sc. Robert Zeps haben mir bei der Arbeit auf dem BAM Testgelände Technische Sicherheit sehr geholfen.

Desweiteren möchte ich Andrea und Frederik für ihre private und fachliche Unterstützung danken. Bei meinen Eltern, Paul und Marion, und meiner Schwester, Anja, bedanke ich mich für die Unterstützung während der gesamten Promotion und darüber hinaus. Ebenfalls möchte ich mich bei meinen Paten, Marlen und Jupp, für ihre fortwährende Unterstützung und ihr Interesse an meinem Lebensweg bedanken.

# 1 Motivation and approach

### Motivation

Dust explosion hazards can be found in a wide range of industrial branches. Most materials, if small enough, can generate dust explosions, this includes dusts in the food industry, mining and others such as flour, coal and aluminum. A dust explosion only occurs if an explosive dust/air mixture and an ignition source with a sufficient amount of energy exist at the same time. Dust explosions can produce temperatures over 1000 °C and pressures over 10 bar. Dust explosion can occur with dust concentrations as low as 30 g/m³ and ignition energies below 1 mJ. A dust specific hazard is secondary explosions, once an explosion took place, deposited dust can be raised and ignited due to the pressure wave and flame. In order to evaluate whether or not an explosion hazard can occur and for the design of preventive and protective safety measures safety characteristics are needed. Safety characteristics of dust/air mixtures consist of, among other things, the ability to form explosive dust/air mixtures, lower explosion limit, maximum explosion pressure and dust explosion constant ($K_{St}$ value). Preventive and protective safety measures can be avoidance of ignition sources, replacement of combustible with non-combustible materials, explosion suppression and explosion venting with vents in order to relieve the explosion pressure. Tests for the determination of safety characteristics are usually performed with methods, which are defined in standards under more or less reproducible conditions such as strength of the ignition source, turbulence intensity and homogeneity of the dust/air-mixture. For example, safety characteristics are used in empirical equations for the determination of the venting area. These empirical equations are based on industrial scale tests that were done with nearly homogenous dust/air mixtures and high turbulence. It is usually assumed that these conditions allow for a conservative evaluation or design. Dusts can vary very much in material, particle shape and size, agglomeration process and behavior in turbulent flow. There is tendency of dusts to form dust clouds due to these properties. This tendency to form clouds is called dustiness and it describes the ability of dust to stay airborne due to a defined mechanical stimulus. Dustiness depends on the properties of the dusts as well as on the determination method as described by **Hauert and Radandt** [1]. Since dustiness depends on the determination method and to achieve a comparable property a new safety characteristic dustiness (see VDI 2263 - Part 9 [2]) has been defined for explosion protection. The safety characteristic dustiness is not taken into account for the design of safety measures in European standards so far.

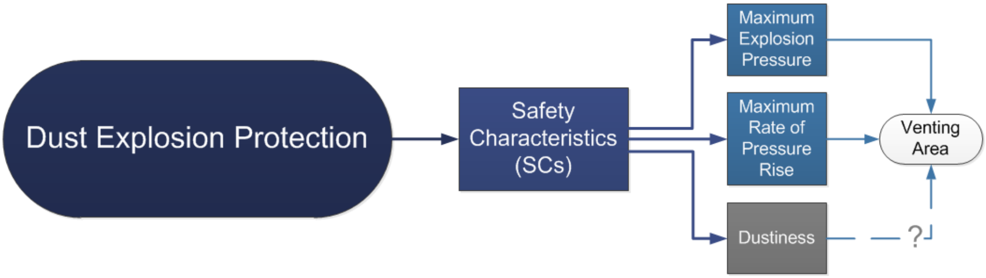

*Figure 1-1. Schematic of dust explosion protection.*

Dustiness probably affects the propagation of a dust explosion, protection measures such as venting, could be optimized based on this parameter, see Figure 1-1. Focus of this work is the influence of dustiness on the course of vented dust explosion regarding adaption of the necessary venting area to practical conditions.

Adaption of the venting area to practical conditions has been done for different phenomena such as turbulence and filling processes, but not for dustiness. So far there is one adaption, which takes dustiness into account indirectly. In practice explosive dust/air mixtures occur very often due to dispersion of a dust layer, conveying of dust or filling up an enclosure. In such processes the dust cloud generated is usually not homogenous and does not spread out over the whole enclosure. **Hauert et al.** [3] showed that for pneumatic conveying with tangential release into silos, lower reduced explosion pressures occur compared to those determined by the standard method as described in the European standard EN 14491 [4]. These effects are now considered for safety measures depending on the filling method in the EN 14491, however, the design depends on $p_{max}$ and $K_{st}$ value and properties of the vessel. Other attempts to better suit practical conditions have been made by **Tamanini** [5] and **Zalosh** [6]. The idea was to take into account different initial turbulence intensities. The influence of initial turbulence on vented dust explosions was also shown by **Scheid et al.** [7]. The American standard NFPA 68 [8] now considers initial turbulence as a parameter for sizing venting areas. A comparative study for sizing venting areas between the standards NFPA 68 and EN 14491 has been made by **Tascon et al**. [9]. It was shown that the venting areas for silos according to the standard NFPA 68 were smaller, therefore less expensive, than the venting areas according to EN 14491, except for length/diameter ratios of one. In conclusion sizing of venting areas according to the European standard EN 14491 can be made more efficient in future.

Other attempts to better suit practical conditions have been made in Europe, e.g. the German guideline VDI 2263 part 7.1 [10] uses the specific conditions of spray dryers to reduce venting areas. This means the mass of combustible material is known in the dryer as well as working conditions (temperature, mass of dust in the vessel), which are used to achieve smaller venting areas.

## Approach

The investigations for this work consist of small-scale and industrial-scale experimental work as well as numerical simulations. Beginning with a literature research about dust explosion protection, small-scale experiments are planned. These experiments are done in a vertical tube apparatus, which is optical accessible and allows dust concentration and pressure measurement. A modular design of the apparatus allows different filling methods. The use of a small apparatus is necessary for reproducible conditions and to save time and material. Results are used to determine the influence of dustiness on vented dust explosions and as input and validation for numerical simulations. As a first preliminary result, six dusts of different dustiness groups were classified according to their dispersion behavior in turbulent flows. Besides, pressure, pressure rises and flame speeds were measured in vented dust explosion experiments to evaluate the influence of dustiness. Additionally the reasons for the different dispersion behavior such as particle size and surface area were investigated.

The results are used to plan industrial-scale experiments in order to verify the results and to determine a first approach to optimize the sizing of venting areas depending on the safety characteristic dustiness.

In safety engineering the use of computational fluid dynamics (CFD) is increasing as well as in many other engineering branches. For future use the possibilities to simulate dust/air mixtures with ANSYS CFX R14 were examined and the Euler/Euler and the Euler/Lagrange approaches were compared. The Euler/Lagrange approach was especially used for various sensitivity studies such as the influence of different particle forces and different particle shapes. In addition the dissertation includes CFD simulations about the possibilities to model the dust/air mixtures with the Euler/Lagrange approach. In order to simulate the settling of dust clouds more realistic the particle surface area was adjusted and the particle size distribution was taken into account. Results were compared to experimentally determined terminal velocities and dust concentrations in small-scale and industrial-scale vessels.

Finally if an influence of dustiness on vented dust explosion can be shown, a suggestion how to change the sizing of the venting area depending on dustiness should be given.

# 2 Combustible dusts

Dust explosions can lead to massive loss in means of process plants or human health. Therefore an appropriate explosion protection is necessary for every facility, which produces, transports or handles dusts. The properties of these dusts, the conditions under which explosive dust/air mixtures occur and their explosion behavior have to be known in order to research combustible dusts in detail and for a proper explosion protection. Understanding dust explosions completely is very difficult. Not only chemical properties are an important influence, e.g. organic, inorganic or metallic and their chemical reactions, but physical properties such as particle size distribution, specific surface area and density alter the reaction behavior immensely.

## 2.1 Dust explosion prevention and protection

The properties of combustible dusts, which are used to plan explosion protection, are described by safety characteristics (SCs). In order to understand the SCs and the special properties of dusts a definition of dust is given here. The word dust is not uniformly defined. Usually the word dust is used for particles smaller than 500 µm [11]. One definition is:

> “Dust – A solid-particle aerosol formed by mechanical disintegration of a parent material, such as by crushing or grinding. Particles range in size from submicrometer to more than 100 µm and usually are irregular.“ [12, p. 4]

SCs are determined on a laboratory scale under defined and reproducible conditions. They are rarely any physical properties of the materials, but linked to part of the practical application or hazard. SCs are used to describe hazardous materials and to obtain comparable decision criteria for designing explosion protection, further details are described by **Eckhoff** [13], **Steen** [14, p. 379ff], **Bartknecht** [15] and **Amyotte** [16].

For dusts a distinction is made between

- characteristics of deposited dusts
- and characteristics of dust/air mixtures.

This work deals with dust/air mixtures only. The determination of the characteristics of dusts is much more difficult than for gases due to the fact, that solid particles have additional properties such as

- different particle size distribution for same type of dust,
- aging of dusts,
- varying water content,
- and widely spread range of densities among different dusts.

Reactivity of dusts is influenced by these properties. Thus the reactivity can differ for samples of the same dust. In order to take appropriate protection measures it is therefore necessary to use samples, which are exactly the same as used in the process or a worst-case sample (dried, sieved) [14, p. 443ff] and [11].

There are various ignition sources, which can cause a dust explosion. Table 2-1 shows different kinds of ignition sources and their averaged probability.

*Table 2-1. Ignition sources acc. to their likeliness [15, p. 161].*

| ignition source | percentage % |
|---|---:|
| mechanical sparks/ heating | 32.7 |
| smouldering spot | 12.7 |
| electrostatic discharge | 8.5 |
| fire | 7.9 |
| hot surface | 4.8 |
| welding | 4.2 |
| electric equipment | 3.2 |
| not known | 17.0 |
| others | 3.0 |

There are different SCs for deposited dusts and suspended dusts. The SCs, which are used, depend on the vessel, process and environmental conditions. Therefore not all SCs have to be determined for a safe operation.

In order to give an overview some SCs for deposited dusts and dust/air mixtures can be found in Table 2-2.

Table 2-2. Overview of SCs.

| safety characteristics | |
|---|---|
| deposited | dust/air mixtures |
| ignitability | explosibility |
| combustion behavior | maximum explosion pressure |
| minimum ignition temperature | maximum rate of pressure rise |
| self-ignition temperature | explosion limits |
| impact sensivity | limiting oxygen concentration |
| | minimum ignition energy |
| | minimum ignition temperature |
| | dustiness* |

*so far not used in European standards

In order to avoid damage to humans or equipment safety measures are designed. Safety measures regarding explosion prevention are all actions to avoid an explosive atmosphere in combination with a sufficient ignition source. Explosion prevention includes

- substitution with a non-combustible material,
- avoidance of explosive dust/air mixtures,
- inertisation,
- and avoidance of ignition sources.

In case of an explosion constructive measures are in place such as

- explosion-resistant design,
- venting,
- explosion suppression
- and explosion isolation.

This work deals with vented dust explosions, therefore only the relevant SCs are described in the following. Further information on dust explosion protection are skipped for brevity and can be found in literature [14] [15] [17] or standards [18] [19] [20] [21].

Venting means reducing explosion pressures with vents, which open in case of an explosion. A pressure curve of a vented dust explosion can be seen in Figure 2-1. The vent opens at a specified activation pressure and the pressure increases until the maximum reduced explosion pressure is reached. Openings reduce the maximum explosion pressure in the vessel below the pressure the vessel can withstand ($p_{vessel\ strength}$). The curve of an unvented explosion with the explosion pressure $p_{ex}$ is shown for comparison.

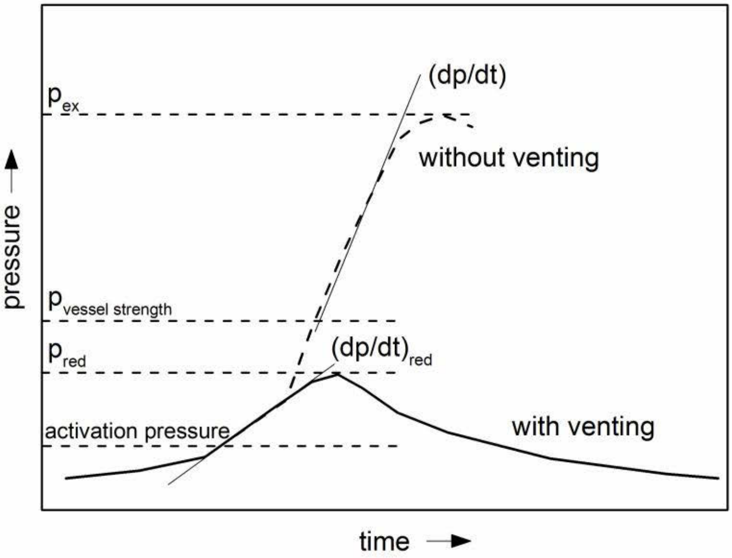

*Figure 2-1. Exemplary pressure curve of a vented explosion (based on [16]).*

A picture of a vented dust explosion in a silo at the Federal Institute for Materials Research and Testing (BAM) test site is shown in Figure 2-2. When designing venting of plants it is necessary to protect humans and environment from flames, pressure and scattering parts in the venting area.

*Figure 2-2. Vented dust explosion in a silo (photo: BAM).*

The development of pressure during an explosion of a dust/air mixture is described by the two properties: maximum explosion pressure $p_{max}$ and maximum rate of pressure rise $(dp/dt)_{max}$ or $K_{St}$ value. These are used in empirical equations together with vessel properties (length/diameter ratio, vessel strength, volume) to size the venting area.

### 2.1.1 Explosion pressure $p_{ex}$ and maximum explosion pressure $p_{max}$

The explosion pressure $p_{ex}$ means the maximum pressure, which is measured during the course of an explosion in a closed vessel (1-m³ vessel or 20-L sphere) for a specified dust concentration, see Figure 2-3.

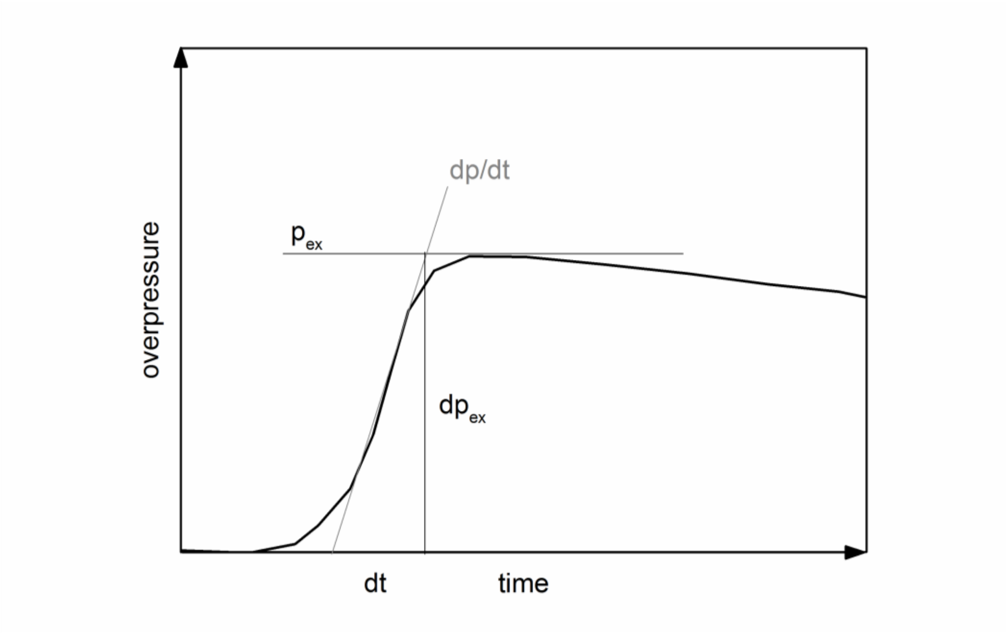

*Figure 2-3. Exemplary course of a pressure time curve in a confined space (based on [20, p. 13]).*

The experimental determination of $p_{max}$ is done with a series of experiments in a confined vessel with systematic variation of the dust concentration. The dust is dispersed with pressurized air and ignited by two pyrotechnical igniters.

### 2.1.2 Maximum rate of pressure rise and $K_{St}$ value

The maximum rate of pressure rise $(dp/dt)_{max}$ of the explosion of a dust-air mixture at an optimum concentration determined in a 1-m³ vessel (or normalized to a volume of 1-m³) is the so-called $K_{St}$ value. The $K_{St}$ value strongly depends on the state of flow and the volume of the test vessel. Up to now the cubic law is used to standardize the results from the 20-L sphere, but as shown by **Krause** in 1998 [22] the cubic law should not be used. Since it is still commonly used for testing with vessels smaller than 1 m³ it is stated in equation 1:

$$dp/dt_{max} \cdot V^{1/3} = konst = K_{St} \qquad \textit{eq. 1}$$

The cubic law is valid only for laminar and spherical flame propagation of homogenously premixed fuel/air mixtures. Usually dust/air mixtures differ very much from these assumptions.

The $K_{St}$ value is used to determine the dust explosion class. Further information about determination of $p_{max}$ and $K_{St}$ value can be found in the standard VDI 2263 – part 1 [23] and EN 14034 – part 1-2 [20] and [21].

### 2.1.3 Dustiness

Dustiness means the tendency of a powder to form airborne dust by a prescribed mechanical stimulus. It is used mainly for health safety so far. Dustiness testing in health care is intended to replicate dust cloud generation as found in workplaces. Dustiness depends on the material as well as on the determination method. Approaches to determine dustiness for pigments and extenders can be found in the standard DIN 55992 - part 1-2 [24], [25] and [26] or in the European standard EN 15051 part 1-3 [27], [28] and [29]. The standards are about workplace exposure and health risks. In 1978 **Wells et al.** [30] described a method to compare powders with respect to their potential to liberate airborne dust in order to choose suitable dusts with lowest emission of respirable dust. This should prevent factory personnel from exposure to dust. Dustiness has been used as characteristic of dusts for some time, but still lacks a complete understanding of physical reasons or comparable results of different test methods. The withdrawn standard ANSI/ASTM D547-41 [31] “Test Method for Index of Dustiness of Coal and Coke” uses a measurement method, which was developed in 1939 to determine dustiness of coal products. Further information on different methods to determine dustiness is given by **Hamelmann** [32] and **Eickelpasch** [33].

In explosion protection dustiness is a new safety characteristic. Dustiness depends very much on the determination method and therefore should be standardized to achieve comparable results. The dependence on determination method and setting was shown by **Breum** for a rotating drum dustiness tester in relation to sample mass, testing time and surface adhesion [34]. These findings are supported by a comparison of four different systems for measuring dustiness by **Bach et al.** [35]**.** There is a statistic correlation between the different methods but no simple way to convert different dustiness values depending on the determination method. Figure 2-4 shows an overview of important influences on dustiness.

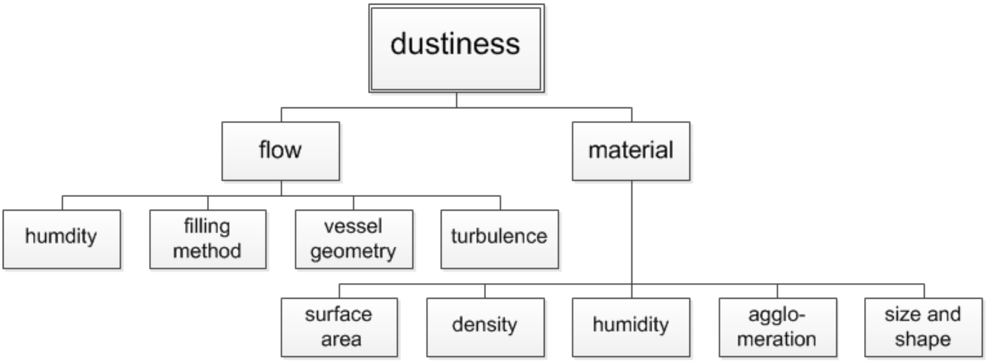

*Figure 2-4. Schematic of factors, which influence dustiness.*

### Dustiness in explosion protection

Dustiness in explosion protection is defined in VDI 2263 – part 9 “Dust fires and dust explosions - Hazards - assessment - protective measures - Determination of dustiness of bulk materials” [36]. The measurement principle described in VDI 2263 – part 9 allows the evaluation of the likelihood of the generation of dust clouds. So far the determination was done for a variety of dusts used in food, mining or metal industries as described by **Hauert and Radandt** [1]. With the measurement apparatus shown in Figure 2-5 the safety characteristic dustiness can be determined. Dusts are divided into dustiness groups. There are six dustiness groups (DG) from one to six (one means little tendency to stay airborne, six the opposite). The equipment consists of a sample container with a feeding system, a dust chamber, a dust concentration meter, a ring ionizer to electrostatically discharge the dust and a computer for data storage and analysis. Electrostatic charge and relative air humidity over 60 % have an influence on dustiness determination as shown by **Lauer** [37]. Electric charge of the sample and/or high relative air humidity reduces the tendency to form dust clouds slightly. A description of the measurement procedure can be found in Figure 2-5.

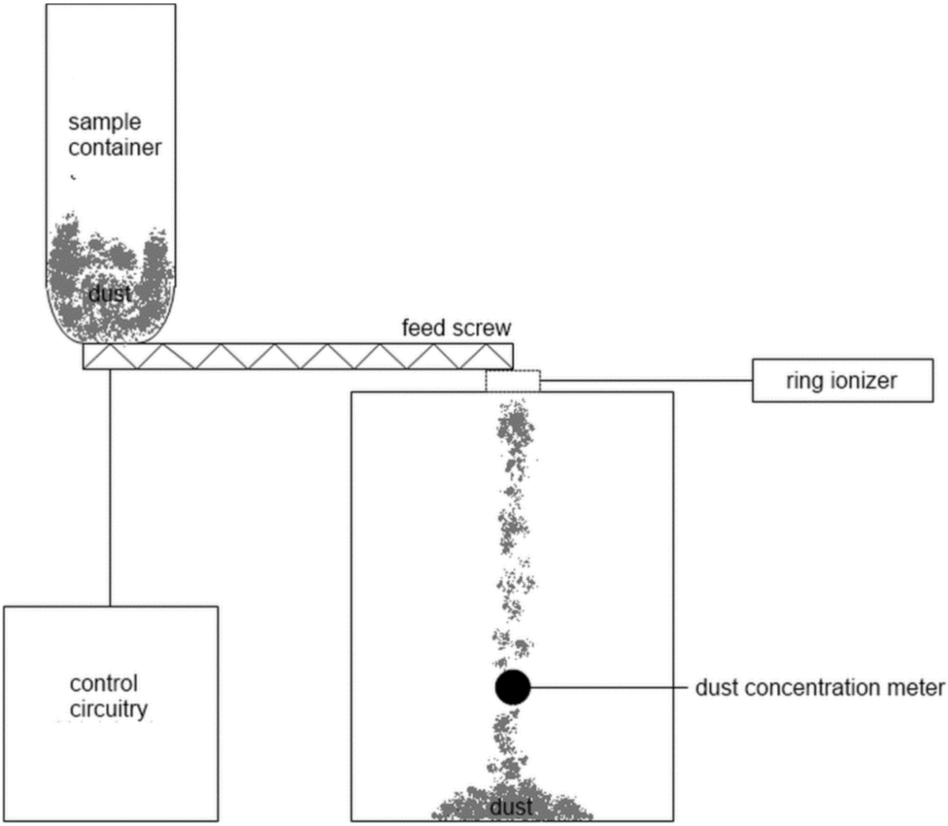

*Figure 2-5. Schematic of the measurement principle.*

Dust is conveyed with a constant volume flow for 300 s. The total time of measurement is 650 s. The local dust concentration over time is calculated with calibration data, which has to be determined for every dust separately. For each of the three measurements the dustiness coefficient $S_i$ is calculated according to eq. 2:

$$S_i = \frac{m^3 / g}{t_F + t_S} \int_0^{t_F+t_S} c(t)dt \qquad \textit{eq. 2}$$

Where c(t) is the measured local concentration, $t_F$ is the time in which the dust is conveyed $(300\ s)$ and $t_S$ is the time of sedimentation $(350\ s)$. $m$ and $g$ are units of length and mass in meter and gram (in order to achieve a dimensionless dustiness number). The average out of the three single values $S_i$is dustiness number S. Dustiness number is used to assign each dust to a dustiness group. A higher dustiness group means a higher tendency to form dust clouds.

Table 2-3. Dustiness groups and dustiness numbers.

| dustiness group | dustiness number S |
|---|---|
| 1 | 0 to 1 |
| 2 | >1-5 |
| 3 | >5-10 |
| 4 | >10-20 |
| 5 | >20-50 |
| 6 | >50 |

For the guideline wheat starch was used as reference material.

## 2.2 Physical properties of dust/air mixtures

Dust/air mixtures belong to the field of aerosols. Aerosol means the dispersion of solid or liquid particles in gas. Dust, mist and smoke belong to the field of aerosols. Due to their importance to technical applications, human health and environmental protection it is necessary to know as much as possible about physical properties of aerosols. Dust/air mixtures are one part of the field of aerosols for which the here described characteristics are meant. **Hinds**, **Baron** and **Elimenech** [12], [38] and [39] described the physical properties and measurement methods related to aerosols as well as the following equations. The wide range of particle sizes of aerosols can be seen in Figure 2-6.

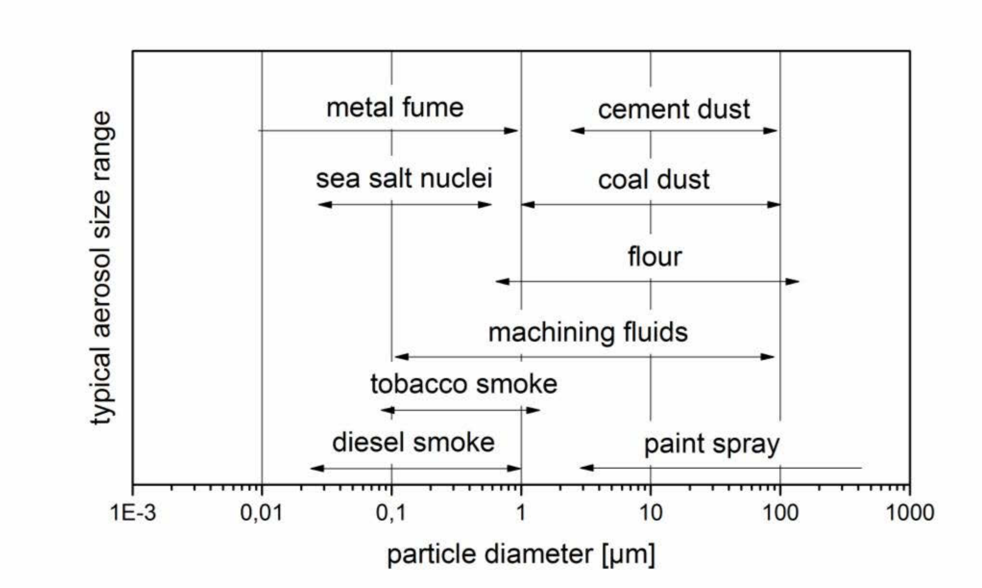

*Figure 2-6. Range of particle sizes of aerosols (based on [12, p. 9]).*

Dust dispersion or the behavior of dust/air mixtures depends on many partly interacting parameters. Even dusts with similar properties such as density and particle size distribution can act very differently as dust/air mixture. The German regulation „Technical Instructions on Air Quality Control - TA-Luft" [40] shows some influences on dust dispersion (see Table 2-4). The parameters, which influence the dispersion behavior, are numerous and partly related. One parameter not related to the material is the conveying method.

Table 2-4 shows the wide range of phenomena, which influence the behavior of dust/air mixtures. These phenomena (material, particle size, turbulent flow, kind of dispersion, humidity) do complicate accurate predictions of any process regarding dust/air mixtures and design of safety measures immensely.

*Table 2-4. Influences on dust dispersion according to [40, p. 52ff].*

| material properties | flow | deposit | transport |
|---|---|---|---|
| material | direction | dump shape | kind of conveying |
| density | velocity | dump size | discharge height |
| particle size distribution | turbulence | angle of slope | impermeability |
| humidity | humidity | area exposed to the wind | |
| particle shape | | surroundings | |
| surface properties | | | |

### 2.2.1 Particle size, shape and density

The particle size or size distribution is one of the most important and most used parameters to describe particles (see **Hinds** [12, p. 8f]). Dusts often have a ratio between smallest and biggest particles of some hundred orders of magnitude of their diameter. In dust explosion protection the median diameter, which is the diameter where 50 % of the sample is finer and 50 % is coarser, is often used to describe the size of dusts. The median diameter can only be taken as hint on the particle size, without more information on the size distribution.

Particle shapes range from spherical to very complex shapes. Most analytical approaches use ideal spherical particles with a density of 1000 kg/m³ instead of more complex models. The influence of shape and different densities can be considered with different diameters or with a correction factor.

Particle density means the density of the particle itself not the dust concentration which is the total mass of the dust in a specified volume in kg/m³. There are some kinds of densities for dusts such as raw density, dry raw density, bulk density, density of the source material and true density (see [41] and [42]):

- Raw density … calculated with all hollow space.
- Dry raw density … determined as the raw density but with completely dried material.
- Bulk density … density of the not-compacted bulk material.
- True density … density of the solid part of a porous material.

### 2.2.2 Drag force and particle Reynolds number

The drag force was already described for solid spheres (cannon balls) by Newton. Unfortunately Newton's considerations are only valid for Reynolds numbers higher than 1000. Particles tend to have much smaller Reynolds numbers, so Stokes' theorem has to be used to calculate the drag force. Figure 2-7 shows the connection between drag coefficient and particle Reynolds number for spheres. The connection between drag coefficient and particle Reynolds number can be determined for other geometries as well.

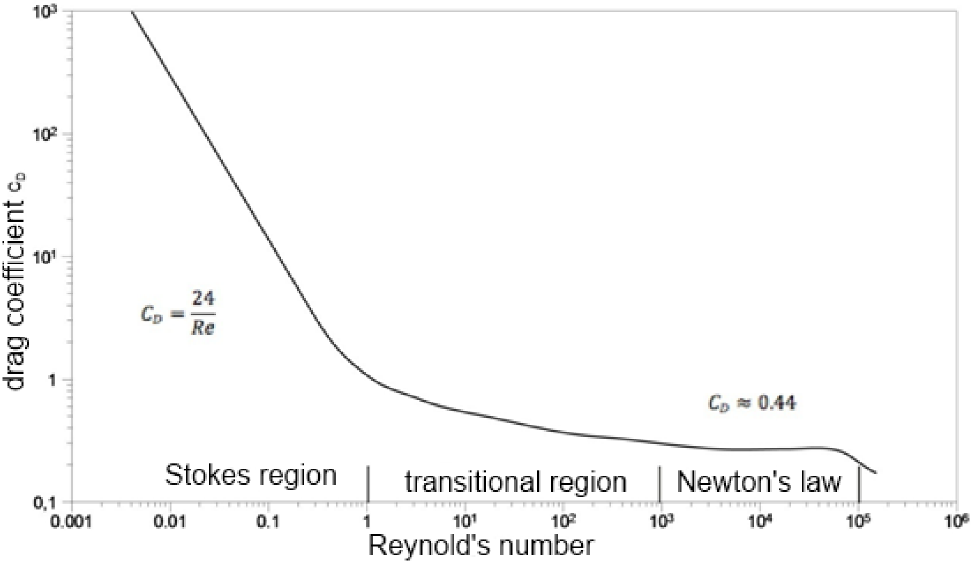

*Figure 2-7. Connection between drag coefficient/particle Reynolds number (based on [12, p. 43]).*

The drag force can be calculated according to eq. 3:

$$\boldsymbol{F_D = C_D \frac{\pi}{8} \rho_\alpha d^2 U^2} \qquad \textbf{\textit{eq. 3}}$$

Where are $C_D$ the drag coefficient, $\rho_\alpha$ density of the gas and $U$ velocity of the flow. The drag coefficient is almost constant for Reynolds numbers between $1000$ and $2 \cdot 10^5$ ($C_D \approx 0.44$). The drag coefficient in the transitional region between Newton and Stokes flow can be calculated according to eq. 4 (see also chapter 3.2.4 for more details on the numerical modeling of the drag force):

$$\boldsymbol{C_D = \frac{24}{Re_p}\left(1 + 0.15 \cdot Re_p^{0.687}\right)} \qquad \textbf{\textit{eq. 4}}$$

For the Stokes region it is assumed that forces due to viscosity are much greater than inertia. Thus, in the Navier-Stokes equations the inertial forces are neglected. Further assumptions for solving the equations are an incompressible fluid, no nearby walls or particles, spherical particles and no-slip surface of the particles. For Reynolds numbers smaller than one the drag coefficient is $C_D = 24/Re_p$. Stokes law can be used if the relative velocity between particle and fluid is much smaller than the speed of sound and the distance of the particle to the wall is at least 10 times the particle diameter.

The particle Reynolds number is defined in eq. 5:

$$\boldsymbol{Re_p = \frac{\rho_\alpha |U_\alpha - U_\beta| d_\beta}{\eta}} \qquad \textbf{\textit{eq. 5}}$$

Where are $U_\alpha$the velocity of the gas, $\rho_\alpha$ the density of the gas, $\eta$ the viscosity of the gas, $d_\beta$ the particle diameter and $U_\beta$ the particle velocity.

### 2.2.3 Corrections for particle density and shape

Particles or dusts have different densities and all kind of shapes. Most analytical and modeling approaches are suitable for spherical particles. Density and shape of particles have an influence on the terminal velocity or behavior in the flow in general.

There are different approaches to take the different shapes into account such as equivalent diameter, Stokes diameter and aerodynamic diameter. These approaches are based on spherical particles with change of diameter and/or density.

The equivalent diameter approach uses a dynamic shape factor (eq. 6):

$$\chi = \frac{\boldsymbol{F_D}}{\boldsymbol{3\pi\eta U d_e}} \qquad \textbf{\textit{eq. 6}}$$

Where $d_e$ is the equivalent diameter. Equivalent diameter means a calculated diameter for a theoretical spherical particle with the same volume as the considered particle. Thus, the Stokes law changes to $F_D = 3\pi\eta U d_e \chi$ and the terminal velocity is now $U_S = \rho_p d_e^2 g/(18\eta\chi)$.

The Stokes diameter uses the density of the source material $\rho_a$, which is easier to determine than the real particle density.

The aerodynamic diameter uses a spherical particle with a normalized density of $\rho_0 = 1000\ kg/m^3$, which has the same terminal velocity as the original particle (treatment as a “solid” water drop). Figure 2-8. shows the differences between the approaches.

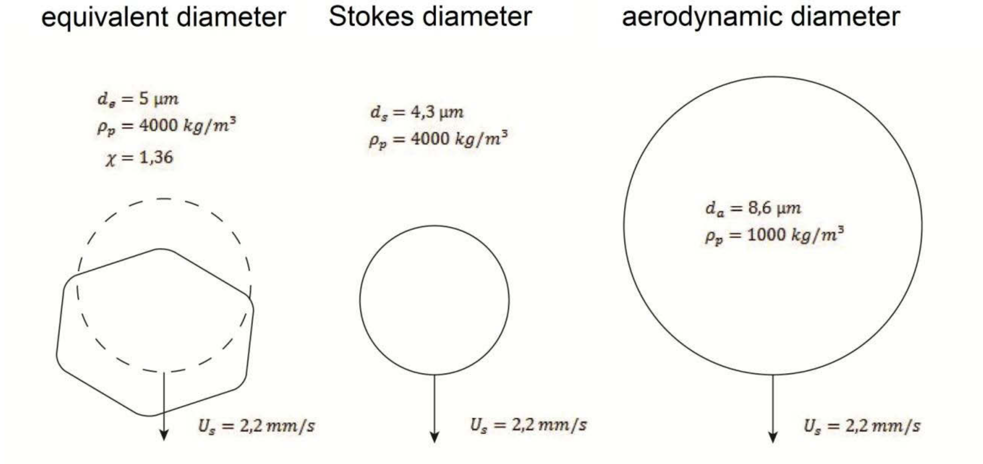

*Figure 2-8. Approaches for different particle shapes (based on [12, p. 54]).*

Thus, it is not always necessary to know the exact shape and/or density of the particle. The different approaches can be converted into each other according to eq. 7.

$$\boldsymbol{d_a} = \boldsymbol{d_e}\left(\frac{\boldsymbol{\rho_\beta}}{\boldsymbol{\rho_0\chi}}\right)^{\mathbf{0{,}5}} = \boldsymbol{d_s}\left(\frac{\boldsymbol{\rho_a}}{\boldsymbol{\rho_0\chi}}\right)^{\mathbf{0{,}5}} \qquad \textbf{\textit{eq. 7}}$$

The following Table (see [12, p. 52]) shows some dynamic shape factors, which were determined in experiments. The results for irregular particles where averaged over all directions within space. The experiments showed that non-spherical particles usually fall slower.

Table 2-5. Exemplary shape factors for different shapes and materials.

| shape | shape factor $\chi$ |
|---|---:|
| sphere | 1.00 |
| cube | 1.08 |
| 3 connected spheres | 1.15 |
| 4 connected spheres | 1.17 |
| lignite | 1.05-1.11 |
| quartz | 1.36 |
| sand | 1.57 |

### Sphericity

For a long time the problem of very different particle shapes has been tried to solve. One approach to describe different particle shapes is sphericity. Sphericity $\Psi_{Wa}$ according to Wadell means the ratio between the surface area of the equal-volume sphere and the real surface area. Therefore spheres have a sphericity of one and all other shapes smaller than one. The sphericity can be calculated with the diameter of the equal-volume sphere $d_v$ and the diameter of the equal-surface sphere $d_o$ (see eq. 8).

$$\boldsymbol{\psi_{Wa}} = \left(\frac{\boldsymbol{d_v}}{\boldsymbol{d_o}}\right)^{\mathbf{2}} \qquad \textbf{\textit{eq. 8}}$$

Figure 2-9 shows sphericities for different shapes determined experimentally by **Rittenhouse** [43].

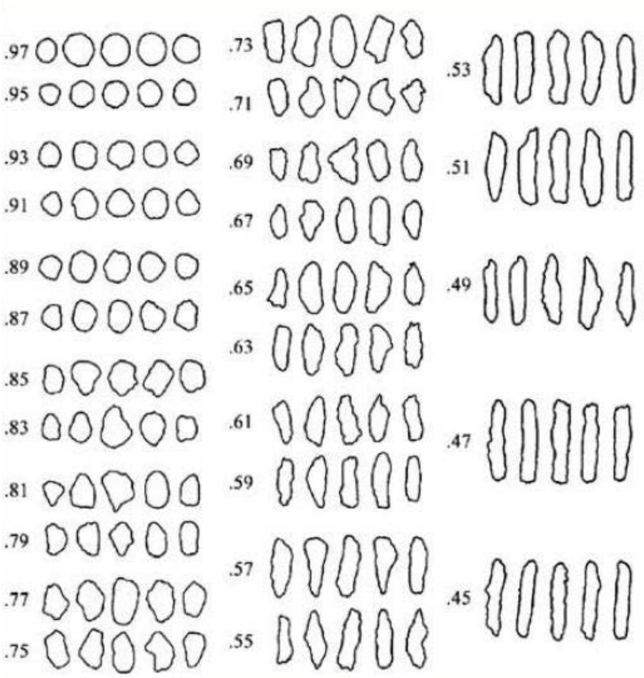

*Figure 2-9. Sphericities according to Rittenhouse [44, p. 415].*

Today new approaches are used to evaluate particle surface characteristics. A combination of optical and X-ray computed-tomography pictures can be used in combination with an automated computer controlled system to describe particles as shown by **Masad et al.** [44]. The method can be used to provide 3D representations of granular material.

### 2.2.4 Particle surface area

The specific surface area means the ratio between the total surface area including all open pores and sample mass [45, p. 2].

The specific surface area influences heat and mass transfer. Higher specific surface areas cause higher burning velocities, which mean more severe explosions [42].

The specific surface area can be determined with the so-called BET theory. The theory was developed by S. Brunauer, P. H. Emmet und E. Teller (BET) in 1938: The theory allows to determine the specific surface area in m²/g. BET is the standard method to determine the specific surface area of solid materials and is also used for development and certification of reference materials (BET „standard materials“) [46].

In order to determine the specific surface gas adsorption is used. Nitrogen, argon or krypton are utilized to do a static, volumetric isothermal measurement. Adsorption takes place with relative pressures between 0.001 bar and 0.3 bar.

### 2.2.5 Terminal velocity of single particles

Particles in motionless air reach their terminal velocity almost immediately. The terminal velocity for single particles can be calculated according to eq. 9. The equation is valid for particle diameters greater than one µm and particle Reynolds numbers smaller than one.

$$\boldsymbol{U_S = \frac{\rho_\beta d_\beta^2 g}{18\eta}} \qquad \textit{eq. 9}$$

Where are $\rho_\beta$ the particle density, the particle diameter $d_\beta$, $\eta$ the gas viscosity and $g$ the acceleration due to gravity.

### 2.2.6 Terminal velocity of dust/air mixtures

Dust/air mixtures in the process industries occur within a wide range of dust concentrations. Dust concentration can be more or less known during the process as in spray driers or vary very much during the process as when filling silos. Assumptions and approaches for single particles are not suitable for higher concentrations. In order to distinguish the two phenomena the term dust cloud is defined here. Dust cloud means a volume of high dust concentration surrounded by a much bigger region of pure air. The behavior of dust clouds is much more complex than of particles, so there is no complete model or analytical approach to describe it.

Figure 2-10 points out the difference between the terminal velocity of single particles and dust clouds. If a certain dust concentration is exceeded the air flow goes around the dust cloud and not through it. This leads to higher particle velocities than for single particles. Usually a mixed form of both phenomena occurs in reality.

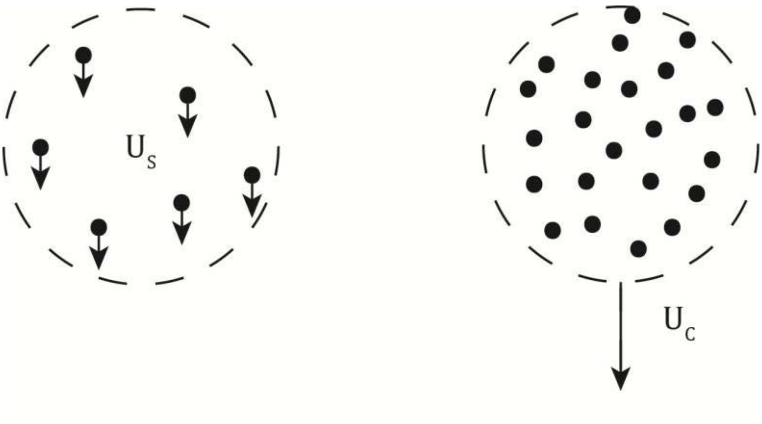

*Figure 2-10. (left) settling of particles (right) settling of dust cloud (based on [12, p. 380]).*

In order to calculate the terminal velocity of dust clouds it is assumed that dust and air have the same velocity inside the cloud. First a cloud density $\rho_c$ is defined (see eq. 10). Cloud density consists of the mass of a spherical dust cloud minus the mass of the displaced air divided by the total volume of the cloud $V_c$. The equation is based on the assumptions that the dust cloud is spherical with a diameter $d_c$, $N$ particles per volume unit, a specified particle diameter $d_\beta$ and a particle density $\rho_\beta$.

$$\boldsymbol{\rho_c = \frac{\rho_c V_c + C_m V_c - \rho_\alpha V_c}{V_c} = dust\ concentration} \qquad \textit{eq. 10}$$

Dust clouds are much bigger than the particles, which are in it. Thus dust clouds can have great Reynolds numbers, which leads to the assumptions that Stokes law cannot be used. For the calculation of the terminal velocity of dust clouds $U_c$ *(see* eq. 11*)* a balance of forces between gravity and Newton's drag force is used.

$$\boldsymbol{U_c = \left(\frac{4\rho_c d_c g}{3C_D \rho_\alpha}\right)^{0.5}} \qquad \textit{eq. 11}$$

This would be the equation for solid spheres, because of the internal circulation of dust clouds the drag force is reduced by approx. 10 %. Detailed information about aerosols and dust settling can be found in [12, p. 379ff] and [39, p. 284ff].

The settling behavior of dust clouds in confined spaces is different from that in free space, if the volume fraction of the dust $r_\beta$ is high and the dust cloud spreads over the whole cross-section. This leads to a higher flow resistance and therefore to smaller terminal velocities (eq. 12).

$$\boldsymbol{U_{Sch} = U_S(1 - r_\beta)^m} \qquad \textit{eq. 12}$$

The exponent $m$ depends on the Reynolds number (approx. 4.8 for laminar and approx. 2.4 for turbulent flows, see [47, p. 62]).

### 2.2.7 Dust concentration

A common parameter to describe dust/air mixtures is the dust concentration. Dust concentration means the present mass of a dust in a certain volume. Dust concentration of combustible dusts is usually given in grams per cubic meter [12, p. 11].

### 2.2.8 Agglomeration

In dust/air mixtures there is agglomeration due to particle/particle collisions. This causes an increasing particle size distribution over time. Thus, it has an influence on the behavior in the flow. Pressure, temperature, viscosity of air and turbulence influence the agglomeration process. Particle size distribution and particle shape have no significant influence.

### 2.2.9 Particle/wall interaction

Particle movement is influenced by collisions with walls. The most important side effects are listed below

- change of direction of particle movement,
- loss of momentum,
- change of particle rotation,
- particle erosion,
- and pressure loss of the flow.

Further information can be found in [48, pp. 22-24].

### 2.2.10 Porosity

The porosity $\varepsilon$ (eq. 13) means the ratio between the hollow space and the total volume *(volume porosity)*

$$\boldsymbol{\varepsilon = \frac{V_H}{V} = 1 - \frac{V_S}{V} = \frac{volume\ of\ hollow\ space}{total\ volume}} \qquad \textit{eq. 13}$$

Where are $V$ the total volume, $V_H$ volume of hollow space and $V_S$ volume of solid. The range of values for $\varepsilon$ is $0 < \varepsilon < 1$.

### Particle Porosity

Particle porosity $\varepsilon_P$ (Figure 2-11) means open (volume $V_{Ho}$) and closed pores (volume $V_{Hg}$) in particles. The particle porosity can be calculated according to eq. 14, where $V_{HP}$ is the volume of all pores and $V_P$ the total volume of the particle.

$$\boldsymbol{\varepsilon_P = \frac{V_{HP}}{V_P} = \frac{V_{Ho} + V_{Hg}}{V_P}} \qquad \textbf{\textit{eq. 14}}$$

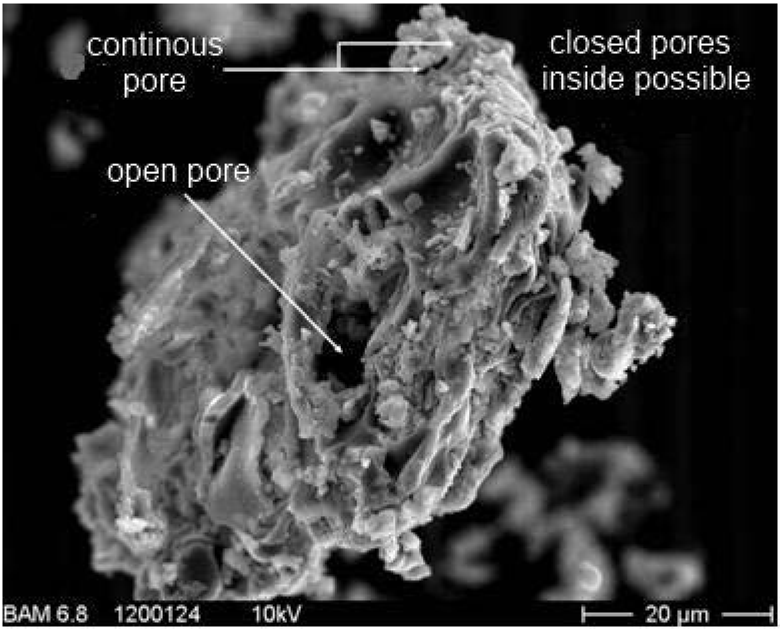

*Figure 2-11. Particle porosity.*

### Agglomeration porosity

Agglomeration porosity $\varepsilon_A$ (Figure 2-12, eq.15) means the ratio between the volume of the particles in an agglomerate $V_{HA}$ to the total volume of an agglomerate $V_A$.

$$\boldsymbol{\varepsilon_A = \frac{V_{HA}}{V_A} = \frac{V_{HA}}{(V_P + V_{HA})}} \qquad \textit{eq. 15}$$

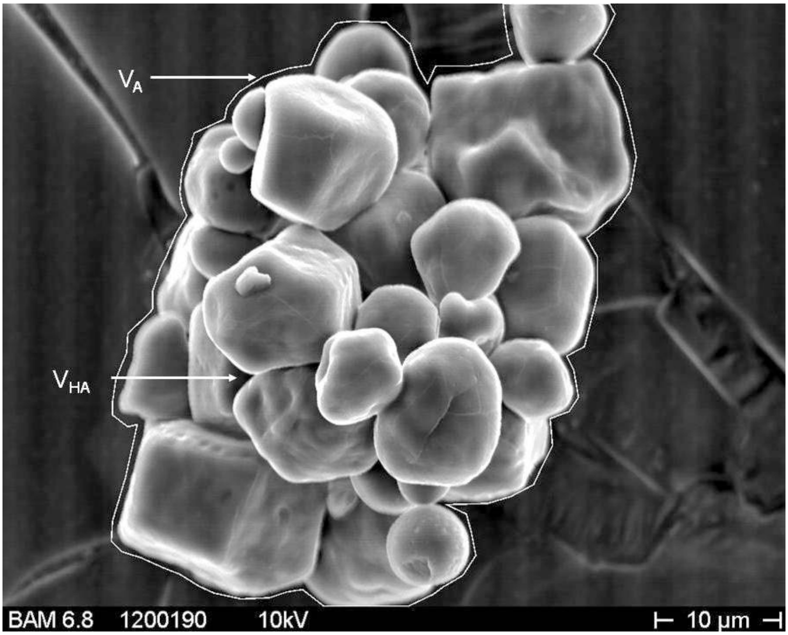

*Figure 2-12. Agglomeration porosity.*

## 2.2.11 Dispersibility

Dust of a certain mass, which is in balance with surroundings, has a finite number of particle bonds. In order to disperse the dust the bonds have to be broken up with a certain amount of work. The minimal work $W_{min}$, which is neccessary to break up all bonds, can be calculated by integration of the needed work for all single bonds. So a maximum dispersibility for all dusts $D_{max}$ can be defined (eq. 16):

$$\boldsymbol{D_{max} = \frac{1}{W_{min}}} \qquad \textit{eq. 16}$$

The defined dispersibility has the dimension mass per energy/work unit. Therefore the dispersibility represents the total dispersion of a certain amount of dust per external supplied energy. In order to take losses in real processes into account an efficiency factor $k$ is used.

$$\boldsymbol{D_{real}} = \frac{\boldsymbol{k}}{\boldsymbol{W_{min}}}, \qquad \mathbf{0} < k < 1 \qquad \textbf{\textit{eq. 17}}$$

$W_{min}$ depends on several influences such as particle size distribution, bulk density, compression and humidity. Compression and humidity increase the minimal needed work. Additionally the dispersibility is influenced by the kind of dispersion and geometric form of the dust. The forces of attraction (Van-Der-Waals force and electrostatic forces) are more effective for small particles. Further information can be found in [49, p. 4].

## 2.3 State of the art

Some severe dust explosions led to constant dust explosion research over the last decades. Findings, which are important for this work, are listed here, including investigations about the influence of dust concentration, initial turbulence and Reynolds number on dust explosions. With increasing computer performance numerical methods (e.g. computational fluid dynamics (CFD)) gained importance in research. CFD is used to simulate dust explosion (based on experimental data). Research on dustiness is very limited so far and regards mostly health aspects.

In 2001 **Krause** [17] summarized experimental and numerical findings in the field of dust explosion research. For example the initial turbulence has a significant influence on the pressure rise, because a higher turbulence leads to an increasing mass, momentum and heat transfer. This can cause faster reactions and higher explosion pressures. Therefore it is very difficult to predict pressure rises in real accidents because of a different turbulent flow at ignition time compared to laboratory results.

The dust concentration has an influence on dust explosions as well. For every dust or dust sample there is an optimal dust concentration where maximum pressures are achieved. In most cases this is a higher than stoichiometric dust concentration due to the fact that the particles are not completely burned.

Flame speeds depend on dust concentration, laminar and turbulent combustion velocity and turbulent flow. There is a combination of optimal dust concentration and Reynolds number for dusts for which a maximum flame speed is achieved.

Up to now there are two common methods to simulate dust explosions. Dust explosions can be seen as gas explosions for example propane or methane explosions or it is divided into a two-phase flow for determination of local dust concentrations and gas phase combustion.

The influence of a stationary initial turbulence at ignition time on dust explosions was examined by **Scheid** [50]. Often there is a stationary turbulent flow as in spray dryers, which is not taken into account when sizing safety measures. In experiments in a 75 L apparatus it was shown that even moderate turbulence intensities (approx. 0.45 m/s) cause higher reduced explosion pressures and rates of pressure rises. For very low and very high static activation pressures for the venting device as well as large venting areas the effect was reduced. This effect was also shown by **Tamanini** [5] and initial turbulence is now used as a parameter to size the venting area in the American standard NFPA 68 [8].

A literature review by the National Fire Protection Association (NFPA) suggests that calculated venting areas are calculated too high with the equations in the NFPA 68 as well as with the equations in EN 14491. In average the calculated venting areas were 1/5 higher than the experimentally determined. Published and confidential experimental data of different vessels, dusts and static activation pressures were used for the investigation. An under prediction of the necessary venting area was only found for very low static activation pressures (below 50 mbar) and very low $K_{St}$ values (below 50 bar*m/s). A need for more experimental data on local dust concentration distribution in vessels as well as turbulence measurements was reported in the study.

The influence of turbulent flow and dust concentration on dust explosions was investigated numerically by **Judel** [51]. CFD was used to simulate turbulent flows and local dust concentrations. In addition dust explosions were simulated. Experimental data was used as input parameters and for validation. It was shown that critical regions with combinations of optimal Reynolds number and dust concentration can be found numerically. This allows pointing out dangerous zones in silos and vessels.

**Tsuji** and **Morikawa** [52] did research in a vertical tube with a laser Doppler anemometer in order to determine the interaction between dust concentration, particle size and turbulent flow. Experiments showed that higher dust concentrations (approx. 6 kg solid per kg air) cause a decrease in air velocity. Furthermore in the experiments small particles decreased turbulence (in terms of RMS value) and bigger particles increased turbulence

**Eickelpasch** [33] investigated the possibilities to characterize dusts with dustiness and the physical reasons for their different behavior. It was shown that dustiness does not only depend on physical properties such as density, humidity, particle size distribution and so on but on the transport method respectively the air flow. In order to characterize dustiness two ratios were used. The first ratio is between the emitted dust mass during a process and the total dust mass, which is conveyed in the process. The second ratio is between the time, which is needed for the sedimentation of all emitted dust, and the total dust mass.

First research with dustiness according to VDI 2263 - part 9 was done by **Hesener und Reinecke** [53]. The dust explosion risk in mixers with moving parts was investigated with respect to the safety characteristic dustiness. The results should be used to develop explosion protection concepts based on dustiness. Numerical simulations were done in order to simulate local dust concentrations. The used Euler/Euler approach produced higher than measured concentrations. The implementation of particle size distribution and density was not sufficient to simulate dustiness.

In order to maintain a certain quality of CFD simulations it is necessary to know the concept and limitations of numerical methods. A detailed description about verification, validation and capabilities of CFD has been done by **Oberkampf et al.** [54]. For numerical investigations a sufficiently fine grid and appropriate physical and mathematical models are needed.

# 3 Computational Fluid Dynamics for multiphase modeling

Only a few problems in fluid mechanics can be solved analytically. A common approach is to use experiments in small or real scale. Unfortunately experiments are often difficult to realize, because they cause much effort and costs or cannot be transferred to real scale. Even if experiments can be carried out the flow can be altered due to measurement equipment or the flow is hardly accessible for measurement equipment. Especially dust/air mixtures depend on many influences such as length/diameter ratio of the vessel, turbulence, wall effects and particle Reynolds number. Thus it is very difficult to transfer laboratory results to industrial scale. Laboratory experiments can be used for proof of general ideas and general direction of the research.

For all these reasons the use of CFD is increasing in many technical fields. It allows the research of many modifications from one basic scenario in real scale without the effort of experiments. The simulations for this work were carried out with ANSYS CFX R14. Further information on CFD, the following explanations and ANSYS CFX guides can be found in [55], [56], [57] and [58].

## 3.1 Computational Fluid Dynamics

Computational fluid dynamics (CFD) allows to numerically calculating flow problems by solving the governing equations of continuity, momentum, and energy and species transport simultaneously. For this purpose the flow region is divided into control volumes for which the governing equations are solved.

In order to solve a problem in fluid mechanics with CFD some steps are necessary:

- Selection of mathematical models (here modified differential equations for the laws of conservation)
- Selection of the discretization method (usually finite volume method)
- Selection of a grid (structured/unstructured)
- Selection of solver method (stationary/instationary)
- Use of suitable convergence criteria and maximum residuals

It has to be clear that numerically achieved solutions are always approximations. The differences between reality and the calculated results consist of simplifications and errors in all steps of the numerical process. These can be

- Differential equations may include simplifications and/or approximations
- Approximations in the discretization process

- Residual error due to the iterative method; accurate solution would be achieved after infinite iterations.

For many phenomena such as turbulence, combustion and multiphase flow there is no exact set of equations. Therefore models have to be used. These models lead to results, which are not an exact replication of reality, even if solved accurately. In order to evaluate the models, experimental data has to be used. Models are often necessary to reduce computing time.

Errors due to discretization can be reduced with more detailed approximations and smaller control volumes. This causes increased computing time.

## 3.2 Simulation of two-phase flows

Flows, which are relevant to process industries, often consist of two or more phases. This work deals with dust/air mixtures only, which belongs to the field of two-phase flows. The two mainly used approaches for multiphase flow modeling are explained in the following.

The most common approaches are the Euler/Lagrange and the Euler/Euler approach.

- Euler/Lagrange approach means solving the Navier-Stokes equations for the continuous phase (air) and the disperse phase (dust) is calculated with a balance of forces. A statistically sufficient number of particles are simulated in the flow, representing all particles. The disperse phase is not really present in the control volumes. A theoretical volume fraction is calculated with the path of the particles.
- The Euler/Euler approach treats every phase as continuous, which means the Navier-Stokes equations are solved for every phase. Both phases are present in the control volumina and interact.

Dust/air mixtures can be divided into three kinds of flows depending on the volume fraction of the dust $\alpha_p$. If the volume fraction of the dust is small the flow dominates the movement of the particles. For an increasing volume fraction the movement of the particles is influenced by the flow and vice versa. The third case for very dense flows adds particle/particle collisions to the second case (see Figure 3-1). $\tau_p$ is the particle relaxation time, which characterizes the time required for particles to adjust its velocity to new boundary conditions/forces. The time is usually very small for small particles but is proportional to the square of particle diameter. For example a one micrometer water droplet in air has a relaxation time of only 0.8 µs. $\tau_k$ is the Kolmogorovian time scale.

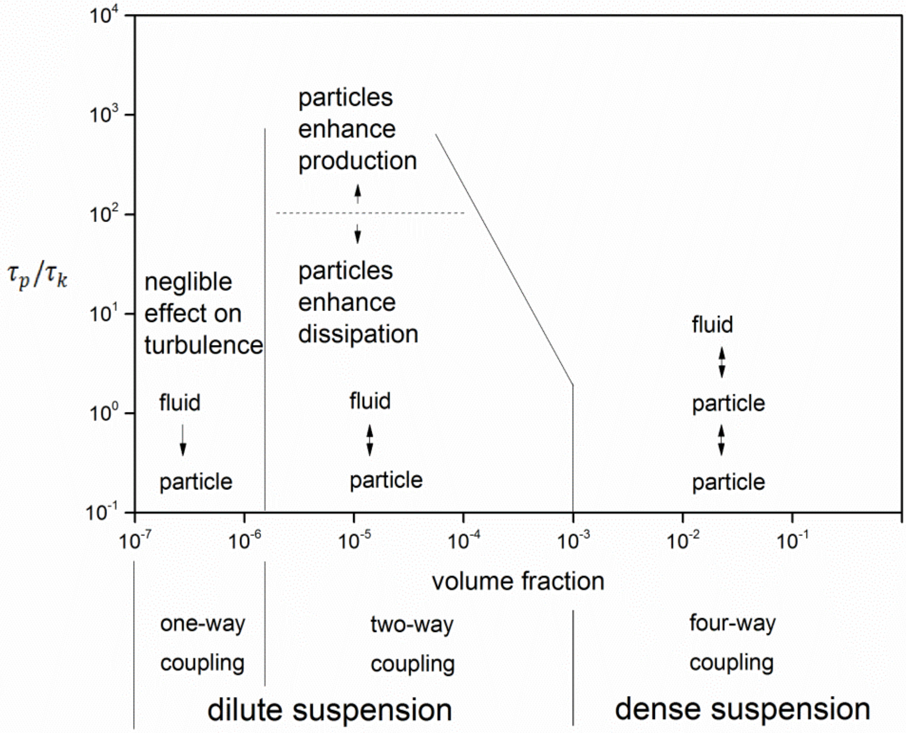

*Figure 3-1. Coupled flow according to Elghobashi [59].*

### 3.2.1 The Euler/Euler approach

With the Euler/Euler approach both phases are treated as continuum, which means the Navier-Stokes equations are solved for both phases. The approach is suitable for flows with volume fractions of both phases higher than $10^{-3}$. Explosive dust/air mixtures usually have volume fractions between $10^{-3}$ and $10^{-2}$, depending on the dust, this means concentrations up to some kilograms per cubic meter. In the field of dust explosion protection the Euler/Euler approach has two drawbacks. On one hand it is only possible to simulate particle size distributions by adding a new phase for each particle size desired which increases computing time. On the other hand there is only a combustion model for particles in the Euler/Lagrange approach in CFX. There are some minor drawbacks such as no collision model. Nonetheless for just one particle size and general results on particle velocities and dust concentration the Euler/Euler approach needs less computing time than the Euler/Lagrange method. A detailed description of the Euler/Euler method used in CFX can be found in the ANSYS Solver Theory Guide [60, p. 101ff].

### Basics of the Euler/Euler approach

The Euler/Euler multiphase approach uses modified momentum and continuity equations. These equations are similar to that for one phase. There are different approaches for different mixtures. There is a distinction between equal phases (e.g. two different gases) or - as used for this paper and described here - particle/gas mixtures. The different phases are marked with the Greek letters $\alpha\ (fluid)$ and $\beta\ (solid)$. The momentum equation can be written as follows (see eq. 18).

$$\begin{aligned}\frac{\partial}{\partial t}(\mathbf{r}_\alpha \boldsymbol{\rho}_\alpha \mathbf{U}_\alpha) + \nabla[\mathbf{r}_\alpha(\boldsymbol{\rho}_\alpha \mathbf{U}_\alpha \otimes \mathbf{U}_\alpha)] \\ = -\mathbf{r}_\alpha \nabla \mathbf{p}_\alpha + \nabla[\mathbf{r}_\alpha \boldsymbol{\mu}_\alpha(\nabla \mathbf{U}_\alpha + (\nabla \mathbf{U}_\alpha)^{\mathbf{T}})] \\ + \sum_{\beta=1}^{\mathbf{N_p}} \left(\boldsymbol{\Gamma}^+_{\alpha\beta}\mathbf{U}_\beta - \boldsymbol{\Gamma}^+_{\beta\alpha}\mathbf{U}_\alpha\right) + \mathbf{S}_{\mathbf{m}\alpha} + \mathbf{M}_\alpha\end{aligned} \qquad \textit{eq. 18}$$

The equation consists of momentum sources due to external forces $S_{M\alpha}$ and the interfacial forces acting on phase *α* due to the presence of other phases $M\alpha$. For example drag force, buoyancy force, virtual mass force, turbulent dispersion force and other influence the total force $M_\alpha$. The term $\left(\Gamma^+_{\alpha\beta}U_\beta - \Gamma^+_{\beta\alpha}U_\alpha\right)$ means momentum transfer due to interphase mass transfer.

The continuity equation (see eq. 19) is equal to that of one phase if the other phases are set to zero. For more than one phase the volume fractions add up to unity.

$$\sum_\alpha \frac{1}{\rho_\alpha}\left[\frac{\partial}{\partial t}(r_\alpha \rho_\alpha) + \nabla(r_\alpha \rho_\alpha U_\alpha)\right] = \sum_\alpha \frac{1}{\rho_\alpha}\left(S_{MS\alpha} + \sum_{\beta=1}^{N_p} \Gamma_{\alpha\beta}\right) \qquad \textit{eq. 19}$$

With the volume fraction of the fluid $r_\alpha$, the density of the fluid $\rho_\alpha$, the velocity $U_\alpha$ and $\Gamma_{\alpha\beta}$ the mass flow rate per unit volume from phase *β* to phase *α*. This term only occurs if interphase mass transfer takes place.

The total pressure of a multiphase flow can be calculated according to eq. 20:

$$p_{tot} = p_{static} + \sum_\alpha \frac{1}{2} r_\alpha \rho_\alpha U_\alpha^2 \qquad \textit{eq. 20}$$

Where $r_\alpha$ is the volume fraction of $\alpha$, $\rho_\alpha$ is the density and $U_\alpha$ is the velocity.

ANSYS CFX uses the effective density $\overline{\rho_\alpha}$ for calculation purposes. For dust/air mixtures the effective density of the solid phase is equal to the dust concentration in $kg/m^3$ (see eq. 21):

$$\overline{\boldsymbol{\rho_\alpha}} = \boldsymbol{r_\alpha \rho_\alpha} \qquad \textbf{\textit{eq. 21}}$$

Interfacial transfer of momentum, heat and mass are directly dependent on the contact surface area between the two phases. This is characterized by the interfacial area per unit volume between the fluid phase *α* and the disperse phase *β*. The surface area is calculated under the assumption that the particle is spherical with a specified diameter.

$$\boldsymbol{A_{\alpha\beta}} = \frac{\boldsymbol{6r_\beta}}{\boldsymbol{d_\beta}} \qquad \textbf{\textit{eq. 22}}$$

### 3.2.2 The Euler/Lagrange approach

The Euler/Lagrange approach is a type of multiphase model, where a statistical sufficient amount of particles is tracked through the flow in a Lagrangian way. The particle track is determined by the forces that act on the particle. The tracking is carried out by forming a set of ordinary differential equations in time for each particle, consisting of equations for position, velocity, temperature, and masses of species. According to Newton the sum of all forces acting on the particle is equal to the change of momentum (as shown in eq. 23 and eq. 24).

$$\frac{\boldsymbol{dx_\beta}}{\boldsymbol{dt}} = \boldsymbol{U_\beta} \qquad \textbf{\textit{eq. 23}}$$

$$\boldsymbol{m_\beta} \frac{\boldsymbol{dU_\beta}}{\boldsymbol{dt}} = \sum_{\boldsymbol{i}} \boldsymbol{F_i} \qquad \textbf{eq. 24}$$

The approach is only valid for dilute flows because the particles do not take up space in the control volume. For reliable results the volume fraction of the disperse phase should not be higher than 0.1. The Euler/Lagrange approach in CFX allows modeling of binary collisions between particles, wall/particle interaction, particle size distributions and particle shape factors. The model makes the so-called four-way coupling possible, which means interaction between fluid, particles and walls.

**Sommerfeld** [61] and **Frank** [62] as well as the ANSYS CFX Solver Theory Guide [60] contain information on the Euler/Lagrange approach.

### 3.2.3 Turbulence

Turbulent flows cover a great bandwidth in time and space. This makes it very difficult to solve problems numerically in detail. Usually turbulence models are used. Increasing computing power might lead to wider use of DNS or LES (Large Eddy Simulation, which is a combination of direct calculation of large eddies and modeling of small ones). Use of LES is increasing already, e.g. when simulating swirl burners [63].

Most of the technical flow problems are turbulent. Therefore it is necessary to calculate or model the turbulence. For this work turbulence was modeled with a so-called (U)RANS turbulence model namely the SST model by **Menter** [64]. This model combines the advantages of k-ω-model near walls with the advantages of k-ϵ-model in the outer area of the boundary layer.

In order to characterize turbulent flows the RMS value $U_{RMS} = \sqrt{\left(\sum_{i=1}^{N} \eta_i (u_i - U)^2\right)}$ is used instead of the non-measurable turbulent fluctuation velocities.

### 3.2.4 Particle forces and effects

Since there are more advantages in the Euler/Lagrange approach to simulate dust/air mixtures such as particle size distributions, particle collisions and a particle shape factor, the Euler/Lagrange approach was chosen after some preliminary simulations (see chapter 7.1). The following explanations are mainly stated for the Euler/Lagrange approach, they differ in some points from the Euler/Euler approach due to the different mathematics. **Sommerfeld** [65] describes all important particle effects and forces in detail, which are explained here in short.

**Buoyancy force**

Buoyancy force due to gravity is equal to the weight of the displaced fluid. For a spherical particle the buoyant force is given by eq. 25 [60, p. 154].

$$\boldsymbol{F_B = \frac{\pi}{6} d_\beta^3 (\rho_\beta - \rho_\alpha) g} \qquad \textit{eq. 25}$$

where $g$ is the gravity vector, $\rho_\alpha$.is the density of the fluid, $\rho_\beta$ the density of the solid and $d_\beta$ is the particle diameter.

**Drag force**

The drag force on a particle is proportional to the slip velocity $U_S$ which means the velocity between particle and fluid. The drag force decelerates the particles. In ANSYS CFX [60, p. 153] it is taken into account with the following formulation (see eq. 26).

$$\boldsymbol{F_D = \frac{1}{2} C_D \rho_\alpha A_{\alpha\beta} |U_S| U_S} \qquad \textit{eq. 26}$$

The equation contains drag coefficient $C_D$, density of fluid $\rho_\alpha$ and $A_{\alpha\beta}$ the effective particle cross section area. The effective particle cross section area can be modified with the shape factor $\chi$ to take the particle shape into account. The drag coefficient $C_D$ depends on the particle Reynolds number and cannot be calculated directly (see eq. 27). For all simulations done a modified Schiller Naumann drag model [66] was used.

$$C_D = r_\alpha^{-1.65} max\left[\frac{24}{Re'}\left(1 + 0.15Re'^{0.687}\right), 0.44\right]$$

***eq. 27***

With $Re' = r_\alpha Re_p$ consisting of the volume fraction of the fluid and the particle [67] Reynolds number.

### Pressure gradient force

The pressure gradient force is applied on the particle due to the pressure gradient in the fluid surrounding the particle caused by fluid acceleration (see eq. 28).

$$F_P = -\frac{m_\alpha}{\rho_\alpha}\nabla p$$

***eq. 28***

### Virtual mass force

The virtual mass force is caused because of the particle motion that accelerates some of the surrounding fluid, leading to an additional drag. That leads to a deceleration of the particles [60, p. 156]. It can be calculated with the formulation used in eq. 29.

$$F_{VM} = m_\alpha \frac{C_{VM}}{2}\left(\frac{dU_\beta}{dt} - \frac{dU_\alpha}{dt}\right)$$

***eq. 29***

### Turbulent dispersion force

The turbulent dispersion force means the influence of turbulence of the main flow on the particle path. Particles are affected by the fluid velocity fluctuating component which leads to a higher mixing rate. The model of turbulent dispersion of particles that is used in the Euler/Lagrange approach is according to **Gosman and Ioannides** [67]. The Euler/Euler approach uses the Favre averaged drag model [68]. The turbulent dispersion force creates a statistical fluctuation of particle velocities and paths but increases computational time.

$$F_{TD} = C_{TD}C_{cd} = \frac{\mu_{t\alpha}}{\sigma_{t\alpha}}\left(\frac{\nabla r_\beta}{r_\beta} - \frac{\nabla r_\alpha}{r_\alpha}\right)$$

***eq. 30***

Where $\sigma_{t\alpha}$ is the turbulent Schmidt number of the fluid and $C_{cd}$ is the coefficient of momentum transfer of multiphase flows.

### Relevance of the forces in dust/air mixtures

**Sommerfeld** [65] and **Hjelmfeld and Mockros** [69] stated that virtual mass force and pressure gradient force cannot be neglected for bigger particles and very turbulent flows.

### Binary particle collisions

Particles can transfer momentum via collisions. This leads to a change of kinetic energy. In dilute flows, as in this work, the particle movement is dominated by the surrounding flow. Nonetheless collisions alter the flow in terms of change of kinetic energy and change of particle size distribution due to agglomeration. With an approach according to **Sommerfeld** [61] the statistical influence of binary particle collisions on the flow can be modeled for a Euler/Lagrange approach. The collision model is based on a stochastic approach, which uses virtual collision elements depending on properties of the solid phase and on the flow. The approach skips the search for real collisions and is therefore faster than modeling “real” collision. Development and validation have been investigated by **Hußmann** [70]**.**

The Euler/Euler approach allows taking collisions into account with additional shear stresses.

### Particle/wall interaction

ANSYS CFX [55] allows momentum transfer between particles and walls. The properties of the collision can be influenced with coefficients of loss and restitution. Rotation of the particle and wall roughness is not taken into account. If collisions are not wanted, it is possible to “collect” particles at the wall. Further information can be found in [70, pp. 14-20].

### Modification of specific surface area – shape factor

The particle shape has a great influence on the sinking rate since it changes the drag force. The shape factor in CFX can be used as one parameter to simulate dustiness. The effect of the shape factor on the particle shape is shown in Figure 3-2. A value of one means a spherical shape (standard value); a higher value means a greater surface in the direction of the flow, so that the particle decelerates. There is no such thing as particle direction in the simulation; a higher value of the shape Χ means a larger surface area in the direction of the flow.

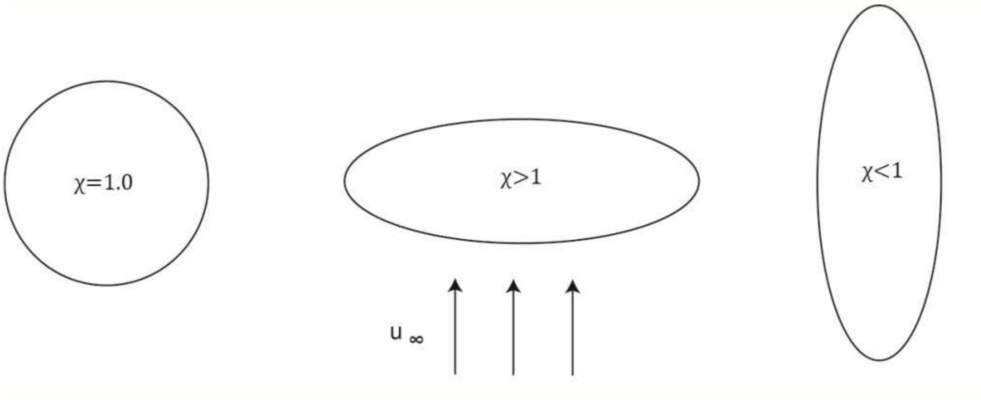

*Figure 3-2. Influence of shape factor.*

### Particle size distribution

The Euler/Lagrange approach allows to define one specific diameter or particle size distributions. Particle size distribution can be chosen manually or chosen to be equally or normally distributed.

In order to realize different particle sizes with the Euler/Euler approach every particle size has to be modeled as additional phase. This increases computing time significantly.

### 3.2.5 Comparison of Euler/Euler and Euler/Lagrange approach in CFX

The Euler/Euler method should be used if high volume fractions of the disperse phase are expected (higher than $10^{-3}$). For up to three phases this method safes computing time compared to the Euler/Lagrange technique. For a wide range of particle sizes each size has to be treated as a single phase which leads to high computing times. If detailed information about the disperse phase is needed, e.g. particle size distributions, different particle shapes and binary collisions between particles the Euler/Lagrange approach is more suitable in CFX. Table 3-1 gives an overview over the effects implemented in the different approaches.

*Table 3-1. Comparison of Euler/Euler and Euler/Lagrange approach.*

| effect | Euler/Lagrange | Euler/Euler |
|---|---|---|
| buoyancy | yes | yes |
| drag force | yes | yes |
| turbulent dispersion force | yes | yes |
| Magnus effect | - | - |
| pressure gradient force | yes | yes |
| virtual mass force | yes | yes |
| wall lubrication force | - | yes |
| 1-way-coppling | yes | - |
| 2-way-coppling | yes | yes |
| particle/particle interaction | yes | limited |
| particle/wall interaction | yes | - |
| shape factor | yes | - |
| particle size distribution | yes | limited |
| multiphase combustion | yes | - |

For further information see [60].

# 4 Dust properties, equipment and preliminary experiments

Experiments were done in order to evaluate an influence of dustiness on vented dust explosions (maximum reduced pressure, rate of pressure rise and flame speed). Additionally the influence of dustiness on the dust concentration over time in a vessel depending on the filling method was investigated. In the beginning small-scale experiments were done because of better controlled conditions, possibility to easily use different setups and dusts as well as small sample quantities. The findings were used to plan and carry out industrial-scale experiments. For the experiments different dusts were chosen and their properties and SCs determined. A total of seven dusts were chosen and examined, not all dusts were used for all tests. Small-scale experiments were done with six dusts and industrial-scale experiments with three dusts. Experiments with dust/air mixtures were done regarding their dispersion behavior, their explosion behavior and terminal velocity. The dusts and their properties as well as first tests regarding the terminal velocity of dust clouds are described in the following.

## 4.1 Choice of dusts

A preselection of suitable dusts was done with VDI Guideline 2263 – part 9 [2] and the BIA-Report „Brenn- und Explosionskenngrößen von Stäuben“ [71]. Six different dusts of different dustiness with comparable maximum explosion pressures $p_{max}$ as well as maximum rate of explosion pressure rise (or $K_{St}$ values) were chosen in order to evaluate the influence of dustiness.

Only dusts, which are not hazardous to health or environment, were chosen. Preselected dusts are shown in Table 4-1. Properties of the actual samples were measured at the BAM and FSA and are stated in the following chapters.

Table 4-1. Choice of dusts.

| dust | dustiness group | $p_{max}$ in bar | $K_{St}$ in bar*m/s |
|---|---|---|---|
| wheat flour | 1 | 6.9 - 8.4 | 55 - 100 |
| wood | 2 | 6.1 – 10.5 | 95 - 192 |
| skimmed milk powder | 3 | 7.4 – 9.4 | 70 - 108 |
| maize starch | 4 | 8.7 – 10.5 | 95 - 200 |
| lignite | 6 | 7.4 – 10.0 | 100 - 150 |
| potato starch | 6 | 7.0 – 9.4 | 36 - 53 |

## 4.2 Properties and safety characteristic of the dusts

Since properties and SCs depend very much on the specific sample, the SCs $p_{max}$ and $K_{St}$ were, after purchasing, determined at the BAM (see chapter 2.1.1). Additionally humidity according to Karl-Fischer method and particle size distribution with MIE scattering principle were determined. Dustiness according to VDI 2263 part 9 was determined by the FSA (Research Establishment for Applied System Safety and Health) in Mannheim, Germany. All dusts were dried until constant in weight.

### 4.2.1 Safety characteristics and particle size

The experimentally determined properties and safety characteristics $p_{max}$, $K_{St}$, dustiness, lower explosion limit, humidity and median diameter are listed in Table 4-2 and Table 4-3. Particle size ranges for all dusts are stated in Table 4-4. Dustiness of wood was not tested as well as one of the wheat flours, reference values were taken instead.

Table 4-2. SCs (part 1).

| dust | dustiness group | $p_{max}$ in bar | $K_{St}$ in bar*m/s | LEL in g/m³ |
|---|---|---|---|---|
| wheat flour | 1[1] | 7.8 | 95 | 60[1] [72] |
| wheat flour* | 1 | 7.3 | 96 | 60[1] [72] |
| wood | 2[1] | 7.6 | 84 | 100[1] [73] |
| skimmed milk powder | 4 | 7.6 | 117 | 60 |
| maize starch | 4 | 8.7 | 167 | 125 |
| lignite | 5 | 8.4 | 196 | 30 |
| potato starch | 5 | 7.0 | 86 | 60[1] [74] |

(*other supplier) / [1] benchmark value from comparable dust

Table 4-3. SCs (part 2).

| dust | humidity in % | median in µm |
|---|---|---|
| wheat flour | 8.62 | 65.4 |
| wheat flour* | 10.91 | 54.2 |
| wood | 4.28 | 260.3 |
| skimmed milk powder | 3.70 | 45.4 |
| maize starch | 4.45 | 13.5 |
| lignite | 8.90 | 37.7 |
| potato starch | 9.52 | 45.7 |

(*other supplier)

One percent by weight Aerosil was added to the maize starch. Wood was sieved (smaller than 500 µm).

Table 4-4 shows the particle size distributions of all tested dusts. Especially wood is much coarser than all other dusts. Maize starch has very small primary particles, but a strong tendency to build agglomerates. The wheat flours have a very similar distribution.

*Table 4-4. Particle size distribution.*

| dust | <500 µm | <250 µm | <125 µm | <80 µm | <63 µm | <32 µm | <20 µm |
|---|---|---|---|---|---|---|---|
| | | | | vol under % | | | |
| wheat flour | 100.00 | 98.61 | 79.84 | 58.76 | 48.50 | 28.76 | 19.03 |
| wheat flour* | 100.00 | 99.47 | 85.34 | 66.19 | 55.82 | 33.76 | 22.21 |
| wood | 81.25 | 47.85 | 20.05 | 10.69 | 7.56 | 2.67 | 1.43 |
| skimmed milk powder | 100.00 | 100.00 | 96.24 | 81.27 | 68.66 | 32.40 | 18.75 |
| maize starch | 100.00 | 100.00 | 100.00 | 100.00 | 100.00 | 99.75 | 86.30 |
| lignite | 99.33 | 90.34 | 75.30 | 65.77 | 61.08 | 47.82 | 38.75 |
| potato starch | 100.00 | 100.00 | 99.99 | 92.14 | 79.43 | 27.03 | 7.53 |

(*other supplier)

### 4.2.2 Raw density, bulk density and porosity

The raw density was determined with the He-pycnometry. The raw density of the dust is used as an input parameter for numerical simulations and to analytically calculate the terminal velocity of single particles.

Bulk density and porosity were determined as well. The bulk density was determined at the BAM and each test was repeated five times. Tests were done according to an internal procedure similar to the test as described in EN ISO 60 / DIN 53468. The bulk density in Table 4-5 is the mean of all five values.

*Table 4-5. Bulk density, porosity and raw density*

| dust | bulk density in kg/m³ | porosity in % | raw density in kg/m³ |
|---|---|---|---|
| wheat flour | 570 | 61.4 | 1474 |
| wood | 184 | 87.2 | 1439 |
| skimmed milk powder | 646 | 48.9 | 1264 |
| maize starch | 602 | 59.9 | 1502 |
| lignite | 491 | 65.6 | 1494 |
| potato starch | 889 | 41.0 | 1505 |

### 4.2.3 Specific surface and analytical terminal velocity (single particle)

The specific surface area was measured with the BET method. BET method means a way to determine the specific surface with gas adsorption. All BET measurements were done with nitrogen and with relative pressures ($p/p_0$) between 0 and 0.3 (see ISO 9277:2010 [75]). A higher surface leads to a higher reactive surface. **Evans et al**. [76] showed that dustiness is not directly correlated to specific surface or primary particle size for nanoscale dusts. Particle size and surface significantly influence the $K_{St}$ value [11], see Table 4-2 and Table 4-3. Table 4-6 shows the experimentally determined specific surface area as well as the analytically calculated terminal velocity for single particles. Since only very few properties of the dust, such as particle diameter, are used in the equation, it should only be considered as tentative indicator on the settling behavior.

*Table 4-6. Specific surface area and terminal velocity.*

| dust | dustiness group | specific surface area (BET) in m²/g | terminal velocity (analytical) in m/s |
|---|---|---|---|
| wheat flour | 1 | 0.4275 | 0.190 |
| wood | 2[1] | 0.8738 | 0.294 |
| skimmed milk powder | 4 | 0.2072 | 0.078 |
| maize starch | 4 | 2.4857 | 0.008 |
| lignite | 5 | 4.9110 | 0.064 |
| potato starch | 5 | 0.2646 | 0.095 |

[1] benchmark value from comparable dust

The terminal velocity was calculated according to $U_S = \frac{\rho_\beta d^2 g}{18\eta}$, where $g = 9{,}81\ m/s$ and $\eta = 0{,}0000181\ kg/(m \cdot s)$.

In order to better understand the measured specific surface areas, for some materials the specific surface areas are compared to those of ideal spherical, non-porous particles. Wheat flour and potato starch have comparable particle median diameters and densities of approximately 50 µm and 1500 kg/m³. This would lead to a specific surface area of 0.080 m²/g for both, compared to measured values of 0.4275 m²/g for wheat flour and 0.2646 m²/g for potato starch. Even without considering shape and porosity smaller particles have higher specific surface areas due to geometrical reasons, for maize starch with a median diameter of 13.5 µm a specific surface area of 0.296 m²/g can be calculated for an ideal, spherical particle compared to a measured value of 2.4857 m²/g.

### 4.2.4 Calorific values

Calorific values were determined at BAM according to ISO 1928 [77]. Calorific values of all dusts are shown in Table 4-7.

*Table 4-7. Calorific values.*

| dust | dustiness group | calorific value in J/g |
|---|---|---|
| wheat flour | 1[1] | 17723 |
| wheat flour* | 1 | 16150 |
| wood | 2[1] | 18387 |
| skimmed milk powder | 4 | 16755 |
| maize starch | 4 | 16279 |
| lignite | 5 | 22115 |
| potato starch | 5 | 16046 |

*other supplier / [1] benchmark value from comparable dust

All tested dusts have calorific values in a narrow range between 16000 J/g and 18000 J/g except lignite.

### 4.2.5 Microscopic pictures

In order to look at the six dusts in detail incident light microscope and scanning electron microscope pictures were made. Figure 4-1 a shows that lignite is very fine and rarely agglomerated. The large surface area determines a high reactivity and dustiness. Potato starch (see Figure 4-1 b) has almost spherical particles with few agglomerates. This correlates with the high tendency to form dust clouds. Maize starch has small particles but large agglomerates, which explains the lower dustiness than that of lignite and the need for use of Aerosil (silicon dioxide, for less agglomeration [78]) (Figure 4-1 c). **Eckhoff** stated that, in general, smaller particles (especially below 10 µm) tend to agglomerate more than larger particles [13, p. 34]. The least tendency to form dust clouds have wheat flour and wood (Figure 4-1 d and f). Milk powder (e) shows all kinds of shapes and lots of single particles as well as large agglomerates.

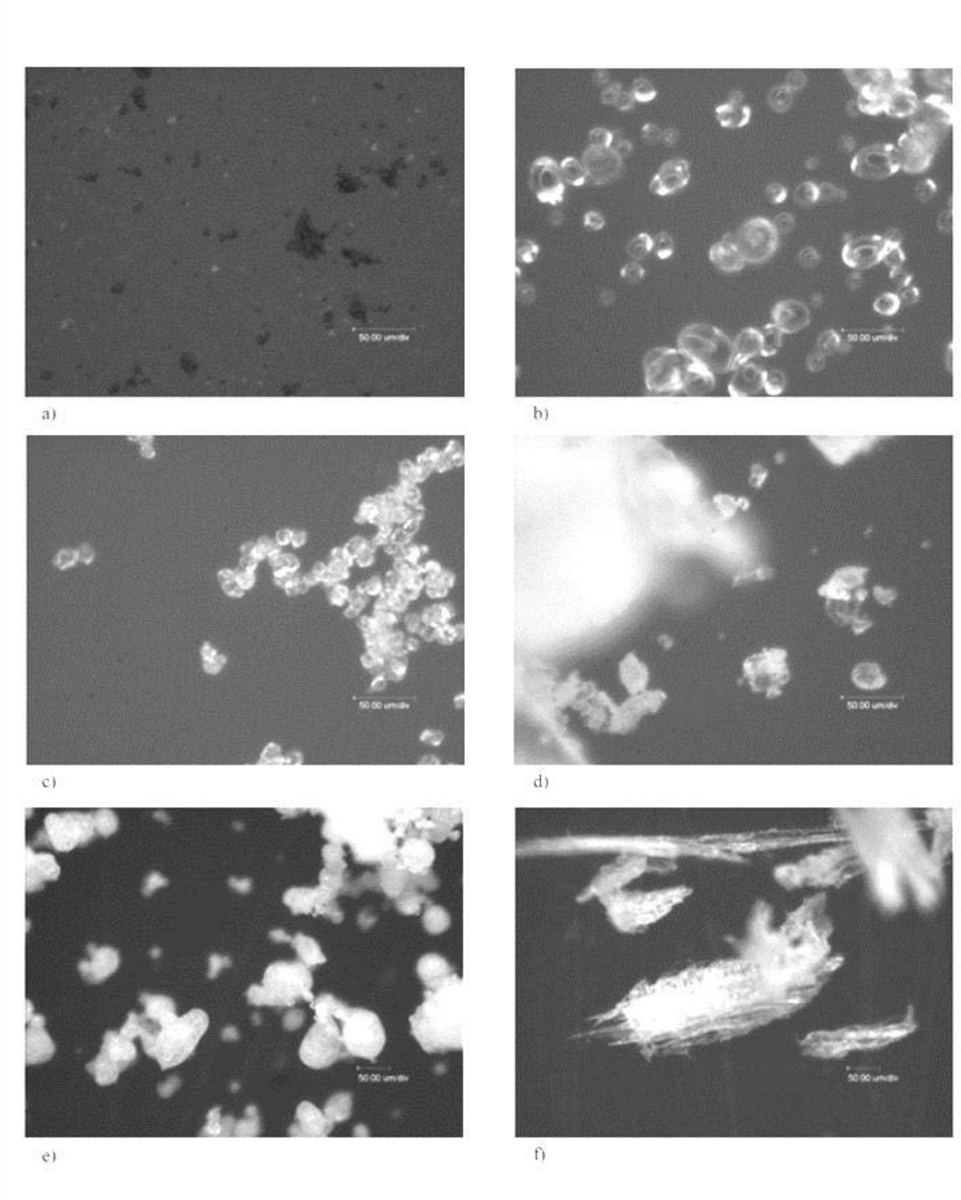

*Figure 4-1: a) lignite (800x) b) potato starch (800x) c) maize starch (800x) d) wheat flour (800x) e) skimmed milk powder (450x) f) wood(450x)*

Further information about shape and size was gained with SEM pictures - as can be seen exemplarily for three dusts (maize starch, lignite, wheat flour; from left to right) in Figure 4-2. The pictures underline that an exact size and shape for dusts is not easy to determine as summarized by **Baron and Willeke** [39, pp. 50-60].

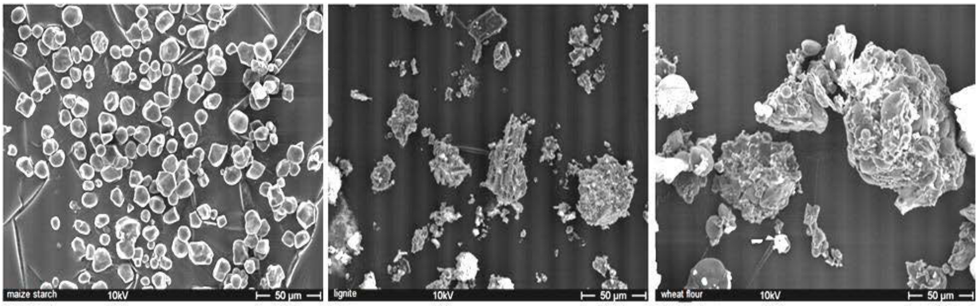

*Figure 4-2. SEM pictures of maize starch (left), lignite (middle) and wheat flour (right).*

### 4.2.6 Dust cloud settling velocity

Velocities of the settling dust clouds were measured for all six dusts. Velocity was determined with a laser Doppler anemometer. Dust was conveyed with 0.022 kg/s. Velocities were measured for five seconds and five times for each dust (see Figure 4-3). A commercial 1D Laser Doppler anemometer by Dantec Dynamics was used to determine the terminal velocity due to gravity. Further information and measurement principle were described in [79].

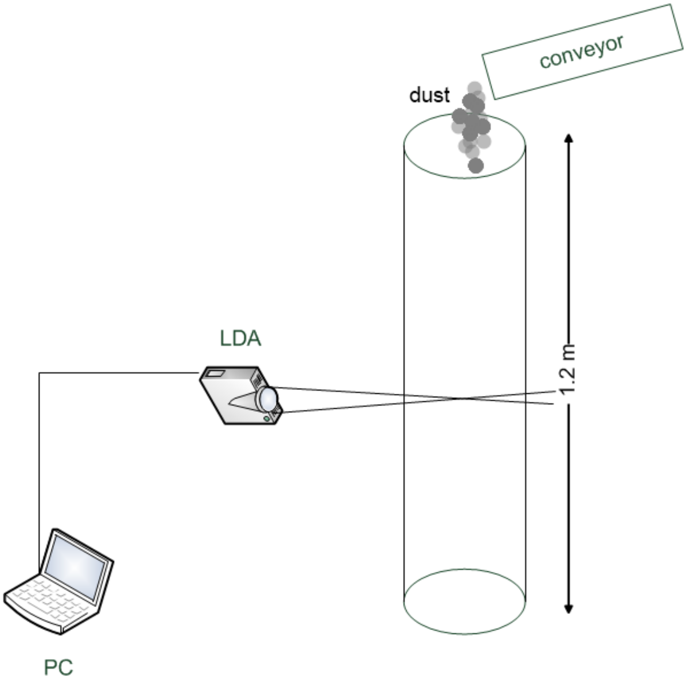

*Figure 4-3. Sketch of the velocity measurement.*

Tests were done with and without mixing Aerosil to the dusts under investigation to examine its assumed effect to reduce agglomeration. Results are listed in Table 4-8 and in Figure 4-4. The mean velocities were not significantly changed by adding Aerosil but the range of velocities for the five tests (or standard deviation) was much higher with Aerosil. If Aerosil reduces agglomerates and therefore more single particles with different sizes fall, a larger range of velocities would result.

*Table 4-8. Measured velocities for dust cloud settling.*

| dust | dustiness group | LDA in m/s | LDA (with Aerosil) in m/s |
|---|---|---|---|
| wheat flour | 1[1] | 0.625 | 0.853 |
| wood | 2[1] | 0.457 | 0.457 |
| skimmed milk powder | 4 | 0.741 | 0.649 |
| maize starch | 4 | 0.425 | 0.422 |
| lignite | 5 | 0.254 | 0.408 |
| potato starch | 5 | 0.541 | 0.689 |

[1] benchmark value from comparable dust

As can be seen in Figure 4-4 Aerosil (silicon dioxide) has an influence on velocity scatter, except for wood, which is not influenced by Aerosil. Skimmed milk powder and maize starch have smaller velocities with Aerosil, which can be explained by smaller agglomerates. Lignite and maize starch have the smallest measured velocities. The other four dusts have measured velocities according to their dustiness as well except for wood. This could be due to the fact that the LDA can only measure small particles and therefore the whole range of particle sizes could not be measured, see as well [80].

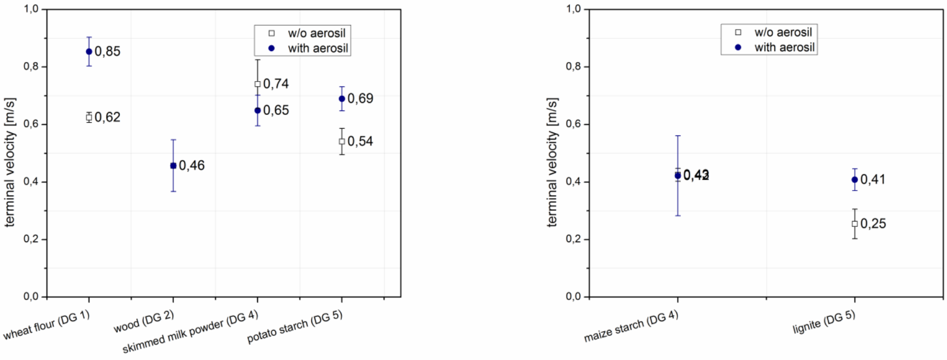

*Figure 4-4. Measured dust cloud velocities and standard deviations.*

## 4.3 Measurement equipment

### 4.3.1 Pressure sensors

In all small-scale experiments pressure was measured with two piezo-resistive sensors 4043A10 and 4043A20 (see Appendix, Table A-1) including measuring amplifier (4603A) by Kistler [81]. Calibration was done with comparative measurements with precision pressure regulator by Fa. GE Sensing GmbH (Typ DPI 515). After calibration the maximum deviation was smaller than 0.1 % FSO/a in the range of 0 to 10 bar.

In all industrial-scale experiments pressure was measured with four piezo-resistive sensors PAA-25 (see Appendix, Table A-2) including measuring amplifier by Kettler. Calibration was done with comparative measurements with precision pressure regulator by Fa. GE Sensing GmbH (Typ DPI 515). After calibration the maximum deviation was smaller than 0.1 % FSO/a in the range of 0 to 5 bar.

### 4.3.2 Laser Doppler Anemometer (LDA)

The velocity at one point in a flow can be determined with laser Doppler anemometry. The method is optical (interference fringe principle) and contact-free. Figure 4-5 shows a schematic interference fringe. The two intersecting laser beams of same frequency can be seen. The distance of the wave front is equal to the wavelength of the light. In the focus there are areas of strong and weak light intensity. A crossing particle reflects light proportional to the velocity of the flow.

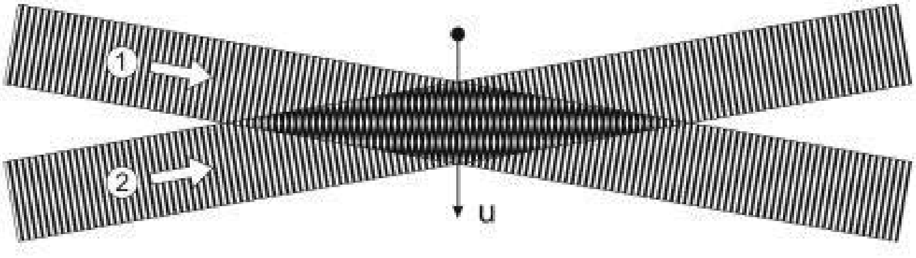

*Figure 4-5. Interference fringe at focus point [82, pp. 7-5].*

The velocity component is calculated with the Doppler frequency according to eq. 31:

$$\boldsymbol{u_z} = \frac{\boldsymbol{\lambda}}{\mathbf{2}\,\mathbf{sin}\left(\frac{\boldsymbol{\theta}}{\mathbf{2}}\right)} \boldsymbol{f_D} \qquad \textit{eq. 31}$$

Where $\lambda$ is the wavelength of the light, $\theta$ is the angle between the laser beams and $f_D$ is the Doppler frequency. The technical data of the LDA can be found in Table A-3 (see Appendix). Due to the reliable measurement principle three repetitive experiments were sufficient. Further information can be found in the manual [82].

### 4.3.3 Dust concentration meter

In order to evaluate the explosion risk of dust/air mixtures it is important to know the local dust concentrations over time. Additionally a suitable dust concentration meter has to have a wide measurement range because many dust show the “optimum” concentration in a relatively high concentration range. In order to measure the dust concentration, light extinction due to the presence of particles in the measuring volume is used (see Figure 4-6).

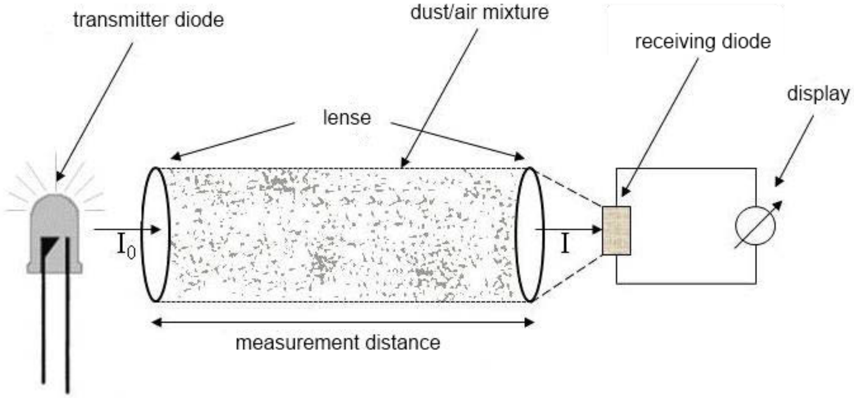

*Figure 4-6. Measurement principle dust concentration meter.*

The measurement unit consists of a transmitter diode (wavelength 950 nm), an emitting diode and two lenses. The transmitter emits light with an intensity $I_0$ and the receiver measures the (reduced) intensity $I$.

The ratio of measured and emitted light intensity $I/I_0$ is called transmission. Extinction $E$ means the negative logarithm of the transmission (derived by the Beer-Lambert law):

$$\boldsymbol{I = I_0 \cdot e^{-klc}} \qquad \textbf{eq. 32}$$

after transposing

$$\boldsymbol{E = -ln\left(\frac{I}{I_0}\right) = \kappa lc} \qquad \textbf{eq. 33}$$

Where $c$ is the dust concentration, $l$ is the measurement distance and $\kappa$ is the extinction coefficient. The extinction coefficient depends on the material and is determined by calibration. Dust concentration $c$ can be calculated according to eq. 34:

$$\boldsymbol{c = -\frac{ln\left(\frac{I}{I_0}\right)}{\kappa l}} \qquad \textbf{\textit{eq. 34}}$$

In order to calibrate all concentration meters for all used dusts, a container filled with methanol was used. The calibration was done by adding stepwise weighted portions of dust to the liquid and elutriating them by a magnetic stirrer. The extinction was proportional to the amount of dust added, see Figure 4-7.

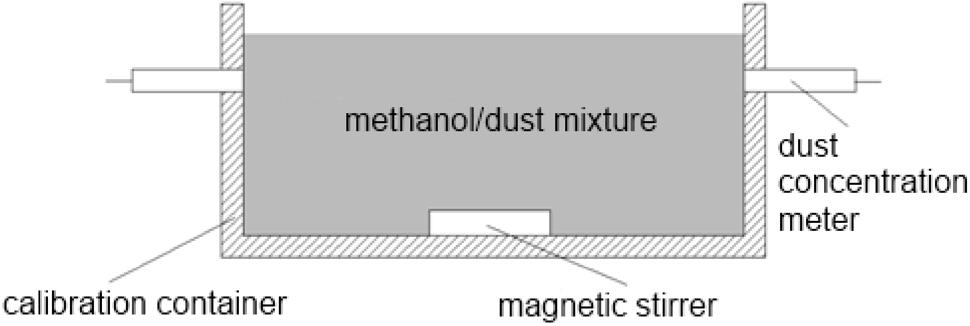

*Figure 4-7. Calibration of dust concentration meter (based on [50, p. 38]).*

Calibration data can be found in appendix A.

**Other Dust Concentration Measurement Principles**

There are some other measurement principles for dust concentration determination. There are scattered light measurement, triboelectric method, radiometric method and sampling methods. Details on these methods can be found in [83], [84] and [85]. Most of them are not suitable for high dust concentrations and/or for determination of dust concentration over time.

### 4.3.4 High-speed camera

The high-speed camera is a Redlake MotionProX4 from 2006 with a maximum frame rate of more than 5000 frames per second (512 x 512 pixels).

# 5 Small-scale experiments with 75 L apparatus

In a first step six dusts were used to carry out experiments in a 75 L vertical tube apparatus. The chosen dusts were wheat flour, wood, skimmed milk powder, maize starch, lignite and potato starch, which are commonly used in process industries and have different dustiness behavior, see chapter 4.2. Experiments included measurement of dust concentrations over time for two filling methods and vented dust explosions with measurement of pressure, pressure rise and flame speeds. Results were used to compare measured pressures to calculated pressures in order to determine an influence of dustiness on the course of dust explosions. Additionally dustiness behavior in the apparatus was investigated depending on the filling method.

## 5.1 Setup

A vertical dust dispersion glass tube apparatus with a 300 mm inner diameter and a volume of 75 L was used for all experiments. Dust was ignited in case of explosion experiments with a 10 J electrical ignition source, which is sufficient for all tested dusts and stronger than most ignition sources under working conditions. Dust was dispersed with two different dispersion methods. Dispersion with a filter plate from the bottom and filling at the top with pressurized air were realized. The filter plate allowed generating a homogenous airflow with reproducible conditions. Additionally dust is often dispersed after deposition due to lack of cleaning or process conditions. With a nozzle at the top of the apparatus a common filling method could be modeled. The second setup led to a more severe scenario as in terms of higher turbulence and total dispersion of all dust. Necessary venting areas were calculated as well as expected explosion pressures in the vessel. This was done to avoid damage to the vessel and to compare measured pressures to calculated ones. Calculated pressures were needed to point out the influence of dustiness on vented dust explosions.

### 5.1.1 Dispersion with filter plate from the bottom

Dust was initially layered on a filter plate with a porosity of less than 40 µm and dispersed by a controlled volume flux of air from the bottom (approx. 23 m³/h) for two seconds in all experiments. For the explosion experiments the dust was ignited by an electrical spark (10 J) after another two seconds. Static activation pressure of 160 mbar and 320 mbar were tested. Dust concentrations were measured at two different positions (37 cm and 70 cm above the filter plate) in the tube apparatus using an infrared light attenuation technique. Pressure was continuously measured during the tests with two piezo-resistive pressure transducers one at the bottom and one in the lid (see Figure 5-1 and Figure 5-2). Measurement equipment is described in chapter 4.3.

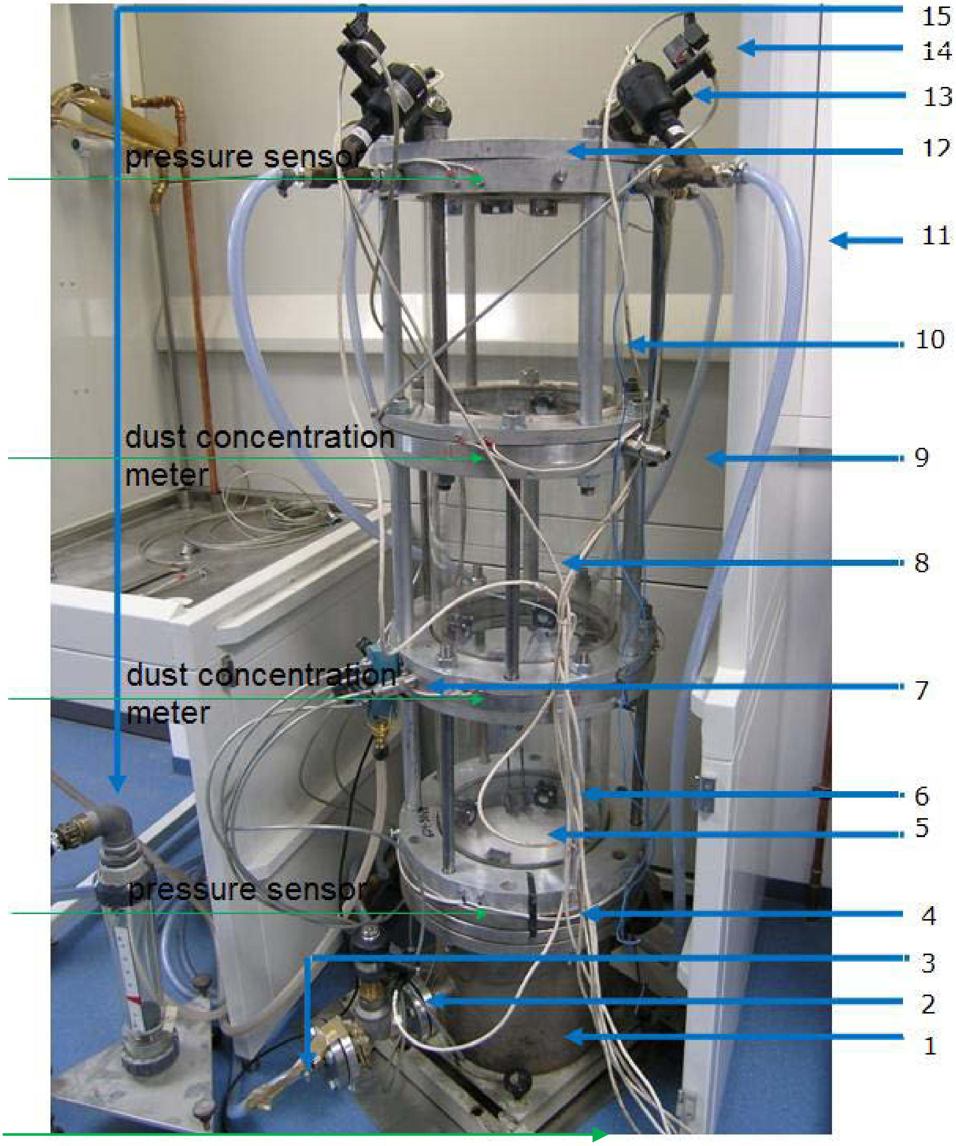

*Figure 5-1. 75 L Apparatus.*

Table 5-1 explains the parts as numbered in Figure 5-1. Locations of pressure sensors and dust concentration meters are marked in Figure 5-1. Three glass segments allowed observing explosions with a high-speed camera. Experiments were repeated at least three times and the apparatus was cleaned after every test.

Table 5-1. Parts of the 75 L Apparatus.

| number | part |
|---|---|
| 1 | bottom vessel |
| 2 | inlet valve |
| 3 | air supply |
| 4 | flange |
| 5 | filter plate |
| 6 | ventilators |
| 7 | air supply for valves |
| 8 | glass |
| 9 | dust concentration meter |
| 10 | supports |
| 11 | outlet hoses |
| 12 | lid |
| 13 | outlet valves |
| 14 | supply |
| 15 | rotameter |

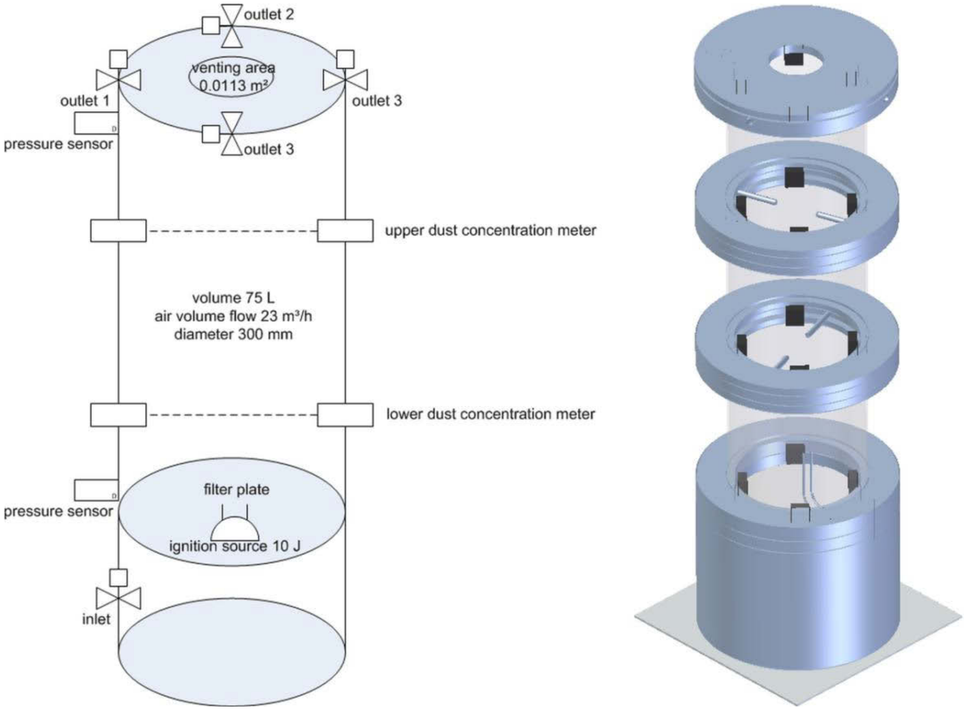

*Figure 5-2. Schematic pictures of the apparatus.*

### 5.1.2 Dispersion with nozzle in the lid

In order to compare dustiness behavior depending on the dispersion methods, the dispersion method of the 75 L apparatus (see chapter 5.1.1) was modified to filling at the top. The total venting area was divided into three parts. Static activation pressure was 160 mbar. The dust was dispersed with a nozzle at the top for 0.8 seconds and ignited after another 0.25 seconds in the explosion experiments (identical 10 J ignition source and location).

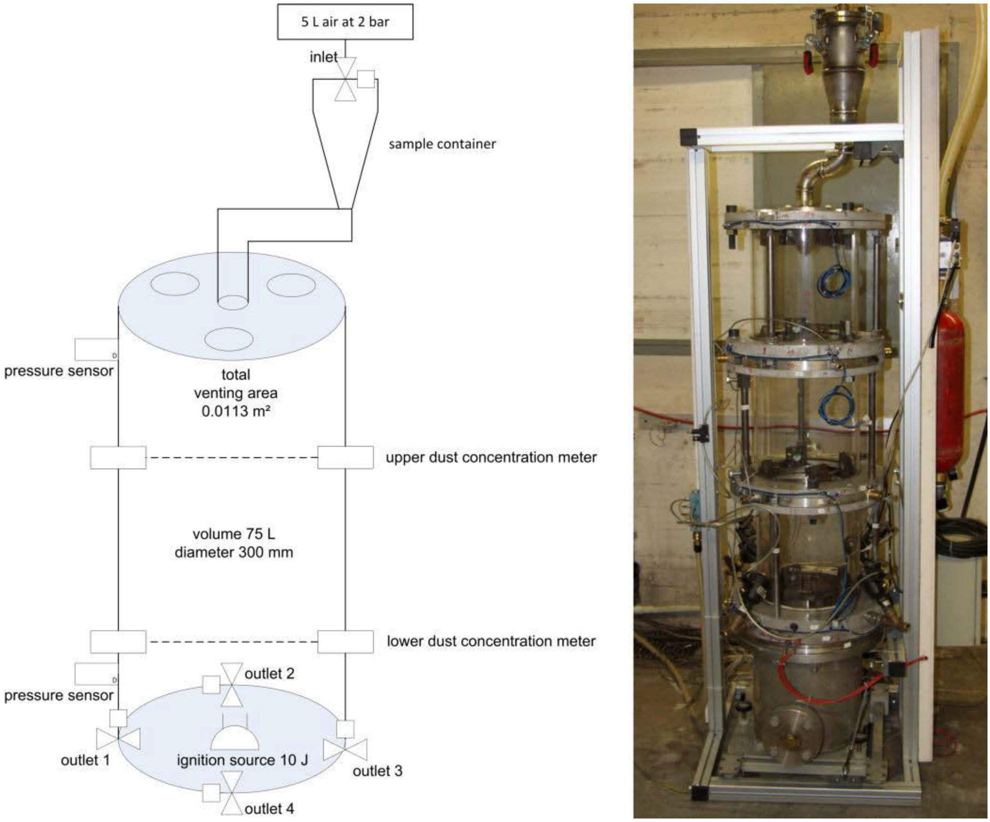

*Figure 5-3. 75 L apparatus with nozzle.*

### 5.1.3 Calculated venting areas

Before any explosion experiments were done, a venting area was calculated for the apparatus according to EN 14491 [86, pp. 6-13]. The apparatus does not have the minimal vessel volume of 0.1 m³, therefore the calculated venting area were used as indicator for the necessary size. Calculation of the necessary venting area depends on the SCs and properties of the vessel (see Figure 5-4). Maximum explosion pressure $p_{max}$ and $K_{St}$ value as well as length/diameter ratio of the vessel have to be known in order to calculate the venting area.

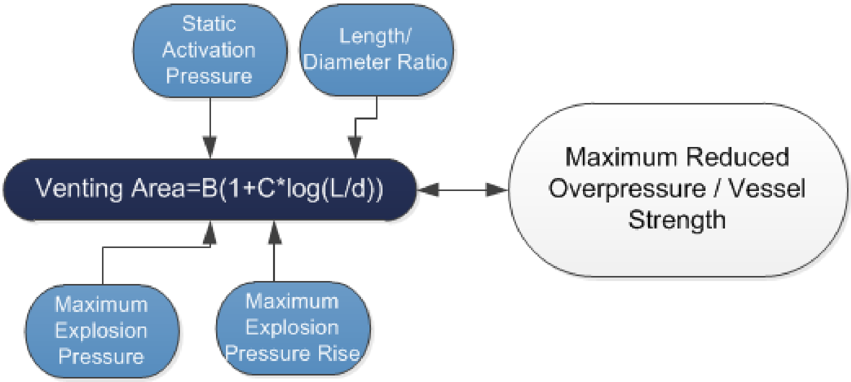

*Figure 5-4. Calculation of the venting area according to standard EN 14491.*

For a maximum reduced pressure of 1.5 bar (for safety reasons and to protect measurement equipment from damage 1.5 bar was used instead of 3 bar, which is the actual strength of the apparatus) the venting area can be calculated according to eq. 35:

$$\boldsymbol{venting\ area} = \boldsymbol{A} = \boldsymbol{B}(\mathbf{1} + \boldsymbol{C} * \boldsymbol{log}(\boldsymbol{l} / \boldsymbol{d})) \qquad \textbf{\textit{eq. 35}}$$

The venting area A can be calculated with the coefficients B and C (for definition see [86, p. 8]). The following venting areas were calculated for three different activation pressures of the venting device (55 mbar; 160 mbar and 320 mbar) as shown in Table 5-3.

*Table 5-2. Venting areas for different activation pressures.*

| dust | venting area in m² $p_{stat}$ 55 mbar | venting area in m² $p_{stat}$ 160 mbar | venting area in m² $p_{stat}$ 320 mbar | chosen venting area in m² |
|---|---|---|---|---|
| wheat flour | 0.00132 | 0.00461 | 0.00963 | 0.01131 |
| wood | 0.00094 | 0.00423 | 0.00925 | |
| skimmed milk powder | 0.00186 | 0.00515 | 0.01017 | |
| maize starch | 0.00394 | 0.00724 | 0.01225 | |
| lignite | 0.00465 | 0.00794 | 0.01296 | |
| potato starch | 0.00081 | 0.00410 | 0.00912 | |

A venting area of 0.01131 m² was chosen. The calculated area for lignite and maize starch was a little bit greater, but the apparatus strength is well over 1.5 bar in reality.

### 5.1.4 Calculated reduced explosion pressures

Additionally the reduced overpressures were estimated in advance of the experiments using the equation for the sizing of the venting area of single enclosures according to EN 14491 [4], equation 2 in the standard EN 14491 [4, p. 8], here equation 35 was transposed so that the maximum expected reduced overpressure could be calculated. Where $A$ is the necessary venting area, $B$ and $C$ are variables, which include the maximum reduced overpressure, maximum overpressure and $K_{St}$ value, $L$ is the maximum length of the vessel and $D$ the diameter. This was done due to the fact that the same venting area was used for all dusts, therefore varying explosion pressures are expected due to different explosion behavior (see $p_{max}$ and $K_{St}$ values, chapter 4.2). According to their dust explosion safety characteristics lignite and maize starch are expected to generate higher explosion pressures, see Table 5-3. The four other dusts are expected to produce comparable explosion pressures due to their comparable safety characteristics. The following table contains the calculated reduced pressures for the six used dusts.

*Table 5-3. Calculated reduced explosion pressures and venting area.*

| dust | $p_{red,max}$ (iterative) in bar $p_{stat}$ 160 mbar |
|---|---|
| wheat flour | 0.75 |
| wood | 0.70 |
| skimmed milk powder | 0.85 |
| maize starch | 1.10 |
| lignite | 1.20 |
| potato starch | 0.70 |

## 5.2 Experiments - dispersion with filter plate

A vertical dust dispersion glass tube apparatus with a volume of 75 L was used for all experiments. The dust was initially layered on a filter plate and dispersed by a controlled volume flux of air from the bottom. For the explosion experiments the dust was ignited by an electrical spark (see chapter 5.1.1).

### 5.2.1 Dustiness experiments

Dust concentration was measured as function of time and at ignition time in order to compare the influence of different dustiness.

Dispersion experiments were done for theoretical concentrations between 250 g/m³ and 2500 g/m³. Theoretical concentration means the concentration which would result from homogenous dispersion of all dust inside the vessel. Dust concentration as function of time is shown for 10 s after ignition time (theoretical). The results are shown exemplary for theoretical concentrations of 250 g/m³ and 1500 g/m³ (see Figure 5-5 and Figure 5-6). The influence of dustiness can be seen for all dusts, when dispersed with filter plate. Dusts with higher dustiness show similar and higher concentrations at the lower and upper sensors, which means, that they tend to produce more homogenous dust concentrations. Comparable results could be shown for the other concentrations.

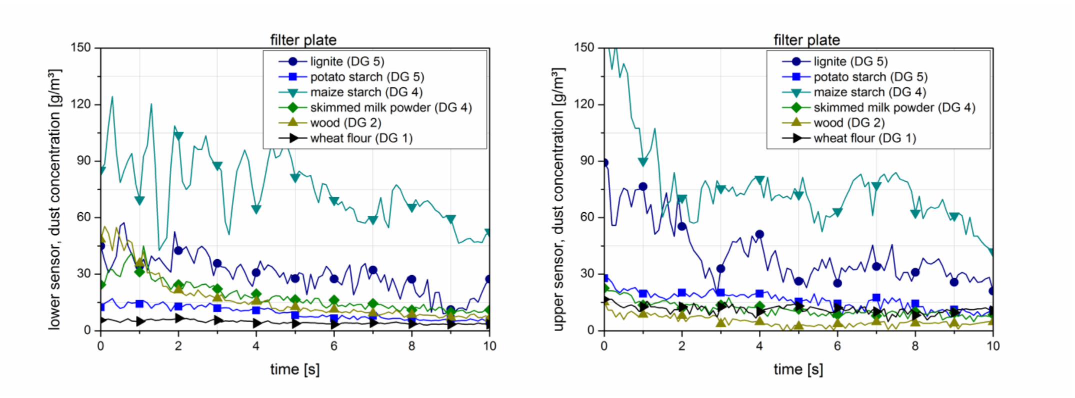

*Figure 5-5. Dust concentration as function of time (250 g/m³).*

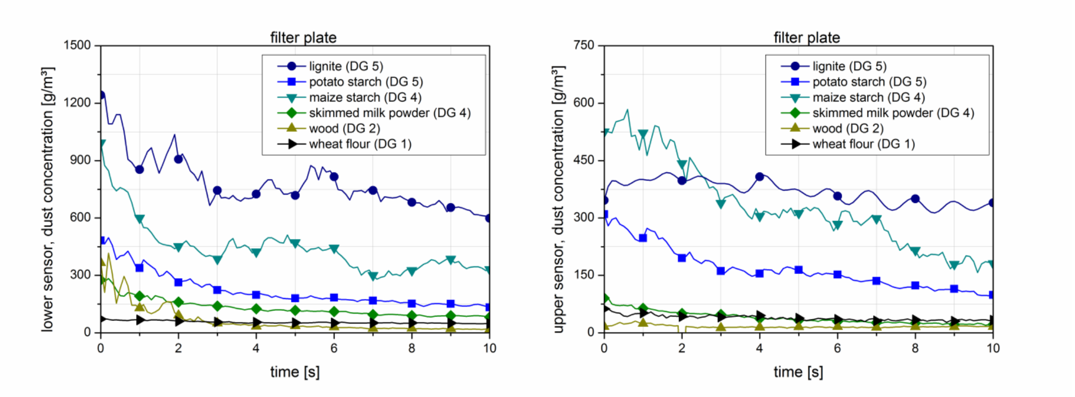

*Figure 5-6. Dust concentration as function of time (1500 g/m³).*

Figure 5-7 shows the measured concentration at ignition time (4 s after beginning of dispersion) as a function of the theoretical concentration, which means the concentration where all filled-in dust would have been dispersed homogenously. The influence of dustiness can be seen for all dusts at ignition time.

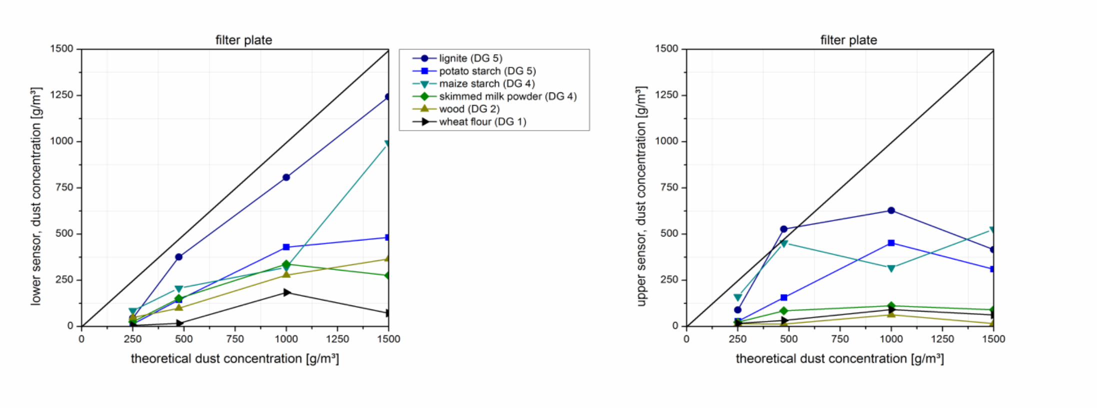

*Figure 5-7. Measured dust concentration at ignition time.*

**Remarks**

Some dust remains on the filter plate, especially wood and wheat flour. Some dust is conveyed out of the outlet valves. The dust concentration meters showed sensitivity to the filling process (approx. first 3 seconds) and had to be adjusted after every test due to drift. Improved dust concentration meters have been used for all following tests.

### 5.2.2 Vented dust explosions

Reduced explosion pressures, pressure rises and flame speeds were measured. The results are shown in the following chapters. All explosion experiments were vented. Tests were done over a wide range of dust concentrations and repeated three times.

### 5.2.3 Reduced explosion pressures $p_{stat}$ 160 mbar

The dust was dispersed for two seconds and ignited with an electrical spark after another two seconds. The venting area was chosen after calculating a venting area (see [4, p. 8]) for the most violent reacting dust (lignite), which was used and for reduced maximum overpressure of 1.5 bar (vessel strength). The venting device was a foil at the top with a venting area of 0.0113 $m^2$. The activation pressure was 160 mbar and was determined with a slow increase of compressed air. For the explosion experiments the theoretical dust concentration, which means the concentration where all filled-in dust would have been dispersed homogenously, was varied between 500 $g/m^3$ and 2500 $g/m^3$.

Figure 5-8 shows the average reduced explosion pressures as function of the theoretical dust concentration. Wheat flour could not be ignited.

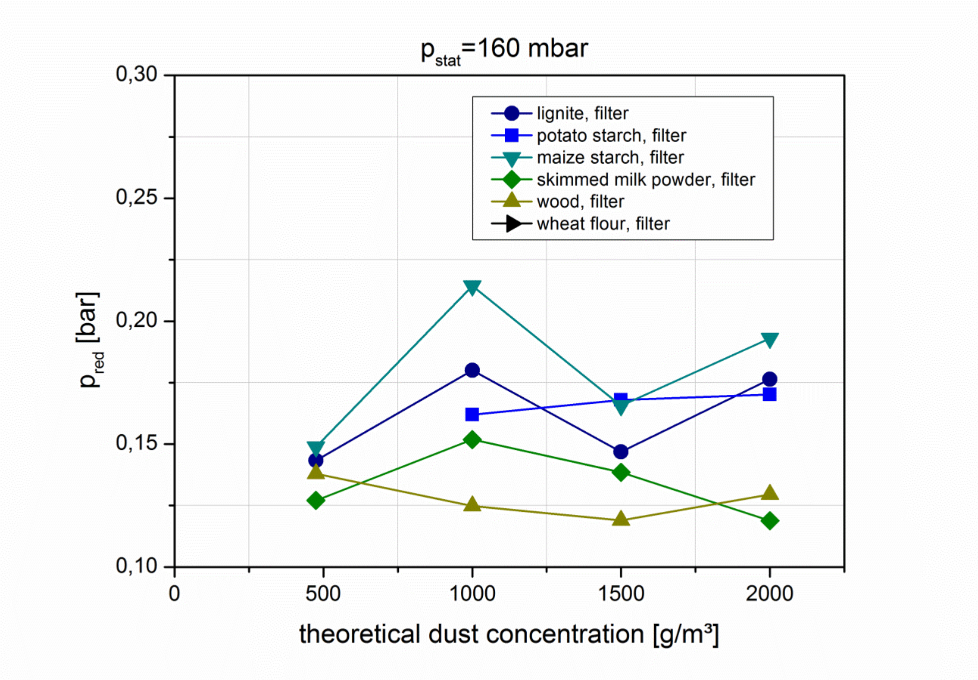

*Figure 5-8. Reduced explosion pressures as function of theoretical concentration.*

The measured and calculated reduced overpressures can be seen in Table 5-4.

*Table 5-4. Calculated and measured reduced explosion pressures for venting area of 0.01131 m².*

| dust | $p_{red,max}$ (iterative) in bar $p_{stat}$ 160 mbar | $p_{red,max}$ (filter) in bar $p_{stat}$ 160 mbar |
|---|---|---|
| wheat flour | 0.75 | - |
| wood | 0.70 | 0.159 |
| skimmed milk powder | 0.85 | 0.185 |
| maize starch | 1.10 | 0.234 |
| lignite | 1.20 | 0.255 |
| potato starch | 0.70 | 0.185 |

All measured reduced overpressures were well below the calculated overpressures. This could be due to the fact that the standard EN 14491 is for turbulent and homogenous worst-case scenarios and is valid only for vessel bigger than 0.1 m³. Potato starch showed higher overpressures compared to the skimmed milk powder and wood, but were expected to have the lowest due to the lower safety characteristics. This could be due to the good dustiness. The wheat flour could not be ignited due to the fact that most of it stayed on the filter plate because of the bad dispersion behavior. The lower explosion limit was probably not reached at ignition source. The difference between calculated and measured overpressures for the four dusts with comparable safety characteristics can be seen in Figure 5-9.

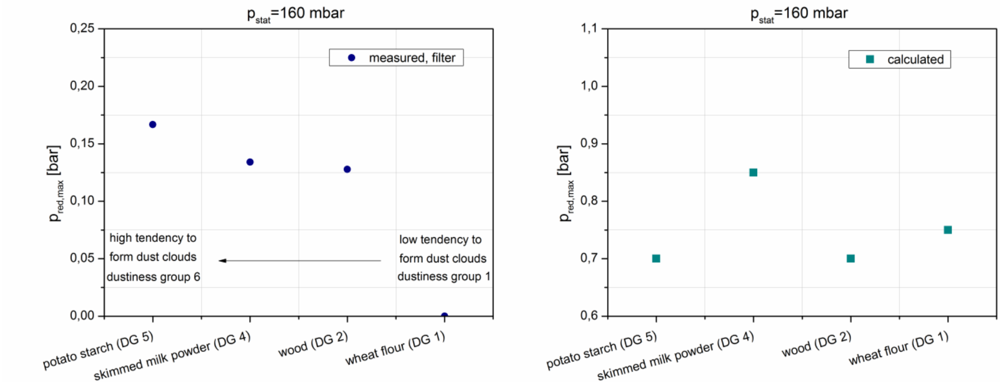

*Figure 5-9. 4 dusts measured and calculated reduced explosion pressures.*

The left diagram shows the actual measured maximum reduced overpressures in the 75 L apparatus. The left diagram shows the calculated pressures for comparison. Figure 5-10 shows comparison of calculated and measured explosion pressures for maize starch and lignite. They have similar dustiness behavior and similar explosion pressures. Higher pressures of dust explosions with lignite compared to maize starch explosions could not be achieved, opposite to the expected values.

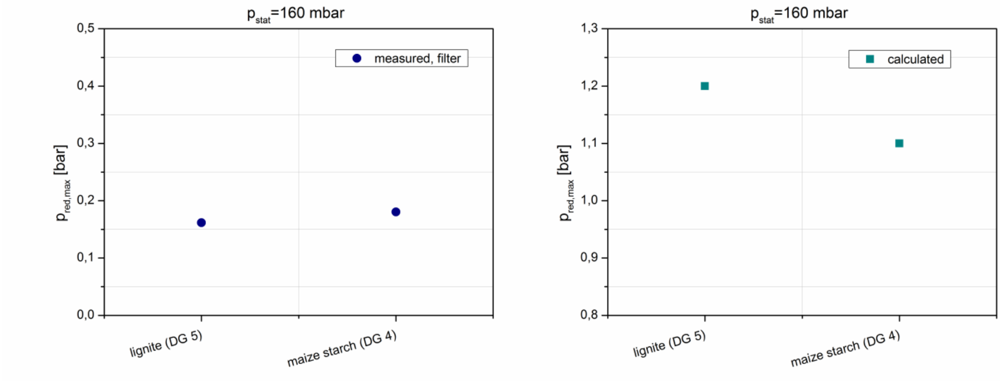

*Figure 5-10. 2 dusts measured and calculated reduced explosion pressures.*

### 5.2.4 Reduced explosion pressures $p_{stat}$ 320 mbar

Explosion experiments with higher static activation pressures showed that the effect due to dustiness can be observed for the higher activation pressures in the 75 L apparatus as well. This effect can be seen in Figure 5-11 and Figure 5-12 for the four dusts with comparable safety characteristics $p_{max}$ and $K_{St}$ value. The diagrams show the measured pressures compared to measured pressures for static activation pressures of 160 mbar and to calculated pressures.

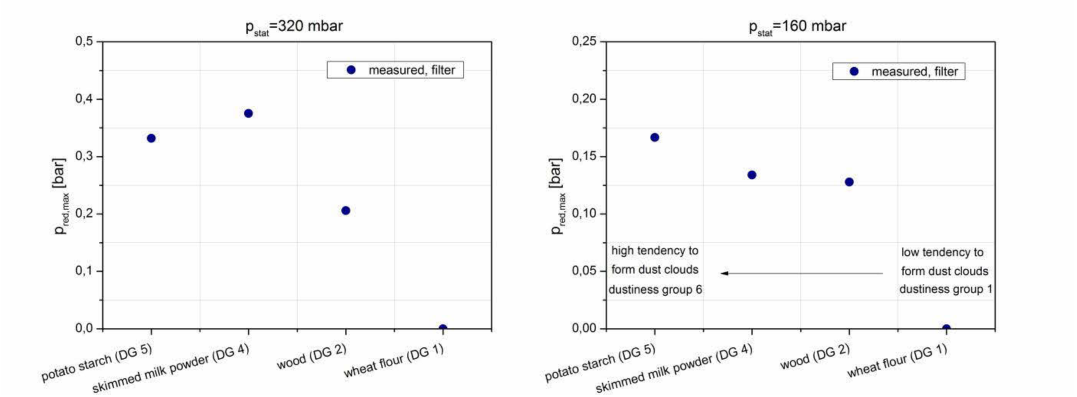

*Figure 5-11. 4 dusts reduced explosion pressures for $p_{stat}$ 320 mbar and 160 mbar.*

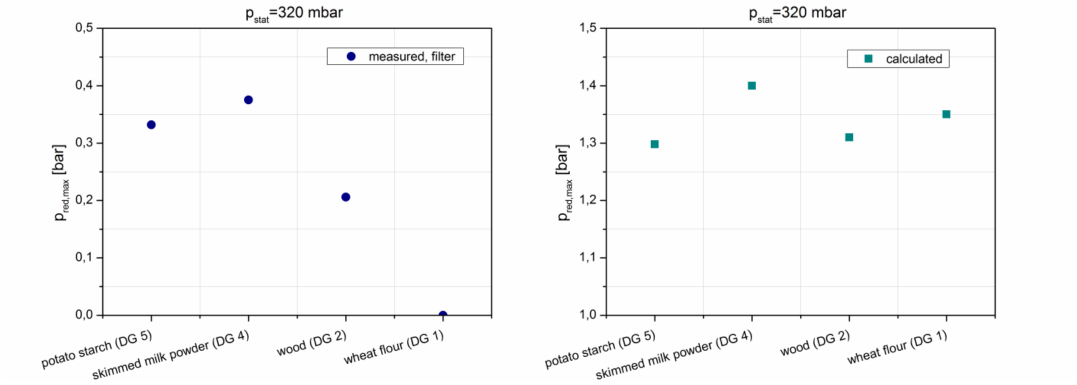

*Figure 5-12. 4 dusts measured and calculated reduced explosion pressures for $p_{stat}$ 320 mbar.*

Figure 5-13 shows that lignite and maize starch have comparable dustiness and pressures as well for a static activation pressure of 320 mbar. A comparison of calculated pressures showed comparable results to those with static activation pressure of 160 mbar and are not displayed here, for comparison see Figure 5-10.

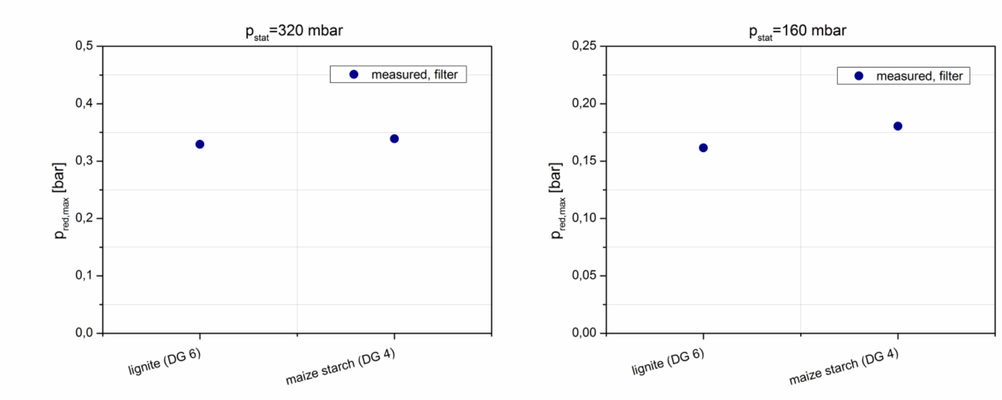

*Figure 5-13. 2 dusts reduced explosion pressures for $p_{stat}$ 160 mbar and 320 mbar.*

### 5.2.5 Maximum pressure rise $p_{stat}$ 160 mbar

All pressure rises were evaluated with the software Origin 8.6G. The evaluation was done graphically with a linear polynomial fit (such as y = Intercept + pressure rise * time) with a maximum deviation of two percent.

The effect of dustiness can be seen for the pressure rise as well. Figure 5-14 shows the pressure rise compared to the $K_{St}$ value for four dusts with comparable $p_{max}$ and $K_{St}$. The measured pressure rises increased with increasing dustiness. Especially potato starch generated higher pressure rises compared to the safety characteristics determined in the 20-L sphere.

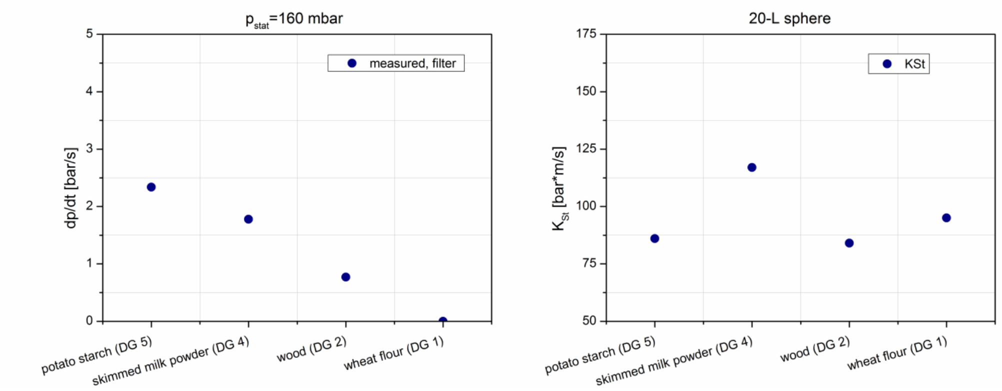

*Figure 5-14. 4 dusts pressure rise compared to $K_{St}$ value.*

Figure 5-15 shows the pressure rise compared to the $K_{St}$ value of the two dusts with higher $p_{max}$ and $K_{St}$. Despite similar dustiness and higher $K_{St}$ values of lignite, maize starch explosions generated higher average pressure rises.

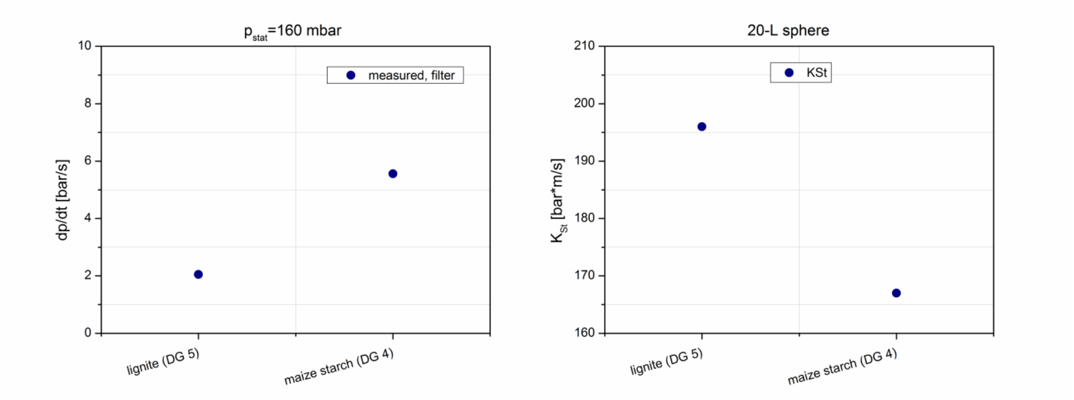

*Figure 5-15. 2 dusts pressure rise compared to $K_{St}$ value.*

### 5.2.6 Maximum pressure rise $p_{stat}$ 320 mbar

Increasing the activation pressure from 160 mbar to 320 mbar leads to higher pressure rises. No other changes can be determined, see chapter 5.2.5. Results are shown in Figure 5-16 and Figure 5-17.

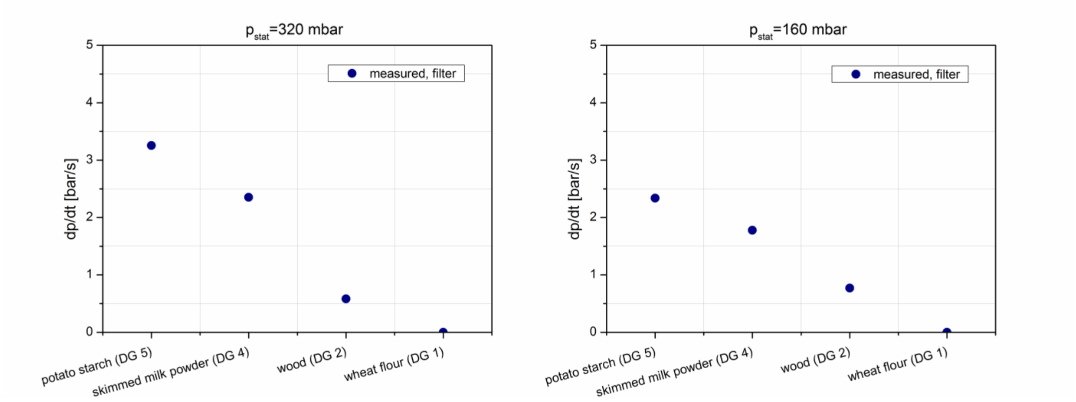

*Figure 5-16. 4 dusts pressure rises for static activation pressures of 160 and 320 mbar.*

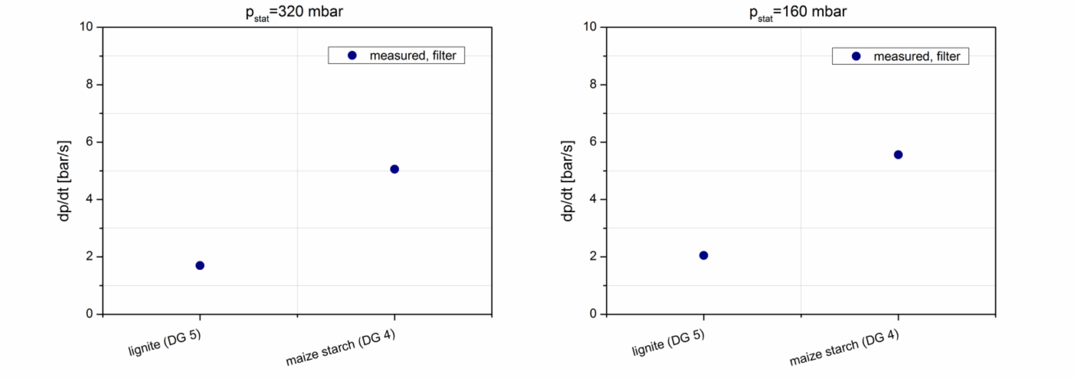

*Figure 5-17. 4 dusts pressure rises for static activation pressures of 160 and 320 mbar.*

### 5.2.7 Flame speeds $p_{stat}$ 160 mbar

Flame speed means the velocity of the flame as seen by a stationary observer. Therefore flame speed is the covered distance in a certain time.

Flame speed depends on many influences such as dust concentration, laminar/turbulent flow and burning velocity. Flame speeds were recorded with a high-speed camera with 250 frames per second.

Flame speed can be divided into laminar and turbulent flame speeds. Laminar flame speed means the flame spreads in a homogenous mixture at rest. The flame in turbulent mixture is accelerated due to the wrinkling of the flame front, so turbulent flame speeds are faster than laminar ones.

The comparison of $K_{St}$ values (Figure 5-18, right) to measured flame speeds in the 75 L apparatus (Figure 5-18, left) shows the influence of dustiness on flame speeds as on the pressure rises. Since flame speed and pressure rise are related this is as expected.

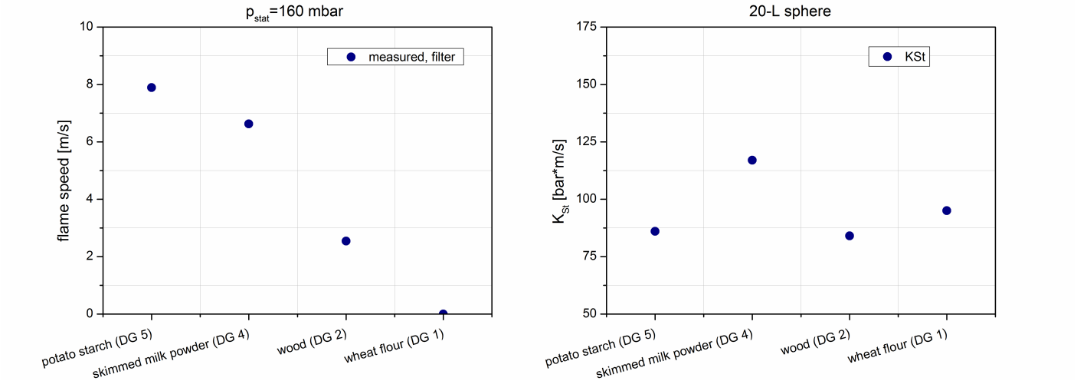

*Figure 5-18. 4 dusts flame speeds and $K_{St}$ values.*

Figure 5-19 shows the comparison of flame speed and $K_{St}$ values for the two dusts with higher safety characteristics. Again no influence of dustiness can be detected, but dustiness is in a similar range, dustiness group 4 and 5.

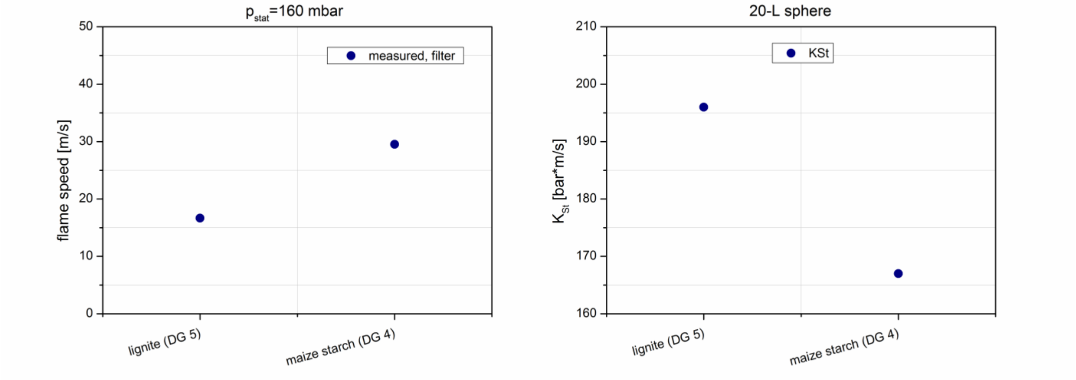

*Figure 5-19. 2 dusts flame speeds and $K_{St}$ values.*

**Remark**

Due to the resolution of the high-speed camera a deviation of 4 ms has to be considered.

## 5.3 Experiments - dispersion with nozzle

In order to create a more critical setup and to evaluate the influence of the dispersion method on dustiness behavior, a second setup was realized. The filling in the following experiments was at the top with a nozzle and pressurized air, for details see chapter 5.1.2.

### 5.3.1 Dustiness experiments

Dispersion experiments were done for theoretical concentrations between 250 g/m³ and 1500 g/m³. Dust concentration was measured for 10 s. The results are shown exemplary for theoretical concentrations of 250 g/m³ (see Figure 5-20 and Figure 5-21, section of time). The influence of dustiness can be seen for all dusts, when filled in at top of the apparatus. Especially potato starch, maize starch and lignite with higher dustiness show high and comparable concentrations at the lower and upper sensors, which means that they tend to produce more homogenous dust concentrations (see Figure 5-21). Comparable results could be shown for the other concentrations.

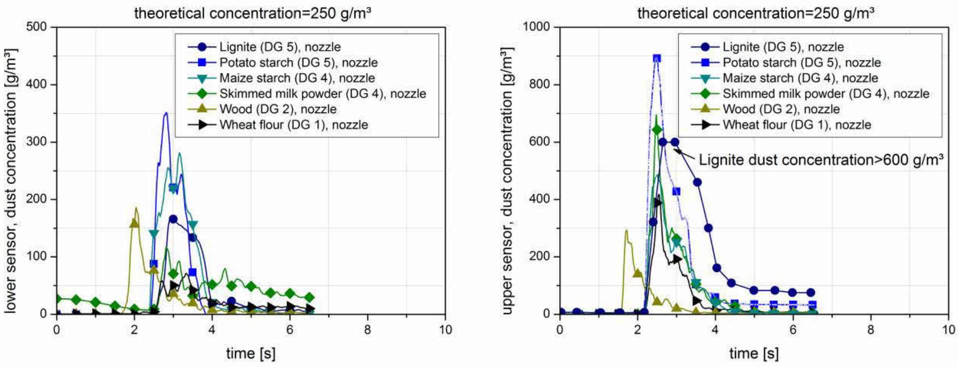

*Figure 5-20. Dust concentration as function of time (250 g/m³).*

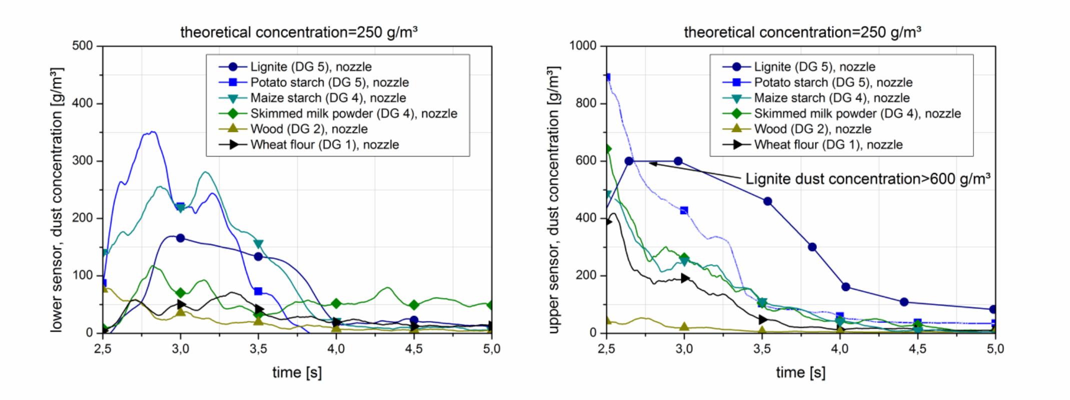

Lignite dust concentration>600 g/m³

*Figure 5-21. Dust concentration as function of time (250 g/m³), section.*

Figure 5-22 shows the measured concentration at ignition time (1.25 s after beginning of dispersion) as a function of the theoretical concentration, which means the concentration where all filled-in dust would have been dispersed homogenously. At ignition time the measured concentrations hint at a homogenous distribution for most dusts. Only maize starch and wheat flour seem to produce less homogenous mixtures.

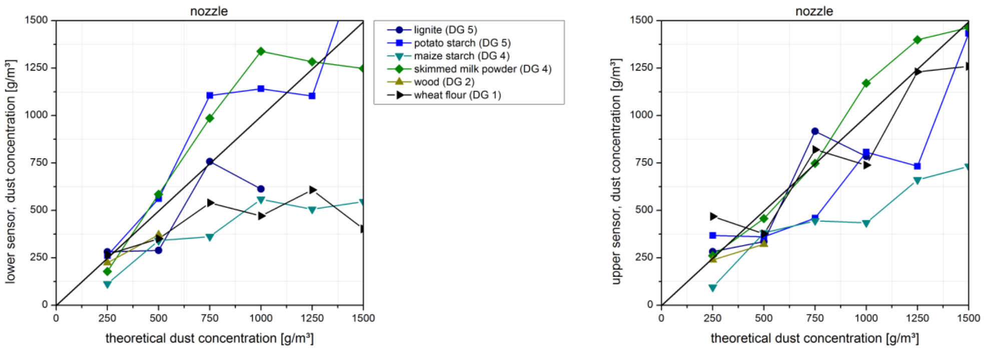

*Figure 5-22. Dust concentration at ignition time.*

### 5.3.2 Comparison of dustiness experiments

Since the behavior of dust/air mixtures depends not only on material properties but on boundary conditions, dust concentration measurements of the two filling methods were used to compare the dustiness behavior depending on the filling method.

Figure 5-23 and Figure 5-24 show dust concentrations at ignition time as function of theoretical concentration for dispersion with the filter plate (left) dispersion at top (right). A more homogenous mixture is achieved at ignition time for dispersion with a nozzle at the top of the apparatus, as expected. Explosion experiments with both filling methods should show, if dustiness influences the course of explosion even if a comparable dust distribution for different dusts is present in the apparatus at ignition time.

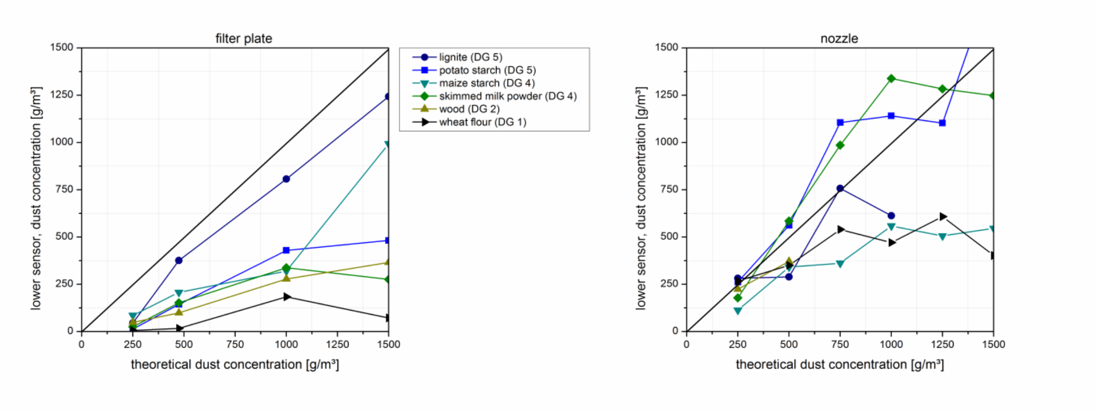

*Figure 5-23. Dust concentration at ignition time, filter plate (left) and nozzle (right).*

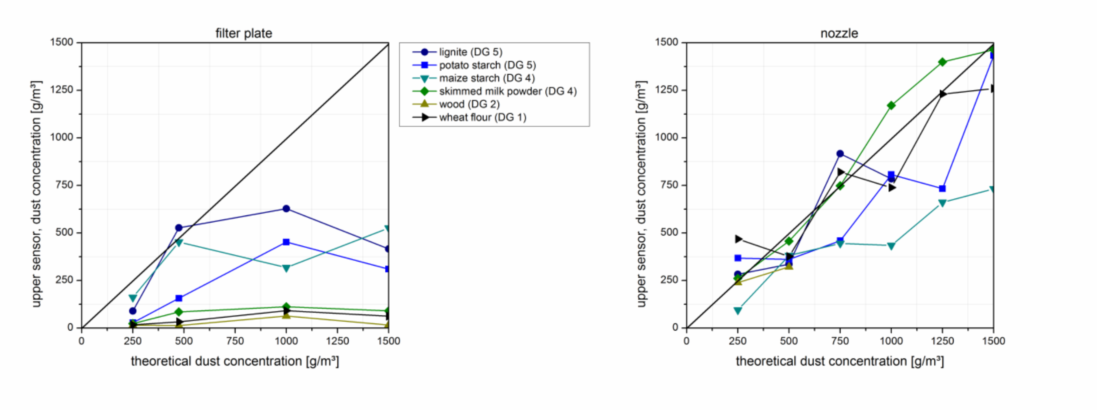

*Figure 5-24. Dust concentration at ignition time, filter plate (left) and nozzle (right).*

Figure 5-25 shows the measured dust concentrations over time for both dispersion methods. Dispersion with the filter plate leads to lower measured concentrations than dispersion at the top for the same sample mass. Influence of dustiness can be seen for both dispersion methods over time.

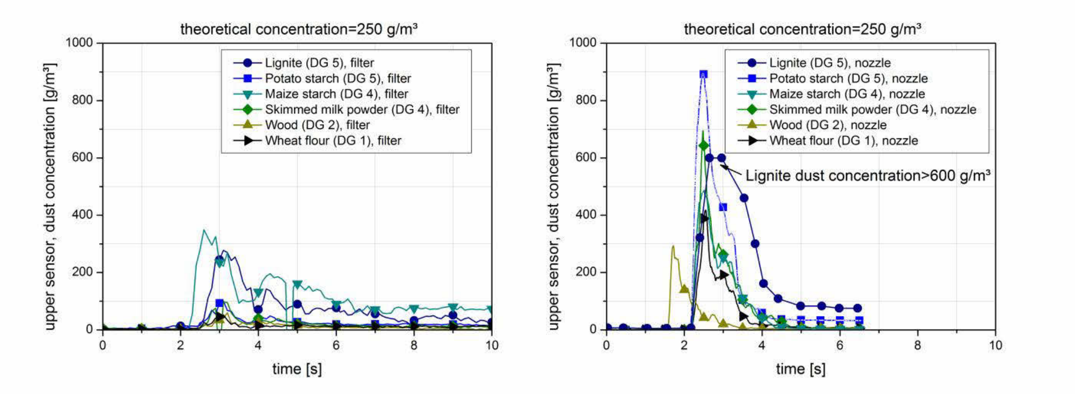

*Figure 5-25. Dust concentration as function of time (250 g/m³), filter plate (left) and nozzle (right).*

## 5.3.3 Comparison of vented dust explosions

Explosion experiments were carried out again with dispersion at the top of the apparatus. Reduced explosion pressures and pressure rises were measured and compared for both filling methods.

## 5.3.4 Comparison of reduced explosion pressures

The comparison between maximum reduced pressures generated with the filter plate and the nozzle show comparable results, but the wheat flour could be ignited and all measured pressures were higher for the dispersion with the nozzle (see Figure 5-26, left). Compared to calculated overpressures (Figure 5-26, right) the influence of dustiness becomes clear again for the four dusts with comparable safety characteristics.

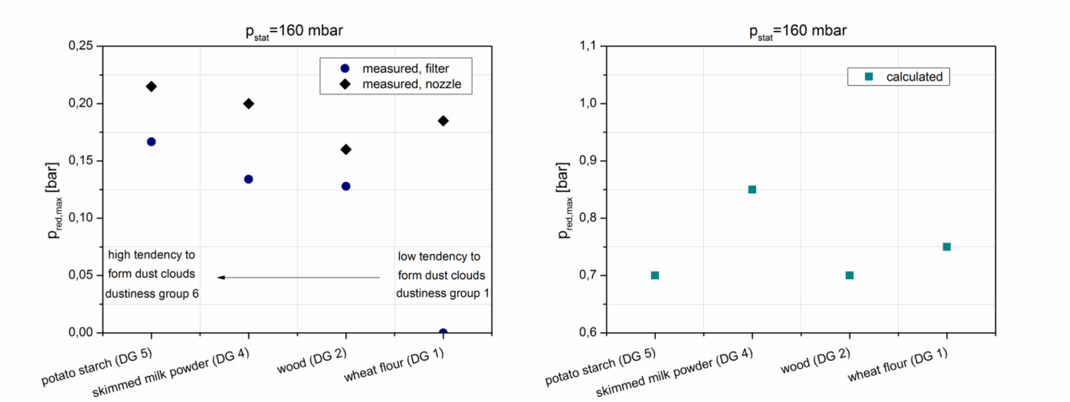

*Figure 5-26. 4 dusts measured and calculated reduced overpressures.*

Figure 5-27 shows the reduced explosion pressures of lignite and maize starch for dispersion with filter and nozzle.

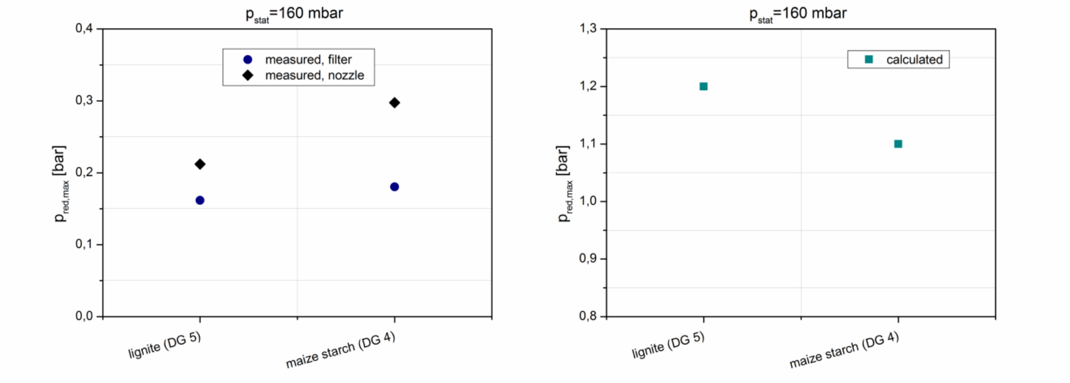

*Figure 5-27. 2 dusts measured and calculated reduced overpressures.*

An overview on all calculated and measured reduced pressures can be found in Table 5-5. Measured and calculated maximum reduced pressures for venting area of 0.01131 m².

*Table 5-5. Measured and calculated maximum reduced pressures for venting area of 0.01131 m²*

| dust | $p_{red,max}$ (iterative) in bar $p_{stat}$ 160 mbar | $p_{red,max}$ (filter) in bar $p_{stat}$ 160 mbar | $p_{red,max}$ (nozzle) in bar $p_{stat}$ 160 mbar |
|---|---|---|---|
| wheat flour (DG 1) | 0.75 | - | 0.169 |
| wood (DG 2) | 0.70 | 0.125 | 0.160 |
| skimmed milk powder (DG 4) | 0.85 | 0.134 | 0.197 |
| maize starch (DG 4) | 1.10 | 0.181 | 0.293 |
| lignite (DG 5) | 1.20 | 0.160 | 0.190 |
| potato starch (DG 5) | 0.70 | 0.167 | 0.209 |

The slightly higher values for the nozzle could be due to the more critical setup and/or because of the division of the venting area into three parts. As stated by **Fakandu et al.** [87] the division into more venting areas with the same total area can lead to higher internal pressures.

## 5.3.5 Comparison of maximum rate of reduced pressure rises

Figure 5-28 and Figure 5-29 show the comparison between pressure rise and $K_{St}$ value for the experiments with filter plate and nozzle. Again the effect of dustiness was observed for the four dusts with comparable safety characterstics, see Figure 5-28 (left). $K_{St}$ values are shown for comparison. Potato starch should react less severe than the other dusts, but the opposite it is.

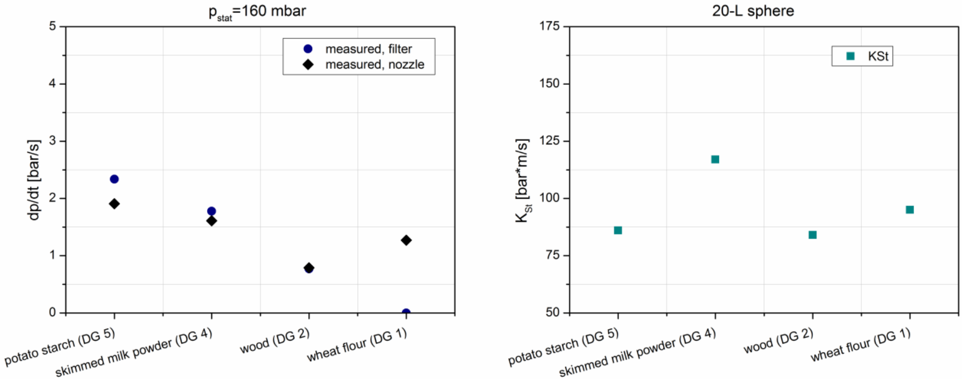

*Figure 5-28. 4 dusts maximum rise of explosion pressure compared to $K_{St}$.*

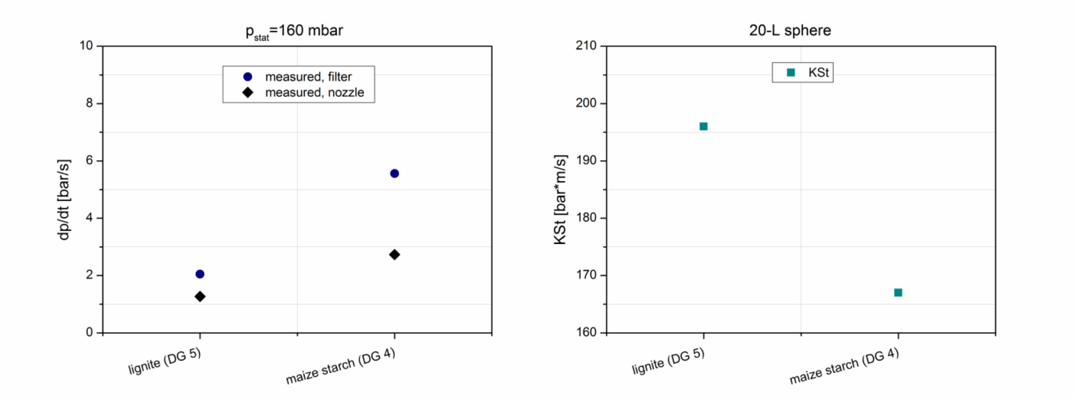

*Figure 5-29. 2 dusts maximum rise of explosion pressure compared to $K_{St}$.*

## 5.4 Conclusion - small-scale-experiments

Experiments in a vented 75 L tube apparatus were done in order to evaluate dustiness behavior depending on the filling method and to investigate the influence of dustiness on the course of explosion under vented conditions. Dustiness means the tendency of a powder to form airborne dust by a prescribed mechanical stimulus. Two dispersion methods, namely dispersion with a filter plate at the bottom and filling at the top with a nozzle, were realized. This provides information about the influence of the dispersion method on dustiness behavior in a vessel. The dispersion at the bottom and the filling at the top were chosen, because these are two common possibilities of dust dispersion as found in work conditions. The dust can be lifted due to air flow or a primary explosion shock wave or is filled in at the top of a vessel, e.g. in a silo. Experiments where the dust concentration was measured over time for the different dispersion methods showed that a general influence of dustiness on the generated dust/air mixture was recorded. Despite this the dispersion method or surrounding air flow influences the total mass of dust in the air and the homogeneity of the mixture. An overview is given in [akl1] and [akl2].

Explosion experiments in a 75 L apparatus showed that potato starch showed higher than expected reduced explosion pressures, pressure rises and flame speeds, compared to the safety characteristics $p_{max}$ and $K_{st}$ value as well as calculated pressures for four selected dusts with $p_{max}$ between 7 bar and 8 bar and $K_{St}$ values around 100 bar*m/s. This could be due to the high dustiness of potato starch. Wheat flour could not be ignited in any experiment with the filter plate, probably because of the low dustiness which lead to dust concentration lower than the lower explosion limit (LEL).

A more homogenous dust distribution at ignition time could be achieved with the filling at the top. The recorded influence of dustiness on the course of explosion in terms of reduced explosion pressure and pressure rise could be shown for comparable dust distributions at ignition time as well, see [88] and [89]. Figure 5-30 shows the ratio of measured and calculated reduced explosion pressures with standard deviation. Dusts were sorted according to their dustiness, if their dustiness group was the same, the dustiness number, their ascending order within the dustiness group, was used. In general measured pressures were below calculated explosion pressures. The measured pressures increased with increasing dustiness, but lignite. Lignite showed the poorest reproducibility as well. Lignite had a very high calculated pressure due to a measured $K_{St}$ value of 197 bar*m/s, which is higher than the highest confirmed value at the GSBL out of 47 samples of 176 bar*m/s (Joint Substance Data Pool of the German Federal Government and the German Federal States) material database [90], which joins safety characteristics of dusts of several institutes.

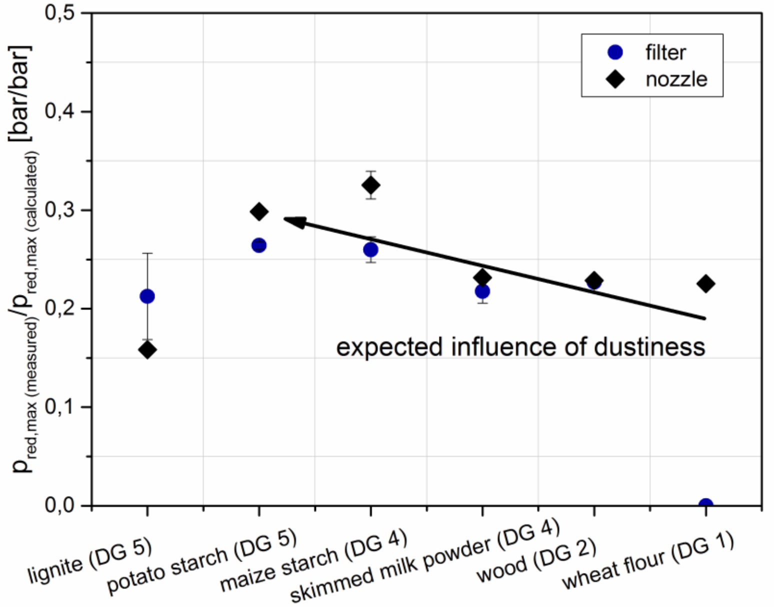

*Figure 5-30. Ratio of measured and calculated reduced explosion pressures for different dispersion methods.*

An approach to adapt the venting area can only be determined with industrial-scale experiments due to the dependence of dust explosions on many parameters. The laboratory vessel was a little bit too small for calculation according to EN 14491. Therefore measured pressures were below the calculated pressures only 25 % - 40 % of calculated $p_{red,max}$ were measured. Since dustiness depends on so many influences starting with a specified scenario seems the only safe approach. If it can be shown for different filling methods and vessel sizes and shapes, a more general approach might be possible. In a next step it is planned to show the influence of dustiness on vented dust explosions for a cylindrical silo with pneumatic filling at top. A 10 % increase reduced maximum pressure (vessel strength) would result in a approx. 10 % decrease of necessary venting area. Therefore it might be possible to use the factor directly on venting area. It is not certain whether a general dustiness as described in [2] can be used for the adaption of the venting area. A reproducible effect has to be shown in industrial scaled experiments as well. Additionally dust properties and boundary conditions must not change during process, e.g. due to changes in the used material or deposition of certain mass fractions.

Future small-scale experiments could deal with the ratio of burnt and unburnt mass depending on dustiness behavior and sample mass. This could help to investigate if more of the dust samples with better dustiness take part in the combustion process. Further investigations regarding turbulence and dustiness could be interesting. Maybe fast and straight sinking dusts with bad dustiness lower turbulence in the vessel and therefore generate less violent explosions. Numerical and experimental investigations regarding the influence of particle size distribution on turbulence have already been made, e.g. by **Sommerfeld** [91].

# 6 Industrial-scale experiments in a 50 m³ silo

In order to evaluate the results from small-scale experiments, dust concentration measurement and vented dust explosion experiments were done in a 50 m³ silo. Three dusts of different dustiness were chosen for all experiments. Dust concentration experiments were done regarding dustiness behavior and reproducibility in a large vessel. Experiments were done with two filling methods, a homogenous injection as worst-case scenario and pneumatic filling at top as found in the process industries. Vented dust explosions were done in a second step for homogenous injection only. Results were compared to calculated pressures in order to verify results regarding the influence of dustiness from small-scale experiments. This should provide information on an influence in an industrial scale, if so, a first approach to adapt the sizing of the venting area should be given.

## 6.1 Setup

The test vessel is a cylindrical silo with a volume of 50 m³ and a diameter of 2.75 m. It has a length/diameter ratio of approx. 3.8 and is designed to withstand overpressures of 0.5 bar. As explosion protection five venting areas are located at the top with a total area of 2.5 m². Dust/air mixtures can be ignited with pyrotechnical igniters at different heights. Pressure is recorded during tests at four locations, two at the middle section and one below and above the middle section. For description of the measurement equipment see chapter 4.3.

Figure 6-1 shows a schematic of the silo with the main properties of the vessel.

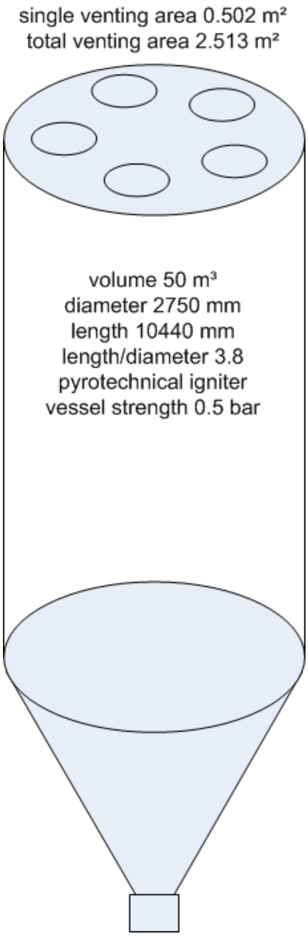

*Figure 6-1. 50 m³ silo.*

### 6.1.1 Choice of dusts and dust properties

For industrial-scale experiments three dusts with different dustiness were used. The dusts are commonly used dusts, namely wheat flour, maize starch and lignite. These are all dusts, which are used in large quantities in process industries, and might lead to severe accidents. Properties of the dusts, such as dustiness group, $p_{max}$, $K_{St}$ values, humidity, specific surface area and particle size distribution, can be taken from Table 6-1 and Table 6-2.

*Table 6-1. Dust properties industrial-scale tests.*

| dust | dustiness group | $p_{max}$ in bar | $K_{St}$ in bar*m/s | humidity in % by weight | raw density in kg/m³ | specific surface area (BET) in m²/g |
|---|---|---|---|---|---|---|
| wheat flour | 1 | 7.2 | 94 | 9.76 | - | - |
| maize starch | 2 | 8.7 | 167 | 10.38 | 1502 | 2.4857 |
| lignite | 5 | 8.4 | 196 | 11.25 | 1494 | 4.9110 |

Table 6-2 gives information about the particle size distribution and lower explosion limit of the dusts. Lower explosion limit of wheat flour was taken from a comparable dust and should only be considered as benchmark value.

Table 6-2. Dust properties industrial-scale tests.

| dust | dustiness group | median in µm | d(0.1) in µm | d(0.9) in µm | lower explosion limit in g/m³ |
|---|---|---|---|---|---|
| wheat flour* | 1 | 54.2 | 10.3 | 143.6 | 60[1] [72] |
| maize starch | 2 | 13.5 | 7.6 | 22.3 | 125 |
| lignite | 5 | 37.7 | 3.8 | 230.5 | 30 |

[1] benchmark value from comparable dust

### 6.1.2 Silo with homogenous injection

In order to create a worst-case scenario, in terms of homogenous dust distribution and high turbulence, dust was injected at eight points through nozzles with pressurized air. A total maximum of 100 L dust can be injected with eight nozzles at three heights. For maize starch with a bulk density of 600 kg/m³ a maximum total mass of 60 kg could be conveyed into the silo. With the total volume of 50 m³ theoretical concentrations up to 1200 g/m³ are possible. Dust was injected for approx. one second in all experiments. Figure 6-2 shows a schematic picture of the silo with the injection points.

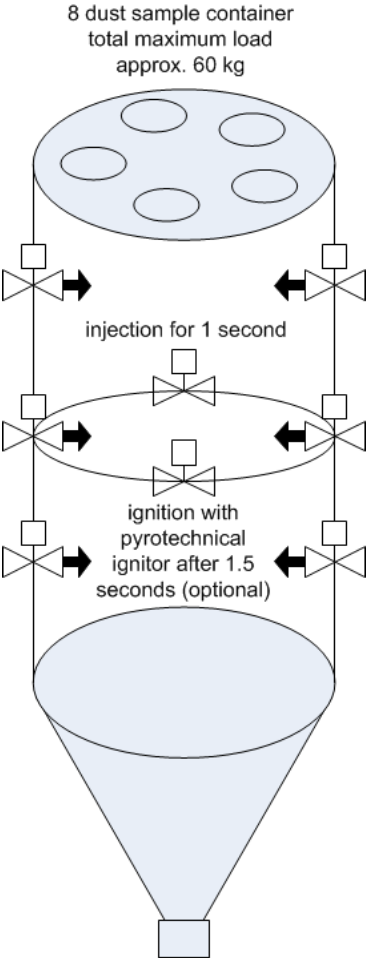

*Figure 6-2. Silo with homogenous injection.*

### 6.1.3 Silo with pneumatic filling at top

The second setup was a pneumatic filling at the top as usually found in the process industries, especially food industry. In order to increase the explosion risk slightly, a deflector plate was installed at the inlet pipe. Dust was conveyed for six seconds in all experiments and, in explosion experiments, ignited after eight seconds with a pyrotechnical igniter. In process industries accidents often occur during filling or handling but in order to avoid damage to the equipment it is not possible to convey until ignition in this configuration. A compromise between filling time, filled-in sample mass and ignition time was chosen. Figure 6-3 shows a schematic picture of the pneumatic filling.

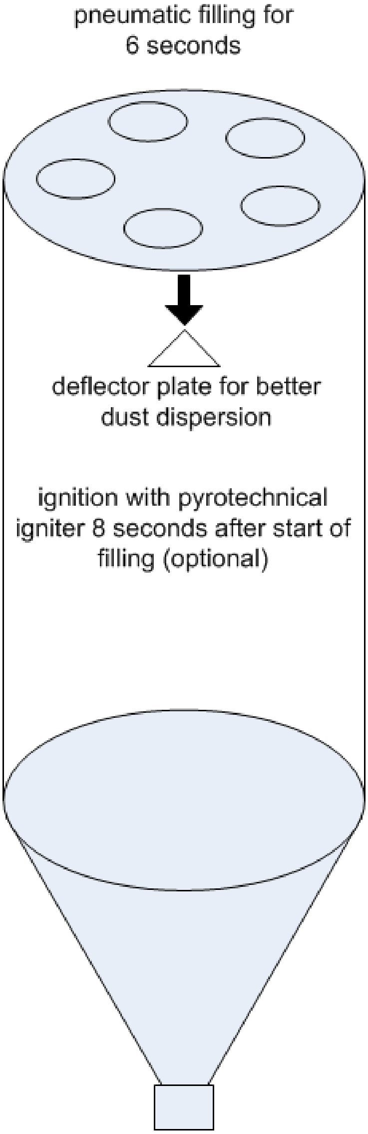

*Figure 6-3. Silo with pneumatic filling at top.*

### 6.1.4 Calculated venting areas

Necessary venting areas were calculated according to EN 14491 for the three tested dusts. For calculation with empirical equations of the standard see chapter 5.1.3. The calculated venting areas for static activation pressures of 80 mbar and 160 mbar are shown in Table 6-3. Activation pressures in process industries are usually very low in order to avoid high pressures in the vessel, which would need thicker and more costly walls.

*Table 6-3. Venting areas for different activation pressures.*

| dust | venting area in m² $p_{stat}$ 80 mbar | venting area in m² $p_{stat}$ 160 mbar | chosen venting area for all experiments |
|---|---|---|---|
| wheat flour (DG1) | 1.05 | 2.29 | 2.5 m² |
| maize starch (DG2) | 2.62 | 3.83 | |
| lignite (DG5) | 3.01 | 4.23 | |

The maximum possible venting area of 2.5 m² was chosen and a static activation pressure of 80 mbar. The total venting area consists of five single vents, each 0.5 m². The calculated area for lignite was a little bit greater; therefore tests have to be made carefully with lignite, e.g. with lower dust concentrations.

### 6.1.5 Calculated reduced explosion pressures

As already done for the small-scale apparatus the expected pressures in the vessel were calculated according to EN 14491, see chapter 5.1.3. Experiments with lignite have to be made carefully. Higher activation pressures than 80 mbar were not used to avoid damage to the silo and are uncommon for these applications in process industries.

*Table 6-4. Calculation of overpressures.*

| dust | venting area 2.5 m² $p_{stat}$ 80 mbar calculated $p_{red,max}$ | venting area 2.5 m² $p_{stat}$ 160 mbar calculated $p_{red,max}$ |
|---|---|---|
| wheat flour (DG1) | 0.21 | 0.47 |
| maize starch (DG2) | 0.52 | 0.75 |
| lignite (DG5) | 0.59 | 0.80 |

## 6.2 Dustiness Experiments and reproducibility in large vessels

Tests were done with maize starch, lignite and wheat flour, which have a range from good to bad dispersion behavior. Tests were used to compare measured dust concentration over time for different dusts. This should allow seeing an influence of dustiness on dust cloud in the vessel. Additionally repeated tests were used evaluating reproducibility of the dust concentration measurement.

### 6.2.1 Dustiness experiments with homogenous injection

A total sample mass of 5 kg was used, which would lead to a theoretical concentration of 100 g/m³ in the silo. Tests with maize starch have been done at two different days, two tests each, total of four tests. All other dusts have been tested on one single day, with a total of three tests. A 30 % range of the average is shown for the tests. This should give information about reproducibility of dust concentration measurements in large vessels and comparison. The test setup is shown in Figure 6-4.

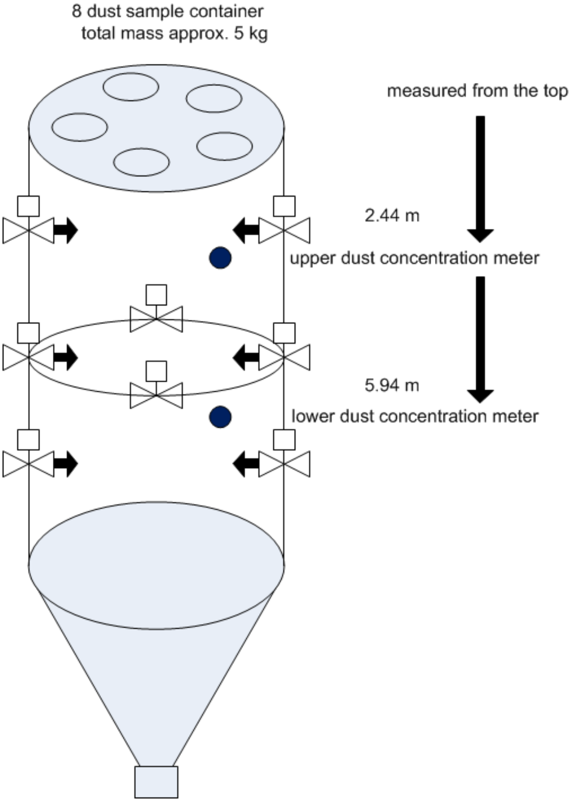

*Figure 6-4. Silo with homogenous injection, 5 kg dust.*

Table 6-5 shows the weather conditions at test day.

*Table 6-5. Weather conditions, homogenous injection.*

| date<br>dd.mm.yy | dust | filling method | T in<br>°C | p in<br>hPa | humidity in<br>% | number of tests |
|---|---|---|---|---|---|---|
| 25.07.13 | maize starch | homogenous | 27 | 1016 | 46 | 2 |
| 01.08.13 | maize starch | homogenous | 23 | 1018 | 83 | 2 |
| 25.09.13 | lignite | homogenous | 14 | 1008 | 72 | 3 |
| 23.04.14 | wheat flour | homogenous | 15 | 1019 | 82 | 3 |

The higher relative humidity seems to lead to lower measured concentrations for maize starch, see Table 6-5 and Figure 6-5. This is supported by the findings of **Lauer** [37], who showed that relative air humidity over 60 % led to lower dust concentrations over time.

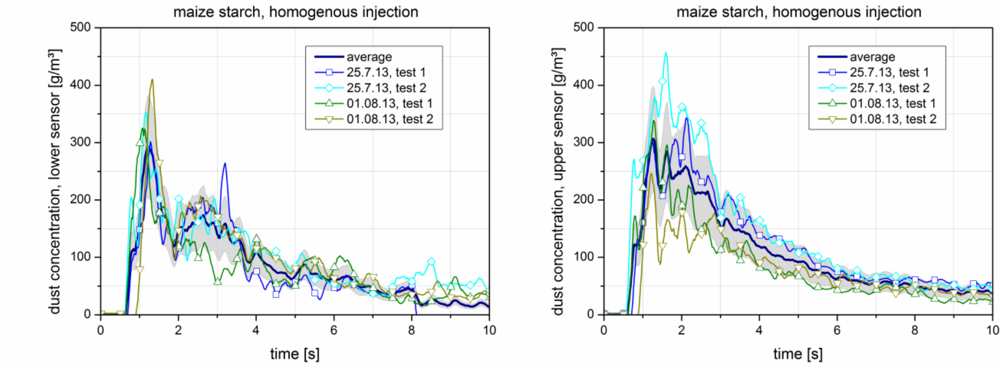

*Figure 6-5. Silo, dust concentration as function of time, homogenous injection maize starch.*

Tests with maize starch (Figure 6-5) and lignite (Figure 6-6) showed comparable results for the dust concentration curve over time. Higher dust concentrations were achieved for tests with lignite, which is in good agreement with the better dustiness.

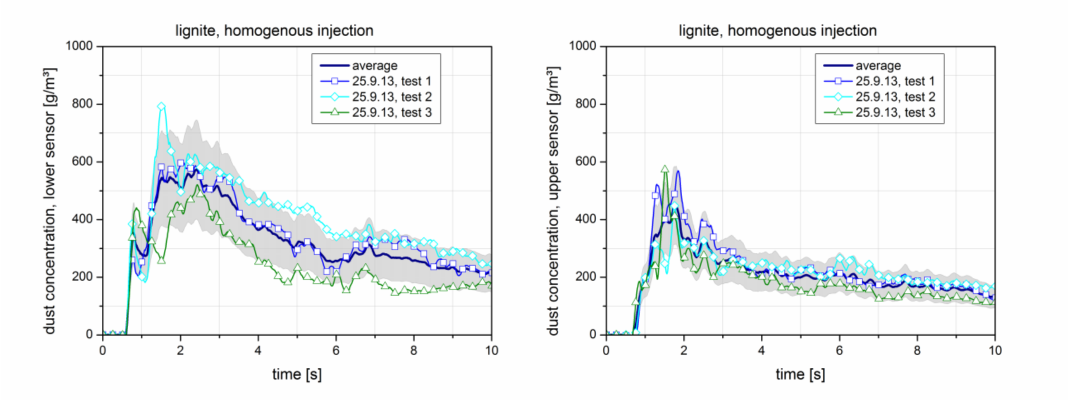

*Figure 6-6. Silo, dust concentration as function of time, homogenous injection, lignite.*

Both tests showed that repeated measurements generated deviations of 30 % and more compared to the average. Figure 6-7 shows the tests with wheat flour. Deviations of 30 % were measured as well. Compared to tests with lignite and maize starch lower dust concentrations over time were reported. Measured dust concentrations decayed earlier compared to the other samples as well.

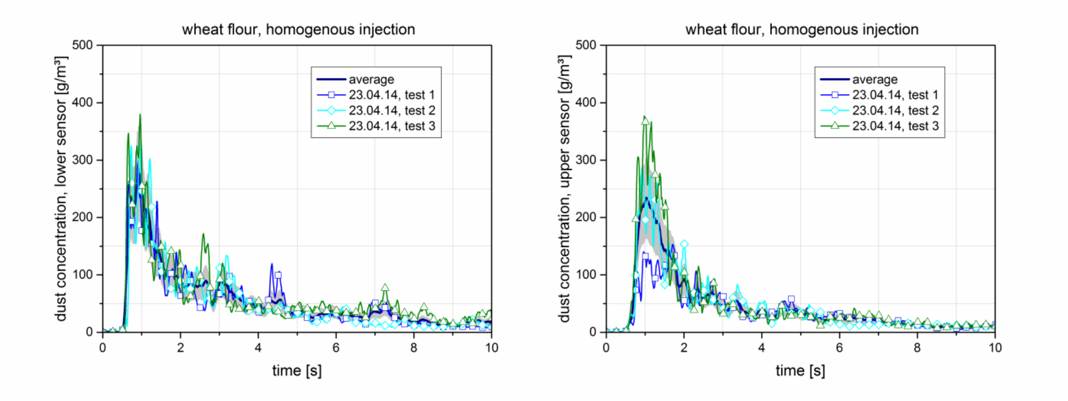

*Figure 6-7. Silo, dust concentration as function of time, homogenous injection, wheat flour.*

### 6.2.2 Dustiness experiments with pneumatic filling

A total mass of approximately 10 kg was used, which would lead to a theoretical concentration of 200 g/m³ in the silo. All dusts have been tested on one single day, with a total of three tests. A 30 % range of the average is shown for the tests. This should give information about reproducibility of dust concentration measurements in large vessels. The test setup is shown in Figure 6-8.

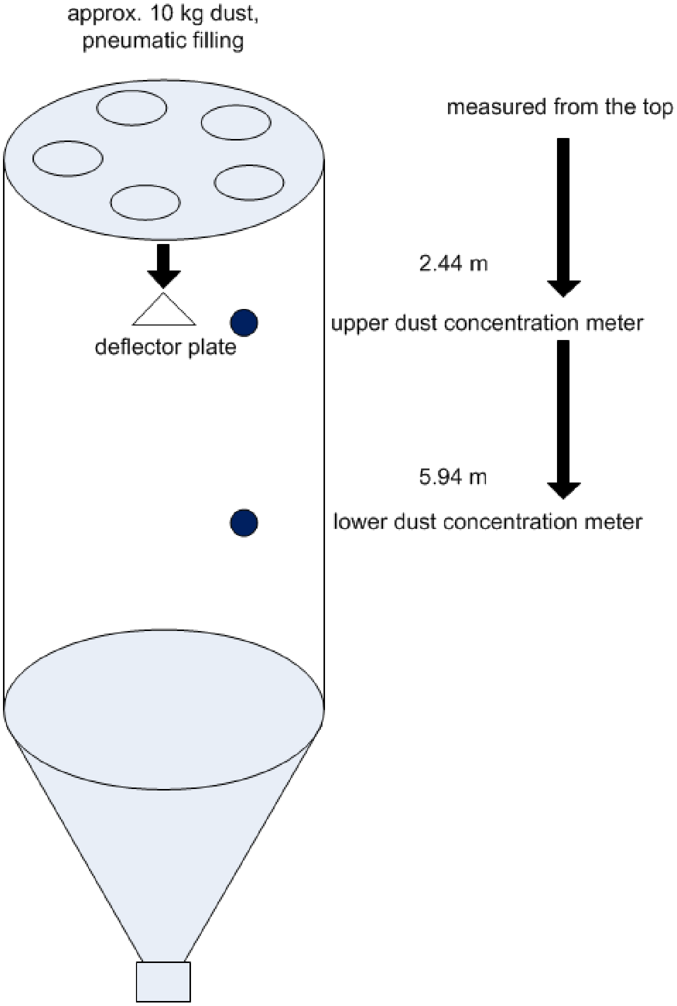

*Figure 6-8. Silo, pneumatic filling 10 kg dust.*

Table 6-6 shows the weather conditions at test day.

*Table 6-6. Weather conditions, pneumatic filling.*

| date<br>dd.mm.yy | dust | filling method | T in<br>°C | p in<br>hPa | humidity<br>% | number of tests |
|---|---|---|---|---|---|---|
| 29.08.13 | maize starch | pneumatic | 21 | 1022 | 62 | 3 |
| 24.10.13 | lignite | pneumatic | 17 | 1006 | 58 | 3 |
| 16.04.14 | wheat flour | pneumatic | 14 | 1034 | 39 | 3 |

The following diagrams show the first dust detection at upper and lower sensor for wheat flour, see Figure 6-9, maize starch, see Figure 6-10 and lignite, see Figure 6-11. This was used to calculate an average settling velocity. Distance between sensors was 3.5 m and this leads to settling velocities of 0.78 m/s for maize starch, 0.66 for wheat flour and 0.54 m/s for lignite. This is in good agreement with the higher tendency of lignite to stay airborne. The lowest tendency of wheat flour to form dust clouds is not represented by the initial detection of dust at the sensors, but can be seen in terms of very low peak dust concentrations and dust concentrations over time.

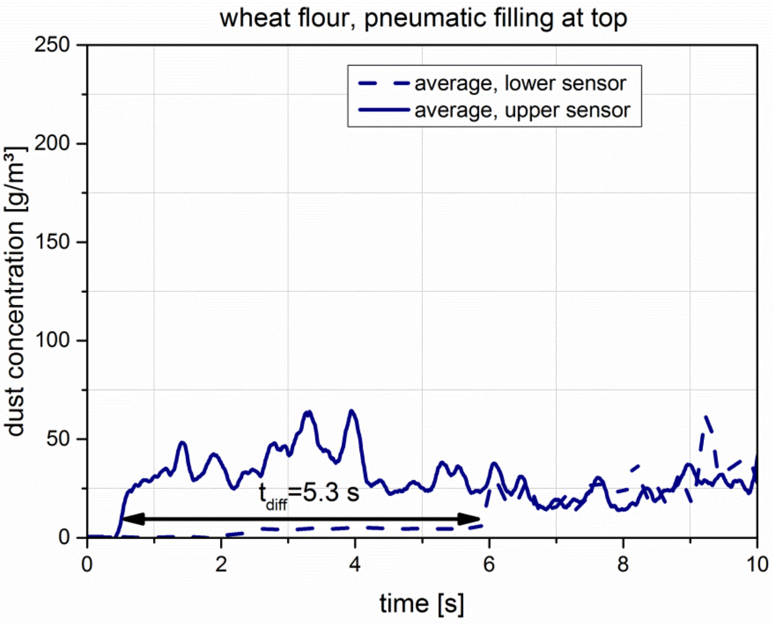

*Figure 6-9. Estimation of cloud settling velocity, wheat flour.*

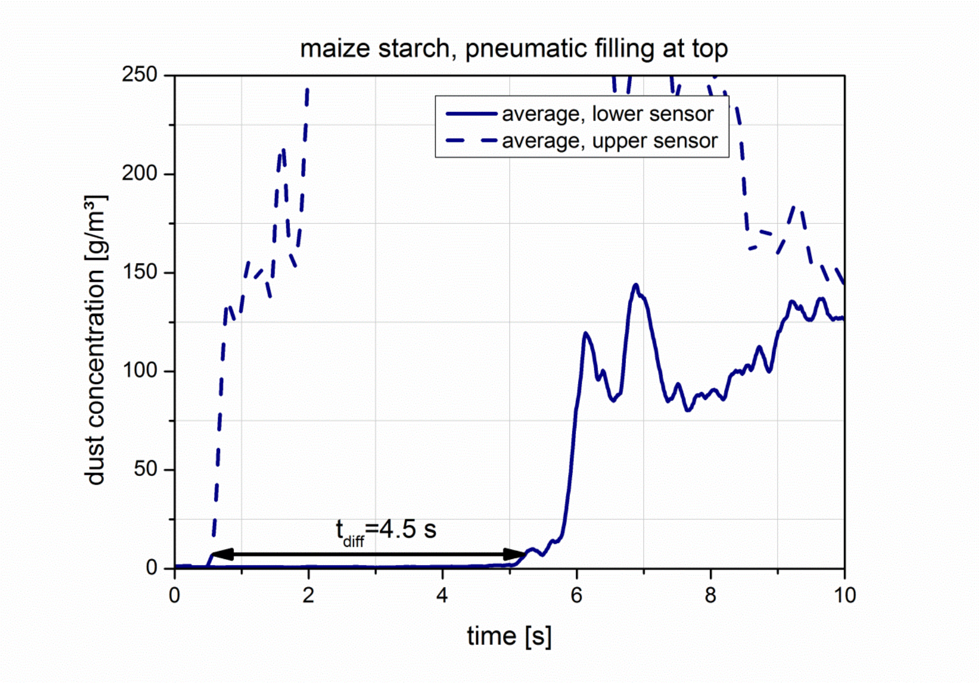

*Figure 6-10. Estimation of cloud settling velocity, maize starch.*

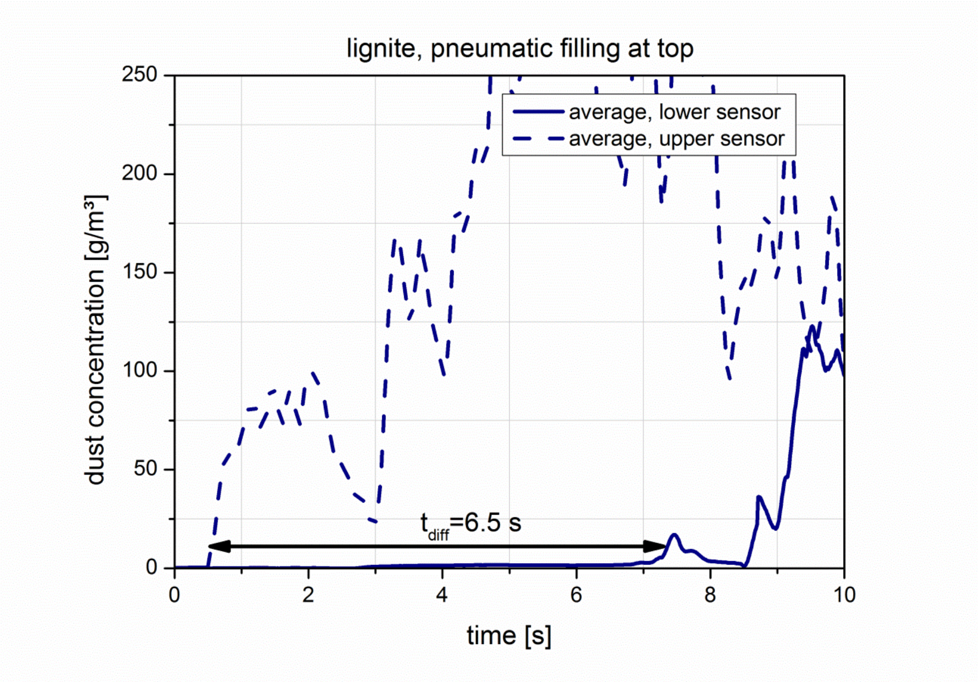

*Figure 6-11. Estimation of cloud settling velocity, lignite.*

Table 6-7 shows a summary of the time difference between first detection of dust at the sensor locations and calculated average cloud settling velocities.

*Table 6-7. Average dust cloud settling velocities.*

| dust | filling method | average time difference in s | average settling velocity in m/s |
|---|---|---|---|
| wheat flour (DG1) | pneumatic | 5.3 | 0.66 |
| maize starch (DG2) | pneumatic | 4.5 | 0.78 |
| lignite (DG5) | pneumatic | 6.5 | 0.54 |

The next diagrams show the dust concentration as function of time for maize starch (see Figure 6-12 and Figure 6-13), and lignite (see Figure 6-14). Especially for the upper sensor near the inlet pipe strong fluctuations can be observed. Deviations over 30 % from the average are present for 10 seconds after first detection of dust. For the lower sensor position there is a reproducible dust concentration curve five seconds after first detection.

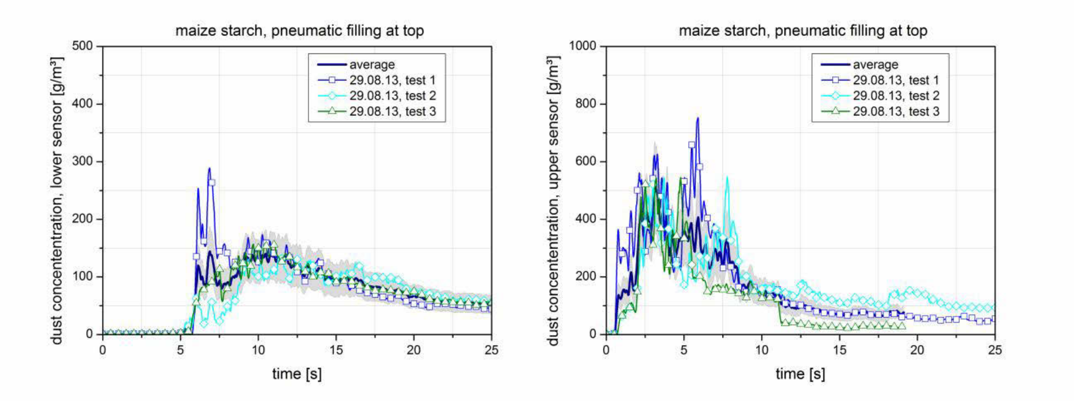

*Figure 6-12. Silo, dust concentration as function of time, pneumatic filling, maize starch.*

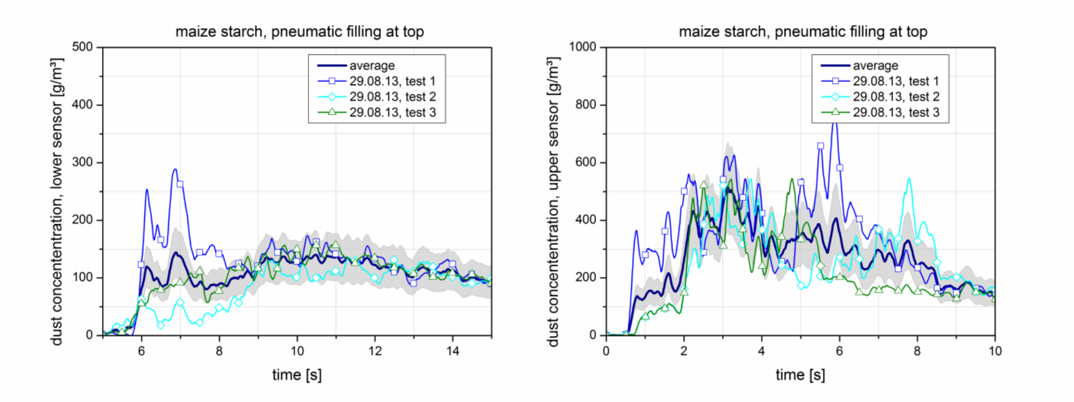

*Figure 6-13. Silo, dust concentration as function of time, pneumatic filling, maize starch, section of time.*

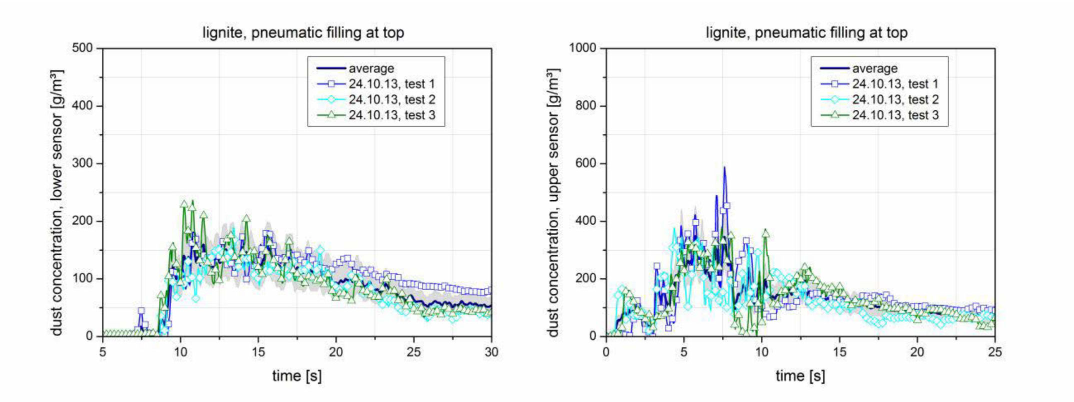

*Figure 6-14. Silo, dust concentration as function of time, pneumatic filling, lignite.*

Figure 6-15 and Figure 6-16 show the measured dust concentration of wheat flour over time for the two sensors. Again a high uncertainty can be observed, exceeding 30 % in repeatedly. There are peaks of three times the averaged measured concentrations from time to time.

In conclusions wheat flour seems to produce very inhomogenous mixtures with chaotic behavior.

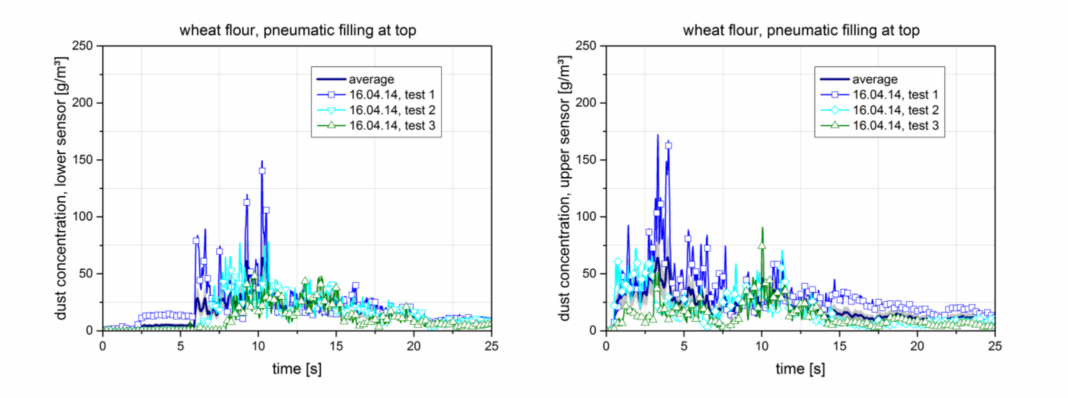

*Figure 6-15. Silo, dust concentration as function of time, pneumatic filling, wheat flour.*

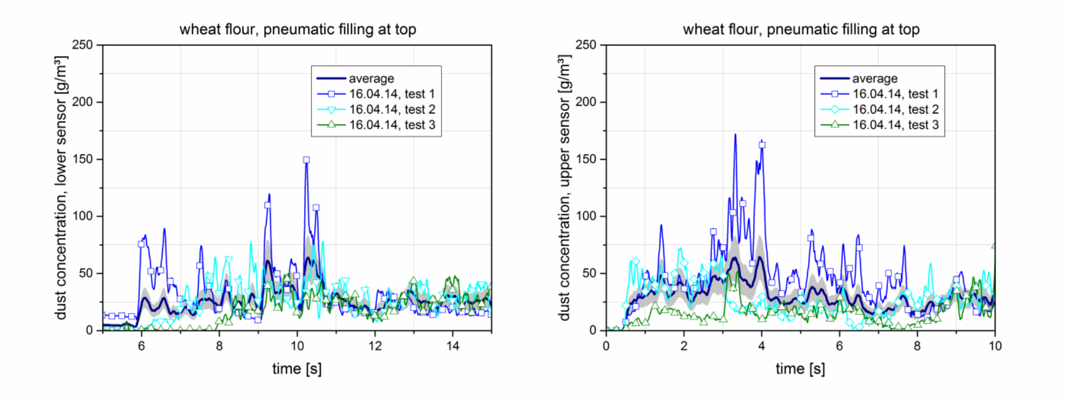

*Figure 6-16. Silo, dust concentration as function of time, pneumatic filling, wheat flour, section of time.*

### 6.2.3 Conclusion - dustiness experiments

Three dusts, wheat flour, maize starch and lignite, were used in combination with two different filling methods for dustiness experiments. Dust concentration was measured over time at two locations and repeated at least three times.

Experiments with pneumatic filling and 10 kg dust were done in the silo. Figure 6-17 shows the averaged dust concentrations over time. Wheat flour produces significantly lower dust concentrations over time compared to the other two dusts with same sample mass.

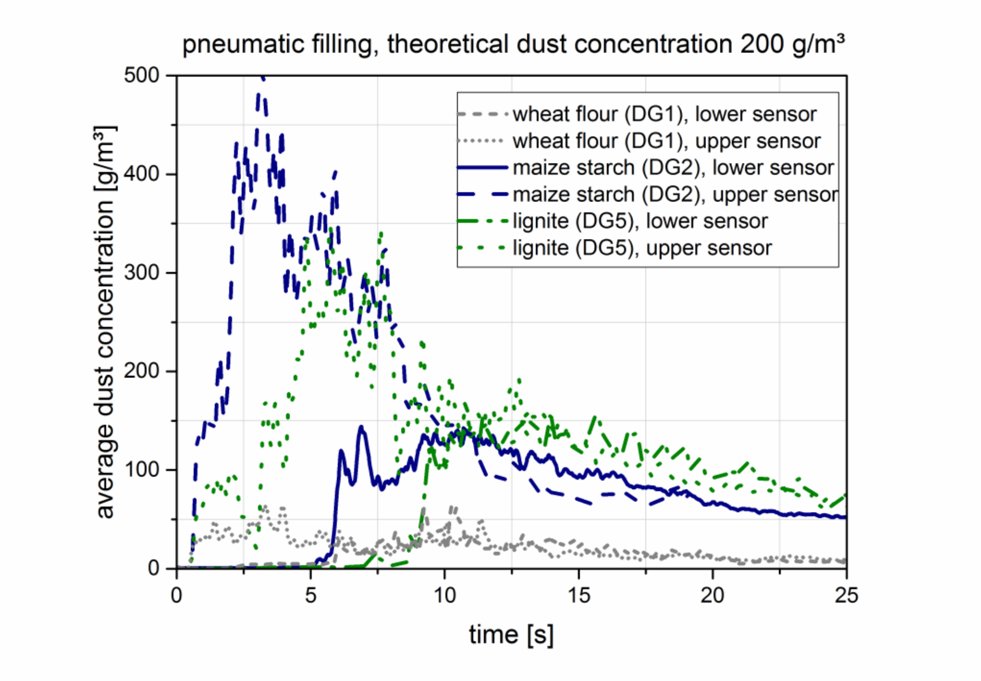

*Figure 6-17. Comparison of average dust concentrations for pneumatic filling, silo.*

Experiments with homogenous injection of 5 kg dust showed comparable results to the small-scale experiments as well as according to the dustiness groups of the samples. Lignite produced higher peak concentrations as well as higher dust concentrations over time. Maize starch and wheat flour have comparable peak values in average, but dust concentration of wheat flour decays fast.

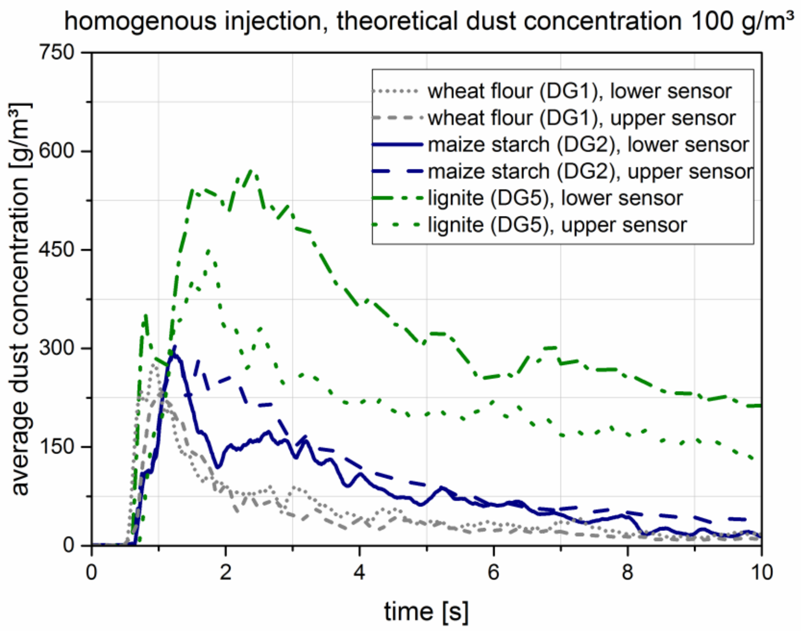

*Figure 6-18. Comparison of average dust concentrations for homogenous injection, silo.*

## 6.3 Explosion experiments

Explosion experiments were carried out in the 50 m³ with homogenous injection and static activation pressures of 80 mbar, see Figure 6-19. Pressure was recorded with four piezo-resistive sensors and the dust/air mixture was ignited with two 10 kJ pyrotechnical igniter. Three dusts were used at three theoretical concentrations (200 g/m³, 500 g/m³ and 1000 g/m³).

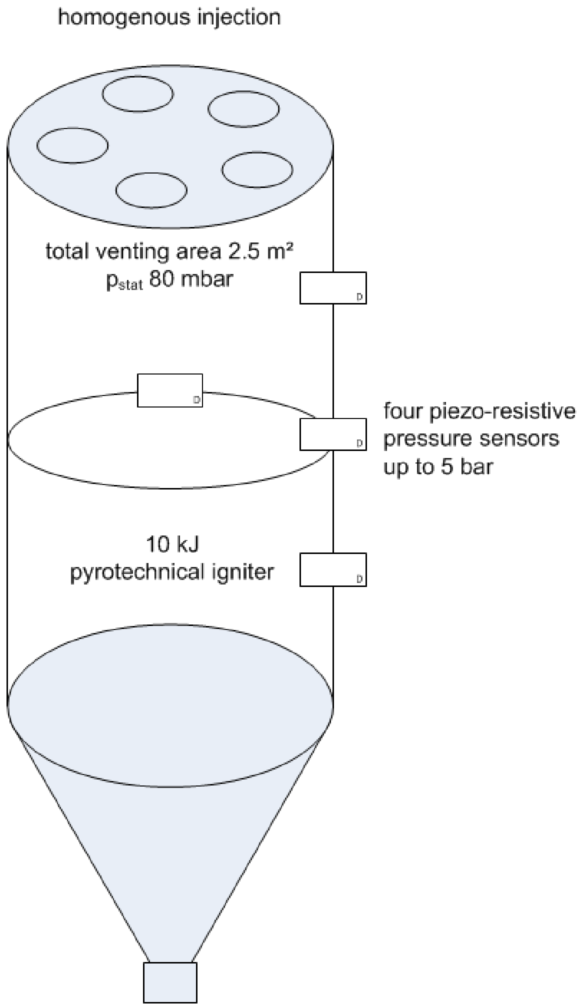

*Figure 6-19. Explosion experiments, 50 m³ silo.*

Boundary conditions of the tests are listed in Table 6-8.

*Table 6-8. Explosion test configurations, 50 m³ silo.*

| dusts | filling methods | theoretical dust concentrations in g/m³ | pyrotechnical igniter in kJ | $p_{stat}$ in mbar | venting area in m² |
|---|---|---|---|---|---|
| wheat flour (DG1) | homogenous | 200 | 2x10 | 80 | 2.5 |
| maize starch (DG2) | | 500 | | | |
| lignite (DG5) | | 1000 | | | |

An example of a recorded pressure curve is shown in Figure 6-20. The reduced explosion pressure was determined in each tests as well as the rate of pressure rise.

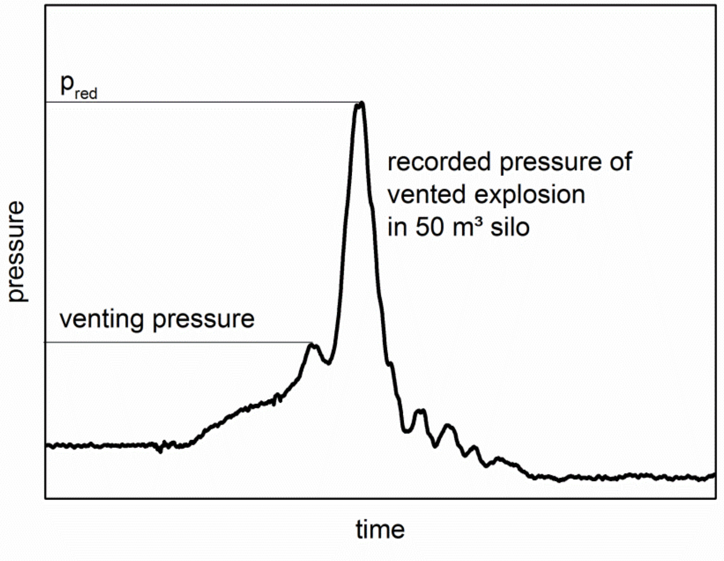

*Figure 6-20. Example of recorded pressure/time curve of a vented explosion in the 50 m³ silo.*

The venting process is visualized for an explosion of a wheat flour/air mixture in Figure 6-21. The opening of the vents due to the pressure rise can be seen in the second picture from the left, followed by the propagating flame. The picture on the right side shows that the venting area has been completely opened by the explosion.

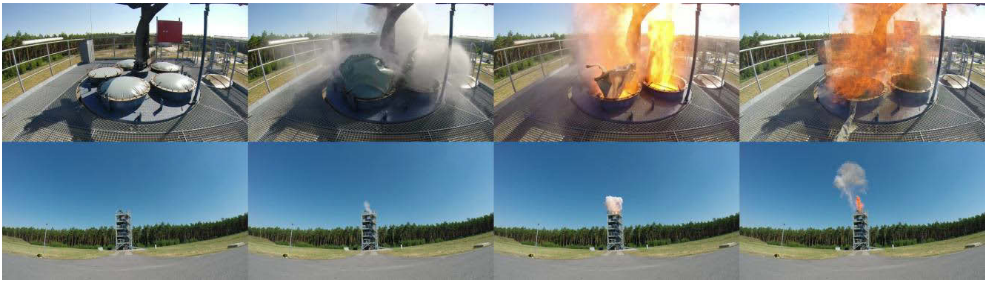

*Figure 6-21. Example of a vented dust explosion in the 50 m³ silo with 25 kg wheat flour.*

### 6.3.1 Explosion experiments with homogenous injection

Results of a first test series are shown in Table 6-9 and Table 6-10. Reduced explosion pressures as well as rates of pressure rises are stated in the tables for the three tested dusts and three theoretical concentrations. One low concentration at 200 g/m³ was tested as well as two higher dust concentrations, which were chosen to take the "optimum" concentration into account. "Optimum" concentrations of the three tested dust in the 20-L-sphere were between 500 g/m³ and 1000 g/m³.

*Table 6-9. Reduced explosion pressures for homogenous injection, 50 m³silo.*

| dust | $p_{red}$, for theoretical concentration of 200 g/m³ | $p_{red}$, for theoretical concentration of 500 g/m³ | $p_{red}$ for theoretical concentration of 1000 g/m³ |
|---|---|---|---|
| wheat flour (DG1) | 0.076 bar | 0.072 bar | 0.046 bar |
| maize starch (DG2) | 0.051 bar | 0.056 bar | 0.140 bar |
| lignite (DG5) | 0.133 bar | 0.091 bar | 0.082 bar |

*Table 6-10. Rates of pressure rise for homogenous injection, 50 m³silo.*

| dust | (dp/dt) for theoretical concentration of 200 g/m³ | (dp/dt) for theoretical concentration of 500 g/m³ | (dp/dt) for theoretical concentration of 1000 g/m³ |
|---|---|---|---|
| wheat flour (DG1) | 0.73 bar/s | 0.83 bar/s | 0.47 bar/s |
| maize starch (DG2) | 1.39 bar/s | 0.83 bar/s | 1.61 bar/s |
| lignite (DG5) | 1.95 bar/s | 0.68 bar/s | 0.59 bar/s |

The diagrams in Figure 6-25 show the reduced explosion pressures and rates of pressures rise as function of the theoretical concentration.

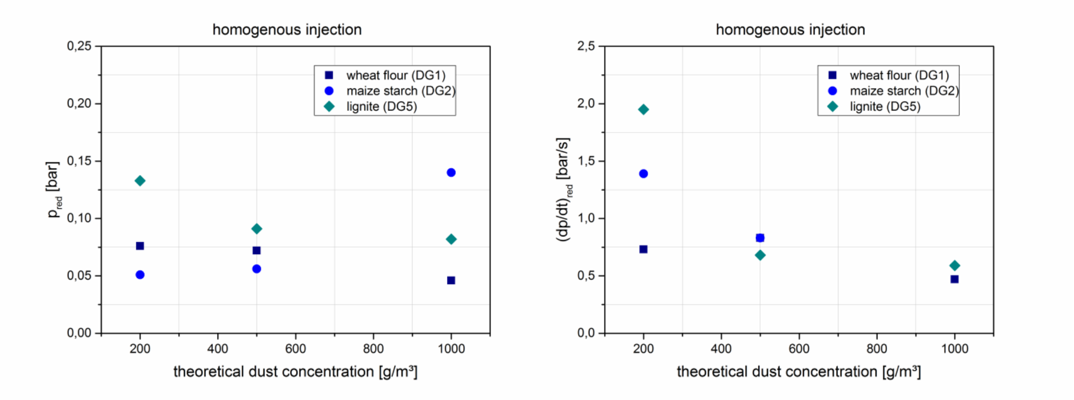

*Figure 6-22. Reduced explosion pressures and (dp/dt) values for homogenous injection, 50 m³ silo.*

### 6.3.2 Conclusion – explosion experiments

As a first result the maximum explosion pressures and rates of pressure rise are given for the first test series. Table 6-11 summarizes the results.

*Table 6-11. Comparison of maximum explosion pressures and pressure rises for homogenous injection.*

| dust | $p_{red,max}$ for homogenous injection bar | $(dp/dt)_{max}$ for homogenous injection bar/s |
|---|---|---|
| wheat flour (DG1) | 0.076 | 0.83 |
| maize starch (DG2) | 0.140 | 1.61 |
| lignite (DG5) | 0.133 | 1.95 |

A comparison of the measured reduced explosion pressures (Figure 6-23, left) to $p_{max}$ values showed that the dusts reacted as in the 20-L-sphere (Figure 6-23, right).

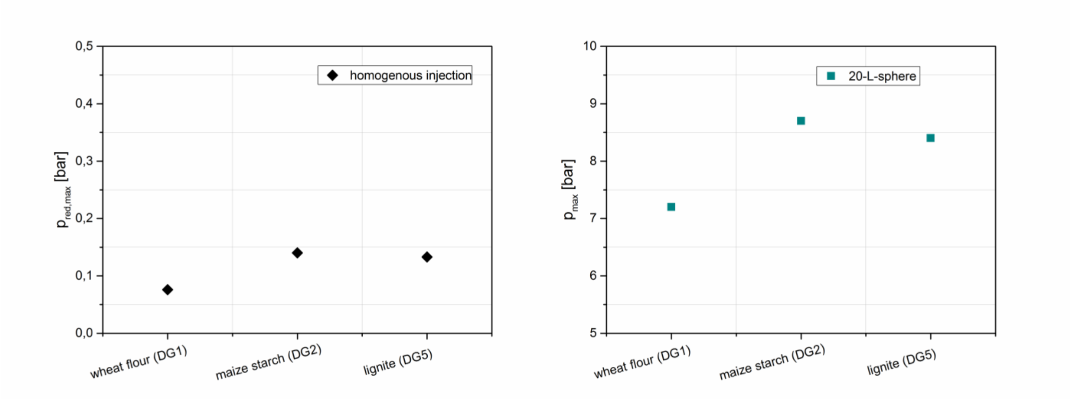

*Figure 6-23. Comparison of maximum reduced explosion pressures of one series to $p_{max}$.*

The maximum reduced rates of pressure rise of the first series (Figure 6-24, left) are compared to the $K_{St}$ values of the three tested dusts (Figure 6-24, right). The maximum reduced rates of pressure rise are in the same order as the $K_{St}$ values of the dusts.

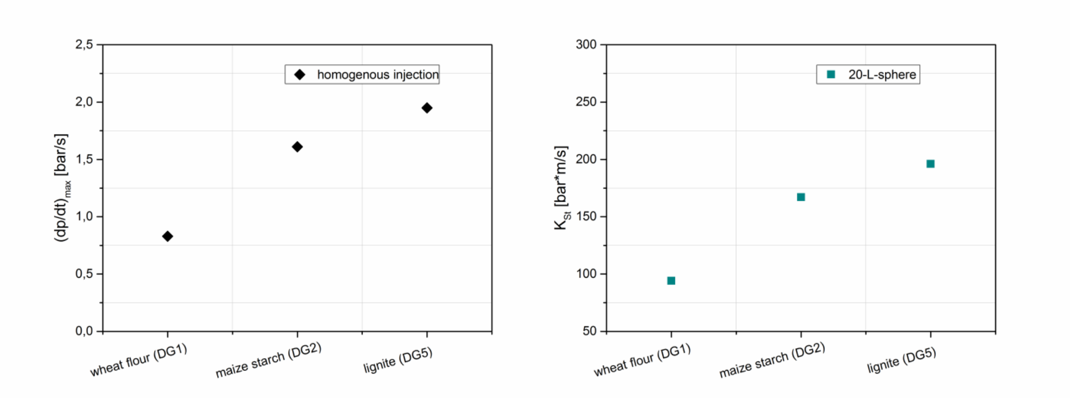

*Figure 6-24. Comparison of maximum reduced rates of pressure rise of one series to $K_{St}$*

Figure 6-25 shows the maximum reduced pressures of the first tests divided by the calculated pressures. All pressures are well below the calculated pressures, similar results were gained in a 500 m³ silo with length/diameter ratio of four by **Eckhoff and Fuhre** in 1984 [13, p. 437]. Experiments showed that all reduced explosion pressures were two to five time lower than the empirical correlations in the VDI 3673 and NFPA 68 suggested. For the experiments in the 50 m³ silo all ratios are in the range of one quarter to one third of the calculated pressures.

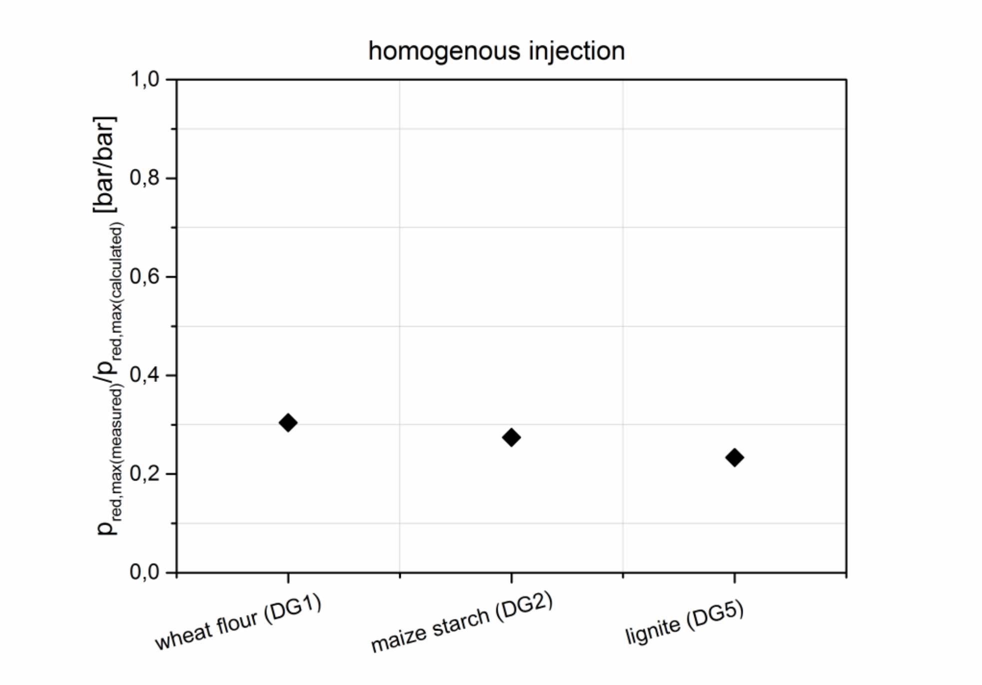

*Figure 6-25. Comparison of reduced explosion pressures to calculated ones, 50 m³ silo.*

## 6.4 Conclusion – industrial-scale experiments

Three dusts of different dustiness, from low to high tendency to form dust clouds, were used for experiments in 50 m³ silo. The chosen dusts were wheat flour, maize starch and lignite. In a first step dust concentrations over time were measured depending on two filling methods, homogenous dispersion with eight nozzles and pneumatic filling at the top of the silo. The dust concentration measurements were used to evaluate findings of the small-scale experiments and to determine if the safety characteristic dustiness can give hints on the dust distribution of different dusts in large vessels. Dustiness experiments in the silo showed that an influence of dustiness on dust concentration over time could be proved for the three dusts. Dust concentration measurements showed a poor reproducibility. There were deviations of 30 % and more compared to the average of measured values, especially for pneumatic filling the measured concentrations differed very much from one test to another. Further research on the dust distribution is recommended to provide more details on the influence of dustiness on vented dust explosion as well as for other safety measures such as help with determining zones and optimal location for suppression systems.

First explosion experiments with a worst-case scenario, which was injection via eight nozzles and pressurized air, showed that all measured reduced explosion pressures were well below the calculated values, despite the critical setup. Reduced explosion pressures and rates of pressure rise were as expected from the 20-L-sphere safety characteristics $p_{max}$ and $K_{St}$. The normalized reduced explosion pressures showed that all pressures were in the range of one third of the calculated pressures. In a next step it would be useful to reduce the venting area until reduced explosion pressures are in the range of the designed vessel strength. This should allow a better evaluation of a potential different behavior of the dusts. Finally explosion experiments with pneumatic filling, which is a commonly used filling method, should be carried out in order to evaluate the influence of dustiness under working conditions. The explosion experiments with pneumatic filling can show the influence of dustiness and can be compared to the worst-case setup for a conservative approach.

# 7 Numerical simulations

The numerical part deals with the simulation of dust/air mixtures. Especially modeling of local dust concentration distributions in small and large vessels and the settling behavior of dust clouds is investigated.

The investigations include preliminary 2D studies of multiphase flow with the Euler/Euler and the Euler/Lagrange approach. Simulations consist of numerical calculation of terminal velocity, influence of shape factor and particle forces on determination of terminal velocities. Preliminary studies were followed by simulation of cloud settling in tube compared to experiments.

In the small-scale 75 L apparatus local dust distributions calculated with the Euler/Euler and Euler/Lagrange approach were compared to measurements. Additionally industrial scaled simulations were done for dust concentration distribution in a 50 m³ silo and determination of zones exceeding the lower explosion limit.

All simulations were carried out with ANSYS CFX R14 with maximum residual criteria of $10^{-3}$ and mass conservation target of 1 %. In order to simulate flows it is necessary to set boundary conditions. These boundary conditions have to be suitable physical conditions, which represent the problem to solve.

## 7.1 Preliminary simulations and sensivity studies for multiphase flow

In order to compare the Euler/Euler with the Euler/Lagrange approach as well as to investigate the shape factor and the influence of different particle forces in Euler/Lagrange method a simplified 2D model of the 75 L test apparatus (see chapter 5.1) was used. The model has a diameter of 300 mm and a height of approx. 1 m and was separated into 34053 computational mesh cells. The following boundary conditions were used. The particles were brought in through an inlet at the bottom for one second with a velocity of 0.5 m/s. All results were recorded after three seconds in which the particles fell down in the direction towards the bottom. The geometry and boundary conditions can be taken from Figure 7-1 and Table 7-1.

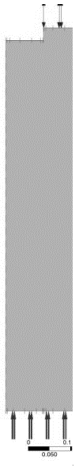

*Figure 7-1. 2D model.*

All simulations were done with drag force and gravity. The simulated particles have a specified diameter of 50 µm and a density of 1000 kg/m³.

Table 7-1. Boundary conditions 2D model.

| | value |
|---|---|
| cells | 34053 |
| minimum grid width (hexaeder) | 0.0002 m |
| maximum grid width (hexaeder) | 0.005 m |
| analysis type | transient |
| time step | 0.005 s |
| total time | 3 s |
| turbulence model | SST |
| fluid | air (25 °C) |
| solid | spherical particle |
| diameter | 50 µm |
| density | 1000 kg/m³ |
| reference pressure | 1 atm |
| inlet | velocity |
| air velocity (for 1 s) | 0.5 m/s |
| volume fraction solid (Euler) | 0.000475 |
| mass flow solid (Lagrange) | 0.00097419 kg/s |
| opening (Entrainment) | 0 bar |

### 7.1.1 Terminal velocity

The terminal velocity, which means the terminal velocity reached by a spherical particle due to gravity, can be estimated with a balance of forces [92, p. 43] $U_S = \frac{\rho_\beta d_\beta^2 g}{18\eta}$. The stationary sinking rate calculated with the Euler/Euler and Euler/Lagrange approach was compared to the analytical solution for one particle, which is approx. 7.5 cm/s. Figure 7-2 shows the averaged particle velocity for the analytical and numerical solutions. The Euler/Euler approach generates particle velocities, which are slightly smaller, whereas the Euler/Lagrange approach produces slightly higher particle velocities. The difference between analytical and numerical methods can be explained due to the fact that the air is not completely still. Besides, there is not just one particle and therefore the particles have an influence on the air flow and vice versa.

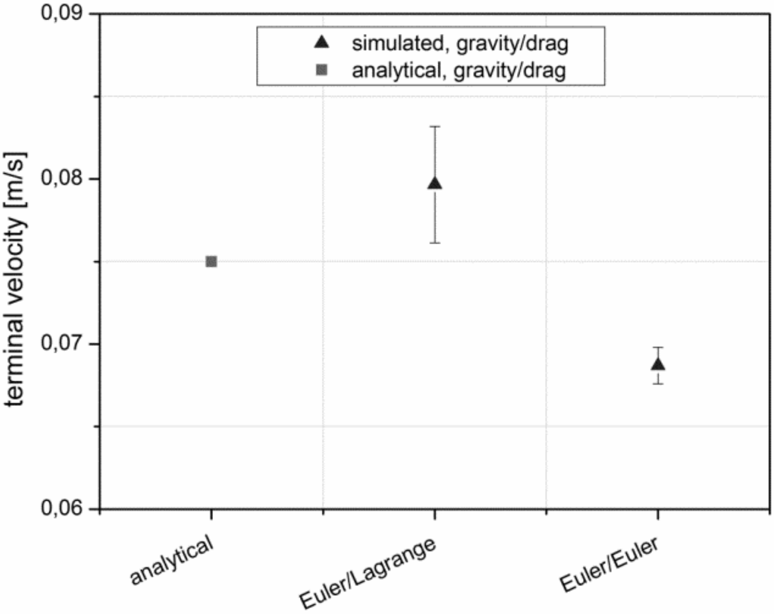

*Figure 7-2. Comparison of simulated and calculated terminal velocities.*

### 7.1.2 Terminal velocity with different shape factors

Simulation of solid particles depends on density and particle size as major influences on the behavior in the flow, but dusts can behave very differently in air even if they have comparable densities and sizes. This can be due to phenomena such as agglomeration, surface area or shape. In order to take the different dustiness into account a shape factor can be used. The factor is used to alter the surface, which lies in direction of the flow and therefore changes the drag force. For explanation of the shape factor in CFX see chapter 3.2.4. A factor of one stands for spherical particles. Different shape factors directly influence the particle velocity. So values higher than one lead to lower mean velocities. The influence of the particle shape on the particle velocity can be seen in Figure 7-3. Therefore the shape factor can be one part simulating different dustiness.

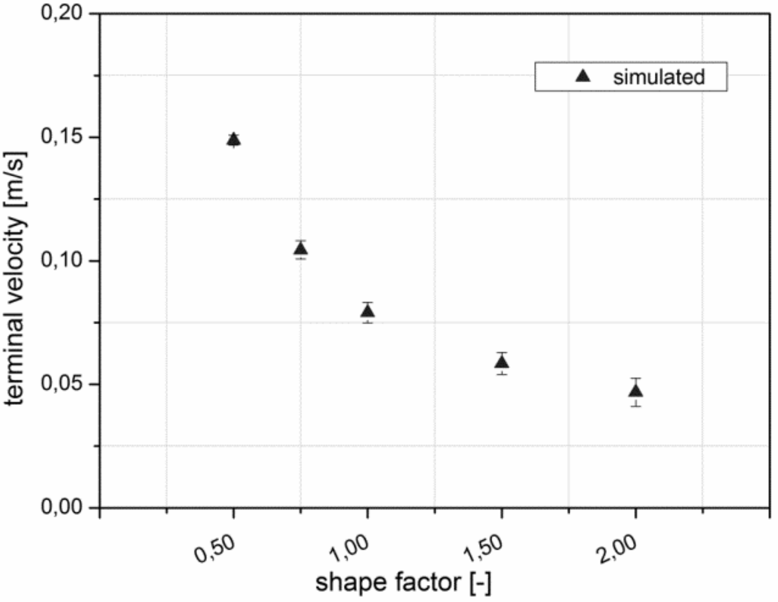

*Figure 7-3. Terminal velocities for different shape factors.*

### 7.1.3 Terminal velocity and additional forces

The motion of a particle is mainly influenced by drag and gravity as well as a possible air flow. This assumption is valid for the most technical dust/air mixtures. Nonetheless there are some additional forces and effects which may influence the particle behavior. As a result, not only drag and gravity were investigated but turbulent dispersion force, pressure gradient force and virtual mass force (see chapter 3.2.4). The diagram in Figure 7-4 shows the occurring and mean particle velocity for the different forces and all forces together. The turbulent dispersion force has substantial influence on the occurring particle velocities and the mean value. If the turbulent dispersion force is used, the pressure gradient and virtual mass force should be enabled as well because of a positive effect on the occurring particle velocities (see Figure 7-4).

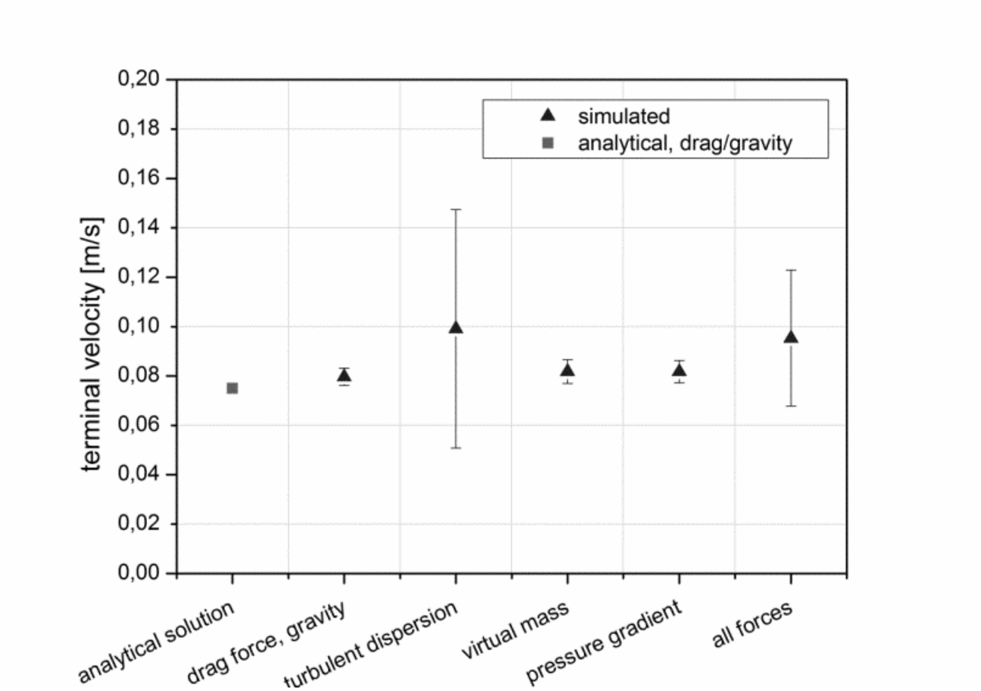

*Figure 7-4. Terminal velocities for different particle forces.*

Without the turbulent dispersion force they do not have much influence on the particle velocities. The pressure gradient force is important, if the densities of the two phases are similar, which is not the case for most dust/air mixtures. Table 7-2 shows an overview of the simulated particle forces.

Table 7-2. Terminal velocities with different particle forces.

| force/effect | |
|---|---|
| gravity | mandatory |
| drag force | mandatory |
| turbulent dispersion force | |
| pressure gradient force | |
| virtual mass force | |
| all forces | all above forces combined |
| analytical | calculated with balance of forces |

### 7.1.4 3D simulation of dust cloud settling

A vertical tube with 15 cm diameter and optical access was used to measure settling velocities of different dusts. Velocity was measured with laser Doppler anemometry. The averaged velocity (measurement time 5 s, see chapter 4.2.6) was compared to simulated ones. Simulations were optimized with the shape factor to model different dustiness or settling behavior of the tested dusts. Additionally a particle size distribution was assumed in the optimized simulations and in a last step additional particle forces and effects. 3D model, boundary conditions and grid can be found in Figure 7-5 and Table 7-3.

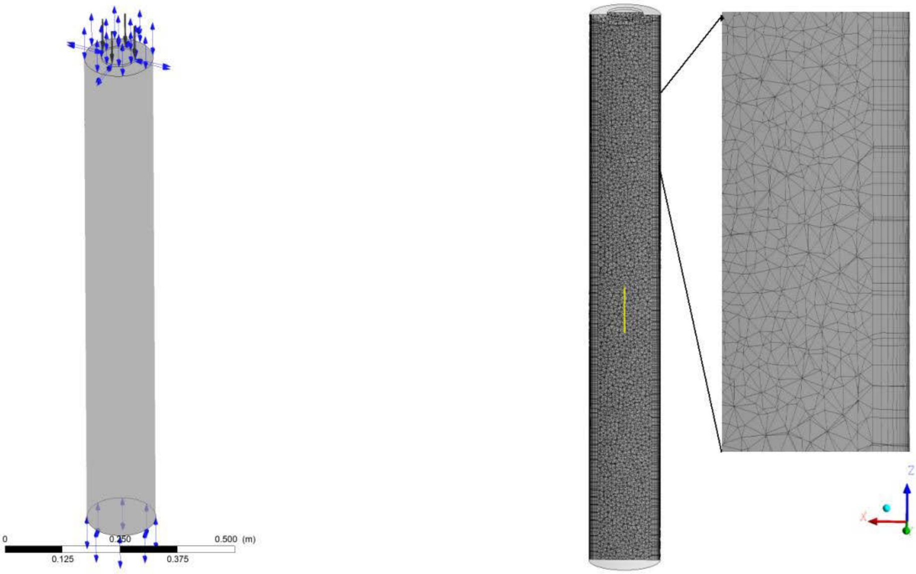

*Figure 7-5. Boundary conditions for 3D terminal velocity simulations.*

Table 7-3. Boundary conditions for 3D terminal velocity simulations

| | value |
|---|---|
| cells | 76561 |
| minimum grid width (tetraeder) | 0.005 m |
| maximum grid width (tetraeder) | 0.015 m |
| number of prism layers | 15 |
| height of first layer | 0.0003 m |
| prism layer growth | 1.3 |
| $y^+$(max) | <1 |
| analysis type | transient |
| time step | 0.01 s |
| turbulence model | SST |
| fluid | air (20 °C) |
| solid | maize starch/lignite/wheat flour/ milk powder/ wood/ potato starch (see chapter 4.2) |
| reference pressure | 1 atm |
| inlet | velocity |
| air mass flow (max) | 0.001 m/s |
| solid mass flow (Lagrange) | 0.0022 kg/s (zero slip velocity) |
| opening (entrainment) | 0 bar |

Experimental and numerical calculations were compared to an analytical estimation of the settling velocity according to $U_C = \left(\frac{4}{3}\,\frac{\rho_C d_C g}{C_D \rho_\alpha}\right)^{0.5} \approx \left(\frac{4}{3}\,\frac{0.61\frac{kg}{m^3} * 0.15\ m * 9.81\ m/s^2}{0.5 * 1.2\ kg/m^3}\right)^{0.5} \approx 1.41\ m/s.$

Where the drag coefficient $C_D$ is assumed as 0.5 in a first step and adjusted to 1.21 for cylindrical shapes as the shape of the test apparatus in a second step [93]. Settling velocity for a spherical dust cloud of 0.15 m is 1.14 m/s and for a cylindrical cloud is 0.91 m/s. Calculated and measured velocities of the six tested dusts can be found in Table 7-4.

*Table 7-4. Comparison of settling velocities*

| dust | analytical (cloud) $C_D$=0.5 in m/s | analytical (cloud) $C_D$=1.21 in m/s | measured (LDA) in m/s | Simulation (Euler/Lagrange approach) in m/s |
|---|---|---|---|---|
| wheat flour (DG1) | 1.41 | 0.91 | 0.853 | 1.368 |
| wood (DG 2) | 1.41 | 0.91 | 0.457 | 1.432 |
| skimmed milk powder (DG 3) | 1.41 | 0.91 | 0.649 | 0.705 |
| maize starch (DG 4) | 1.41 | 0.91 | 0.422 | 0.598 |
| lignite (DG 6) | 1.41 | 0.91 | 0.408 | 0.647 |
| potato starch (DG 6) | 1.41 | 0.91 | 0.689 | 1.463 |

Settings for the three optimized simulations (OS) 1-3 including shape factor and particle size distribution are shown in Table 7-5. Additional effects in OS3 were binary collisions and turbulent dispersion force.

*Table 7-5. Settings for optimized simulations.*

| dust | LDA in m/s | shape factor OS1 / OS2 | shape factor OS3 | Particle size distribution (min;med; max) in µm |
|---|---|---|---|---|
| wheat flour | 0.853 | 2.0 | 6.0 | (10;60;160) |
| wood | 0.457 | 2.5 | 10.0 | (80;260;500) |
| skimmed milk powder | 0.649 | 1.3 | 3.0 | (10;45;100) |
| maize starch | 0.422 | 1.3 | 3.9 | (10;14;25) |
| lignite | 0.408 | 2.0 | 4.0 | (4;38;230) |
| potato starch | 0.689 | 2.5 | 10.0 | (20;45;80) |

Simulations showed that the simulation of gravity and drag for one specific particle size does not lead to satisfying results (see Figure 7-6). The implementation of a shape factor, which means to alter the specific surface, a particle size distribution and additional forces improve the results significantly in some cases, especially for dusts with larger median diameters.

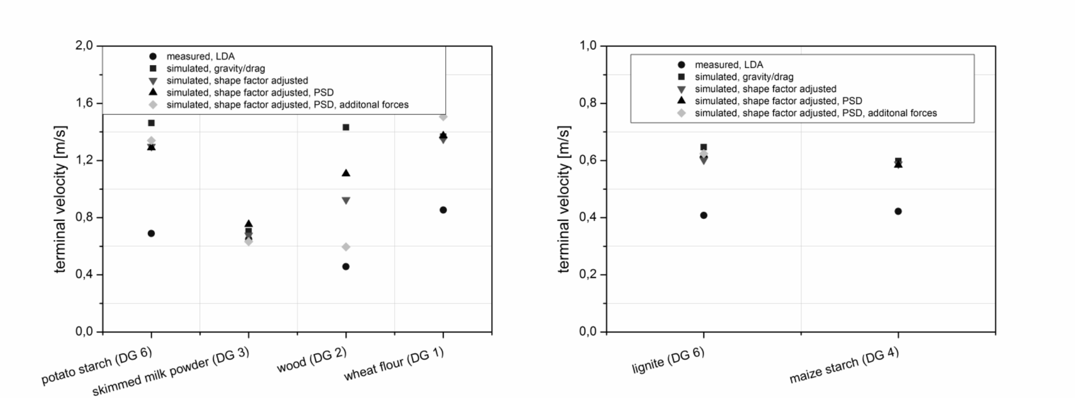

*Figure 7-6. Measured and simulated dust cloud settling velocities.*

An overview over the simulation results is given in Table 7-4. It consists of the averaged velocities of all optimized simulations (OS) compared to the initial simulations, which produced settling velocities higher than the measured velocities for all tested dusts, and to the measured values. Results could be improved especially for wood and potato starch. Simulation of milk powder showed good results from the beginning. Simulation of particles smaller than 50 µm (e.g. maize starch and lignite) showed the biggest discrepancies between simulation and measurement. Improvement could not be achieved or not much improvement. Density, shape factor and particle size distribution are therefore sufficient as input parameter for larger particles (approx. bigger than 100 µm) only. For small particles further modifications are needed such as modification of drag coefficient or modeling of agglomeration.

*Table 7-6. Results of simulated dust cloud settling velocities.*

| dust | simulation in m/s | OS1 in m/s | OS2 in m/s | OS3 in m/s | LDA in m/s |
|---|---|---|---|---|---|
| wheat flour | 1.368 | 1.350 | 1.374 | 1.333 | 0.853 |
| wood | 1.432 | 0.926 | 1.107 | 0.637 | 0.457 |
| skimmed milk powder | 0.705 | 0.677 | 0.753 | 0.753 | 0.649 |
| maize starch | 0.598 | 0.588 | 0.584 | 0.581 | 0.422 |
| lignite | 0.647 | 0.602 | 0.620 | No solution | 0.408 |
| potato starch | 1.463 | 1.299 | 1.290 | 0.813 | 0.689 |

### 7.1.5 Conclusion - preliminary studies

Detailed simulations of dust/air mixtures without major modifications of the code are only possible with the Euler/Lagrange approach. It allows determining local dust concentrations by taking many particle phenomena such as particle size distribution, particle shape (surface area) and particle collisions into account. For high dust concentrations the Euler/Euler approach or a porous media approach is necessary.

The shape factor (influences surface area in the flow) can be used as one tool to simulate different dustiness for otherwise almost identical dusts. Further modifications are needed to better model different dustiness.

The settling velocities of dust clouds due to gravity can only be simulated with a high uncertainty. Only 2D simulations with few particles showed comparable results to the analytical solution. Real scenarios need to be set up carefully with a shape factor or further modifications to improve the settling behavior due to gravity. One approach to optimize the particle behavior might be to adapt the drag coefficient depending on the particle Reynolds number as done by **Morsi et al**. [94] and to implement agglomeration processes. Nonetheless the settling velocities of different dusts, even with similar particle sizes, can differ very much depending on the material properties/dustiness and flow or test methods. Especially for particles smaller than 50 µm results differ very much from measured velocities.

## 7.2 Simulation of 75 L apparatus

A detailed CAD model of the 75 L apparatus, see chapter 5.1, was created. The model was designed in SolidEdge R16 and a negative was converted to ANSYS CFX in order to model the flow regime. CAD and CFD model are shown in Figure 7-7.

*Figure 7-7. CAD model (left) and CFD model (right).*

The model has a diameter of 300 mm and a height of approx. 1.2 m as the original apparatus.

The dispersion of the dust (optional) and influx of the air is simulated with an inlet at the bottom and a mass flow. Four outlets are located at the top as in the experiments. Closing of the valves was modeled with a time-depending expression. Figure 7-8 shows the apparatus with boundary conditions, inlet at the bottom and outlets at the top to avoid overpressures.

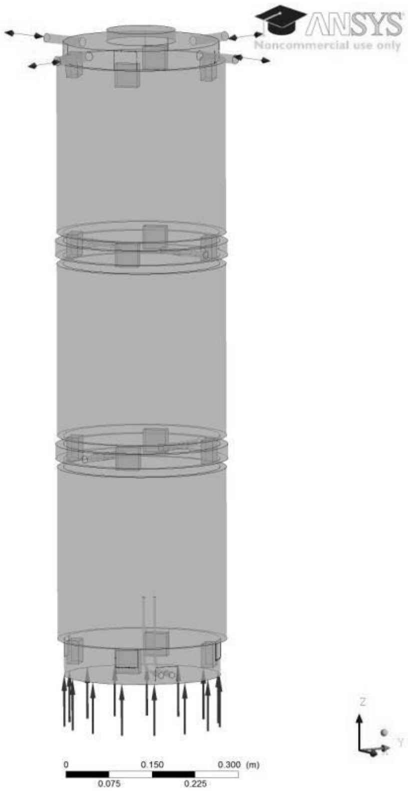

*Figure 7-8. Simulation of 75 L boundary conditions.*

Table 7-7 shows settings and boundary conditions of the 3D model of the 75 L apparatus.

Table 7-7. Settings 3D model of 75 L apparatus.

| | value |
|---|---|
| cells | 3392701 |
| minimum grid width (tetraeder) | 0.001 m |
| maximum grid width (tetraeder) | 0.02 m |
| number of prism layers | 15 |
| height of first layer | 0.0008 m |
| prism layer growth | 1.3 |
| $y^+$(max) | <2 |
| Inlet | mass flow |
| mass flow air (max) | 0.0532 kg/s |
| opening (entrainment) | 0 bar |

### 7.2.1 Grid independence

Grid independence was investigated with a stationary air flow and three grids. The finest grid was taken as best solution, since there is no exact solution and results should tend to the exact solution of the numerical approach. Difference to the coarser grids is evaluated for velocity. This is done over the diameter and the height for one line each and for all grids errors are calculated globally. The meshing tool ANSYS ICEM CFD was used to create the grids. After creating the finest grid the other two were generated with a „global scale factor“ (*gsf*), which can be used to scale cell sizes. More information on how to prove grid independence is explained by **Shyy et al**. [95, pp. 139-164].

Information on setup and boundary conditions can be found in Figure 7-8 and Table 7-8.

Table 7-8. Simulation parameters for grid independence.

| grid | fine | middle | raw |
|---|---|---|---|
| global scale factor | 1 | 3 | 6 |
| cells | 3392701 | 2403041 | 1101983 |
| nodes | 1413444 | 997143 | 427483 |
| minimum grid width | 0.001 m x global scale factor | | |
| maximum grid width | 0.02 m x global scale factor | | |
| $y^+$(max) | <2 | <3 | <4 |
| max. residuum | 0.0001 | | |
| mass flow | 0.0532 kg/s | | |
| opening (entrainment) | 0 bar | | |

Simulated velocities for all three grids are shown as function of normalized diameter in the middle of the apparatus (left) and height (right), Figure 7-9. All Grids show comparable results.

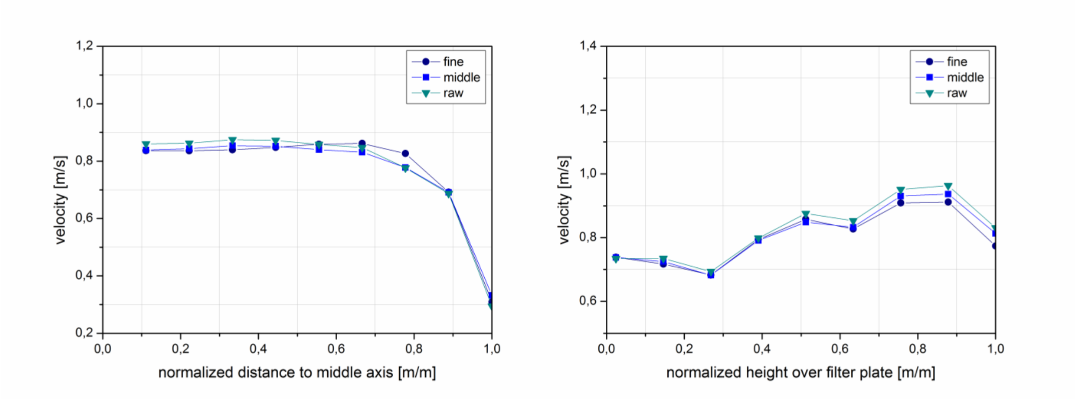

*Figure 7-9. Velocity as function of diameter (left) and height (right).*

Figure 7-10 shows the simulated velocities of the coarser and coarsest grid as function of the velocities of the finest grid. All velocities differ only up to 5 % from the finest grid.

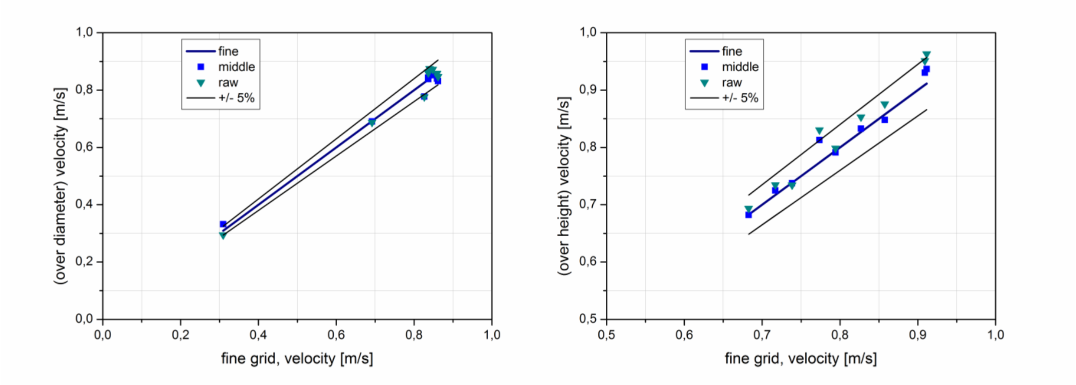

*Figure 7-10. Velocity as function of velocity of fine grid, diameter (left) and height (right).*

In order to evaluate the grid dependence of the solution the simulated velocities U and the velocity in main direction of the flow $u_Z$ were compared between the three grids globally. Therefore three values were defined, 1-norm, 2-norm and max-norm, which can be calculated according to the following equations 36 to 38.

$$\|\boldsymbol{U}\|_1 = \frac{1}{N}\sum_{k=1}^{N} f_k$$ ***eq. 36***

$$\|\boldsymbol{U}\|_2 = \sqrt{\frac{1}{N}\sum_{k=1}^{N} f_k^2}$$ ***eq. 37***

$$\|\boldsymbol{U}\|_{max} = \boldsymbol{max}(\boldsymbol{f_k}) \qquad \textit{\textbf{eq. 38}}$$

1-norm means the average error over all nodes, 2-norm is the average squared error and max-norm is the maximum error in the regime. The error $f_k$ can be calculated according to eq. 39.

$$\boldsymbol{f_k} = \left|\boldsymbol{U_{k,fein}} - \boldsymbol{U_{k,gsf}}\right| = \sqrt{\sum_{i=1}^{3}\left(\boldsymbol{u_{i,k,fein}} - \boldsymbol{u_{i,k,gsf}}\right)^2} \qquad \textit{\textbf{eq. 39}}$$

In order to evaluate the error the difference between the velocity at a node k of the fine grid is compared to that of the coarser grid. Therefore the grid dependence of the solution can be estimated, even without a precise solution.

Table 7-9 shows the calculated errors for the velocity U and for the velocity component $u_Z$ in main direction of the flow compared to the solution of the finest grid.

Table 7-9. Overview of error in comparison to finest grid.

| grid | fine | middle | raw |
|---|---|---|---|
| 1-norm (U) | - | 0.000908 | 0.00179 |
| 1-norm ($u_Z$) | - | 0.000035 | 0.0005 |
| 2-norm (U) | - | 0.00924 | 0.0131 |
| 2-norm ($u_Z$) | - | 0.00751 | 0.0105 |
| max-norm (U) | - | 0.0515 | 0.0517 |
| max-norm ($u_Z$) | - | 0.0400 | 0.0515 |

A graphical evaluation showed that the largest differences were located at the outlet tubes, which are closed most of the time in the following simulations.

In conclusion the solution develops towards a convergent result. All following simulations were done with the finest grid to achieve the best results.

### 7.2.2 Comparison of Euler/Euler and Euler/Lagrange approach

Experiments with the 75 L apparatus and maize starch were simulated with the Euler/Lagrange and Euler/Euler approach. This was used to evaluate both models regarding their quality to simulate dust/air mixtures in vessels. The setup was dispersion with the filter plate (see chapter 5.1.1). Boundary conditions and settings were chosen according to the experiments and can be found in Table 7-10 and Table 7-11. Air and dust were injected with a mass flow inlet for two seconds. Outlet valves closed after four seconds.

Table 7-10. Parameter for comparison of Euler/Euler and Euler/Lagrange approach.

| parameter | |
|---|---|
| cells | 3392701 |
| smallest grid width (Tetraeder) | 0.001 m |
| largest grid width (Tetraeder) | 0.02 m |
| number of prism layers | 15 |
| height of first layer | 0.0008 m |
| growth rate | 1.3 |
| $y^+$(max) | <2 |
| calculation scheme | transient |
| time step | 0.005 s |
| total time | 20 s |
| turbulence model | SST |
| fluid | air |
| solid | maize starch (see Table 7-11) |
| reference pressure | 1 atm |
| inlet | Mass flow |
| mass flow air | 0.0532 kg/s (for 2 s) |
| volume fraction (Euler) | 0.000679 (for 2 s) |
| mass flow solid (Lagrange) | 0.0175 kg/s (for 2 s) |
| opening (entrainment) | 0 bar |

Dust concentrations were compared at the measurement locations. Additionally dust concentrations were graphically compared.

*Table 7-11. Material data, maize starch.*

| maize starch | |
|---|---|
| density | 1502 kg/m³ |
| median diameter | 14 µm |
| d(0.1) | 10 µm |
| d(0.9) | 25 µm |

The following figures Figure 7-11, Figure 7-12, Figure 7-13 and Figure 7-14 show the simulated dust concentrations over time on a plane through the middle of the 75 L apparatus.

Results of the Euler/Euler approach are on the left and results of the Euler/Lagrange approach on the right side.

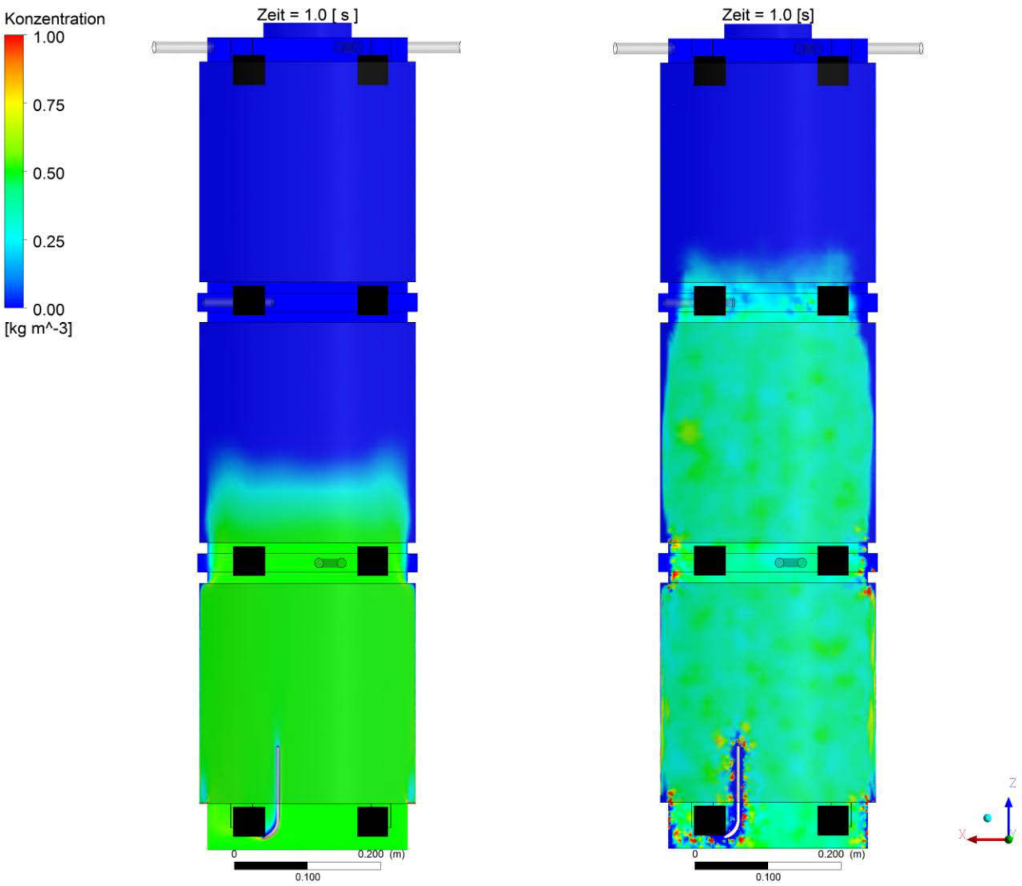

*Figure 7-11. Dust concentration after 1 s, Euler/Euler (left) and Euler/Lagrange (right).*

Figure 7-11 shows that the dust spreads faster in the apparatus with the Euler/Lagrange approach compared to the Euler/Euler approach, despite comparable setups.

Figure 7-12 shows that the dust spreads out more in the apparatus for the Euler/Lagrange approach. Simulated dust distribution with the Euler/Euler approach looks more like two liquids with different densities; this is due to the mathematical method.

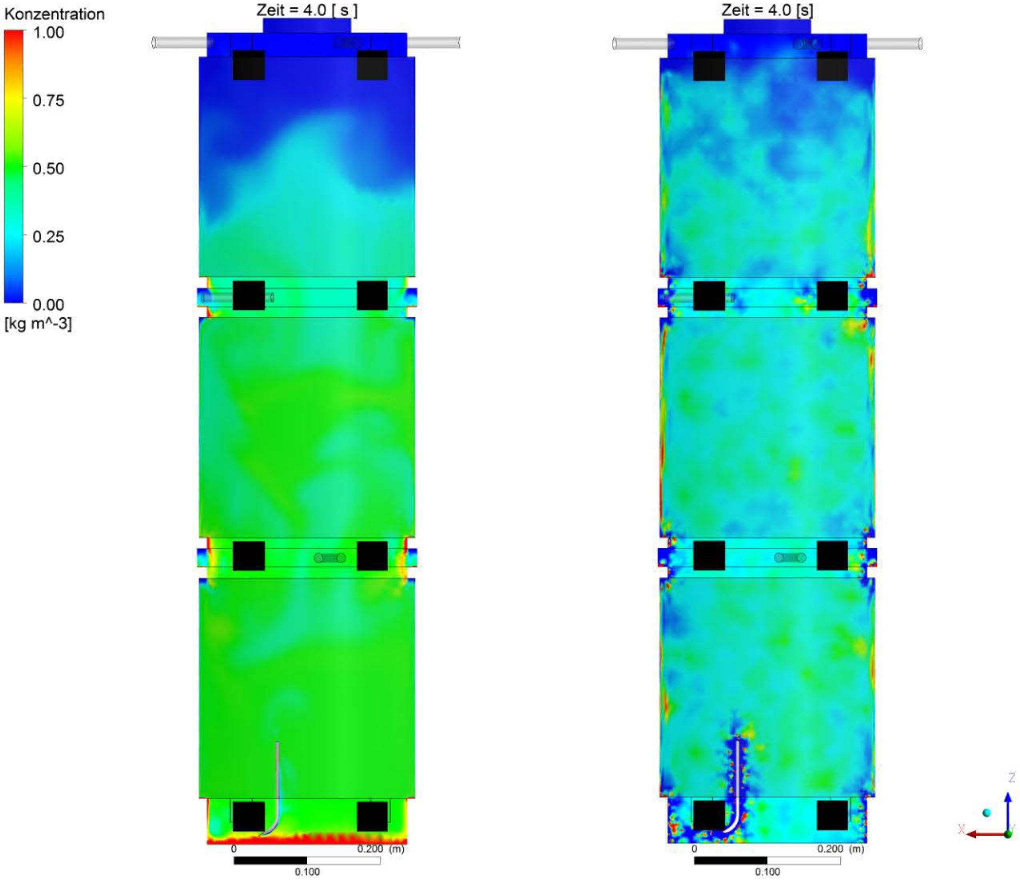

*Figure 7-12. Dust concentration after 4 s, Euler/Euler (left) and Euler/Lagrange (right).*

Dust distribution with the Euler/Lagrange approach (Figure 7-13, right) shows more local differences than that of the Euler/Euler approach.

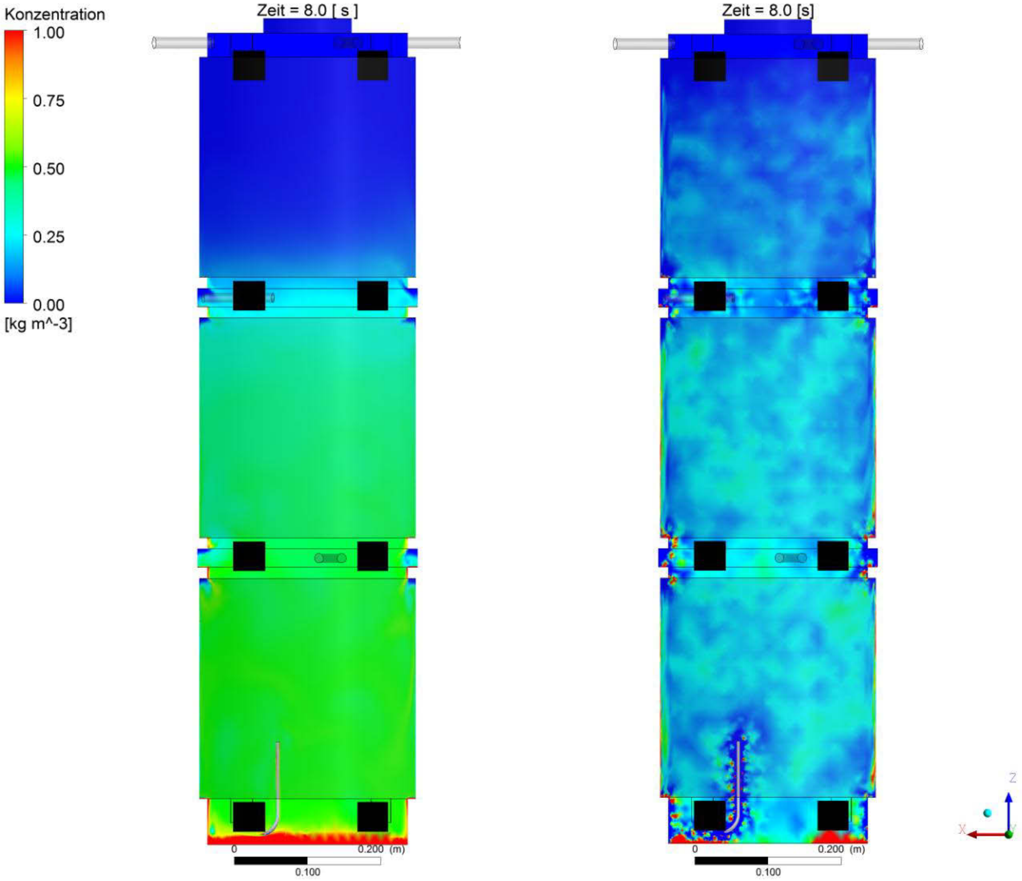

*Figure 7-13. Dust concentration after 8 s, Euler/Euler (left) and Euler/Lagrange (right).*

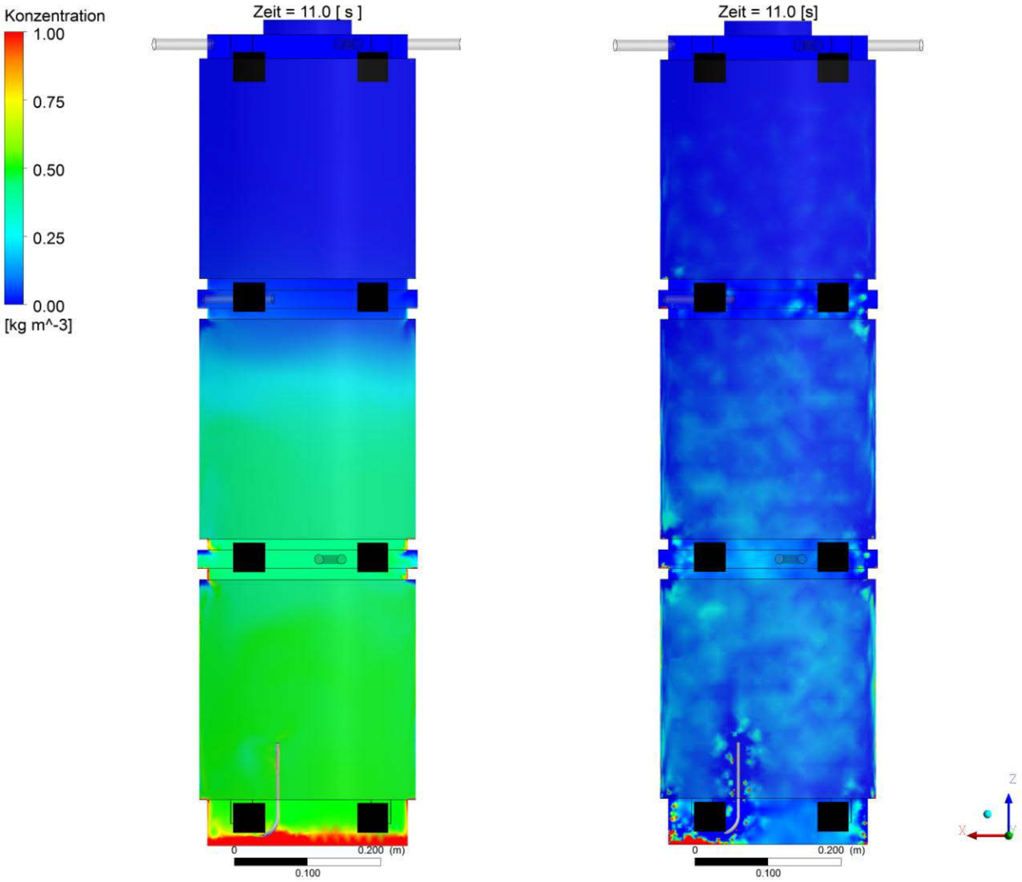

*Figure 7-14. Dust concentration after 11 s, Euler/Euler (left) and Euler/Lagrange (right).*

After 11 seconds only little dust is in the air with the Euler/Lagrange approach, Figure 7-14 right. Dust is only slowly retreating with the Euler/Euler approach. This effect can be seen in the diagrams in Figure 7-15 (left) as well. Dust concentration for the lower sensor stays high, when simulated with the Euler/Euler approach. The simulated dust concentrations at the upper location are in good agreement for both approaches (on the right).

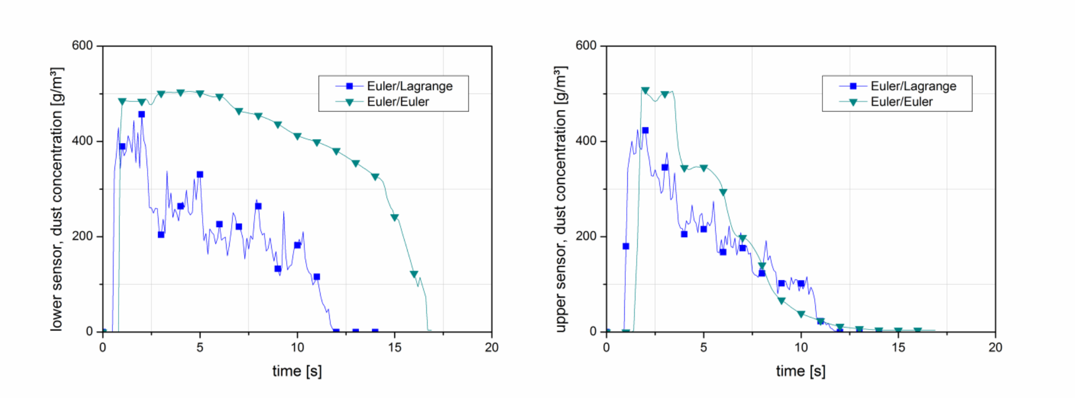

*Figure 7-15. Comparison of simulated dust concentrations with Euler/Euler and Euler/Lagrange approach at measurement locations (lower, left and upper, right).*

Figure 7-16 shows the simulated dust concentrations compared to the measured concentrations at the lower (left) and upper location (right). The fluctuations of the local dust concentration can only be seen for the Euler/Lagrange approach.

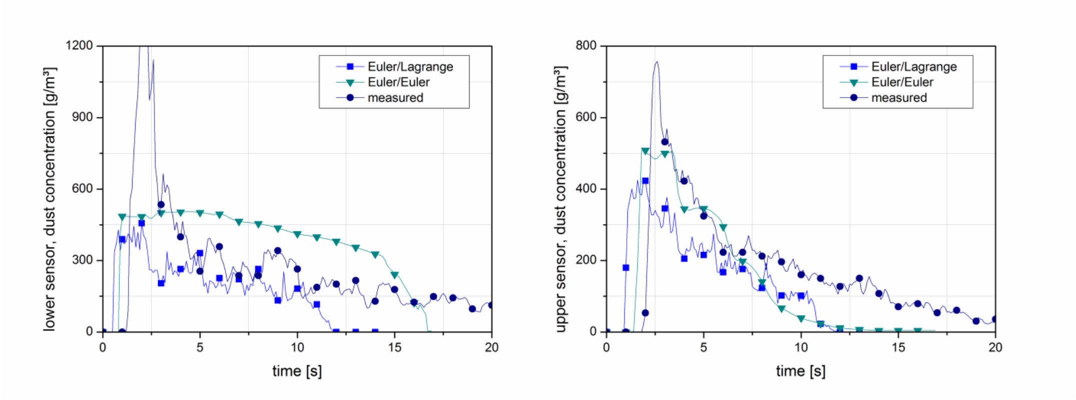

*Figure 7-16. Comparison of simulated dust concentrations with Euler/Euler and Euler/Lagrange approach at measurement locations (lower, left and upper, right) to measured dust concentrations.*

Figure 7-17 shows the measured and simulated dust concentrations at (theoretical) ignition time. Results for both approaches differ from the measured values. The Euler/Lagrange approach has better agreement for comparable concentrations at the two locations.

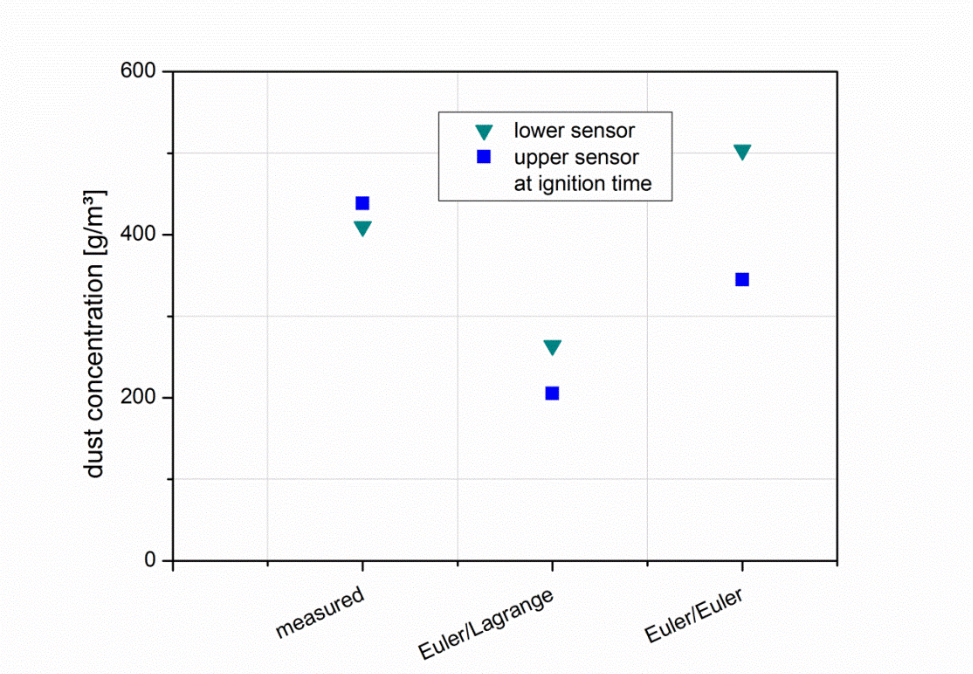

*Figure 7-17. Comparison of simulated and measured dust concentrations at (theoretical) ignition time.*

### 7.2.3 Conclusion - simulation of 75 L apparatus

A comparison of Euler/Euler and Euler/Lagrange approach in order to evaluate simulation capabilities of both approaches regarding dust/air mixtures, especially local dust distribution, showed general differences. The Euler/Euler approach, which treats both phases as fluids, leads to a homogenous distribution of the dispersed dust, nearly without local differences. Dust distribution simulated with the Euler/Lagrange approach in the 75 L apparatus looks more natural with local peaks and lows of dust concentration. Comparison to measured data showed differences for both approaches, but the uncertainties of the measurement with the dust concentration meters have to be taken into account. The devices were especially sensitive to the filling process (approx. first three seconds). Both approaches need further modification to better model dust concentration as a function of time. The Euler/Lagrange approach allows for particle size distributions with particle collisions, further particle forces and the particle shape factor as proposed in chapter 7.1.2. The Euler/Lagrange approach is used in all following simulations with particle size distribution, additional particle forces, binary collisions and a material depending shape factor.

In a next step measured data with improved dust concentration meters is compared to simulated dust concentrations in a large vessel.

## 7.3 Simulation of dust dispersion in the 50 m³ Silo

In process industries dust is often handled in large quantities and vessels of all sizes. A 50 m³ silo is modeled with two different filling processes and measured and simulated dust concentrations over time are compared. One setup is a homogenous injection with eight nozzles as worst-case scenario with a homogenous dust cloud and high turbulence. As second setup pneumatic filling at top is used as found in process industries. In a last step three configurations are compared regarding parts of the vessel where the lower explosion limit is exceeded (see [96]).

### 7.3.1 Simulation of homogenous injection

Filling of the silo was modeled for 15 s with a theoretical concentration of 100 g/m³. Dust was injected at eight positions. An Euler/Lagrange approach is used to model the dispersion of maize starch. The input of parameter studies and simulation of dust cloud settling is used to adapt maize starch input parameters (see Table 7-12 and chapter 0). An unstructured mesh was used. Figure 7-18 shows grid and measurement locations (right) and injection points (left).

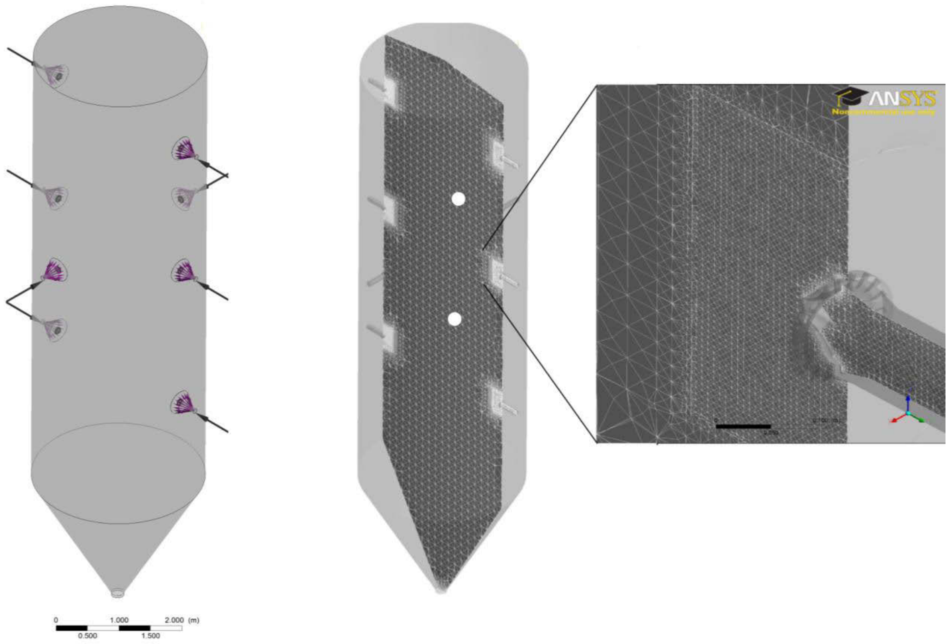

*Figure 7-18. Homogenous injection, boundary conditions and mesh.*

A schematic of the silo and measurement locations can be seen in Figure 7-18.

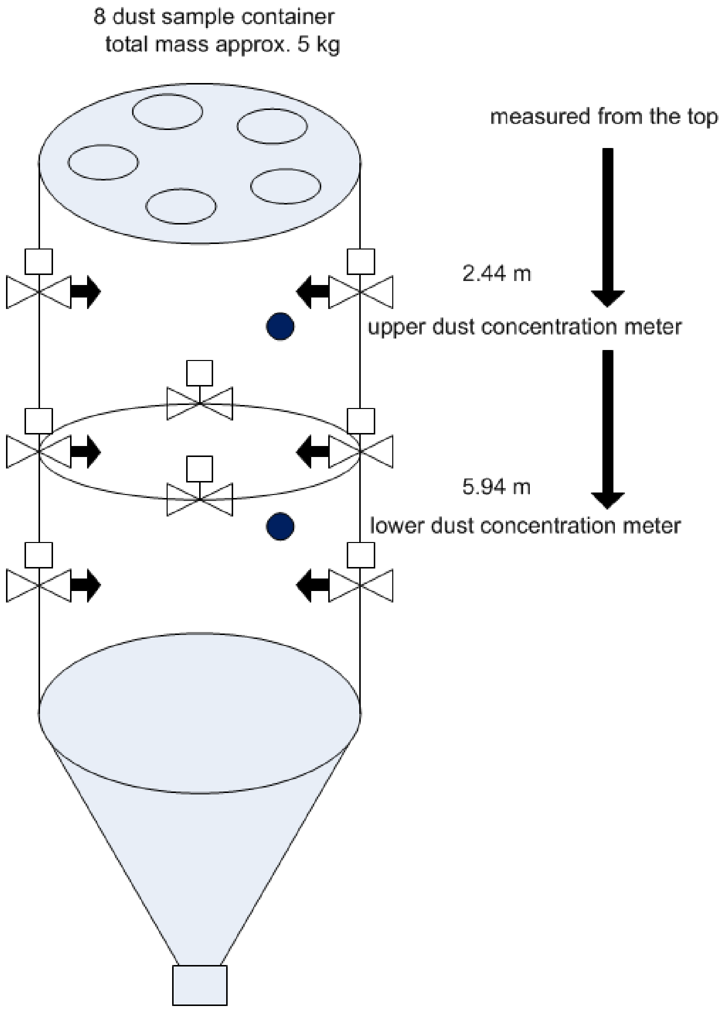

*Figure 7-19. Silo with homogenous injection, schematic.*

Table 7-12. Maize starch.

| maize starch | |
|---|---|
| density | 1502 kg/m³ |
| median diameter | 14 µm |
| d(0.1) | 10 µm |
| d(0.9) | 25 µm |
| shape factor | 3.9 |

Table 7-12 shows density, particle size distribution and shape factor as used to describe maize starch in the simulations.

All eight nozzles were modeled as in reality. Figure 7-20 and Figure 7-21 show the modeled nozzle with injection of dust.

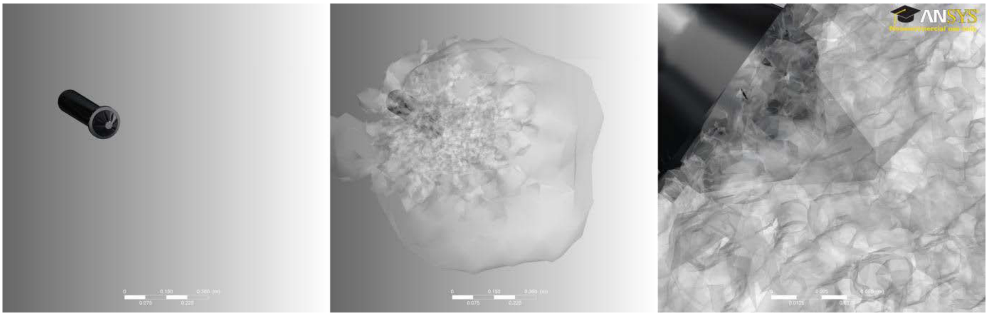

*Figure 7-20. Nozzle with injection of maize starch.*

The nozzle was developed to allow dust dispersion in all direction simultaneously. Figure 7-20 shows the nozzle at start of simulation (left) and after 0.5 seconds. Dust concentrations of 500 g/m³ and above are shown. The same concentration range is shown in Figure 7-21 as point cloud.

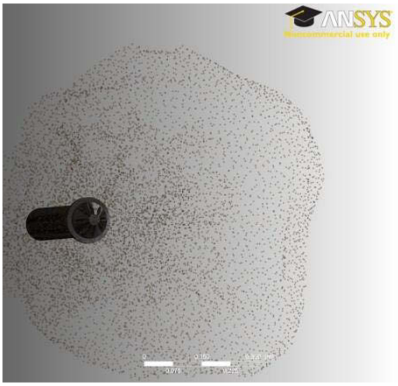

*Figure 7-21. Injected dust as point cloud.*

Table 7-13 shows the settings of the simulations. Dust is injected for one second at eight locations with a total mass of five kilograms. Turbulence was modeled with a shear stress (SST) model.

Table 7-13. Simulation parameters, homogenous injection, 50 m³ Silo.

| parameter | |
|---|---|
| cells | 8524039 |
| smallest grid width (Tetraeder) | 0.001 m |
| largest grid width (Tetraeder) | 0.25 m |
| number of prism layers | 15 |
| height of first layer | 0.008 m |
| growth rate | 1.3 |
| $y^+$(max) | <2 |
| calculation scheme | transient |
| time step | 0.01 s |
| total time | 15 s |
| turbulence model | SST |
| fluid | air |
| solid | maize starch |
| reference pressure | 1 atm |
| inlet | velocity |
| velocity of air (max) | 36 m/s |
| injection time | 1 s |
| mass flow solid | 0.625 kg/s each nozzle |

Figure 7-22 shows the velocity field in the silo in the first eight seconds of injection.

*Figure 7-22. Velocity from second 1 to second 8, homogenous injection.*

Figure 7-23 and Figure 7-24 show a comparison of measured and calculated dust concentrations at two measurement locations. A general agreement of dust concentration over time could be achieved. Simulated values are slightly lower than the measured average most of the time.

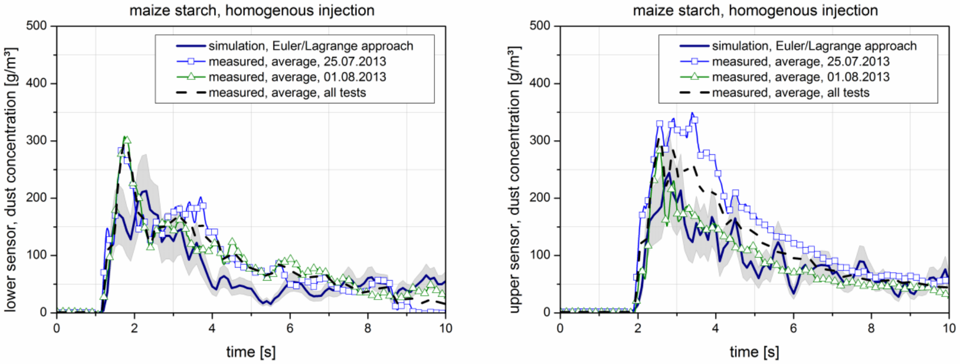

*Figure 7-23. Measured and simulated dust concentration at lower (left) and upper (right) location.*

,

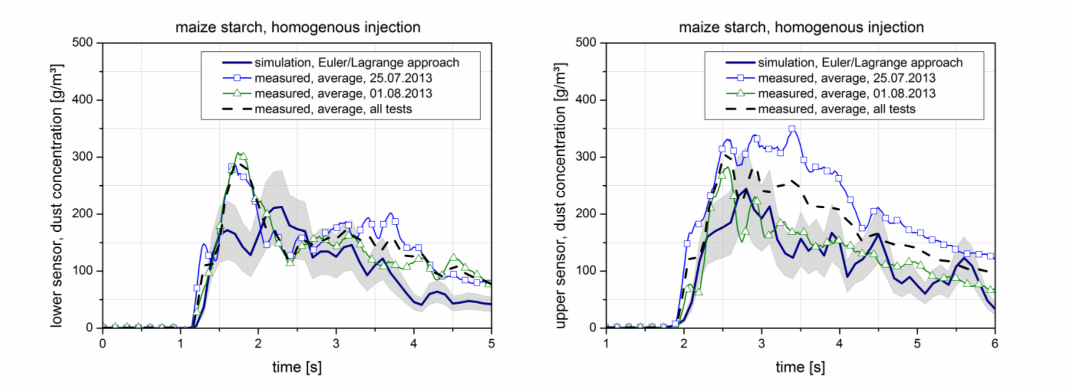

*Figure 7-24. Measured and simulated dust concentration at lower (left) and upper (right) location, section of time.*

With means of CFD it is possible to evaluate local dust concentrations in vessels. This allows pointing out areas where the lower explosion limit (LEL) is exceeded. This could help to develop filling methods, for which the LEL is not reached in most of the vessel.

Figure 7-25 and Figure 7-26 show the development of dust concentrations at LEL and two times LEL for four seconds for homogenous injection into the silo. Only five kilograms of maize starch are sufficient to fill large parts with an explosive dust/air mixture just above LEL. After four seconds dust concentrations are below two times LEL in most parts of the vessel, see Figure 7-26 (lower row).

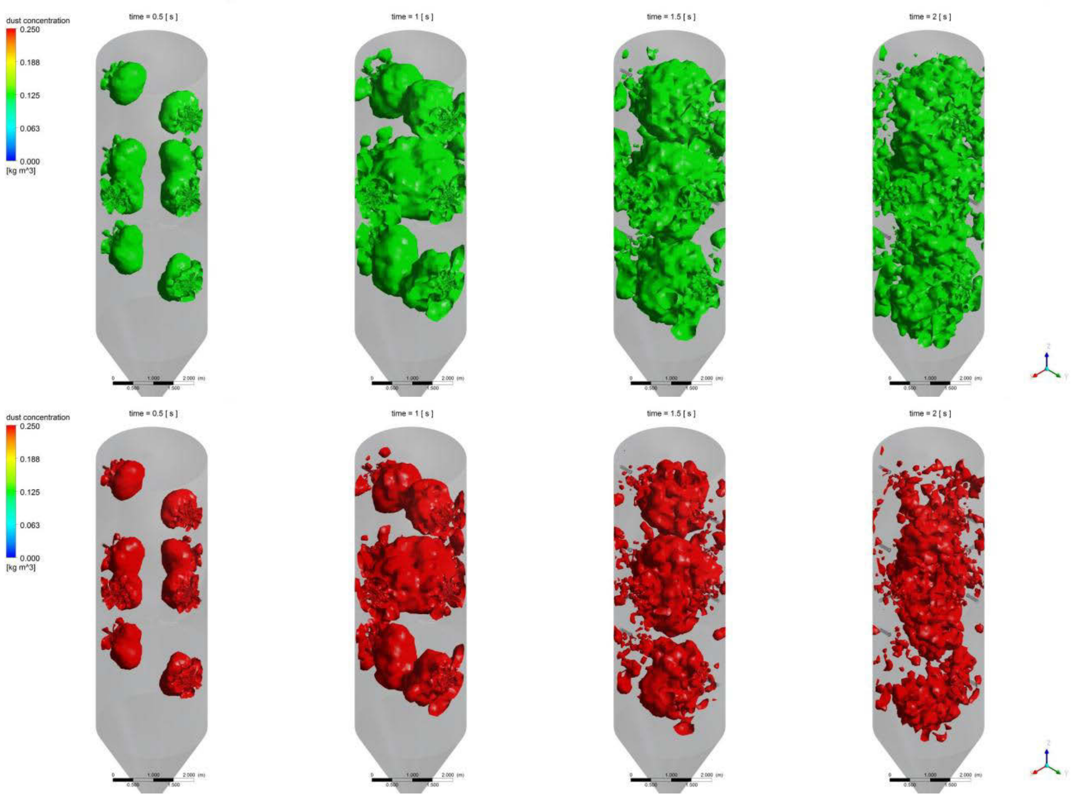

*Figure 7-25. Homogenous injection, development of volume with dust concentrations at LEL (upper row) and two times LEL (lower row) for first two seconds.*

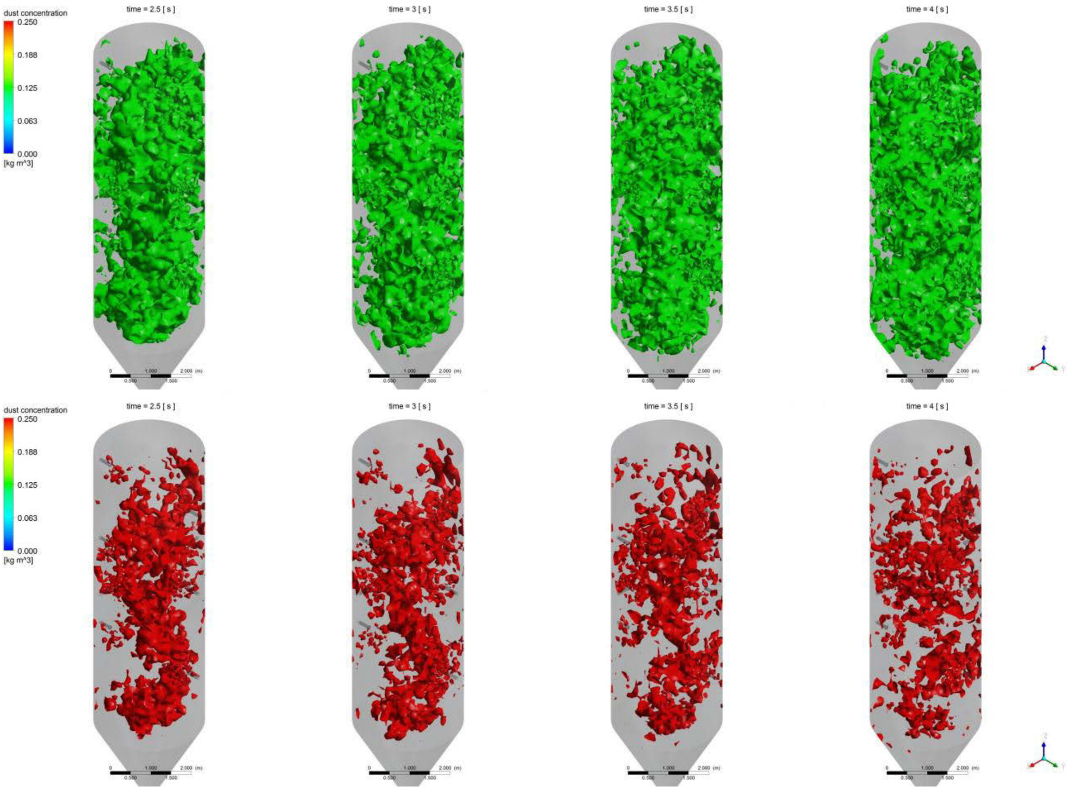

*Figure 7-26. Homogenous injection, development of volume with dust concentrations at LEL (upper row) and two times LEL (lower row) for 2 to 4 seconds after injection.*

### 7.3.2 Simulation of pneumatic filling

Pneumatic filling of the silo was modeled for 15 s with a theoretical concentration of 200 g/m³. Dust was injected at the top for six seconds. An Euler/Lagrange approach is used to model maize starch. The input of parameter studies and simulation of dust cloud settling is used to adapt maize starch input parameters (see Table 7-12 and chapter 0). The setup with measurement locations and grid can be seen in Figure 7-27 and Figure 7-28. A structured mesh was used.

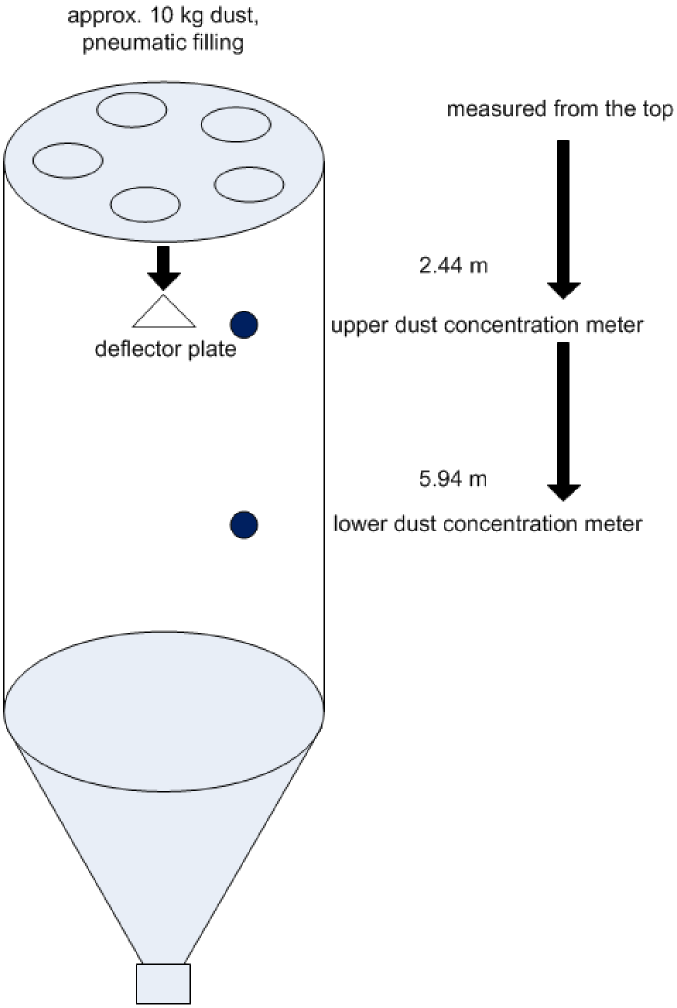

*Figure 7-27. Silo with homogenous injection, schematic.*

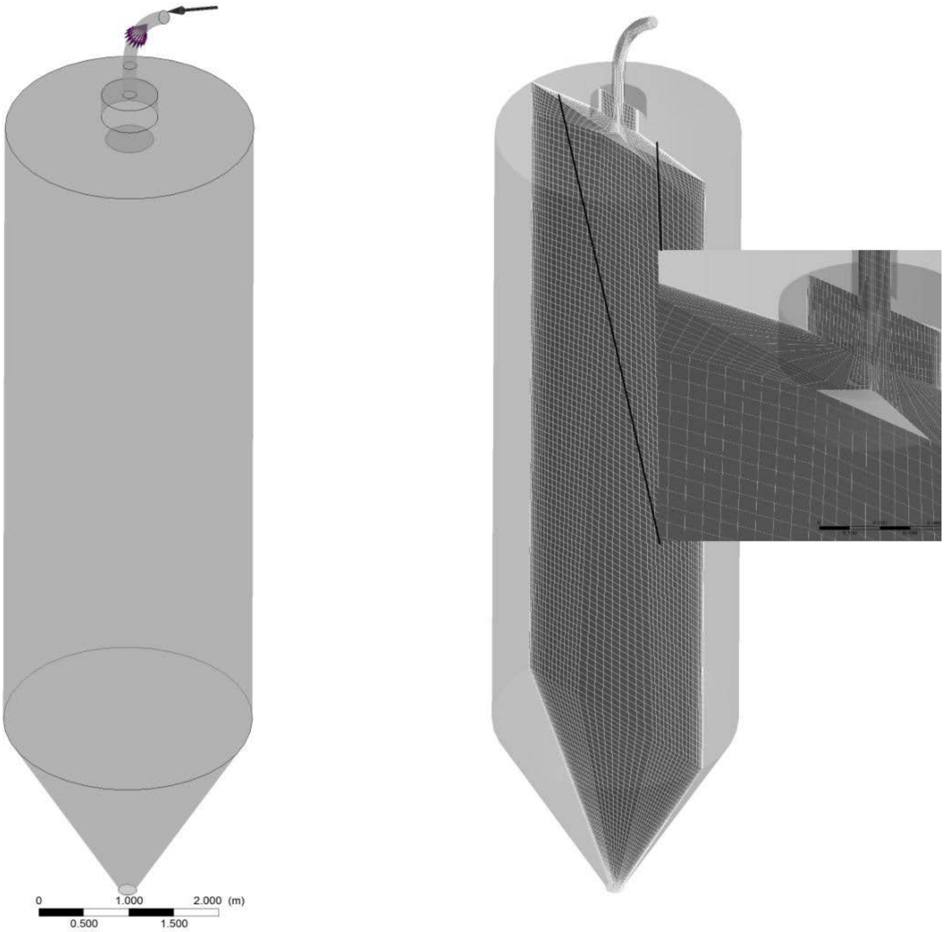

*Figure 7-28. Pneumatic filling, boundary conditions and mesh.*

Table 7-14 shows the settings of the simulations. Dust is injected for one second at eight locations with a total mass of five kilograms. Turbulence was modeled with a shear stress (SST) model.

*Table 7-14. Simulation parameters, pneumatic filling, 50 m³ Silo.*

| parameter | |
|---|---|
| cells | 164223 |
| smallest grid width (hexaedra) | 0.0075 m |
| largest grid width (hexaedra) | 0.25 m |
| height of first layer | 0.0001 m |
| number of prism layers/ growth rate | 15 /1.3 |
| $y^+$(max) | <2 |
| calculation scheme | transient |
| time step | 0.01 s |
| total time | 15 s |
| turbulence model | SST |
| fluid | air |
| solid | maize starch |
| reference pressure | 1 atm |
| inlet | mass flow |
| mass flow air | 0.0532 kg/s |
| conveying time | 6 s |
| mass flow solid | 1.665 kg/s |
| opening (at bottom cone during filling) | 0 bar |

Figure 7-29 shows the velocity field in the silo in the first eight seconds of injection.

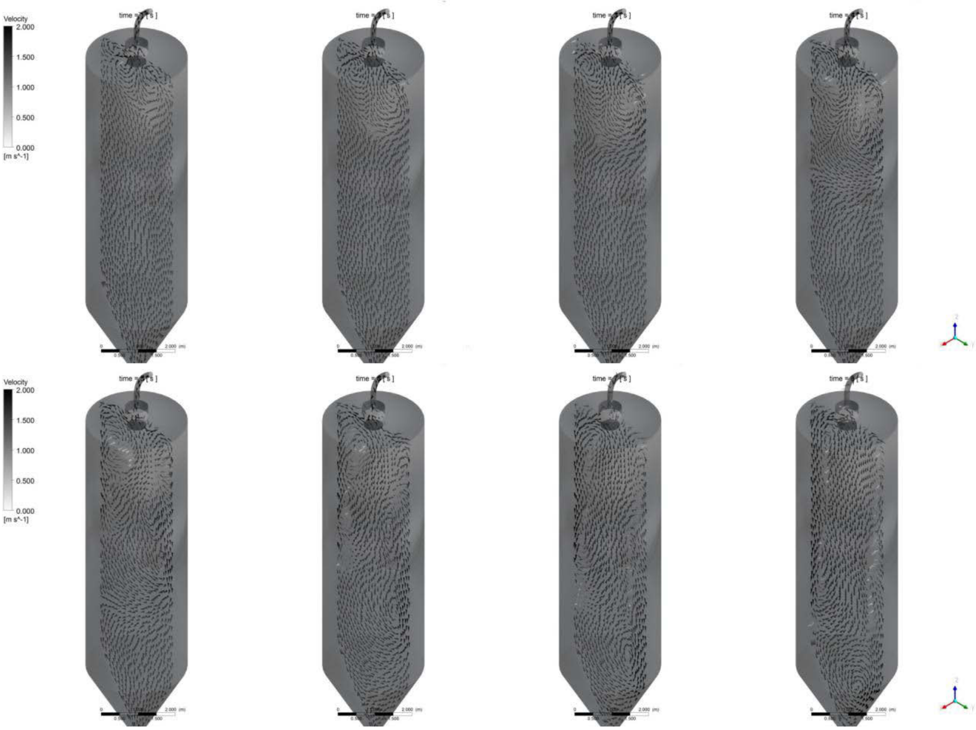

*Figure 7-29. Velocity from second 1 to second 8, pneumatic filling.*

As a first evaluation the average sinking velocity of the dust cloud is calculated from first detection of dust at the sensor locations. The time difference in combination with the path to calculate an average velocity, which is compared to measured values. The measured time difference between dust detection at the sensor locations is in average $t_{diff} = 4.5$ s for maize starch. This leads to an average dust cloud velocity of $U_{DC} = 0.78$ m/s.

Figure 7-30 (left) shows the averaged measured time difference between dust detection at lower and upper sensor location. Simulated curves are shown in Figure 7-30 (right), the results are shown for the shape factor, as taken from preliminary studies (see chapter 0) and a doubled shape factor.

The original simulation leads to an average dust cloud velocity of $U_{DC} = 1.7$ m/s, which is approximately twice the measured value and with a doubled shape factor it is still 1.13 m/s, which is better but still too high.

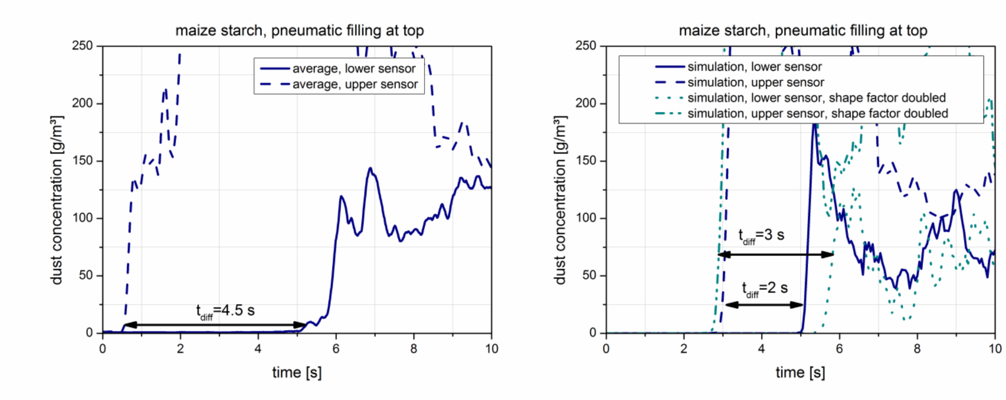

*Figure 7-30. Measured and simulated dust detection times at sensor locations.*

Instead of increasing the specific surface area with a shape factor, it is possible to modify the behavior of particles with an equivalent density, see chapter 2.2.3. An equivalent density can be calculated with the diameter of the particle, the specific surface area and the density of the particle:

$$\rho_{eq} = \frac{\textit{surface area of spherical particle}}{\textit{surface area determined with BET}} * \textbf{measured density of particle} \qquad \textbf{eq. 40}$$

which is 0.119 * particle density for maize starch as used here as example. For particles with high specific surface areas this would lead to very low densities of single particles. Measured specific surface area of maize starch is 2.4857 m²/g but the specfic surface area of a spherical particle with a diameter of 13.5 µm would be 0.2959 m²/g. The calculated equivalent density for maize starch would approximately be 180 kg/m³. First simulations showed that densities as low as 180 kg/m³ would lead to cloud settling velocities lower than 0.35 m/s. Therefore a standard density of 1000 kg/m³ was chosen, which leads to cloud settling in the simulations of 0.70 m/s, which is slightly lower than the measured average of 0.78 m/s. Smaller corrections could now be made with the shape factor. An equivalent density approach allows to modify the settling velocity significantly, but changes other parameters. Since the program assumes spherical particles, the number of particles is increasing for a constant mass flow. For the planned simulation of dust explosions it lowers the fuel per particle. Figure 7-31 shows the time differences at which the dust is detected at sensor locations for the different approaches. The shape factor allows some medium changes of settling behavior, whereas a change of density of 1/3 of the original density alters the settling behavior immensely.

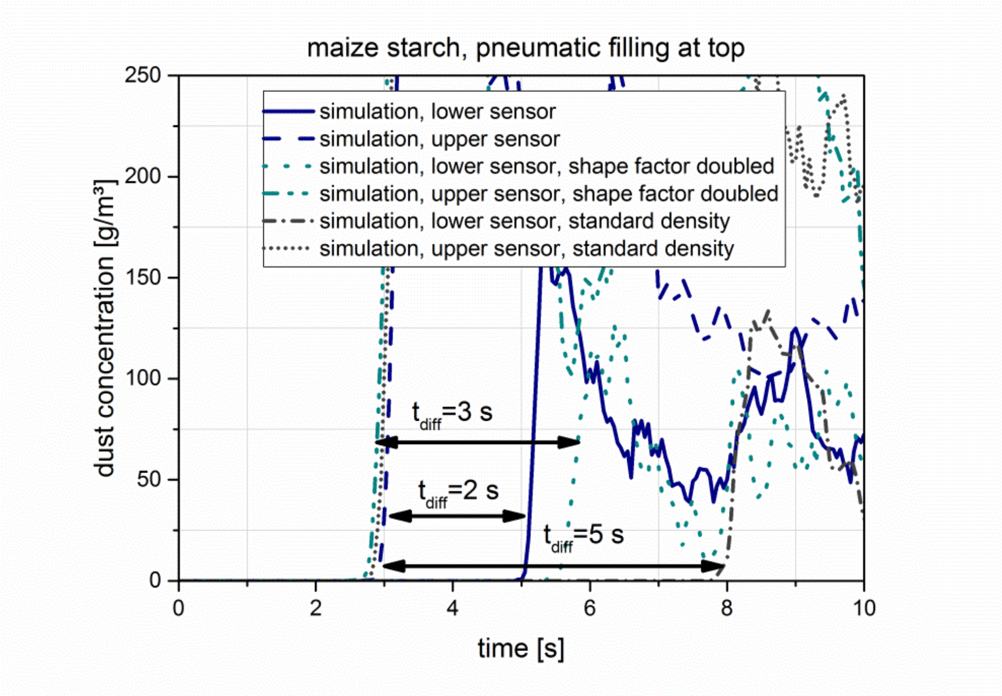

*Figure 7-31. Simulated dust detection times at sensor locations with different settings.*

Figure 7-32 gives an overview of measured and simulated cloud settling velocities. Velocities were determined with the detection times between sensors. The measured averaged velocity is shown with standard deviation. A further modification of the shape factor improves the results but a modified density shows best results in terms of settling velocities.

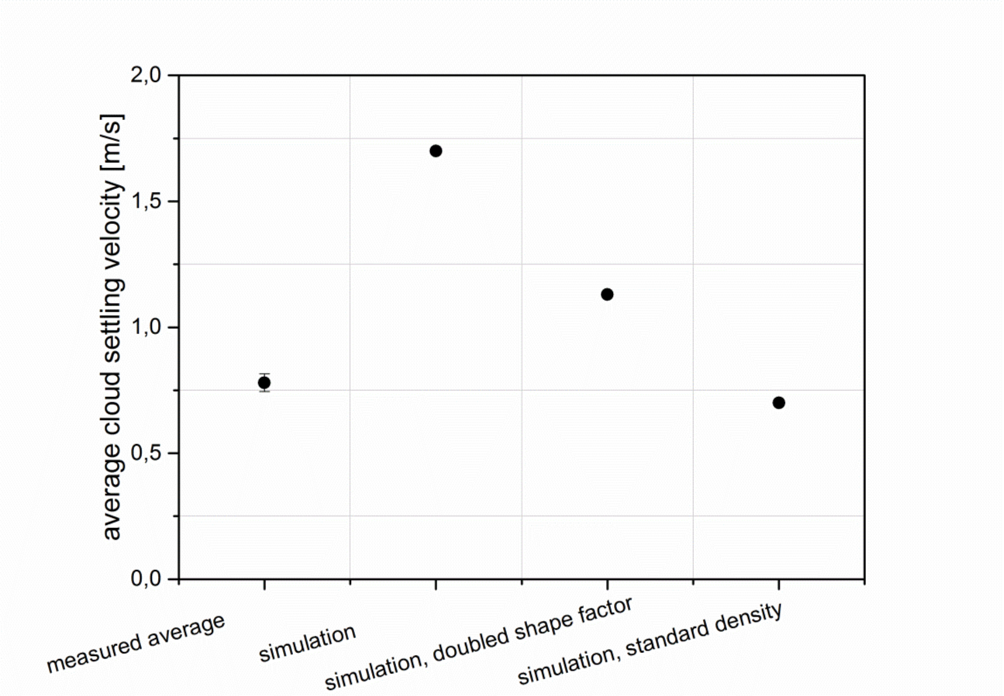

*Figure 7-32. Measured and simulated cloud settling velocities, pneumatic filling.*

Figure 7-33 shows the measured and simulated dust concentrations at sensor locations for the different settings. All simulations show good agreement in dust concentration distribution but not in time. This is at least partly, because the exact beginning of conveying in measurement could not be determined due to setup, therefore the timeline is not completely synchronized.

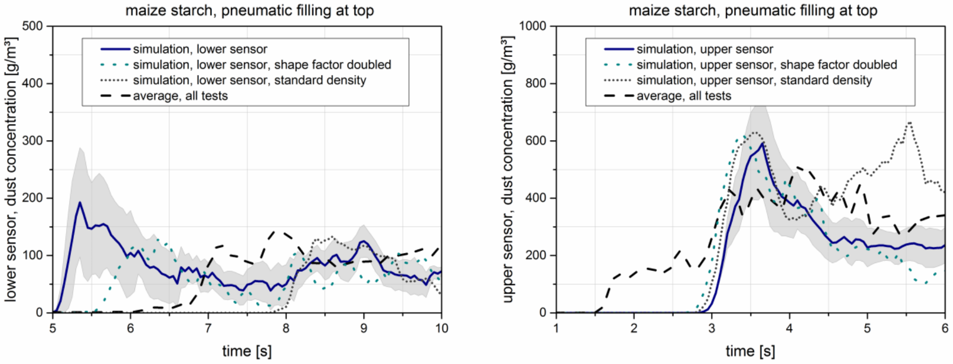

*Figure 7-33. Measured and simulated dust concentration at lower (left) and upper (right) location.*

Figure 7-34 and Figure 7-35 show the development of the isosurfaces with dust concetrations at LEL (upper row) and two times LEL (lower row) for eight seconds. The isosurfaces of LEL and two times LEL develop simulatanously from top to bottom for a total sample mass of 10 kg maize starch.

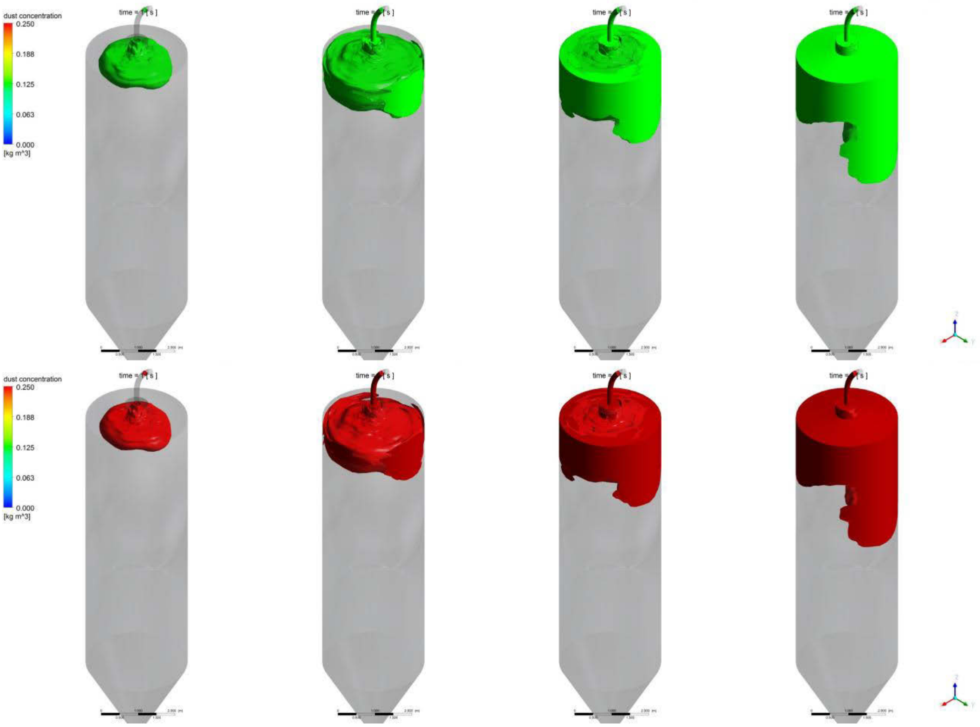

*Figure 7-34. Pneumatic filling, development of volume with dust concentrations at LEL (upper row) and two times LEL (lower row) for first two seconds.*

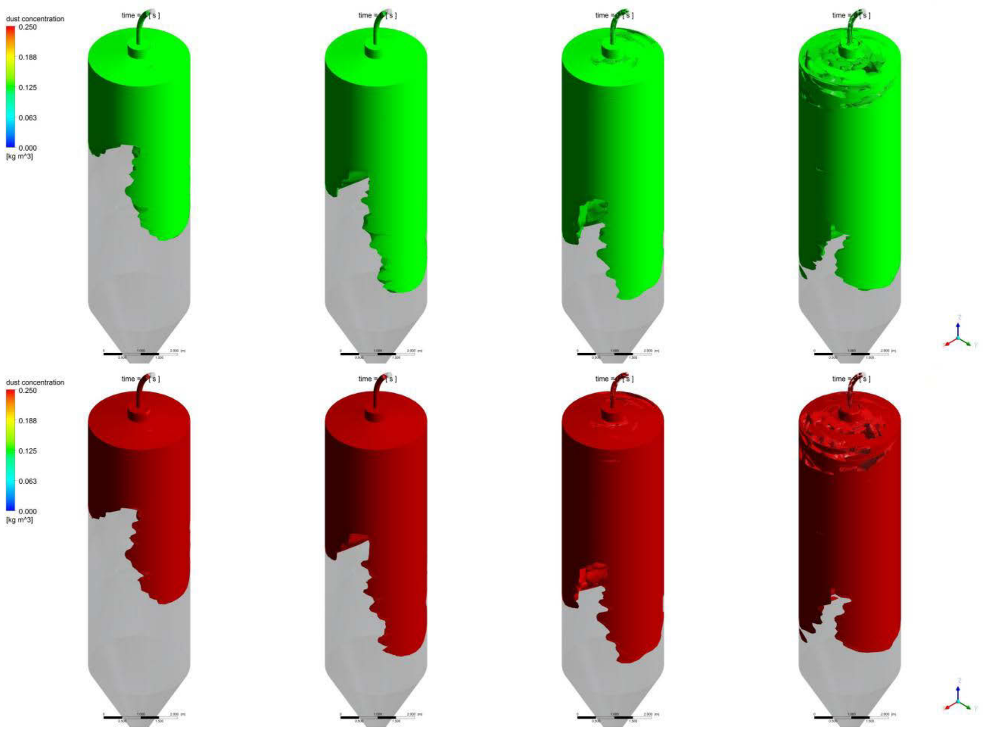

*Figure 7-35. Pneumatic filling, development of volume with dust concentrations at LEL (upper row) and two times LEL (lower row) for four to eight seconds after injection.*

### 7.3.3 Simulation of pneumatic filling – different dustiness

Simulations with pneumatic filling and three dusts of different dustiness were carried out. In order to evaluate the possibility to model different dustiness numerically results were compared to experimental data. Simulation parameters and boundary conditions can be found in chapter 7.3.2. For simulation of the three dusts a constant density approach was used. Dustiness was taken into account with different particle size distributions and shape factors. Material parameters are described in Table 7-16.

Table 7-15. Wheat flour, maize starch and lignite.

| | wheat flour | maize starch | lignite |
|---|---|---|---|
| dustiness group | 1 | 2 | 5 |
| density | 1000 kg/m³ | 1000 kg/m³ | 1000 kg/m³ |
| median diameter | 60 µm | 14 µm | 38 µm |
| d(0.1) | 10 µm | 10 µm | 4 µm |
| d(0.9) | 160 µm | 25 µm- | 230 µm |
| shape factor | 6 | 7.8 | 13 |

Simulated dust concentrations over time of the three dusts for the lower and upper sensor location are shown in Figure 7-15 (left). Lower dust concentrations are simulated for wheat flour compared to the other two dusts, which is in good agreement with the lowest tendency to form dust clouds of wheat flour. Lignite and maize starch produce higher dust concentrations over time compared to wheat flour. Dust concentrations of all three dusts decrease faster than the measured dust concentrations (right). In the simulations dust can be detected after approx. three seconds at the lower sensor points, whereas dust detection in experiments was in the range of four to six seconds. The simulated dust concentrations of wheat flour are twice as high as measured in average. Simulated dust concentrations of lignite and maize starch are quantitatively in the range of the measured data.

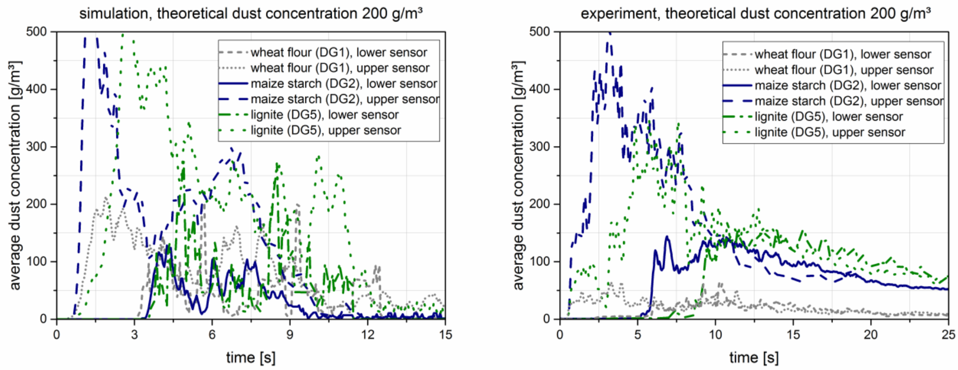

*Figure 7-36. Comparison of simulated and measured dust concentrations for pneumatic filling, 50 m³ silo.*

### 7.3.4 Comparison of different filling methods regarding LEL

CFD could provide an aid when designing conveying methods in order to create configurations, where the lower explosion limit is not reached in most parts of the vessel. An approach is to model different injection points and angles in combination with an evaluation of the volume of the vessel where the lower explosion limit is exceeded. Additionally CFD allows finding a configuration where the turbulence intensity is especially low, which would lead to lower explosion pressures in case of a dust explosion. A summary is given in [akl5]. Figure 7-37 shows three exemplary configurations, which are used to illustrate the approach. A homogenous injection (left) was modeled as worst case scenario with only 5 kg dust, but eight injection points. This should generate an as homogenous as possible dust/air mixture. For comparison two different inlet geometries for the pneumatic filling were modeled. A 60° bent pipe (middle) as in the experiments was realized and a straight inlet (right). 10 kg dust was filled in for configurations, where dust was injected at the top.

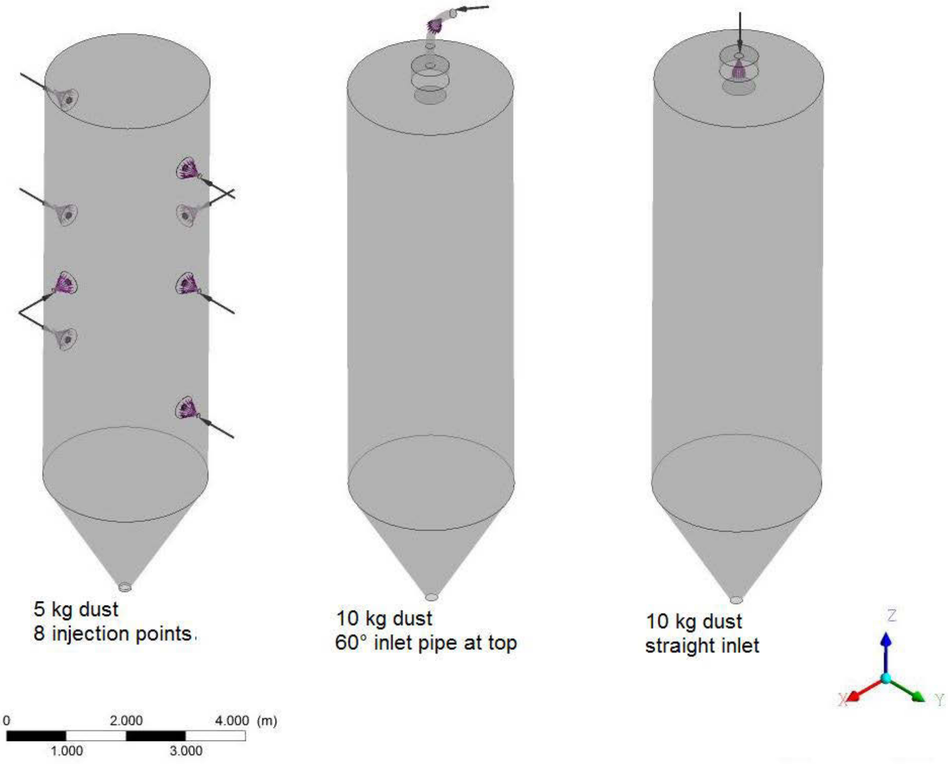

*Figure 7-37. Comparison of homogenous injection (left), pneumatic filling at top with 60° pipe as in experiments (middle) and pneumatic filling with straight inlet (right).*

Figure 7-38 shows the development of dust distribution in the silo for the three configurations during the first seven seconds.

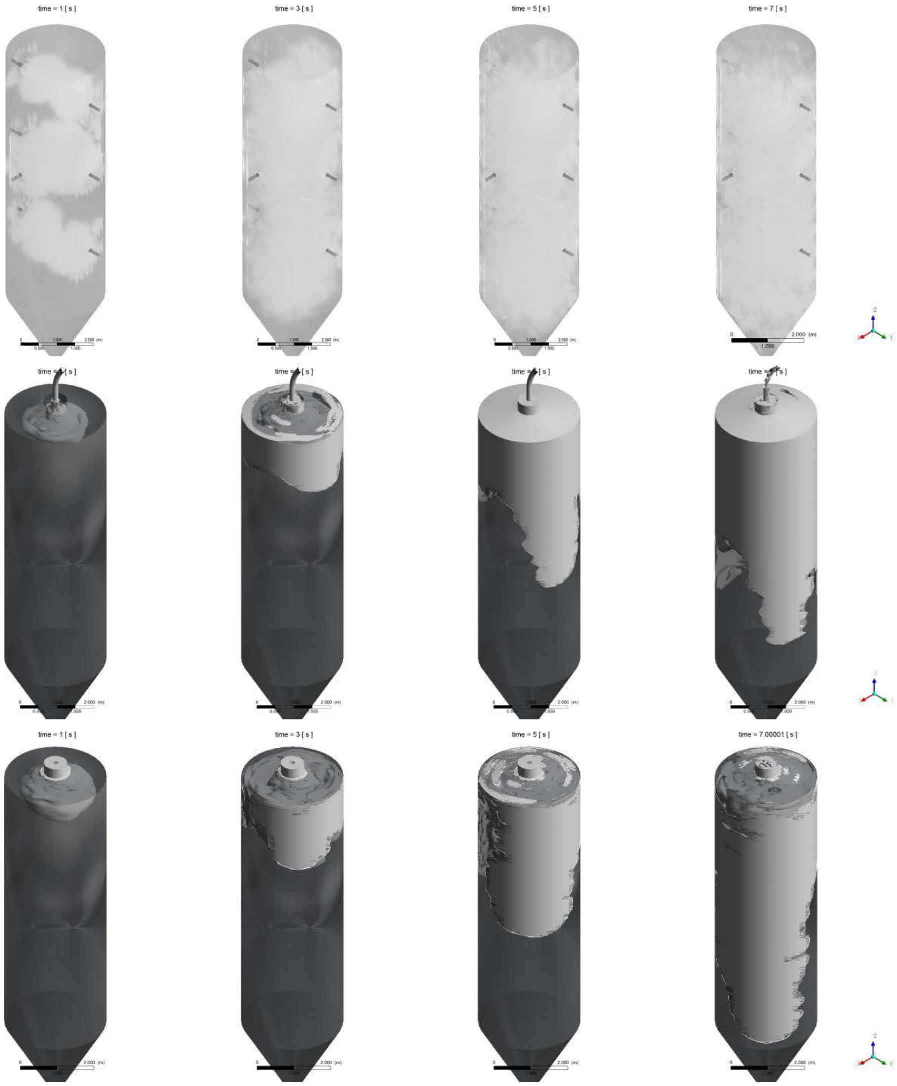

*Figure 7-38. Comparison of dust injection for homogenous injection (upper row), pneumatic filling with 60° bent pipe (middle row) and pneumatic filling with straight inlet (lower row).*

For all three configurations the volume, where the dust concentration exceeds the lower explosion limit was determined as function of time. Figure 7-39 shows the volume of the vessel, which is filled with an explosive atmosphere, in percent as function of time after beginning of injection. The homogenous injection leads to an explosive atmosphere in more than 40 % of the vessel in two seconds for only 5 kg of sample mass, whereas the pneumatic filling with bend pipe leads to an explosive dust/air mixture in almost 60 % of the vessel after eight seconds with a doubled sample mass of 10 kg. A straight pipe leads to a smaller explosive volume compared to the bend pipe for the filled-in sample mass and geometry. In terms of explosion protection configuration with straight inlet would be better for pneumatic filling into the vessel in this work.

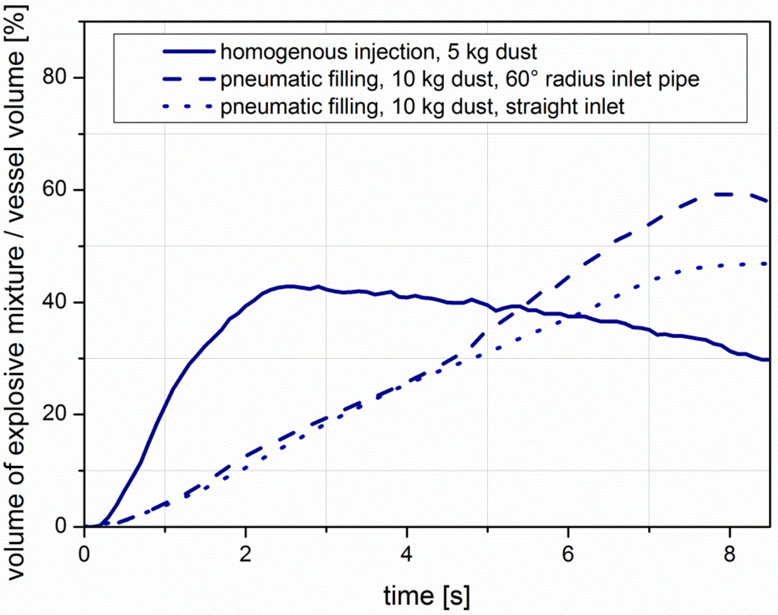

*Figure 7-39. Comparison of volume of explosive dust/air mixture for different setups.*

### 7.3.5 Turbulence for different conveying velocities

Dust explosion severity depends very much on initial turbulence among other influences such as dust concentration distribution, particle size and so on. In order to show an approach to investigate a good compromise between conveying velocity and low initial turbulence RMS velocities in the silo are compared for different inlet velocities. Simulation parameters can be found in Table 7-16.

*Table 7-16. Simulation parameters, pneumatic filling, 50 m³ Silo, different turbulence intensities.*

| parameter | |
|---|---|
| cells | 164223 |
| smallest grid width (hexaedra) | 0.0075 m |
| largest grid width (hexaedra) | 0.25 m |
| height of first layer | 0.0001 m |
| number of prism layers/ growth rate | 15 /1.3 |
| $y^+$(max) | <2 |
| calculation scheme | stationary |
| turbulence model | SST |
| fluid | air |
| solid | maize starch |
| reference pressure | 1 atm |
| inlet | velocity |
| air velocity $u_{in}$ | 6;12;24;36;48 m/s |
| mass flow solid | 1.665 kg/s |
| opening (at bottom cone during filling) | 0 bar |

Air velocity was chosen according to common conveying velocities for pneumatic filling systems, which are usually between 3 and 45 m/s air flow depending on the desired product mass flow [97]. Inlet velocities of 6; 12; 24; 36; and 48 m /s were chosen to evaluate the initial turbulence in the silo depending on the inlet velocity. Findings of **Tamanini** for corn starch and coal suggest that RMS velocities in m/s should be 2 m/s, or below this guarantees significantly lower reduced explosion pressures [98], since this is difficult to determine axial and tangential velocities below 20 m/s are suggested in [8].

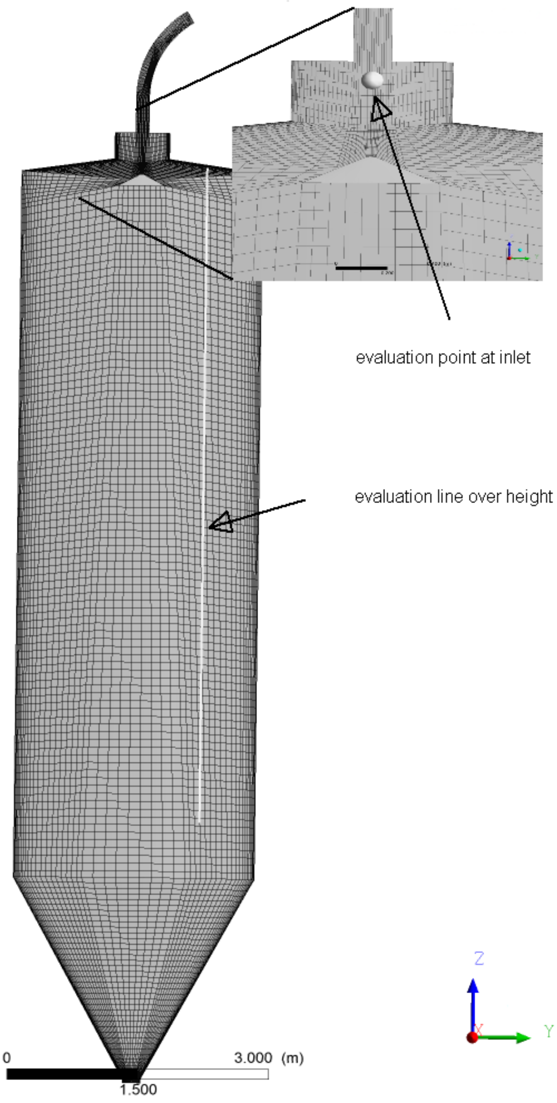

*Figure 7-40. Grid of 50 m³ silo and evaluation locations.*

RMS velocities were evaluated near the tube exit (see Figure 7-40) and over the height of the silo, with some distance to the center due to the deflection plate. The results are summarized in Table 7-17 and Figure 7-41. It can be seen that for inlet velocities higher than 24 m/s velocities and RMS velocities are increasing significantly. This supports the findings of **Tamanin**i [98], and [8]. Therefore it is useful to avoid velocities of 20 m/s and higher behind the conveying tube.

*Table 7-17. Velocities and RMS velocities for different inlet velocities.*

| | $u_{in}$ = 6 m/s | $u_{in}$ = 12 m/s | $u_{in}$ = 24 m/s | $u_{in}$ =36 m/s | $u_{in}$ = 48 m/s |
|---|---|---|---|---|---|
| $u_{xpoint}$ in m/s | 0.5 | 0.4 | 0.6 | 9.1 | 2.0 |
| $u_{ypoint}$ in m/s | 1.3 | 1.0 | 3.1 | 3.5 | 2.3 |
| $u_{zpoint}$ in m/s | 1.4 | 2.1 | 3.58 | 28.6 | 52.0 |
| $RMS_{point}$ in m/s | 1.51 | 5.38 | 10.8 | 32.6 | 63.4 |
| RMS (vol. averaged) in m/s | 0.146 | 0.59 | 0.64 | 1.67 | 1.96 |

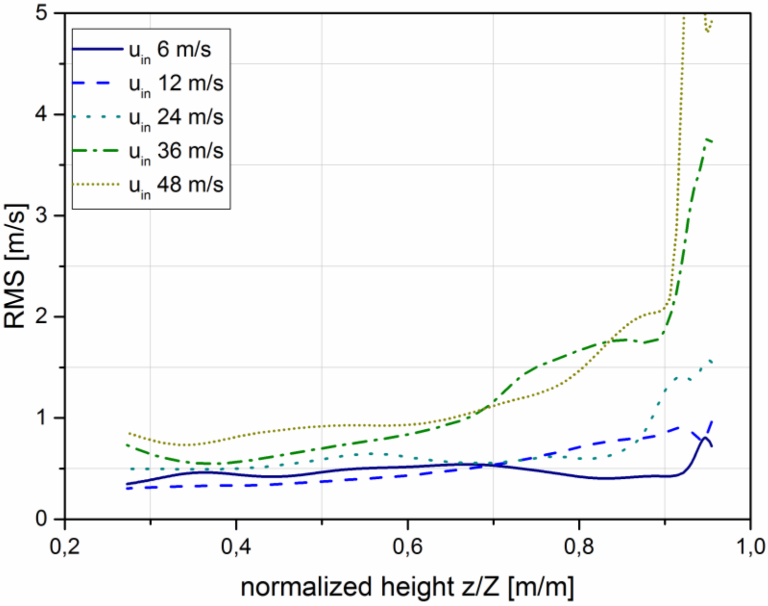

*Figure 7-41. Comparison of RMS velocities over height for different inlet velocities.*

In order to undermine the results above, Figure 7-42 shows a comparison of the RMS velocities for inlet velocities of 12, 24 and 36 m/s.

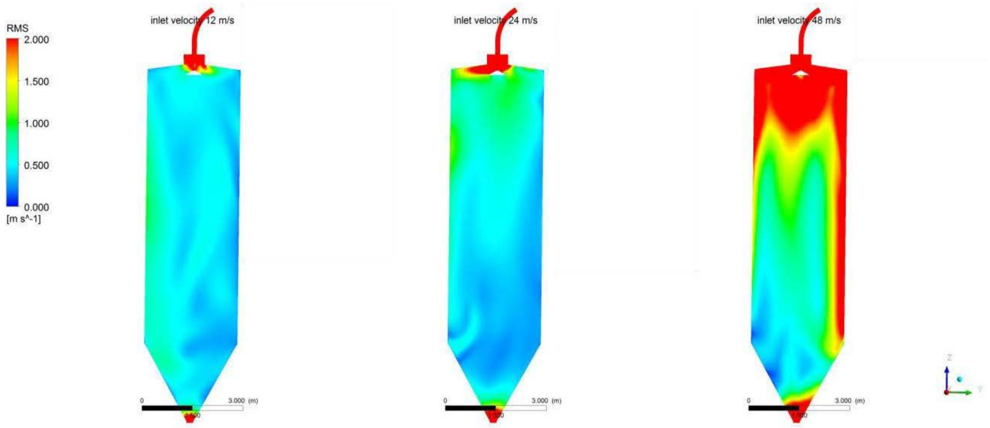

*Figure 7-42. Exemplary RMS velocities for 12, 24 and 48 m/s inlet velocities, y-z-plane.*

### 7.3.6 Conclusion - simulation of 50 m³ silo

Two different filling processes were modeled with an Euler/Lagrange approach. A homogenous injection at eight points in the silo was investigated. This should provide information about a worst-case scenario in terms of dust distribution and turbulence. Second configuration was a pneumatic filling process as found in many industrial branches. Dust concentrations over time were compared to measured values over time. Modeled dust concentrations showed general agreement of measured and simulated data. Especially the homogenous injection could be modeled in good agreement with time and quantity. Modeling of pneumatic filling led to an over prediction of the settling velocity of the dust cloud, but good agreement of dust concentrations. It seems in cases where gravity outweighs the influence of the surrounding flow the settling velocities are predicted as too fast. Simulation of the behavior of dust/air mixtures can still be improved in order to achieve more detailed information on development of dust distribution over time. Since particle shape and surface area as well as agglomeration processes have an influence on the behavior, it is very difficult to model dust/air mixtures sufficiently. Up to now it is not possible to model the total number of particles in industrial-scale simulations. Therefore collisions and agglomeration processes cannot be calculated directly. A first approach could be to use a standard density of 1000 kg/m³, shape factors and/or particle sizes to modify the behavior of particles in the flow in combination with experimental data. Particle size distribution as well as particle collisions and additional particle forces should always be considered, see chapter 4.2.6 and chapter 7.1.3. First simulations with constant density, particle size distributions and shape factors for different dustiness of three dusts and a pneumatic filling process showed that different dustiness can be modeled in general. Compared to measured data all three dust still sink faster in the simulations and dust concentration is under predicted over time. Further improvements should include considering a Reynolds depending drag coefficient, particle rotation and agglomeration. The turbulence effects of particles and flow could be researched further, since they can differ very much, e.g., if particles bounce of walls or each other their RMS values differ from the fluid flows. First numerical and experimental work has been done by **Sommerfeld** [91].

Three configurations of filling processes were compared regarding differences between the developments of the volumes exceeding the lower explosion limit in the vessel as function of time. Two pneumatic filling configurations with bend and straight inlet pipe showed that a straight inlet would be the safer choice for the setup of this work. This means for this setup and the filled-in sample less volume is filled with an explosive dust/air mixture than in the other configurations. In future it would be possible to use an Euler/Lagrange approach to compare different filling methods or injection points or angles, inlet geometries regarding the local distribution of dust over time when designing a vessel. This could lower the probability of an accident, if a setting can be found where the lower explosion limit is not reached in most of the vessel during the filling process. Additionally a setting could be found with a low turbulence intensity, which would lead to lower explosion pressures in case of an accident. This could be done in addition or at the same time when developing a pneumatic filling system, which is as efficient as possible, with CFD methods. If only intake geometry is modified (angle, position) this could be done without lowering efficiency of the filling process. Indirectly this is already taken into account when sizing venting areas for tangential filling at the top according to DIN EN 14491. For tangential release of dust into a silo the empiric equations take the inhomogenous distribution of dust and lower turbulence into account, when sizing the venting area. This based on investigations by **Hauert et al.** [3], where the lower explosion limit in a silo was only reached near the walls of the silo when dust was released tangential at the top.

In addition the RMS velocity regarding the turbulence intensity in the silo was investigated for different inlet velocities and pneumatic filling. Higher RMS velocities lead to more severe dust explosions due to better mixing of fuel and air. With this approach a compromise between high intake velocities, high mass flows of dust and as low as possible RMS velocities can be found. In reverse a worst case scenario can be found with this approach, in combination with parameter study regarding an optimal dust concentration distribution in the silo a setting can be found where severe dust explosions can be expected. Simulations regarding optimal dust concentration distribution with fluent where already done by **Judel** [51] in 1998 and further investigations regarding turbulence were proposed. Findings of **Tamanin**i [98], [8] were supported by the numerical simulations, which suggested velocities below 20 m/s in vessels in order to reduce turbulence significantly and therefore lower dust explosion severity in case of an explosion.

# 8 Conclusions

The influence of a safety characteristic named dustiness on the course of vented dust explosions was evaluated. The investigations aim on the adaption of the necessary venting area to practical conditions, up to now the design depends on $p_{max}$ and $K_{St}$ value and properties of the vessel only. Dustiness is the tendency of dusts to form dust clouds due to a prescribed mechanical stimulus. Dustiness is not taken into account for the design of safety measures in European standards so far. In a first step the influence was investigated with a small-scale, vented 75 L apparatus. It could be shown that dustiness influences reduced explosion pressures as well as rates of pressure rise and flame speeds. Reduced explosion pressures were compared to calculated pressures. Dusts with little tendency to form dust clouds generated lower pressures compared to the expected values than dusts with higher dustiness. Dust concentration measurements as function of time in the 75 L apparatus showed that dusts with higher dustiness generated higher dust concentrations over time for same boundary conditions. Experiments were done with six dusts and two filling methods.

In order to verify the results from small-scale experiments, a 50 m³ silo was used for industrial-scale tests. Tests were done with three dusts and two filling methods. Dust concentrations measurements confirmed that dusts with higher tendency to form dust clouds generate higher dust concentrations over time in a large vessel as well. But dust concentration measurements showed that especially for pneumatic filling at top results vary 30 % and more compared to the average. Even for simultaneous injection at different points dust concentrations varied up to 30 % from test to test. Despite the high uncertainty dust concentration measurements suggested that dusts with higher dustiness produce dust clouds, which stay in the air for a longer time and spread out more homogenously in the vessel, see Figure 8-1. Further research is needed, which evaluates not only the dust concentration over time but dust distribution across the vessel. This may lead to improvements when determining zones (20, 21, 22) as well. Dustiness could be a useful parameter for the determination of zones.

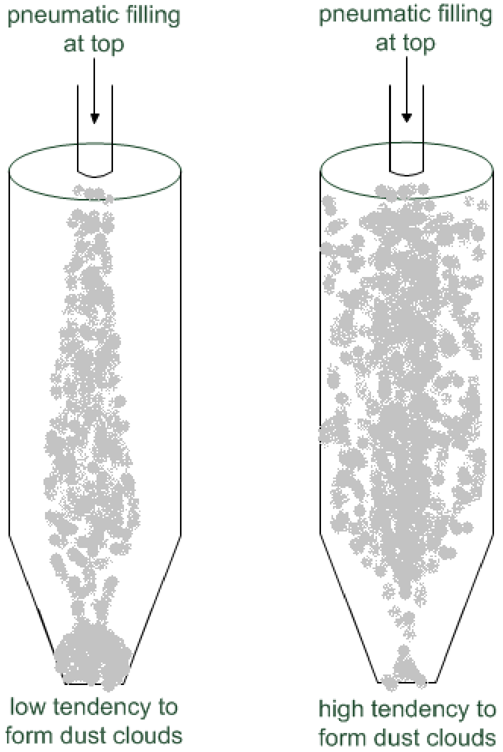

*Figure 8-1. Schematic dust distribution depending on dustiness.*

First explosion experiments with homogenous injection showed that for a worst-case scenario of dust injection with nozzles no influence of dustiness could be detected for the three tested dusts. As expected for a more or less homogenous dust cloud with early ignition.

In order to develop an approach to adapt the venting area depending on dustiness at least a total of 18 dusts should be tested to confirm influence of dustiness on vented dust explosion. Dusts should be organic and inorganic, metallic dusts can be very different in their behavior and should be left out. Every dustiness group from one to six should be included. If the influence can be confirmed for an industrial-scale silo, an adaption for the empirical equations should be found for cylindrical silos with axial, pneumatic filling. Transfer of results to different processes and vessel geometries was not shown yet and was found to be unlikely since filling process has an major influence on the behavior of dust/air mixtures.

But even using a proven effect should be considered carefully. Influences such as changing humidity, air pressure, conveying etc. have to be taken into account. A conservative approach could be to determine dustiness with dried dusts only. In this case industrial-scale experiments have to be made with dried dusts only as well and on days with relative air humidity below 60 %, e.g. a very hot and dry summer could change dustiness behavior in the vessel. Another change in dustiness behavior could happen due to the process itself where a different particle size distribution could be generated e.g. when a certain fraction is deposited. Therefore boundary conditions have to be considered carefully if an adaption is proposed. Not only dispersion method, but particle size distribution, specific surface, density and humidity of dust (see [88]) have an influence on dustiness behavior and course of explosion. The course of explosion in general depends on various phenomena such as dust nature (as described in this work), pre-ignition turbulence, length/diameter ratio of the enclosure and vent activation overpressure ( [7], [5] and [6]).

In addition possibilities to model dust/air mixtures with a commercial CFD code ANSYS CFX R14 were investigated. Two common multiphase approaches were used and compared. One approach is the Euler/Euler approach, which treats every phase as continuum and the other approach is the Euler/Lagrange approach, which uses a balance of forces to calculate disperse phases. First studies showed that the Euler/Lagrange approach is more suitable for modeling dust/air mixtures. The Euler/Lagrange allows easily including particle size distribution, additional particle forces, such as turbulent dispersion force and virtual mass force, as well as a model for binary particle collisions and particle/wall interaction. In addition it is possible to modify the particle shape or surface area with a shape factor, which is important to model different dustiness. Simulations of a small-scale and an industrial-scale vessel showed that dust concentration could be modeled in good agreement with measured data, especially for flow governed dust distribution as in cases where dust is injected with nozzles and pressurized air. For gravity driven dust settling time difference between measured and simulated data was decreased with further corrections, such as shape factor and equivalent density. A detailed comparison of measured and simulated dust distribution for dusts of different dustiness in a large vessel is recommended, because first findings indicate that the dust distribution inside the vessel is under predicted for dusts with high tendency to form dust clouds. In future it could be useful to implement a particle Reynold’s number depending drag coefficient as done by **Morsi et al.** [94], agglomeration processes and an approach for particle rotation in addition to the wall/particle model, see [65].

# References

[1] F. Hauert and S. Radandt, “Determination of dustiness of bulk materials,” in *Proccedings of the 8th International Confernece on Measurement and Control of Granular Materials*, 2009.

[2] Verein Deutscher Ingenieure, *VDI 2263- part 9:2008:05 "Dust fires and dust explosions - Hazards - assessment - protective measures - Determination of dustiness of bulk material",* Berlin: Beuth Verlag, 2008.

[3] F. Hauert, H. Fogt, A.Vogl, D. Wennerberg und S. Radandt, „Staubverteilung und Staubverteilung und Geschwindigkeitsparameter in einem pneumatisch befüllten Silo mit numerischen Simulationen,“ *VDI–Berichte 1272, 1996: Sichere Handhabung brennbarer St äube,* 1996.

[4] DIN, *EN 14491:2012-10 "Dust explosion venting protective systems",* Beuth Verlag, 2012.

[5] F. Tamanini, „The role of turbulence in dust explosions,“ *Journal of Loss Prevention in the Process Industries,* Bd. 11, Nr. 1, pp. 1-10, 1998.

[6] R. Zalosh, „New dust explosion venting design requirements for turbulent operating condtions,“ *Journal of Loss Prevention in the Process Industries,* Bd. 20, Nr. 4-6, pp. 530-535, 2007.

[7] M. Scheid, A. Geißler und U. Krause, „Experiments on the influence of pre-ignition turbulence on vented gas and dust explosions,“ *Journal of Loss Prevention in the Process Industries,* Nr. 2-3, pp. 194-199, 2006.

[8] National Fire Protection Association, NFPA 68 Guides for venting of deflagration, Quincy, MA, 2013.

[9] A. Tascon, P. Aguado und A. Ramirez, „Dust explosion venting in silos: A comparison of standards NFPA 68 and EN 14491,“ *Journal of Loss Prevention in the Process Industries,* Bd. 22, pp. 204-209, 2008.

[10] Verein Deutscher Ingenieure, VDI 2263 -part 7.1:2013-03 "Dust fires and dust explosions - Hazards - assessment - protective measures - Fire and explosion protection in spraying and drying integrated equipment - Examples", Berlin: Beuth Verlag, 2013.

[11] Verein Deutscher Ingenenieure, VDI 2263:1992-05 "Dust fires and dust explosions; hazards, assessment, protective measures", Berlin: Beuth, 1992.

[12] W. Hinds, Aerosol Technology, USA: Wiley-Interscience, 1999.

[13] R. Eckhoff, Dust Explosions in the Process Industries, 3. Hrsg., Golf Pub Co, 2003.

[14] H. Steen, Handbook of Explosion Prevention and Protection, Deutschland: WILEY-VCH Verlag GmbH, 2004.

[15] W. Bartknecht, Dust Explosions: Course, Prevention, Protection, 1. Hrsg., Berlin – Heidelberg – New York: Springer, 1989.

[16] P. Amyotte, An Introduction to Dust Explosions - Understanding the Myths and Realities of Dust Explosions for a Safer Workplace, 1 Hrsg., Elsevier, 2013.

[17] U. Krause, Wärme- und Stofftransportvorgänge bei sicherheitstechnischen Untersuchungsverfahren für Staubbrände und Staubexplosionen, 1. Hrsg., Aachen: Shaker Verlag, 2002.

[18] DIN, *DIN EN 14460:2007-07 "Explosion resistant equipment",* Berlin: Beuth Verlag, 2007.

[19] DIN, *DIN EN 14797:2007-03 "Explosion venting devices",* Berlin: Beuth Verlag, 2007.

[20] DIN, *DIN EN 14034-1:2011-04 Determination of explosion characteristics of dust clouds - Part 1:" Determination of the maximum explosion pressure pmax of dust clouds",* Berlin: Beuth, 2011.

[21] DIN, *DIN EN 14034-2:2011-04 Determination of explosion characteristics of dust clouds - Part 2: "Determination of the maximum rate of explosion pressure rise (dp/dt)max of dust clouds",* Berlin: Beuth, 2011.

[22] U. Krause, BAM Forschungsbericht 194: Ein Beitrag zur mathematischen Modellierung des Ablaufs von Explosionen, Berlin: BAM, 1993.

[23] Verein Deutscher Ingenieure, *VDI 2263 - part 1:1990-05 " Dust fires and dust explosions; hazards, assessment, protective measures; test methods for the determination of the safety characteristic of dusts",* Berlin: Beuth Verlag, 1990.

[24] DIN, *DIN 55992,* Berlin: Beuth Verlag GmbH, 1999.

[25] DIN, *DIN 55992-1:2006-06 "Determination of a parameter for the dust formation of pigments and extenders - Part 1: Rotation method",* Berlin: Beuth Verlag, 2006.

[26] DIN, *DIN 55992-2_1999-10 "Determination of a parameter for the dust formation of pigments and extenders - Part 2: Dropmethod",* Berlin: Beuth Verlag, 1999.

[27] DIN, DIN EN 15051-1:2011-11 "Workplace exposure - Measurement of the dustiness of bulk materials - Part 1: Requirements and choice of test methods", Berlin: Beuth, 2011.

[28] DIN, DIN EN 15051-2:2011-11 "Workplace exposure - Measurement of the dustiness of bulk materials - Part 2: Rotating drum method", Berlin: Beuth, 2011.

[29] DIN, DIN EN 15051-3:2011-11 "Workplace exposure - Measurement of the dustiness of bulk materials - Part 3: Continuous drop method", Berlin: Beuth, 2011.

[30] A. Wells und D. Alexander, „A method for estimating the dust yield of powders,“ *Powder Technology,* pp. 271-277, March-April 1978.

[31] ANSI, ANSI/ASTM D 547-41 "Standard Test Method for Index of Dustiness of Coal and Coke", ASTM International, 1980 (withdrawn 1986).

[32] F. Hamelmann und E. Schmidt, „Messverfahren zur Bestimmung des Staubungsvermögens von dispersen Pulvern,“ *Chemie Ingenieur Technik,* pp. 1666-1676, 12 2002.

[33] D. Eickelpasch, Methodik zur Bestimmung diffuser Staubemissionen beim Schüttgutumschlag, Dortmund: Universität Dortmund, 1996.

[34] N. Breum, „The rotating drum dustiness tester: Variability in dustiness in relation to sample mass, testing time, and surface adhesion,“ *The Annals of Occupational Hygiene,* Bd. 43, Nr. 8, pp. 557-566, November 1999.

[35] S. Bach, U. Eickmann und E. Schmidt, „Comparison of Established Systems for Measuring the Dustiness of Powders with the UNC Dustiness Tester Developed Especially for Pharmaceutical Substances,“ *Ann. Occup. Hyg.,* Bd. 8, Nr. 57, pp. 1078-1086, 2013.

[36] Verein Deutscher Ingenieure, VDI-Richtlinie 2263 part 9 "Dust fires and dust explosions - Hazards - assessment - protective measures - Determination of dustiness of bulk materials", Beuth Verlag, 2008.

[37] K. Lauer, Untersuchung des Einflusses der elektrostatischen Aufladung von Stäuben auf die Neigung dieser Stäube zur Staubwolkenbildung, Mannheim: FSA Forschungsgesellschaft für angewandte Systemsicherheit und Arbeitsmedizin, 2003.

[38] M. Elimelech, J. Gregory, X. Jia and R. Williams, Particle Deposition and Aggregation, 1. ed., USA: Butterworth Heinemann, 1995.

[39] K. Willeke and P. Baron, Aerosol Measurement, 2. Edition ed., USA: Wiley-Interscience, 2001.

[40] Federal Ministry for Environment, Nature Conservation and Nuclear Safety, Technical Instructions on Air Quality Control – TA Luft, Germany: Joint Ministerial Gazette (GMBl), 2002, p. 202.

[41] P. M. Schnell und P. K. Volland, „Virtuelle Hochschule Bayern," [Online]. Available: http://www.lrz.de/~volland/vhb/einblicke/grundlagen/pskript11_1.pdf. [Zugriff am 13 April 2012].

[42] M. Stieß, Mechanische Verfahrenstechnik 1, 2. ed., Berlin: Springer Verlag, 1995.

[43] G. Rittenhouse, Sedimentation near junction of Maquoketa and Mississippi Rivers, discussion, Journal of Sedimentary Research, 1943, pp. 40-42.

[44] E. Masad, S. Saadeh, T. Al-Rousan, E. Garboczi und D. Little, „Computations of particle surface characteristics using optical and X-ray CT images," *Computational Materials Science,* Bd. 34, pp. 406-424, 2005.

[45] D. P. Klobes, „Bundesanstalt für Materialforschung und -prüfung," Januar 2011. [Online]. Available: http://www.bam.de/de/fachthemen/referenzverfahren/kapitel_4.htm. [Zugriff am 11 Juni 2012].

[46] DIN, *DIN ISO 9277:2014-01 "Determination of the specific surface area of solids by gas adsorption - BET method",* Berlin: Beuth, 2014.

[47] H. Schubert, Mechanische Verfahrenstechnik, 3. ed., Leipzig: Deutscher Verlag für Grundstoffindustrie, 1990.

[48] J. Kussin, Dissertation - Experimentelle Studien zur Partikelbewegung und Turbulenzmodifikation in einem horizontalen Kanal bei unterschiedlichen Wandrauhigkeiten, Halle: ULB Sachsen-Anhalt, 2004.

[49] R. Eckhoff, "Are enhanced dust explosion hazards to be foreseen in production, processing and handling of powders consisting of nano-size particles?," *Journal of Physics: Conference Series 304,* pp. 1-21, 2011.

[50] M. Scheid, Dissertation - Experimentelle Untersuchungen zum Ablauf von Gas- und Staubexplosionen in druckentlasteten Reaktionsgefäßen, Berlin: Bundesanstalt für Materialforschung und -prüfung (BAM), 2005.

[51] P. Judel, Diplomarbeit - Untersuchungen zum Einfluss von Strömungsfeld und Partikelkonzentration auf den Ablauf von Staubexplosionen, Berlin: TU Berlin, 1998.

[52] Y. Tsuji und M. Y., „LDV measurements of an air-solid-twophase flow in a vertical pipe,“ *Journal of Fluid Mechanics,* Bd. 120, pp. 385-409, 1982.

[53] U. Hesener und M. Reinecke, „Staubexplosionsrisiko an Mischern mit bewegten Werkzeugen zur Erstellung und Abgrenzung möglicher Explosionsschutzkonzepte,“ Dekra EXAM GmbH, Bochum, 2012.

[54] W. Oberkampf und T. H. C. Trucano, Verification, Validation, and Predictive Capability in Computational Engineering and Physics, 02: Sandia National Laboratories, 2003.

[55] ANSYS, CFX 14.0 - Modeling Theory Guide, ANSYS, 2009.

[56] J. Ferziger and M. Peric, Numerische Strömungsmechanik, 3. ed., Berlin Heidelberg New York: Springer, 2008.

[57] P. Gerlinger, Numerische Verbrennungssimulation, Berlin Heidelberg New York: Springer, 2005.

[58] F. Joos, Technische Verbrennung, 1. Hrsg., Hamburg: Springer, 2006.

[59] S. Elghobashi, „On Predicting Particle-Laden Turbulent Flows,“ in s *Proc. Of the 7th Workshop on Two-Phase Flow Predictions*, 1994.

[60] ANSYS, CFX 14.0 - Theory Guide, ANSYS, 2009.

[61] M. Sommerfeld, Modellierung und numerische Berechnung von partikelbeladenen turbulenten Strömungen mit Hilfe des Euler-Lagrange-Verfahrens., Aachen: Shaker Verlag, 1996.

[62] T. Frank, Parallele Algorithmen für die numerische Simulation dreidimensionaler, disperser Mehrphasenströmungen und deren Anwendung in der Verfahrenstechnik, Aachen: Shaker Verlag, 2002.

[63] A. Warzeche und A. Boguslawski, „Simulations of pulverized coal oxy-combustion in swirl burner using RANS and LES methods,“ *Fuel Processing Technology,* pp. 130-135, March 2014.

[64] F. Menter, “Two-Equation Eddy-Viscosity Turbulence Models for Engineering Applications.,” *AIAA Journal 32,* vol. Nr. 8, pp. 1598-1605, 1994.

[65] M. Sommerfeld, *Theoretical and Experimental Modelling of Particulate Flows,* Bde. %1 von %2Lecture Series No.2000-6, Karman Institute for Fluid Mechanics, 2000, pp. 1-62.

[66] C. Wen and Y. Yu, “Mechanics of Fluidization,” in *Chem. Eng. Prog. Symp.Ser. 62*, 1966.

[67] A. Gosman und E. Ioannides, „Aspects of Computer Simulation of Liquid Fuelled Combustors,“ *Journal of Energy,* Bd. 7, pp. 482-490, 1983.

[68] A. Burns, T. Frank, I.Hamill und J.-M. Shi, „Drag Model for Turbulent Dispersion in Eulerian Multi-Phase Flows,“ in s *5th International Conference on Multiphase Flow, ICMF’04*, Yokohama, 2004.

[69] J. A. T. Hjelmfeld und M. L.F., „Motion of Discrete Particles in a Turbulent Fluid,“ *Applied Scientific Research,* Nr. 16, pp. 149-161, 1966.

[70] B. Hußmann, Dissertation - Modellierung und numerische Simulation der zweiphasigen Strömungs- und Verbrennungsvorgänge in einem Staustrahltriebwerk mit Bor als Festtreibstoff, München: Universität der Bundeswehr München, 2008.

[71] H. Beck, N. Glienke and C. Möhlmann, BIA-Report "Brenn- und Explosionskenngrößen von Stäuben, Sankt Augustin: Hauptverband der gewerblichen Berufsgenossenschaften, 1997.

[72] IFA, 11 09 2013. [Online]. Available: http://staubex.ifa.dguv.de/explokomp.aspx?nr=859&lang=.

[73] IFA, 11 09 2013. [Online]. Available: http://staubex.ifa.dguv.de/explokomp.aspx?nr=5678&lang=.

[74] IFA, 09 11 2013. [Online]. Available: http://staubex.ifa.dguv.de/explokomp.aspx?nr=181&lang=.

[75] *ISO 9277 "Bestimmung der spezifischen Oberfläche von Feststoffen durch Gasadsorption nach dem BET-Verfahren",* Berlin: Beuth Verlag, 2010-09.

[76] D. Evans, L. Turkevich, C. Roettgers, G. Deye und P. Baron, „Dustiness of Fine and Nanoscale Powders,“ *ANNALS OF OCCUPATIONAL HYGIENE,* Bd. 57, Nr. 2, pp. 261-277, March 2013.

[77] ISO, *ISO 1928:2009-06 “Solid mineral fuels - Determination of gross calorific value by the bomb calorimetric method and calculation of net calorific value”.,* ISO, 2009.

[78] V. S. B. 1. T. Vongsurakrai, A. S. B. 1. T. Vongsurakrai und S. S. B. 1. T. Varavinit, Verbesserungen bei der Agglomeration von Stärke / Thailand Patent 0000823439, 11.08.2005.

[79] J. Abbiss, T. Chubb and E. Pik, “Laser Doppler anemometry,” *Optics and Laser Technology,* vol. Volume 6, no. 6, pp. 249-261, Deccember 1974.

[80] A. Klippel, M. Scheid und U. Krause, „Progress on the Research into the Influence of Dustiness on Dust Explosions,“ in s *7th International Seminar on Fire and Explosion Hazards*, Providence, R.I., 2013.

[81] Kistler, „Datenblatt Drucksensoren Kistler 4043A,“ Kistler, [Online]. Available: http://www.kistler.com/mediaaccess/000-003d-10.09.pdf. [Zugriff am 29 03 2012].

[82] Dantec Dynamics, BSA Flow Software - Installation and User's guide, 7. ed., Skovlunde: Dantec Dynamics, 2002.

[83] M. Stiess, Mechanische Verfahrenstechnik - Partikeltechnologie 1, 3 ed., Springer, 2009.

[84] Sick AG, “Mitteilung Achema,” Frankfurt, 2009.

[85] Durag GmbH, “Mitteilung Achema,” Frankfurt, 2009.

[86] DIN, *EN 14491:2012-10 "Dust explosion venting protective systems",* Berlin: Beuth Verlag, 2012.

[87] B. Fakandu, Z. Yan, H. Phylaktou und G. Andrews, „The Effect of Vent Area Distribution in Gas Explosion Venting and Turbulent Length Scale Influence on the External Explosion Overpressure,“ in s *7th International Symposium on Fire and Explosion Hazards*, Providency, R.I., USA, 2013.

[88] A. Klippel, M. Scheid und U. Krause, „Investigations into the influence of dustiness on dust explosions,“ *Journal of Loss Prevention in the Process Industries: Special Edition ISHMPIE 9,* Bd. 26, Nr. 6, pp. 1616-1626, 2013.

[89] A. Klippel, M. Scheid, J. Koperski, M. Wappler und U. Krause, „Influence of dustiness on small-scale vented dust explosions,“ *Journal of Loss Prevention in the Process Industries,* Bd. 26, Nr. 6, pp. 1433-1441, 2013.

[90] Umweltbundesamt, „GSBL Joint Substance Data Pool of the German Federal Government,“ [Online]. Available: http://www.gsbl.de/eng_home.htm. [Zugriff am 15 01 2014].

[91] M. Sommerfeld, „Particle Dispersion in Turbulent Flow: THe Effect of Particle Size Distribution,“ *Particle and Particle Systems Characterization,* Bd. 7, Nr. 1-4, pp. 209-220, 1990.

[92] W. Hinds, Aerosol Technology, 2. Hrsg., Los Angeles: John Wiley & Sons, Inc., 1999.

[93] G. Bruschi, T. Nishioka und K. W. R. Tsang, Drag Coefficient of a Cylinder, 2003.

[94] S. Morsi und A. Alexander, „An investigation of particle trajectories in two-phase flow systems,“ *Journal of Fluid Mechanics,* Nr. 55(2), pp. 193-208, 1972.

[95] W. Shyy, M. Garbey, A. Appukuttan and J. Wu, *Evaluation of Richardson Extrapolation in Computational Fluid Dynamics In: Numerical Heat Transfer, Part B: Fundamentals 41,* vol. 2, 2002.

[96] A. Klippel, M. Schmidt, O. Mücke und U. Krause, „Dust concentration measurements during filling of a silo and CFD modeling of filling processes regarding exceeding the lower explosion limit,“ *Journal of Loss Prevention in the Process Industries,* Bd. 29, pp. 122-137, May 2014.

[97] solids solutions group, „solids Pneumatische Fördersysteme,“ solids solutions group , 2014. [Online]. Available: http://www.solids.de/de/anlagen-systeme/pneumatische-foerdersysteme/uebersicht-pneumatische-foerdersysteme.html. [Zugriff am 24 03 2014].

[98] R. Zalosh, „Explosion Venting Data and Modeling - Literature Review,“ NFPA, Quincy, MA, 2008.

## Own Publications

[akl1] A. Klippel, M. Scheid and U. Krause, "Investigations into the influence of dustiness on dust explosions," *Journal of Loss Prevention in the Process Industries: Special Edition ISHMPIE 9,* vol. 26, no. 6, pp. 1616-1626, 2013.

[akl2] A. Klippel, M. Scheid, J. Koperski, M. Wappler and U. Krause, "Influence of dustiness on small-scale vented dust explosions," *Journal of Loss Prevention in the Process Industries,* vol. 26, no. 6, pp. 1433-1441, 2013.

[akl3] A. Klippel, M. Scheid and U. Krause, "Progress on the Research into the Influence of Dustiness on Dust Explosions," in *7th International Seminar on Fire and Explosion Hazards*, Providence, R.I., 2013

[akl4] A. Klippel, M. Schmidt, M. Scheid und U. Krause, „11. Fachtagung Anlagen-. Arbeits- und Umweltsicherheit," *Einfluss des Staubungsverhaltens auf druckentlastete Staubexplosionen"*, Köthen, 2013.

[akl5] A. Klippel, M. Schmidt, O. Mücke and U. Krause, "Dust concentration measurements during filling of a silo and CFD modeling of filling processes regarding exceeding the lower explosion limit," *Journal of Loss Prevention in the Process Industries,* vol. 29, pp. 122-137, 2014.

# Appendix A: Experimental equipment and calibration

Appendix A consists of a description of the experimental equipment and calibration data for all dusts of the dust concentration meters.

## A.1 Technical data of measurement equipment

In all small-scale experiments pressure was measured with two piezo-resistive sensors 4043A10 and 4043A20 (Table A-1)

*Table A-1. Data Sheet Pressure sensors, small-scale experiments.*

| | 4043A10 | | 4043A20 |
|---|---|---|---|
| measurement range | 0…10 bar | | 0…20 bar |
| temperature range | | -40 - 70 °C | |
| sensivity | 50 mV/bar | | 25 mV/bar |
| eigenfrequency | > 120 kHz | | > 150 kHz |
| calibration power | | 2…5 mA | |
| reference power | | 4 mA | |
| input impedance | | ≈3 kΩ | |
| stability of sensivity | | < 0.2 %/a | |
| stability of zero point | | < 0.5 %FSO*/a | |
| thermal zero point change | | ± < 0.5 %FSO*/a | |
| thermal sensivity change | | < ± 1.0 % | |
| acceleration sensivity | | 0.3 mbar/g | |
| shock resistance | | 1000 g | |
| protection | | IP65 | |

*FSO…full scale output

In all industrial-scale experiments pressure was measured with four piezo-resistive sensors PAA-25 (see Table A-2).

*Table A-2. Data Sheet Pressure sensors, industrial-scale experiments.*

| | PAA-25 |
|---|---|
| measurement range | 0…5 bar |
| temperature range | -40 - 100 °C |
| voltage range | 0…10 V |
| stability of sensivity | < 0.2 %/a |
| stability of zero point | < 0.1 %FSO*/a |
| thermal zero point change | ± < 0.2 %FSO*/a |
| protection | IP68 |

*FSO…full scale output

The technical data of the LDA can be found in Table A-3.

Table A-3. Technical data LDA.

| | Dantec Dynamics |
|---|---|
| processor | F60 |
| laser | Flowlite 1D |
| method | Nd:YAG-Laser |
| wavelength | 532 nm |
| focus | 401.2 mm |
| distance between beams | 39.21 mm |
| high voltage | 800 - 1600 V |
| scope zoom | 450 % |

## A.2 Calibration of dust concentration meters

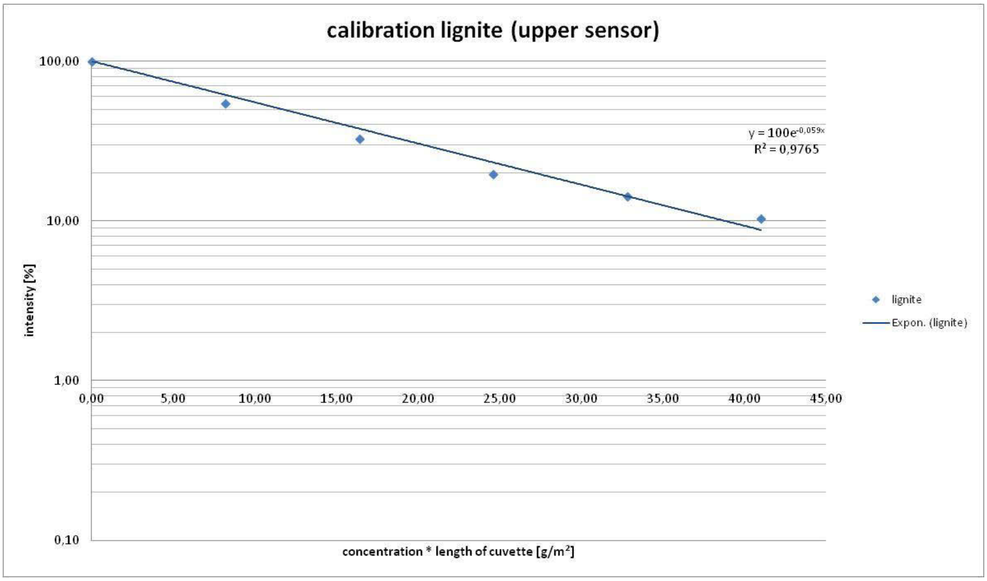

*A 1. Calibration for dust concentration meters, upper sensor, lignite.*

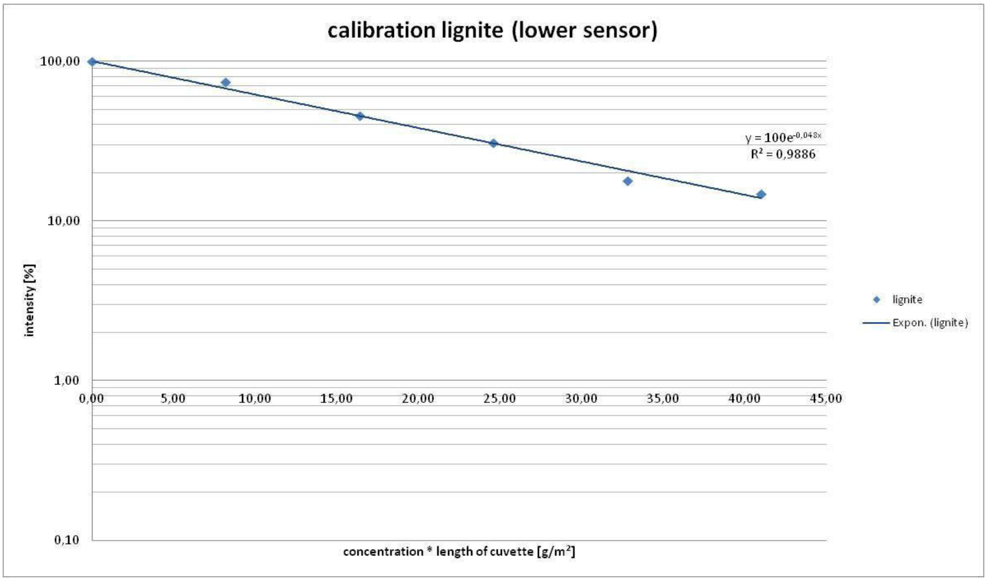

*A 2. Calibration for dust concentration meters, lower sensor, lignite.*

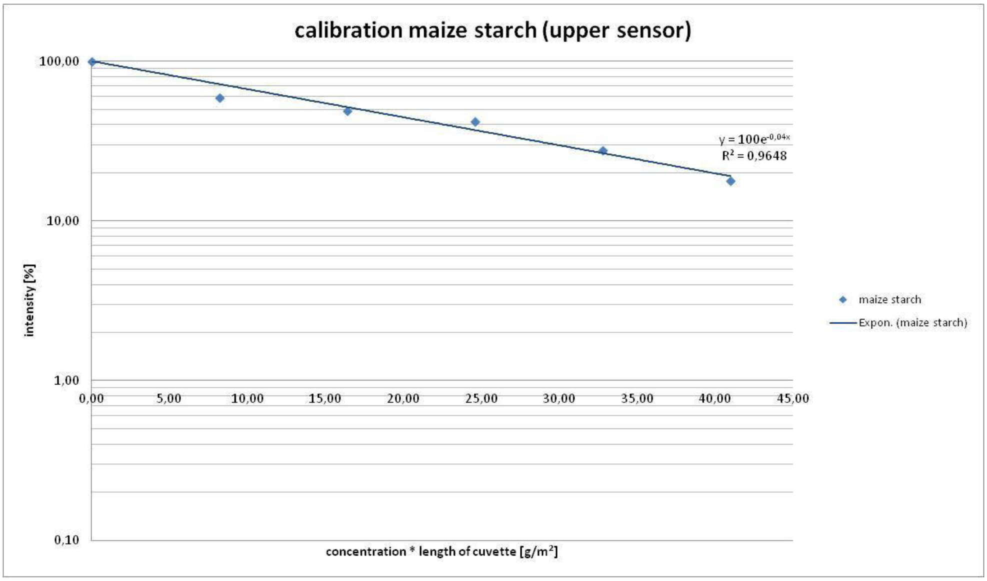

*A 3. Calibration for dust concentration meters, upper sensor, maize starch.*

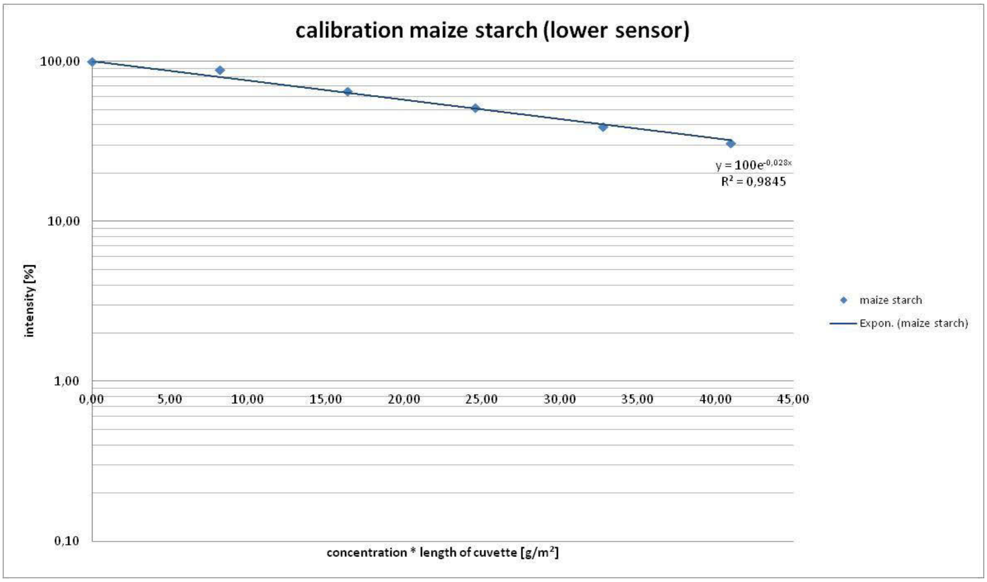

*A 4. Calibration for dust concentration meters, lower sensor, maize starch.*

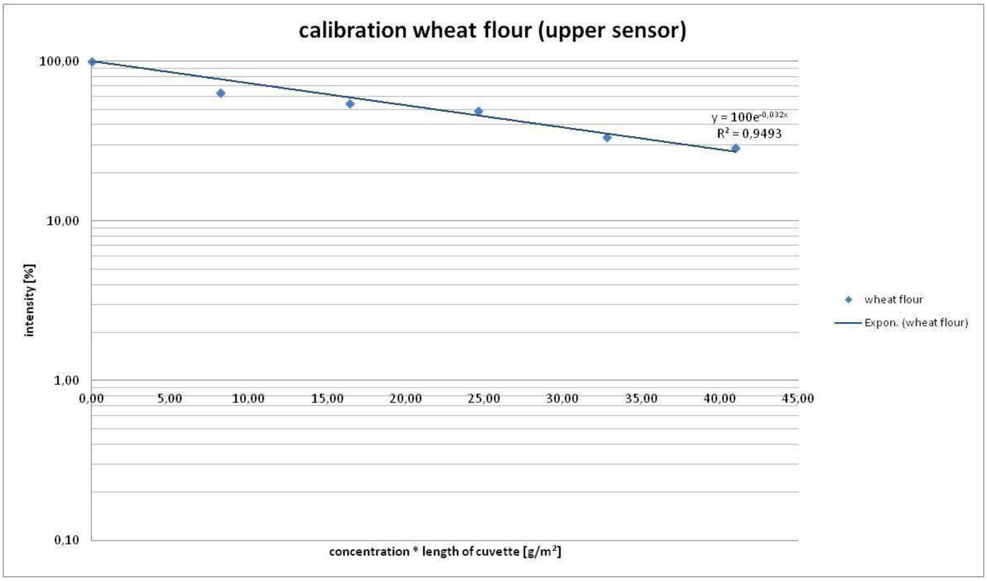

*A 5. Calibration for dust concentration meters, upper sensor, wheat flour.*

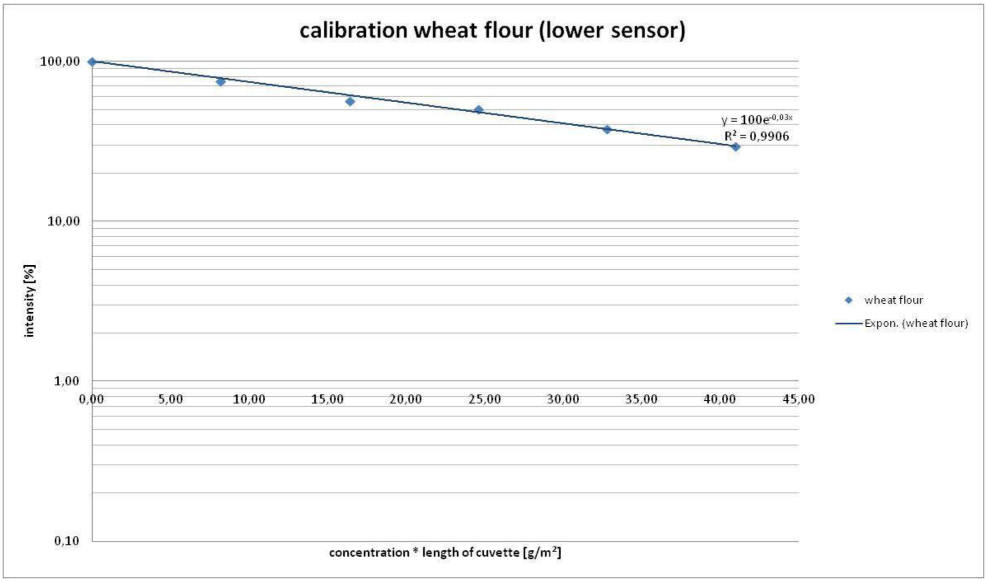

*A 6. Calibration for dust concentration meters, lower sensor, wheat flour.*

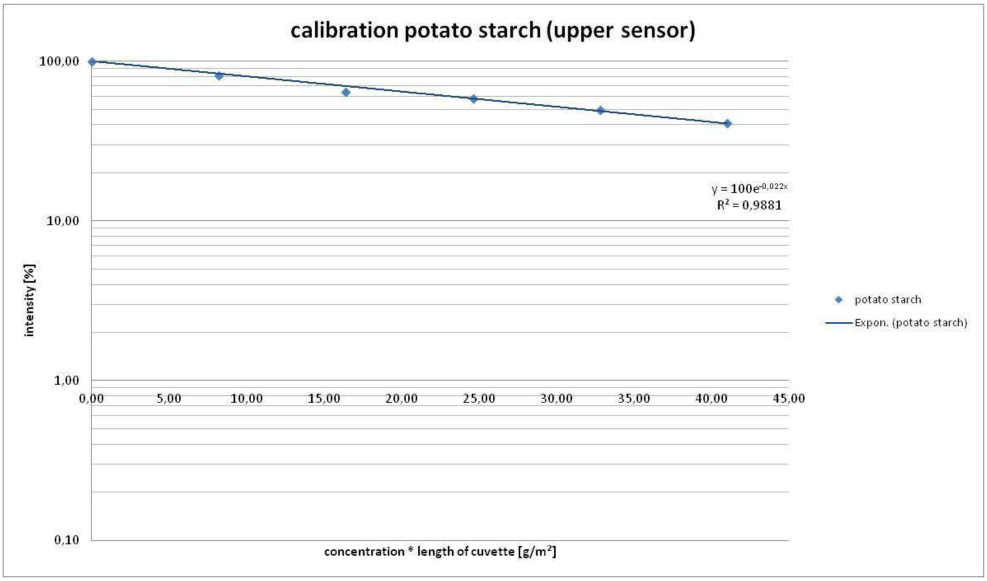

*A 7. Calibration for dust concentration meters, upper sensor, potato starch.*

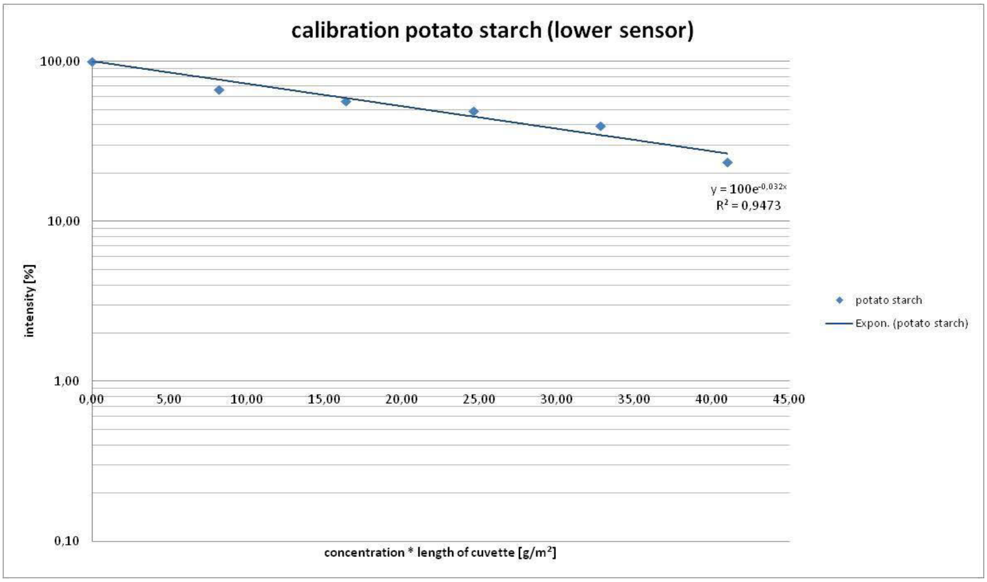

*A 8. Calibration for dust concentration meters, lower sensor, potato starch.*

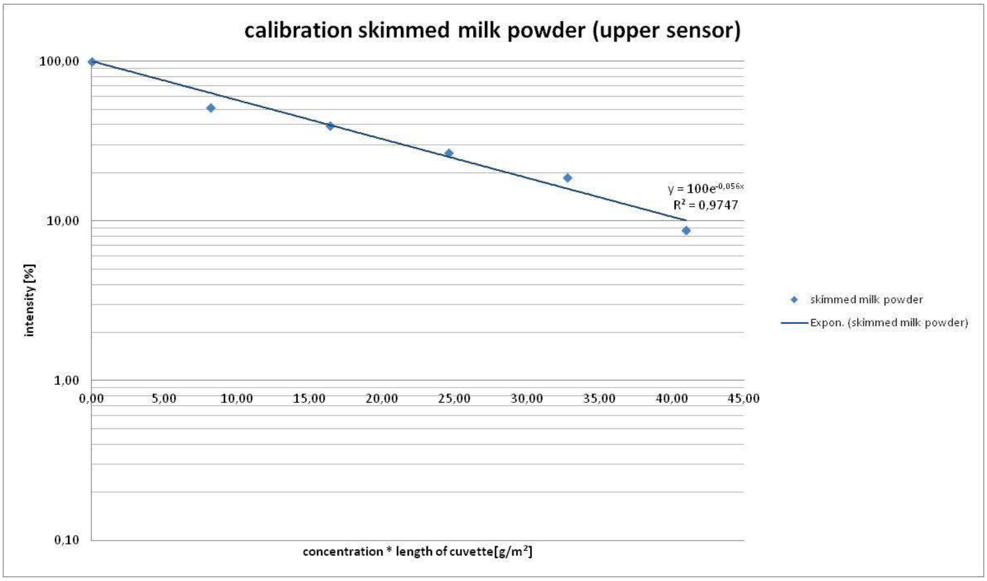

*A 9. Calibration for dust concentration meters, upper sensor, milk powder.*

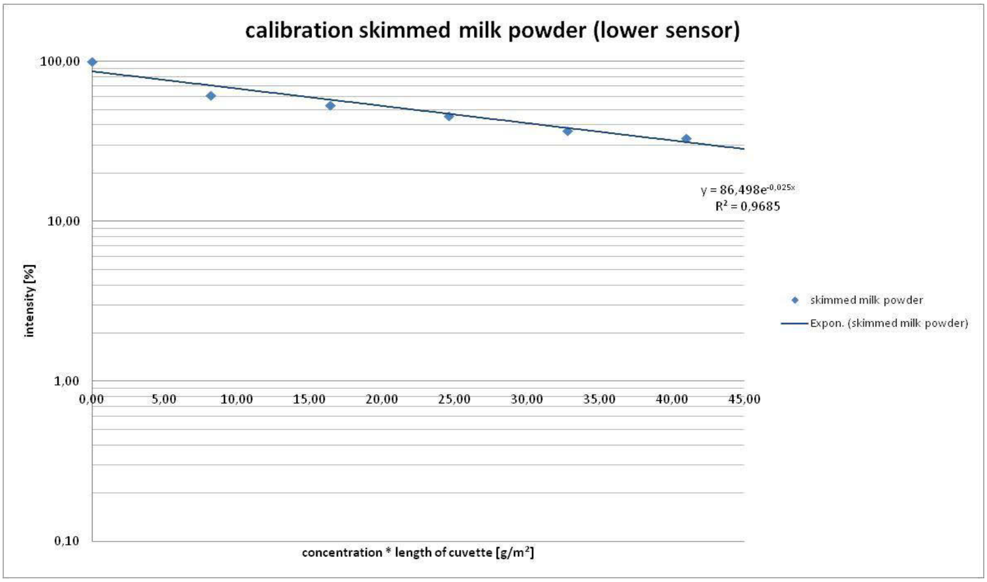

*A 10. Calibration for dust concentration meters, lower sensor, milk powder.*

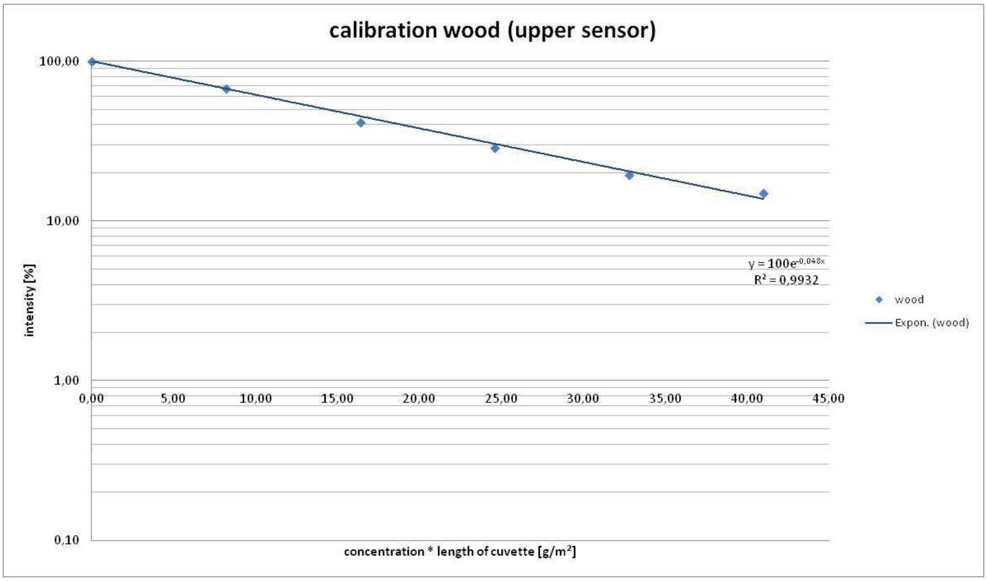

*A 11. Calibration for dust concentration meters, upper sensor, wood.*

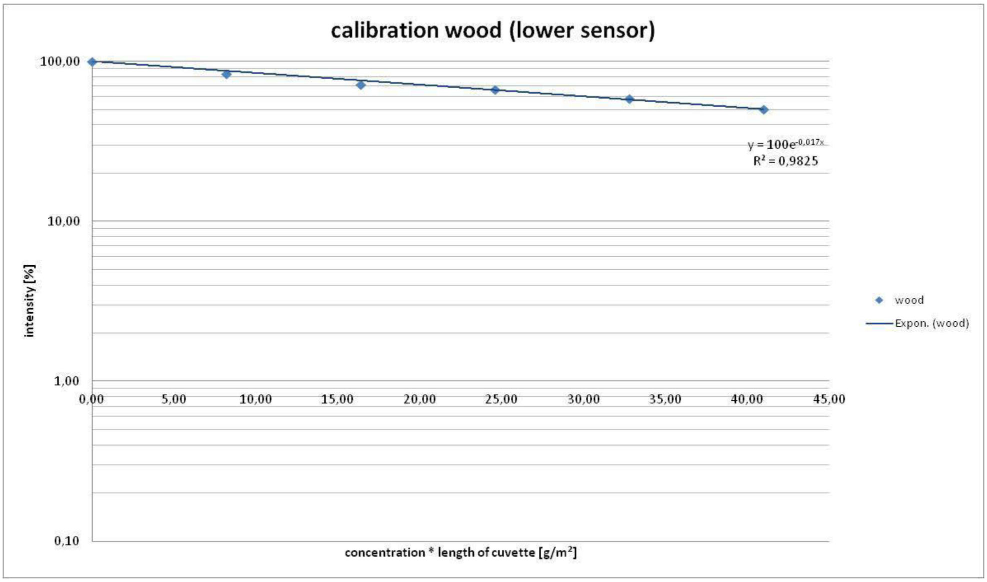

*A 12. Calibration for dust concentration meters, lower sensor, wood.*

## A.3 Calibration of improved dust concentration meters

For later small-scale experiments an improved dust concentration meter was used.

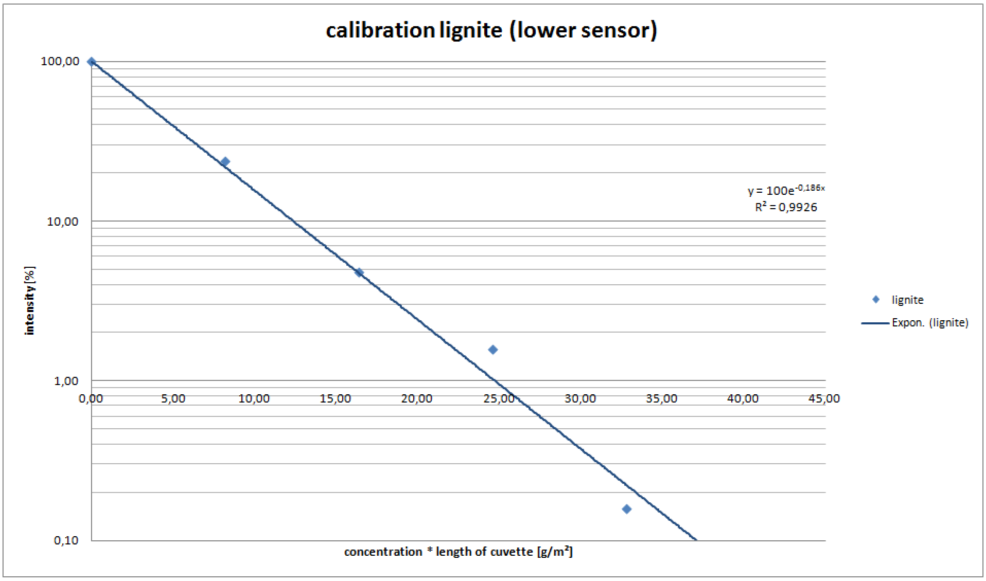

*A 13. Calibration for dust concentration meters, lower sensor, lignite.*

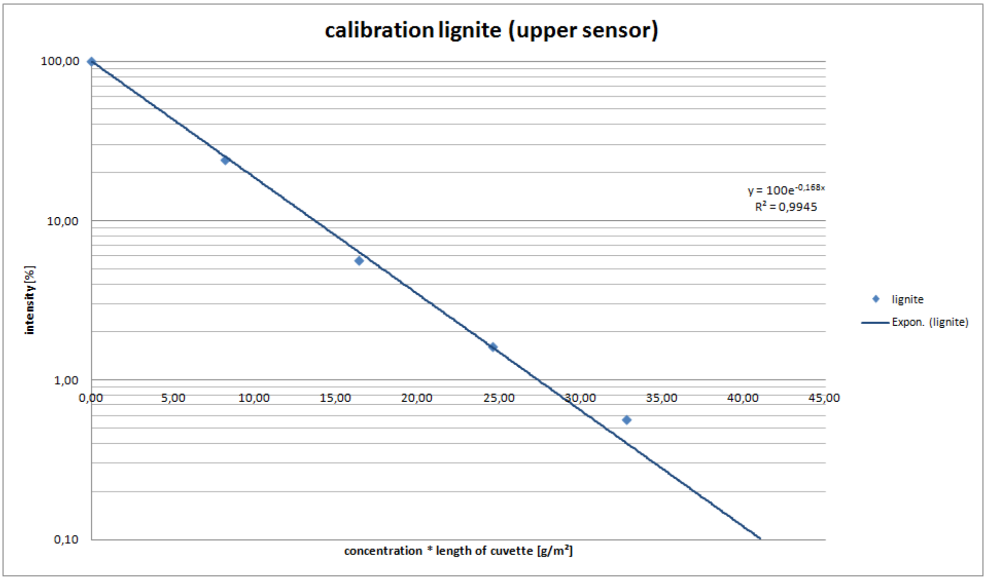

*A 14. Calibration for dust concentration meters, upper sensor, lignite.*

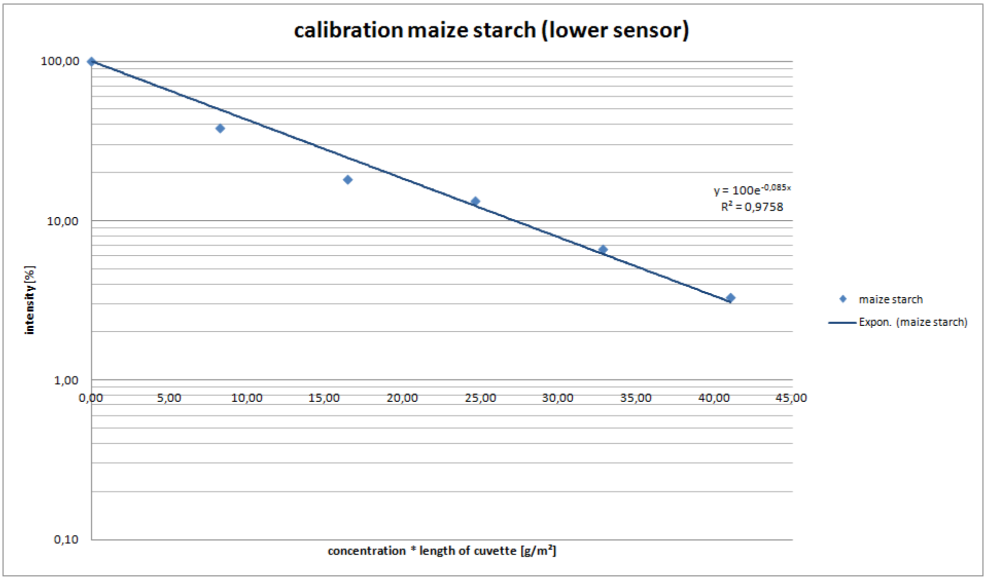

*A 15. Calibration for dust concentration meters, lower sensor, maize starch.*

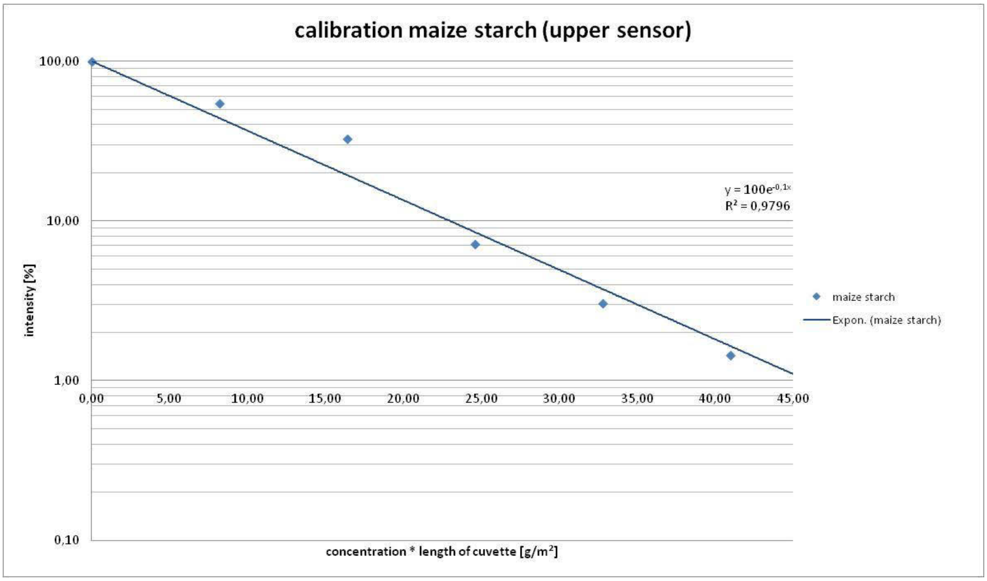

*A 16. Calibration for dust concentration meters, upper sensor, maize starch.*

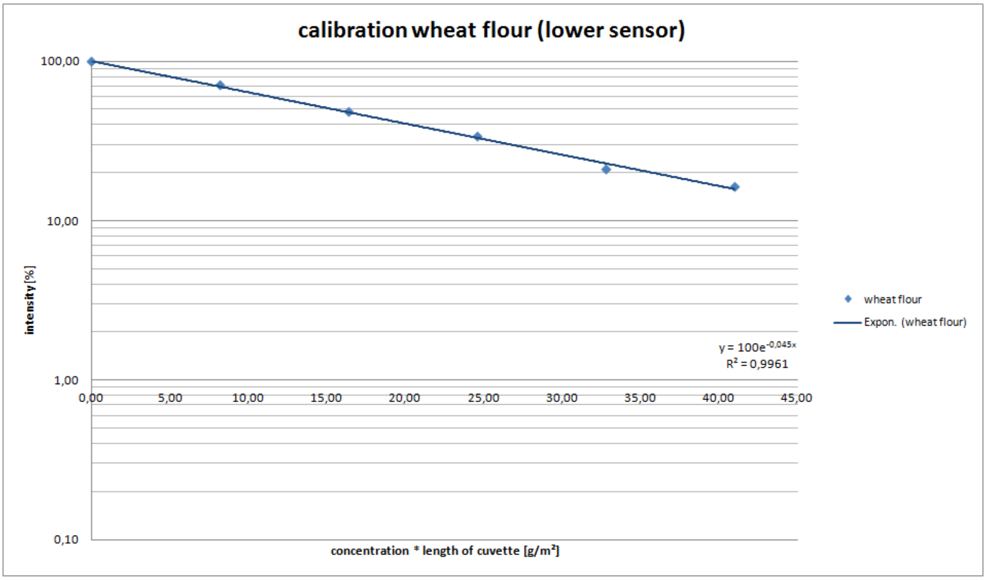

*A 17. Calibration for dust concentration meters, lower sensor, wheat flour.*

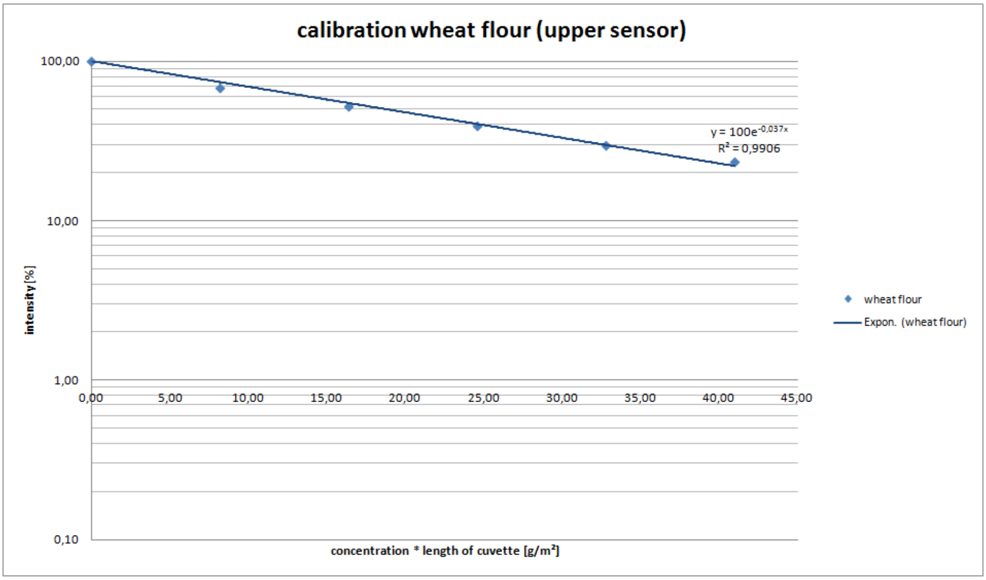

*A 18. Calibration for dust concentration meters, upper sensor, wheat flour.*

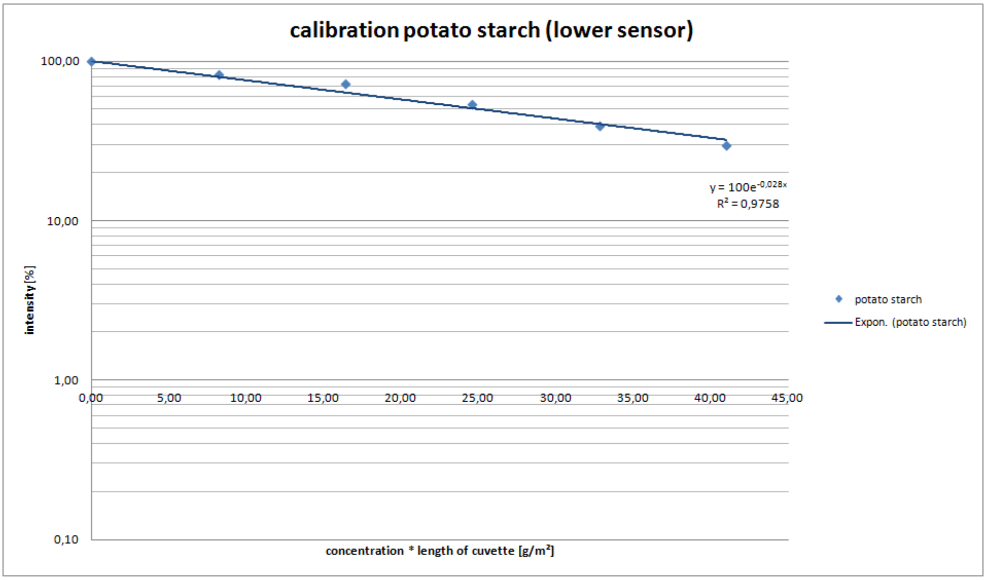

*A 19. Calibration for dust concentration meters, lower sensor, potato starch.*

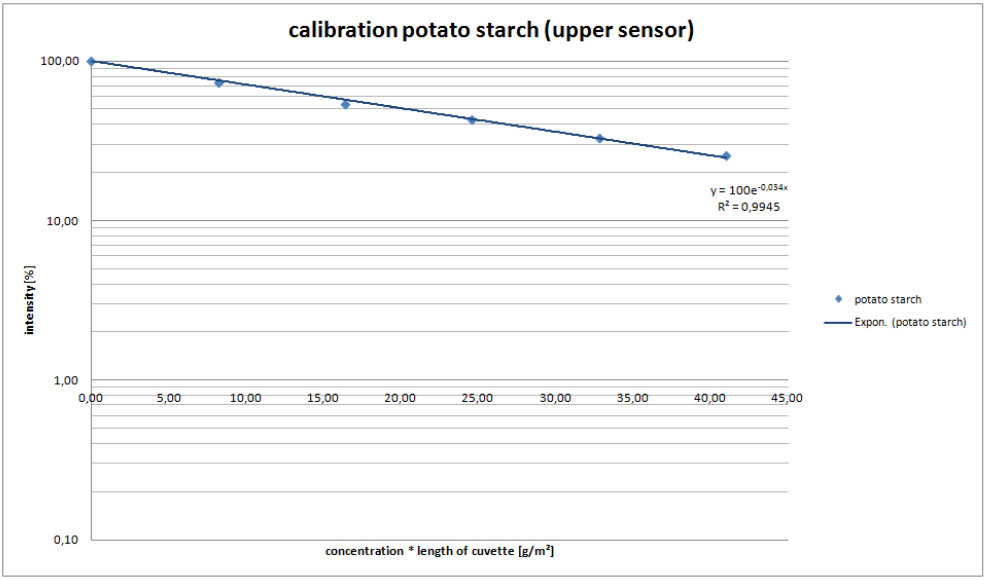

*A 20. Calibration for dust concentration meters, upper sensor, potato starch.*

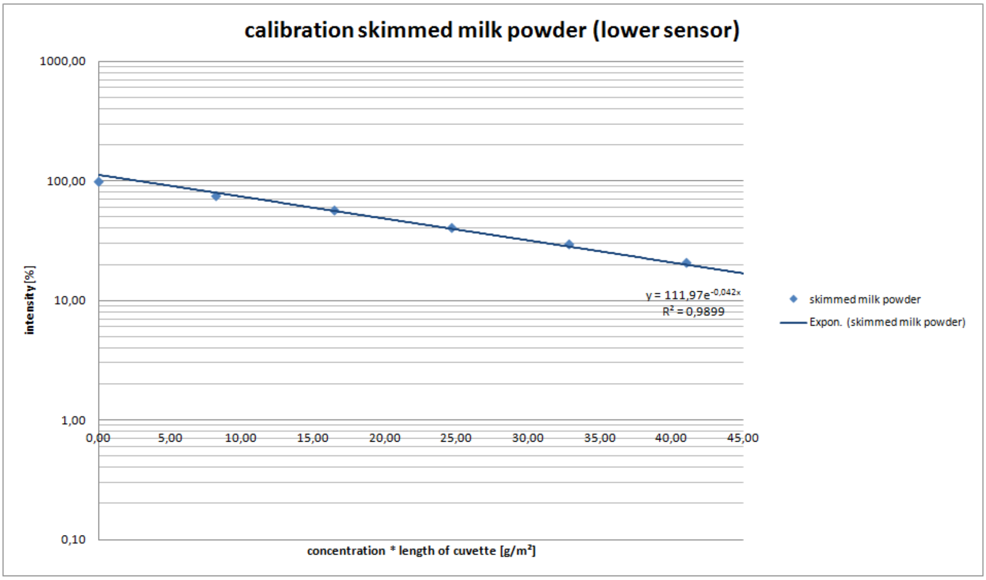

*A 21. Calibration for dust concentration meters, lower sensor, milk powder.*

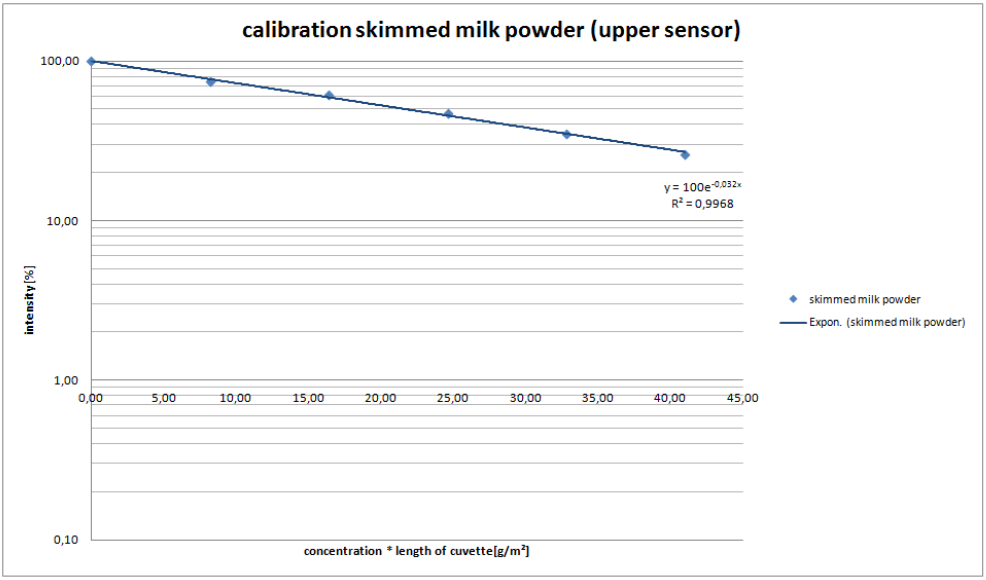

*A 22. Calibration for dust concentration meters, upper sensor, milk powder.*

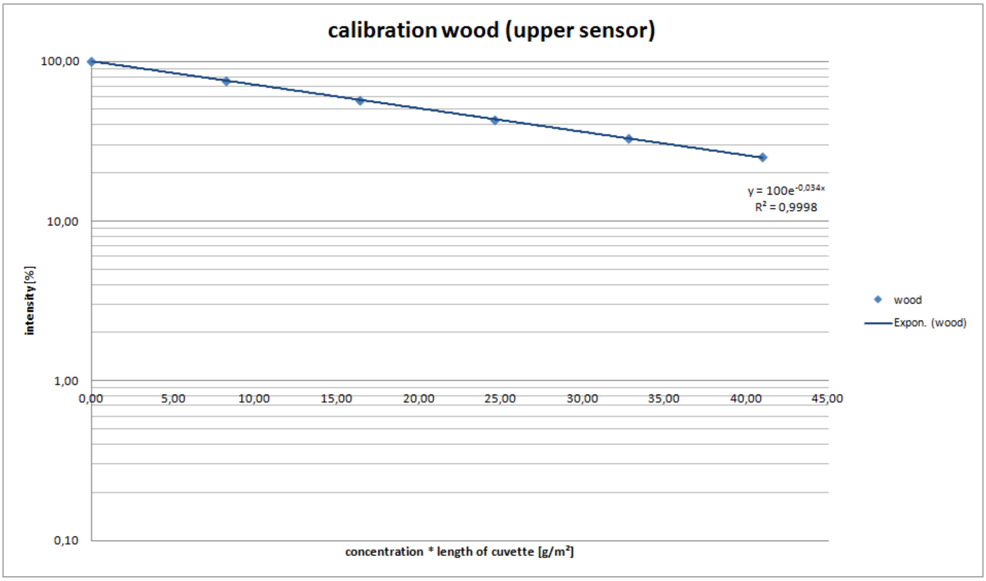

*A 23. Calibration for dust concentration meters, upper sensor, wood.*

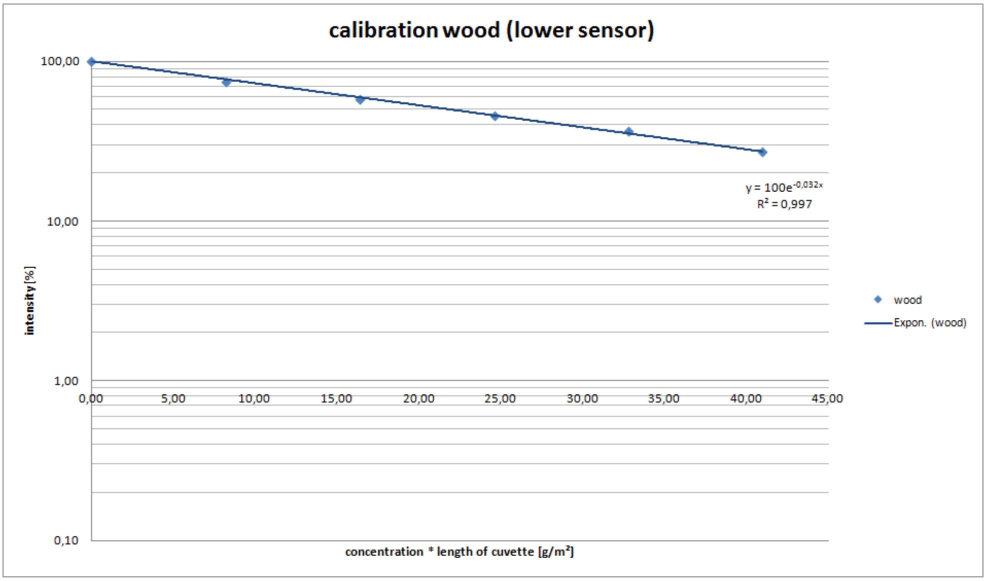

*A 24. Calibration for dust concentration meters, lower sensor, wood.*

## A.4 Calibration of dust concentration meters for large-scaled experiments

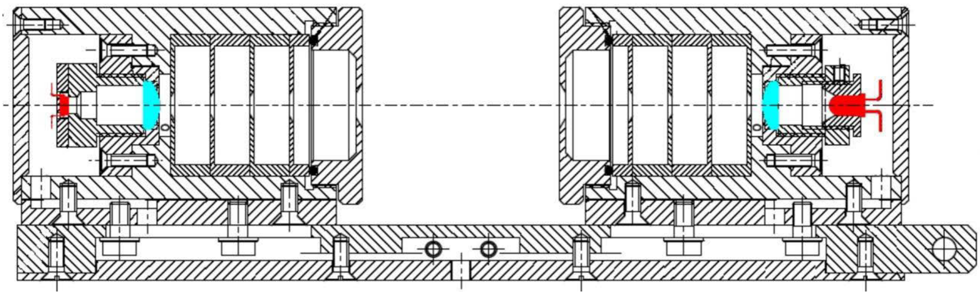

A 25. Improved dust concentration meter for large-scale experiments.

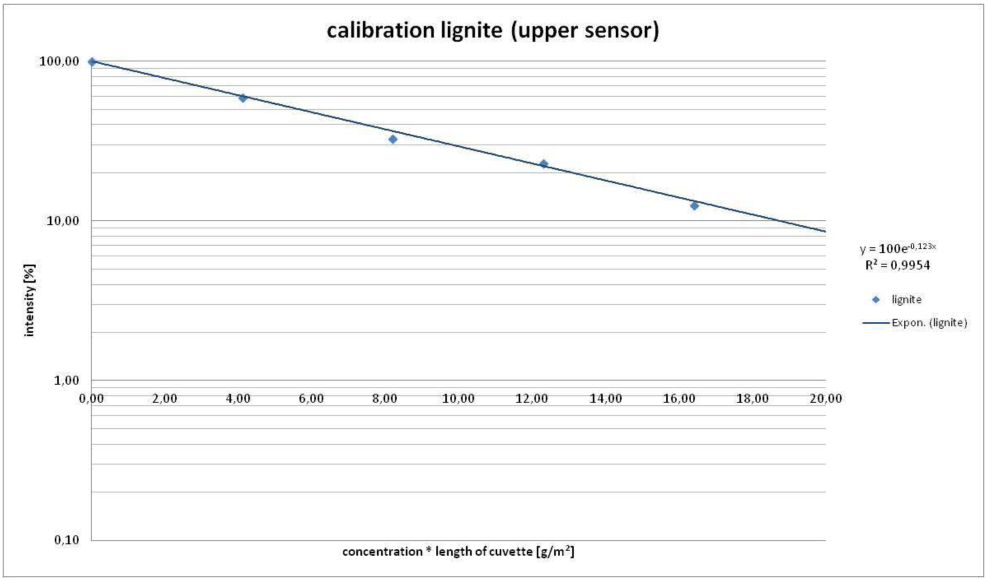

A 26. Calibration for dust concentration meters, upper sensor, lignite.

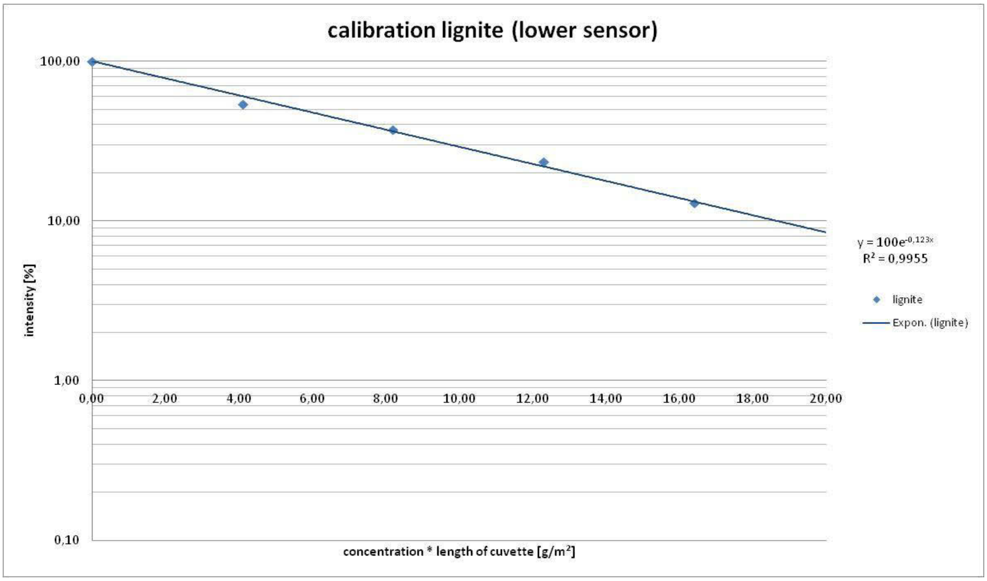

*A 27. Calibration for dust concentration meters, lower sensor, lignite.*

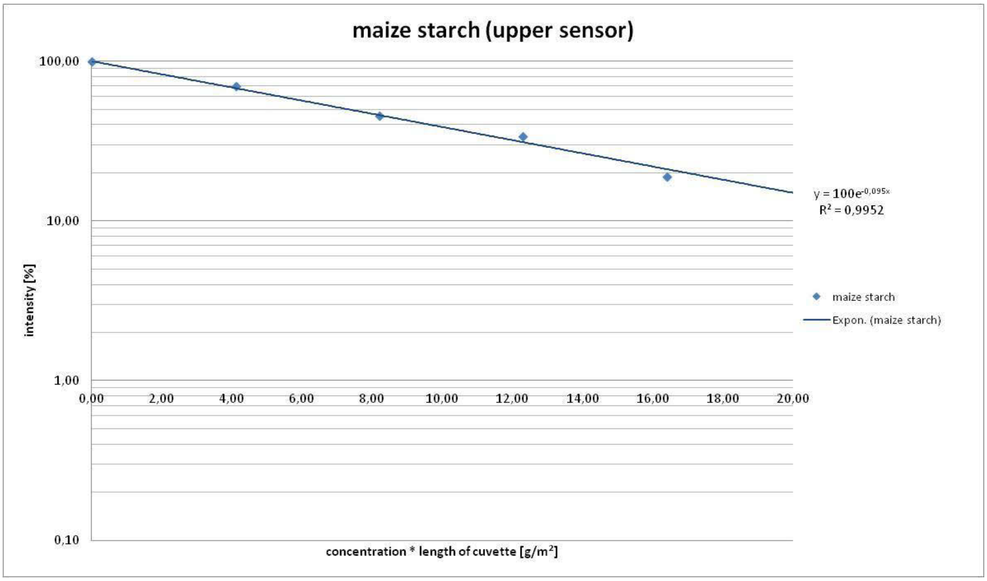

*A 28. Calibration for dust concentration meters, upper sensor, maize starch.*

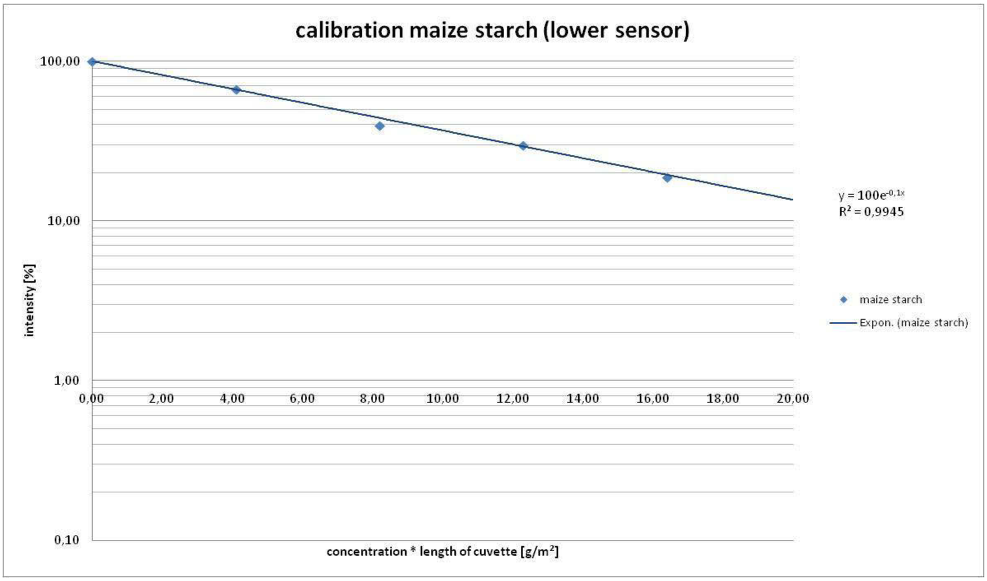

A 29. Calibration for dust concentration meters, lower sensor, maize starch.

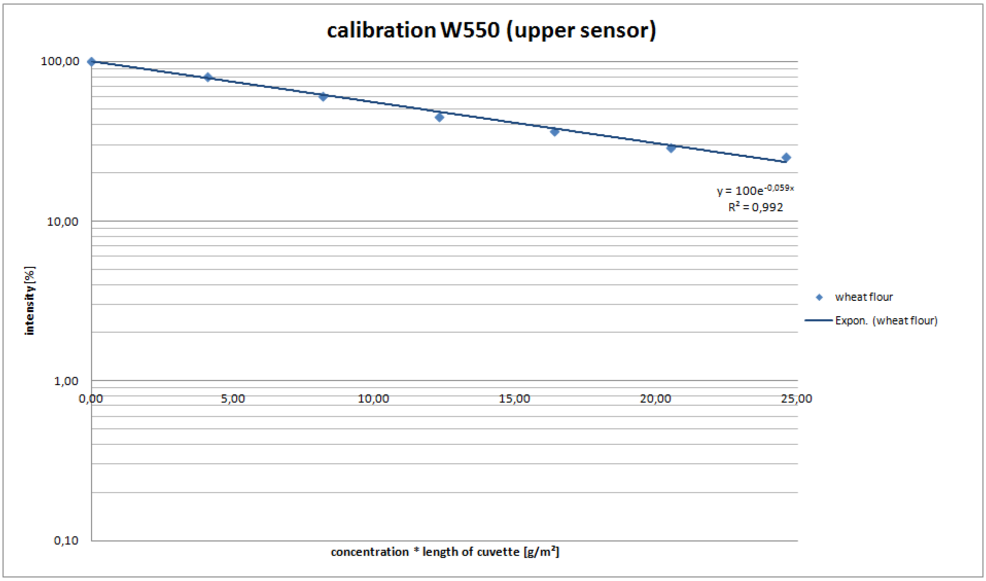

A 30. Calibration for dust concentration meters, upper sensor, wheat flour.

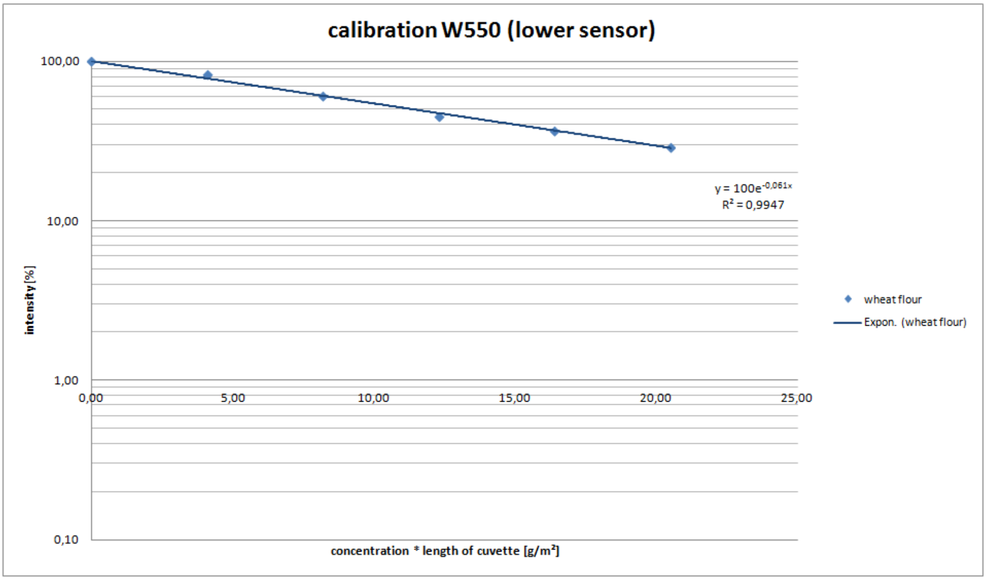

*A 31. Calibration for dust concentration meters, lower sensor, wheat flour.*